

AMERICAN UNIVERSITY OF BEIRUT

UPHEAVAL BUCKLING OF BURIED OFFSHORE
PIPELINES

by
SAHAR ALI ISMAIL

A thesis
submitted in partial fulfillment of the requirements
for the degree of Master of Engineering
to the Department of Civil Engineering
of the Faculty of Engineering and Architecture
at the American University of Beirut

Beirut, Lebanon
April 2016

AMERICAN UNIVERSITY OF BEIRUT

THESIS/UPHEAVAL BUCKLING OF BURIED OFFSHORE
PIPELINES

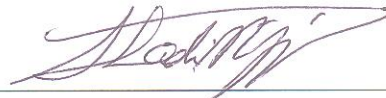
by
SAHAR ALI ISMAIL

Approved by:



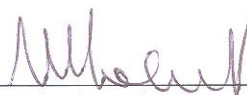
Dr. Salah Sadek, Professor
Civil and Environmental Engineering Department

Advisor



Dr. Shadi Najjar, Associate Professor
Civil and Environmental Engineering Department

Advisor



Dr. Mounir Mabsout, Professor
Civil and Environmental Engineering Department

Member of Committee

Date of thesis defense: April 18, 2016

AMERICAN UNIVERSITY OF BEIRUT

THESIS, DISSERTATION, PROJECT RELEASE FORM

Student Name: Tomaï Sahar Ali
Last First Middle

Master's Thesis Master's Project Doctoral Dissertation

I authorize the American University of Beirut to: (a) reproduce hard or electronic copies of my thesis, dissertation, or project; (b) include such copies in the archives and digital repositories of the University; and (c) make freely available such copies to third parties for research or educational purposes.

I authorize the American University of Beirut, three years after the date of submitting my thesis, dissertation, or project, to: (a) reproduce hard or electronic copies of it; (b) include such copies in the archives and digital repositories of the University; and (c) make freely available such copies to third parties for research or educational purposes.

Sahar Tomaï

May 3, 2016

Date

ACKNOWLEDGMENTS

I would like to express my gratitude to my advisors Professor Salah Sadek and Associate Professor Shadi Najjar for their guidance, support and encouragement through the study. Also, I would like to thank Professor Mounir Mabsout for his guidance and assistance while learning the finite element software and the engineering IT department for their help in computer work.

I would like to thank my family, my fiancée and my friends for their help, support and patience at all times.

AN ABSTRACT OF THE THESIS OF

Sahar Ali Ismail for Master of Science
Major: Civil Engineering

Title: Upheaval Buckling of Buried Offshore Pipelines

Offshore pipelines are used to transport oil and gas in different areas of the world. The economic importance of offshore pipelines has increased in recent years with the development of oil and gas transportation systems. Hydrocarbons are transported in the pipelines at high temperature and pressure in order to facilitate the flow of oil and to prevent its “solidification”. However, these high temperatures and pressures may force the pipeline to buckle either in the horizontal (lateral) or in the vertical direction (upheaval). The latter buckling mode may lead to pipeline failure that could cause massive oil leakage and severe environmental damages. Several studies have investigated the uplift resistance of buried pipelines. The objective of this thesis is to assess the effects of several parameters (soil burial depth, soil and pipeline properties and geometries) on the upheaval buckling of buried offshore pipelines by using the finite element software Abaqus to build the 3D model considering all pertinent factors. A new simplified empirical design approach is presented based on the parametric studies and analytical solutions explored and/or developed in the thesis herein.

ILLUSTRATIONS

Figure		Page
1.1.	Upheaval buckling of an offshore pipeline (after Friis-Hansen, 2000).....	3
1.2.	a) The vertical slip model (after Schaminee et al. (1990)) and b) Sliding block mechanism with shear planes at ψ to the vertical (after White et al., 2001).....	7
1.3.	Force Analysis of a pipeline section with vertical buckling presented by Hobbs (1981, 1984) (after Liu and Yan, 2013).....	9
1.4.	Basic types of initial imperfection configurations (Taylor and Tran, 1996).....	10
1.5.	Uplift test results for cohesionless soil (after Schaminee et al., 1990).....	12
1.6.	The normalized uplift resistance (P/HD) versus the burial depth (H/D) for a) $ID=0-20\%$, b) $ID=20-50\%$ and c) $ID=50-80\%$ (after White et al., 2001).....	14
1.7.	Correlation of pullout test results with different mechanisms ($D/D_0=2$) (after Schupp et al. 2006).....	16
1.8.	The modified vertical slip model used to predict experimental results (after Byrne et al., 2013).....	18
1.9.	Load-displacement data for pipeline tests carried out at different velocities (saturated sand: $H/D=3$ and $D=0.048m$) (after Bransby et al.,2009).....	19
1.10.	Flow around mechanism at a pipe displacement of $0.5D$ in a)dense coarse sand, b)dense fine sand, c)loose dense sand and d)loose fine sand (after Cheuk et al.,2008).....	20
1.11.	Summary of the parametric experimental and numerical study a) peak mobilization distance normalized by H and b) peak mobilization distance normalized by D (after Robert and Thusyanthan, 2014).....	22
1.12.	FE model of pipeline upheaval buckling (after Zeng et al., 2014).....	26

1.13.	Model geometry and soil support idealization (after Liu et al., 2015)..	27
1.14.	Nonlinear soil springs used to represent clay resistance on pipe uplift displacement (after Liu et al., 2015).....	27
1.15.	Comparison between experimental (test data) and numerical (calculation results) using the non-linear spring models (after Liu et al., 2015).....	28
1.16.	Normalized vertical force as a function of embedment ratio (after Newson and Deljoui, 2006).....	30
1.17.	Shallow and deep embedment contours for breakaway and bonded cases (after Newson and Deljoui, 2006).....	30
1.18.	Plain strain finite element model for buried offshore pipeline (after Liu et al., 2013).....	31
1.19.	Influence of a) the soil cover depth, b) the friction coefficient and c) the soil strength on the temperature difference versus buckle amplitude (after Liu et al., 2013).....	32
1.20.	Finite element uplift resistance results compared with experimental results for a) H/D=6 and b) H/D=8 (after Robert and Thusyanthan, 2014).....	33
1.21.	The dimensionless mobilization versus H/D for D=200mm for loose and dense sand compared with DNV and ASCE guidelines (after Robert and Thusyanthan, 2014).....	34
1.22.	Finite element analysis results for upward pipeline movement a) medium sand, H/D=4, b) dense sand, H/D=4, c) medium sand, H/D=13 and d) dense sand, H/D=13 (after Yimsiri et al., 2004).....	35
1.23.	Design chart for upward pipe movement (after Yimsiri et al., 2004)...	36
1.24.	2D finite element model (after Liu et al., 2014).....	37
1.25.	3D finite element model a) pipeline without initial imperfection and b) pipeline with initial imperfection (after Liu et al., 2014).....	37
1.26.	Midpoint pipeline buckling amplitude versus operational temperature difference for different models (after Liu et al., 2014).....	38
1.27.	Comparison of finite element models and analytical solution a) lateral deformation, b) axial stress, c) maximum buckling amplitude versus temperature difference and d) maximum buckling amplitude versus axial stress (after Liu et al., 2014).....	38

2.1	Geometry and model mesh distribution.....	45
2.2	Load displacement curves of the full model and its quarter.....	46
2.3	Load displacement curves of the pipe wall- fixed and restrained axially boundary conditions.....	47
2.4	Load displacement curves of the reduced and non reduced element types.....	48
2.5	a) Undeformed and b) Deformed shape of Triaxial Test of MMC soil model.....	53
2.6	Vertical stress versus axial strain of MC and MMC triaxial test at 10 and 50 kPa confinement.....	54
2.7	Mohr Coulomb Envelope for the medium dense sand with fines for the MC model and the MMC at peak states.....	54
2.8	Mohr Coulomb Envelope for the medium dense sand with fines for the MMC model at residual states.....	55
2.9	Different mesh sizes sections of the 3D finite element model.....	57
2.10	Load displacement curves of the mesh sensitivity analyses.....	57
3.1	Upheaval buckling of an offshore pipeline (after Friis-Hansen, 2000)	58
3.2	Pipeline effective length using "cutoff slope" value of 0.0014.....	60
3.3	Normalized mobilization distance- tangent intersection method.....	61
3.4	Pipeline buckling amplitude along the length of the pipe for different water levels.....	67
3.5	Load displacement curves- F (divided by L_p) versus $disp/H_c$ for different water levels.....	67
3.6	Pipeline buckling amplitude at 1% H_c upward pipeline displacement along the length of the pipe for different pipeline diameters-Medium Dense Sand with Fines.....	70
3.7	Load displacement curves- F (divided by L_p) versus $disp/H_c$ for different pipeline diameters-Medium Dense Sand with Fines.....	70

3.8	Load displacement curves- F (divided by L_{eff}) versus $disp/H_c$ for different pipeline diameters-Medium Dense Sand with Fines.....	71
3.9	a) Maximum uplift resistance and b) maximum normalized mobilization distance for different pipe diameters -Medium Dense Sand with Fines.....	71
3.10	Pipeline buckling amplitude at 1% H_c upward pipeline displacement along the length of the pipe for different embedment depths-Medium Dense Sand with Fines.....	73
3.11	Load displacement curves- F (divided by L_p) versus $disp/H_c$ for different embedment depths (H/D) -Medium Dense Sand with Fines.	74
3.12	Load displacement curves- F (divided by L_{eff}) versus $disp/H_c$ for different embedment depths (H/D) -Medium Dense Sand with Fines.	74
3.13	a) Maximum uplift resistance and b) maximum normalized mobilization distance for different embedment depths -Medium Dense Sand with Fines.....	75
3.14	Pipeline buckling amplitude at 1% H_c upward pipeline displacement along the length of the pipe for different pullout lengths (% L) - Medium Dense Sand with Fines.....	78
3.15	Load displacement curves- F (divided by L_p) versus $disp/H_c$ for different pullout lengths-Medium Dense Sand with Fines.....	78
3.16	Load displacement curves- F (divided by L_{eff}) versus $disp/H_c$ for different pullout lengths-Medium Dense Sand with Fines.....	79
3.17	Maximum uplift resistance and b) maximum normalized mobilization distance for different pullout lengths -Medium Dense Sand with Fines	79
3.18	Variation of the relative change in effective length $(L_{eff}-L_p)/L_p$ for different pullout lengths at different diameter to wall thickness ratios – Medium Dense Sand with Fines.....	81
3.19	Load displacement curves- a) F divided by L_p and b) F divided by L_{eff} versus $disp/H_c$ for different pullout lengths at different diameter to wall thickness ratios-Medium Dense Sand with Fines.....	83
3.20	Maximum uplift resistance: a) F divided by L_p and b) F divided by L_{eff} versus pullout lengths at different diameter to wall thickness ratios-Medium Dense Sand with Fines.....	84
3.21	Maximum normalized mobilization distance for different pullout lengths at different diameter to wall thickness ratios-Medium Dense Sand with Fines.....	84

3.22	Pipeline buckling amplitude at 1%Hc upward pipeline displacement along the length of the pipe for different soil cohesion values-Medium Dense Sand with Fines.....	86
3.23	Load displacement curves- F (divided by Lp) versus disp/Hc for different soil cohesion values and pullout lengths-Medium Dense Sand with Fines.....	87
3.24	Load displacement curves- F (divided by Leff) versus disp/Hc for different soil cohesion values and pullout lengths-Medium Dense Sand with Fines.....	87
3.25	Maximum uplift resistance: a) F divided by Lp and b) F divided by Leff versus pullout lengths at different soil cohesion values-Medium Dense Sand with Fines.....	88
3.26	Maximum normalized mobilization distance for different pullout lengths at different soil cohesion values-Medium Dense Sand with Fines.....	88
3.27	a) Maximum uplift resistance and b) mobilization distance for loose, medium dense and dense sand with fines for different pipe diameters..	92
3.28	a) Maximum uplift resistance and b) mobilization distance for loose, medium dense and dense sand with fines for different embedment depths.....	92
3.29	a) Maximum uplift resistance and b) mobilization distance for loose, medium dense and dense sand with fines for different pullout lengths.	93
3.30	a) Maximum uplift resistance and b) mobilization distance for loose, medium dense and dense sand with fines for different soil cohesion...	93
3.31	Load displacement curves F versus disp/Hc for loose, medium and dense sand with fines for different pipe diameters.....	94
3.32	Load displacement curves F versus disp/Hc for loose, medium dense and dense sand with fines for different embedment depths.....	96
3.33	Load displacement curves F versus disp/Hc for loose, medium dense and dense sand with fines for different pullout lengths.....	98
3.34	Load displacement curves F versus disp/Hc for loose, medium dense and dense sand with fines for different soil cohesion and pullout lengths.....	101
3.35	a) Vertical slip model (after Schaminee et al. (1990)) and b) Sliding block mechanism with shear planes at ψ to the vertical (after White et al. (2001)).....	102

3.36	Uplift soil resistance versus Soil Cohesion for Loose Sand with Fines- 100% pullout length FE results and Analytical Solutions.....	104
3.37	Bias Factor versus soil cohesion Analytical Solutions-Loose Sand with Fines.....	104
3.38	Uplift soil resistance versus Soil Cohesion for Medium Dense Sand with Fines- 100% pullout length FE results and Analytical Solutions..	105
3.39	Bias Factor versus soil cohesion Analytical Solutions-Medium Dense Sand with Fines.....	105
3.40	Uplift soil resistance versus Soil Cohesion for Dense Sand with Fines- 100% pullout length FE results and Analytical Solutions.....	106
3.41	Bias Factor versus soil cohesion Analytical Solutions- Dense Sand with Fines.....	106
3.42	Uplift soil resistance versus pipe diameter a)Loose b)Medium Dense and c)Dense sand with Fines- FE and Vertical Slip Model Analytical Solutions.....	109
3.43	Uplift soil resistance versus embedment depth a)Loose b)Medium Dense and c)Dense sand with Fines - FE and Vertical Slip Model Analytical Solutions.....	110
3.44	Uplift soil resistance versus pullout length a)Loose b)Medium Dense and c)Dense sand with Fines - FE and Vertical Slip Model Analytical Solutions.....	111
3.45	Uplift soil resistance versus soil cohesion a)Loose b)Medium Dense and c)Dense sand with Fines - FE and Vertical Slip Model Analytical Solutions	112
3.46	a) Local and b)Global soil failure modes.....	114
3.47	Uplift soil resistance versus pipe diameter a)Loose b)Medium Dense and c)Dense sand with Fines - FE and DNV Analytical Solutions.....	116
3.48	Uplift soil resistance versus embedment depth a)Loose b)Medium Dense and c)Dense sand with Fines - FE and DNV Analytical Solutions.....	117
3.49	Uplift soil resistance versus pullout length a)Loose b)Medium Dense and c)Dense sand with Fines - FE and DNV Analytical Solutions.....	118
3.50	Uplift soil resistance versus soil cohesion a)Loose b)Medium Dense and c)Dense sand with Fines - FE and DNV Analytical Solutions.....	119
3.51	Shear strain plot.....	121

3.52	Uplift soil resistance versus pipe diameter a)Loose b)Medium Dense and c)Dense sand with Fines - FE and Inclined Failure Surface Analytical Solutions.....	122
3.53	Uplift soil resistance versus Embedment Depth a)Loose b)Medium Dense and c)Dense sand with Fines - FE and Inclined Failure Surface Analytical Solutions.....	123
3.54	Uplift soil resistance versus pullout length a)Loose b)Medium Dense and c)Dense sand with Fines - FE and Inclined Failure Surface Analytical Solutions.....	124
3.55	Uplift soil resistance versus soil cohesion a)Loose b)Medium Dense and c)Dense sand with Fines - FE and Inclined Failure Surface Analytical Solutions.....	125
4.1	Variation of a) normalized uplift resistance exponential regression for different embedment depths, b) pipeline diameter linear regression correction coefficient, c) pullout length linear regression correction coefficient and d) soil cohesion power regression correction coefficient.....	128
4.2	Example.....	130
4.3	Variation of the measured (FE results) with the predicted uplift resistance for analytical and empirical solutions- Loose sand with fines.....	132
4.4	Variation of the bias factor with a) pipe diameter, b) embedment depth c) pullout length and d) soil cohesion for analytical and empirical solutions- Loose sand with fines.....	132
4.5	Variation of the measured (FE results) with the predicted uplift resistance for analytical and empirical solutions- Medium dense sand with fines.....	133
4.6	Variation of the bias factor with a) pipe diameter, b) embedment depth c) pullout length and d) soil cohesion for analytical and empirical solutions-Medium dense with fines.....	133
4.7	Variation of the measured (FE results) with the predicted uplift resistance for analytical and empirical solutions- Dense sand with fines.....	134
4.8	Variation of the bias factor with a) pipe diameter, b) embedment depth c) pullout length and d) soil cohesion for analytical and empirical solutions-Dense sand with fines.....	134

TABLES

Table	Page
1.1. Recommended mobilization distance values from DNV-RP-F110 (DNV 2007).....	8
2.1. Soil and pipe model parameters used in the Finite Element Analyses (FE).....	51
2.2. Mesh sensitivity analysis: mesh sizes sections and respective computational time.....	56
3.1. Medium Dense Sand with Fines simulation cases (GROUP-1)....	62
3.2. Medium Dense Sand with Fines simulation cases (GROUP-1-continued).....	63
3.3. Loose Sand with Fines simulation cases (GROUP-1).....	64
3.4. Dense Sand with Fines simulation cases (GROUP-1).....	65
3.5. Maximum uplift soil resistance and normalized mobilization distance-effect of pipe diameter- Medium Dense Sand with Fines.....	69
3.6. Maximum uplift soil resistance and normalized mobilization distance-effect of embedment depth- Medium Dense Sand with Fines.....	73
3.7. Maximum uplift soil resistance and normalized mobilization distance-effect of pullout length- Medium Dense Sand with Fines.....	77
3.8. Pipe stiffness for different diameter sizes and diameter to wall thickness ratios.....	81
3.9. Maximum uplift soil resistance and normalized mobilization distance-effect of soil cohesion- Medium Dense Sand with Fines.....	86

CONTENTS

ACKNOWLEDGEMENTS	v
ABSTRACT.....	vi
LIST OF ILLUSTRATIONS.....	vii
LIST OF TABLES.....	xviii

Chapter

I. INTRODUCTION, BACKGROUND AND SCOPE.....	1
A. Introduction.....	1
B. Background.....	1
1. Analytical Studies	5
a. Vertical Slip Model.....	5
b. Sliding Block with Included Failure Surface.....	5
c. Det Norske Veritas Guidelines.....	7
2. Experimental Studies.....	10
a. Effect of Pullout Rate.....	16
b. Effect of Soil Particle Size	19
c. Mobilization Distance.....	21
3. Numerical Studies.....	24
C. Scope and Objectives of the Research.....	41
1. Objectives of the Proposed Study.....	41
2. Scope of Work.....	41
3. Organization of the Thesis.....	42
II. FINITE ELEMENT MODEL OF UPHEAVAL	44
BUCKLING OF BURIEOFFSHORE.PIPELINE.....	44
A. Software	44

B. Problem Definition.....	44
C. Constitutive Models.....	48
D. Mesh Sensitivity Analysis	55
III. Results and Analysis.....	58
A. Overview of Analyses/ Parametric Study.....	58
B. Effect of Water Level.....	66
C. Case-1 Medium Dense Sand with Fines.....	68
1. Effect of Pipeline Diameter, D.....	68
2. Effect of Embedment Depth, H.....	72
3. Effect of Pullout Length, L_p	76
4. Effect of Pipeline Diameter to Wall Thickness Ratio, D/t	80
D. Effect of Soil Properties.....	85
1. Soil Cohesion, c	85
2. Soil Denseness.....	89
E. Analytical Solutions.....	102
1. Vertical Slip Models.....	107
2. DNV.....	113
3. Sliding Block with Inclined Failure Surfaces.....	120
IV. Simplified Approach to Calculate the Uplift Resistance....	126
A. Empirical Approach.....	126
B. Example.....	123
C. Simplified Approach Validation.....	131
V. Conclusions and Recommendations.....	135
REFERENCES.....	145

Appendix

I. USDFLD Code.....	115
II. Load Displacement Curves.....	153
A. Loose Sand with Fines.....	176
B. Medium Dense Sand with Fines.....	178
C. Dense Sand with Fines.....	180
III. Variation of the Bias Factor for Different Analytical Solutions.....	195
IV. Shear Strain Plots.....	195

CHAPTER I

INTRODUCTION, BACKGROUND AND SCOPE

A. INTRODUCTION

The worldwide economic importance of offshore pipelines has increased in recent years with the development of oil and gas transportation. In fact, two-thirds of the oil and natural gas transport in developed countries is done via pipelines. The transport of hydrocarbons in pipelines is typically done at high temperature and pressure to facilitate flow and to prevent “solidification” of the oil. However, these high temperatures and pressures may force the pipeline laid offshore to buckle either in the horizontal or in the vertical direction (lateral or upheaval buckling, respectively). The latter buckling mode may lead to pipeline failure which can, not only cause massive oil leakage and loss of billions of dollars, but also result in severe environmental damage to sea fauna and flora along with the seabed itself, shoreline, etc. These failures can have equally severe secondary economic impacts on tourism, industry, etc. Some recent examples of offshore oil leaks are those that occurred in the Deepwater Horizon in the Gulf of Mexico (April 2010), in Montara West Atlas rug in Australia (August 2009) and in Bohai in the Gulf in China (June 2011).

B. BACKGROUND

Offshore pipelines, also known as subsea pipelines, are placed *on* (unburied pipelines) or *in* the seabed in a trench (buried pipelines). They have been used since the 1970s to transport oil and/or gas to onshore storage facilities and refineries. Several factors

are considered in designing and constructing offshore pipelines. These include: the current use(s) of the seabed in the area, geohazards (geology of the area, geotechnical and environment conditions: submarine landslides, currents, waves, ice-related issues, etc.), societal/political context, etc. From a technical perspective, the most important factors to consider are the seabed ability to withstand the weight of the pipelines and associated loads, in addition to geohazards associated with the area, if any.

Offshore pipelines have typical diameters of around 76 mm (3 inches) for gas lines and can be up to 1800 mm (72 inches) for high capacity oil lines. In addition, the wall thickness of these pipes varies from 10 to 75 mm (0.39 to 3 inches). Pipeline walls are made of steel and coated for corrosion and abrasion (Gerwick, 2007 and Dean, 2010).

Offshore pipelines are very slender elements given their substantial length (on the order of kms). These pipelines carry high temperature oil and gas. The temperatures inside the pipelines produce internal pressure or thermal expansion that is resisted by the friction between the pipe and the soil or the seabed surrounding this pipe; this leads to high compressive forces within the pipe which may result in “Euler buckling” of the pipeline.

The buckling behavior of pipelines can be divided into two modes: local and global (whole) buckling. Local buckling refers to the local instability of the pipe wall and was investigated by several researchers: Bouwkamp and Stephen (1973), Sherman (1976), Reddy (1979), Gresnigt and Foeken (2001), among others. Whole buckling, also known as beam buckling, is like Euler buckling for slender columns where the pipeline experiences a large displacement in the vertical direction (uplift, upheaval buckling) or lateral direction (lateral buckling) (Run Liu and Shuwang Yan, 2013).

Upheaval buckling, under a given temperature and pressure, is controlled by the soil resistance acting on the pipeline. This soil resistance depends on several factors such as the soil cover or burial depth, soil properties, amplitude of the pipeline buckling and direction of the pipeline movement (Liu et al., 2013).

When the water depth is less than about 60 meters, pipelines must be buried in a trench to insure the minimal interference between the pipeline and the marine activities and to provide thermal insulation. Burying sections of the pipeline has several advantages: the soil cover provides thermal insulation by retaining the pipe cool-down time and additional resistance to the pipeline against axial expansion and “pipeline walking”. Upheaval buckling is a major problem for buried pipelines because it is associated with large axial forces that lead to high values of strain, therefore potential yielding of the pipeline leading to failure (Cheuk et al., 2006 and Sun et al., 2011) (Figure 1.1).

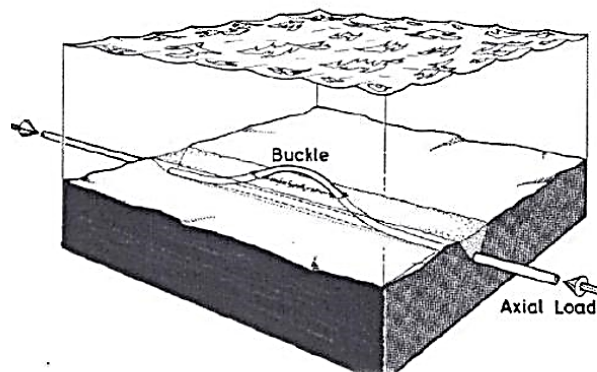


Figure 1.1 Upheaval buckling of an offshore pipeline (after Friis-Hansen, 2000)

Studies on upheaval buckling analysis of subsea pipelines go back to 1974 when Palmer and Baldry (1974) conducted a small scale experiment modeling buckling of a pipeline due to an increase in the pipe internal pressure. Hobbs (1981 and 1984) summarized the basic models of buckling of subsea pipelines. A series of upheaval buckling of offshore pipeline incidents occurred in the 1980s in the North Sea and resulted in severe economic and environmental impacts and costs (Guijt, 1990 and Nielsen et al. 1990). Since the 1990s, and given the increased use and interest in exploitation of offshore gas and oil reserves worldwide, several researchers focused on developing the state of knowledge and practice in reference to pipeline design and stability against upheaval buckling through analytical, experimental and numerical studies. In what follows, a summary of the main efforts and findings is presented. .

1. Analytical Studies

The key factor associated with the resistance to uplift of buried pipelines is the Uplift Resistance Force, F , provided by the embedment soil, expressed in units of F/L (e.g. kN/m). Several researchers presented empirical formulae to obtain the maximum uplift resistance force. These formulae vary in reference to the models and assumptions used to derive them and are included in this section:

a. Vertical Slip Model (ref. Figure 1.2a)

- Schaminee et al. (1990)
 - Cohesionless soil: $F = \gamma'HD + H^2 \gamma' K \tan \phi$
 - Cohesive soil: $F = \gamma'HD + 2Hc_u$
- Palmer et al. (1990)
 - Cohesionless soil: $F = \gamma'HD + f \gamma' H^2$
 - Cohesive soil: $F = c_u D \cdot \min[3, H/D]$
- Branby et al. (2002)
 - Cohesionless soil: $F = \gamma'HD [1 + 0.1D/H + K_o \tan \phi (H/D) (1 + D/(2H))^2]$
 - Cohesive soil: $F = \gamma'HD [1 + 0.1D/H + 2c_u / (\gamma'H) (H/D + 0.5)]$

b. Sliding Block with Inclined Failure Surface (ref. Figure 1.2b)

- White et al. (2001)
 - $F = \gamma'HD + \gamma'H^2 \tan \psi + \gamma'H^2 (\tan \phi_{\text{peak}} - \tan \psi) [(1 + K_o)/2 - (1 - K_o)(\cos 2\psi)/2]$
- Ng and Sprigman (1994)
 - Cohesionless soil: $F = \gamma'HD + H^2 \gamma' \tan \phi_{\text{max}}$
- Vermeer and Sutjiadi (1985)
 - Cohesionless soil: $F = \gamma'HD + H^2 \gamma' \tan \phi_{\text{max}} \cos \phi_{\text{crit}}$

Where:

F =peak uplift resistance per unit length (kN/m)

$F/(\gamma'HD) = P_d$ = uplift resistance factor

γ' =effective unit weight (kN/m³)

H =soil cover height (m)

D =pipeline diameter (m)

c_u =undrained shear strength

Ψ =dilation angle (°)

Φ =internal friction angle (°)

ϕ_{peak} =peak friction angle (°)

ϕ_{crit} = critical friction angle (°)

$K_o = 1 - \sin \phi$

K =coefficient of lateral earth pressure (the ratio of the horizontal and vertical effective stresses)

f = experimental coefficient determined experimentally, taken as 0.5 for dense materials and 0.1 for loose materials (after Palmer et al. (1990))

L = loose sand

VL = very loose sand

R = rock

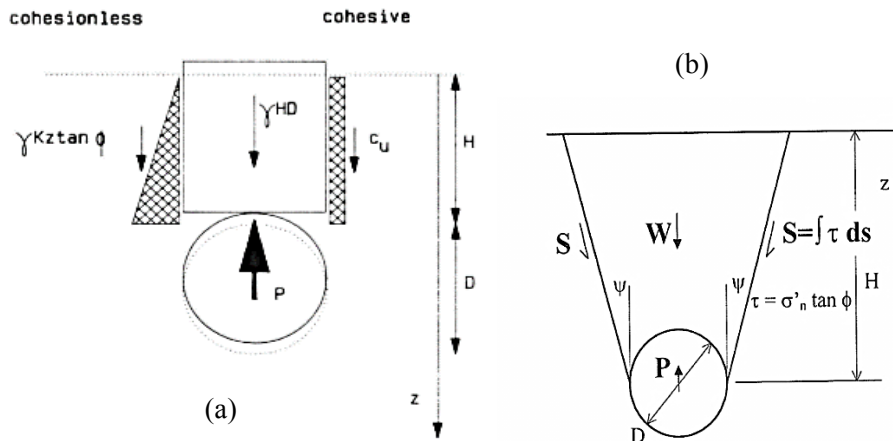


Figure 1.2 a) The vertical slip model (after Schaminee et al. (1990)) and b) Sliding block mechanism with shear planes at ψ to the vertical (after White et al., 2001)

c. Det Norske Veritas Guidelines (DNV, 2007)

The DNV (Det Norske Veritas, 2007) Offshore Specifications indicate that the peak uplift resistance of pipelines in sand may be obtained as follows:

- Cohesionless soil: $F = \gamma'HD[1 + (0.5 - \pi/8)D/H + f_p / (\gamma'HD)(H + D/2)]$
- Cohesive soil: $F = \gamma''HD + \gamma'D^2(0.5 - \pi/2) + 2c_u(H + D/2)$

(Global soil failure model, shallow shear failure)

Where:

R_{peak} = peak uplift resistance per unit length (kN/m)

f_p = Pedersen uplift factor (as described in Table 1)

γ' = effective unit weight (kN/m^3)

H = soil cover height (m)

D = pipeline diameter (m)

DNV states, as described in Table 1.1, that the pipe movement at peak mobilization of a buried pipe in sand, δ_f , is between 0.005H and 0.008H and independent of the embedment depth ratio H/D.

Table 1.1 Recommended mobilization distance values from DNV-RP-F110 (DNV 2007)

BACKFILL SOIL TYPE	MOBILIZATION DISTANCE δ_f	PEDERSEN UPLIFT FACTOR f_p	DNV LIMITATION
loose sand	0.5-0.8%H	0.1-0.3	$3.5 \leq H/D \leq 7.5$
medium or dense sand	0.5-0.8%H	0.4-0.6	$2 \leq H/D \leq 8$
rock	20-30mm	0.5-0.8	$2 \leq H/D \leq 8$, particle size (25-75 mm)

The effect of pipeline initial imperfection was not included in any of the basic models of buckling for long pipelines summarized by Hobbs (1981, 1984). The “initial imperfection” effect is mainly produced by an uneven seabed profile or by the existence of a prop under the pipeline. These initial imperfections constitute weak points in the pipeline that are quicker to undergo upheaval buckling when compared to other sections of the pipeline. The basic models of Hobbs have been modified throughout the years and updated by considering the pipeline initial imperfections that are produced by the pipe lay-out techniques as shown in Figure 1.3. Several researchers considered this problem such as Taylor and Tran (1993, 1996), Ballet and Hobbs (1992), Matlaby and Calladine (1995), Croll (1997) and Hunt and Blackmore (1997). Taylor and Tran (1993, 1996) presented

three types of typical imperfection configuration of subsea pipelines (Figure 1.4) and developed symmetric buckle models of pipelines (trenched or buried, continuous or discrete). Ballet and Hobbs (1992) and Hunt and Blackmore (1997) considered the asymmetric buckling in the prop case and seabed imperfection.

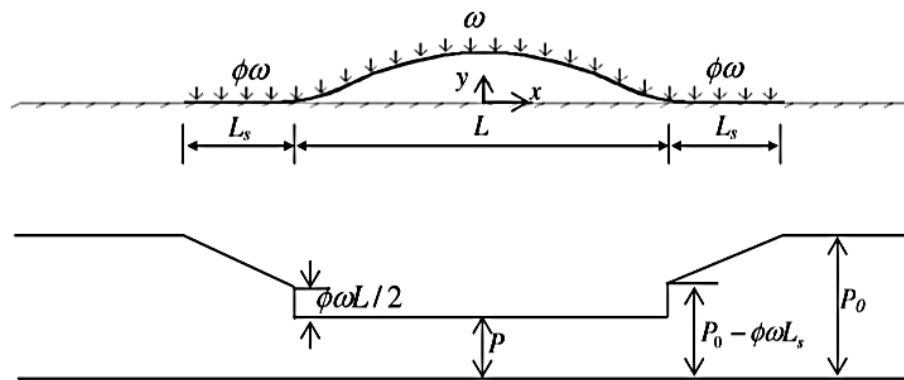


Figure 1.2 Force Analysis of a pipeline section with vertical buckling presented by Hobbs (1981, 1984) (after Liu and Yan, 2013)

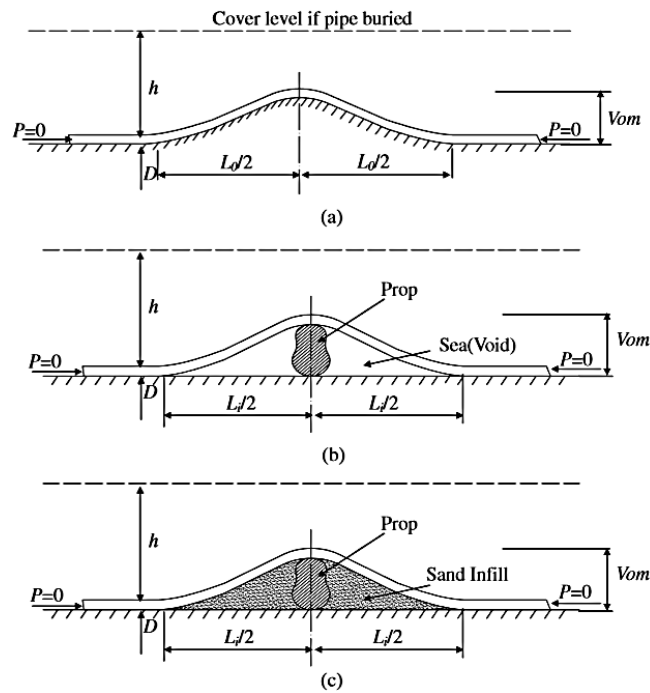


Figure 1.3 Basic types of initial imperfection configurations (Taylor and Tran, 1996)

2. Experimental Studies

Lab-scale studies on upheaval buckling of offshore pipelines include pipe-soil interaction that is associated with pullout and friction experiments. These experiments focus on the force-displacement relationship of the upheaval buckling of buried pipelines.

The first published work on the pipe-soil interaction was in 1981 where Anand and Agarwal (1981) conducted large-scale experiments to study the frictional resistance between the soil and concrete-coated pipes in the horizontal and vertical directions. Tian et al. (2010) performed physical model experiments to obtain load-displacement curves for the behavior of pipelines subjected to horizontal and vertical loading. In addition, Gao et al.

(2010) carried out centrifuge displacement-control pipe-soil interaction experiments to obtain the underlying pipe-soil mechanism by studying the effects of the pipe surface roughness, end-constraints and initial embedment.

Starting in 1990 and since, several researchers performed uplift or pullout physical model and centrifuge experiments of buried pipelines in sand. Those include Schaminee et al. (1990), Ng and Springman (1994), White et al. (2001), Bransby et al. (2001), Gao et al. (2011), Chin et al. (2006), and Schupp et al. (2006). In some of the more recent work, Byrne et al. (2008 and 2013) and Bransby and Ireland (2009) examined the effect of pullout rates on the results obtained. Other studies focused on uplift mobilization distance of the buried pipelines in sand, such as the work of Bransby et al. (2001), Stone (2006), Cheuk et al. (2008), Wang et al. (2012) and Robert and Thusyanthan (2014). The mechanisms of failure were observed and interpreted by Ng and Springman (1994), Bransby et al. (2001), White et al. (2001), Schupp et al. (2006), Stone (2006), Cheuk et al. (2008) and Byrne et al. (2008 and 2013). Finally, Ng and Springman (1994) White et al. (2001), Chin et al. (2006) and Byrne et al. (2008) presented and discussed a modification to the vertical slip model which was originally suggested by Schaminee et al. (1990).

Going back to the original study by Schaminee et al. (1990), the work included conducting full-scale experiments on uplift and axial resistance of a 4'' pipe embedded in saturated soil for the cases of dense sand, loose sand, remolded clay and rock, with various soil cover depth to pipeline diameter conditions ($H/D = 4$ to 12) to provide data and to link between the in-situ and lab conditions. They showed (Figure 1.5) that the uplift force increases with the increase in H/D and the values for the uplift force for sand and rock are

greater than the values that were presented in the literature to date. In addition, the uplift force values were greater for clayey soil than for sandy soil for the same displacement.

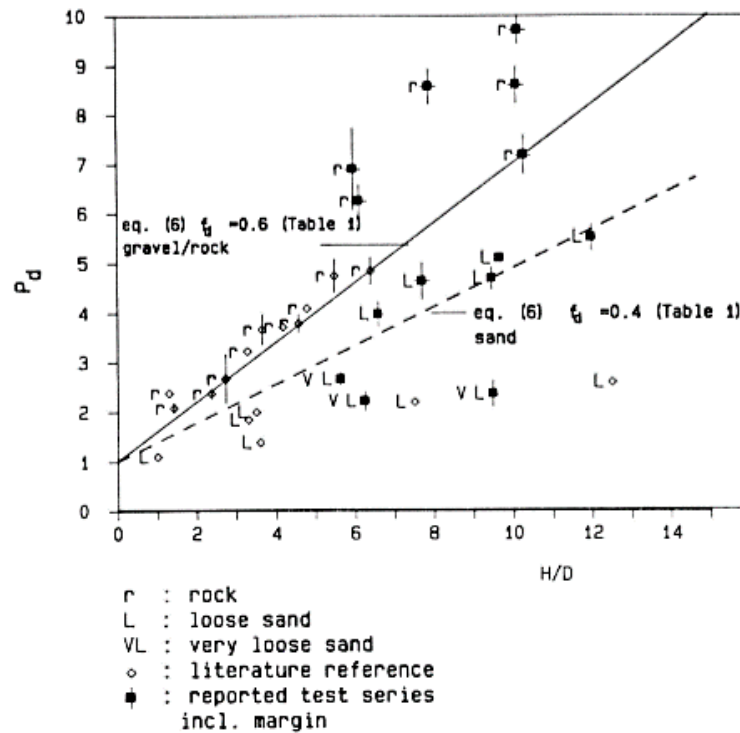


Figure 1.4 Uplift test results for cohesionless soil (after Schaminee et al., 1990)

Ng and Springman (1994) measured the uplift resistance of pipelines buried in sand and in sand overlain by rockfill using a mini-drum centrifuge (drained conditions). The failure mechanisms during pipe pullout were observed. The authors suggested a modification to the vertical slip model for cohesionless soils that was presented by

Schaminee et al. (1990), to account for soil dilation. As reported by Ng and Springman (1994), the peak uplift resistance is not affected by whether the sand backfill is above the gravel backfill or vice versa. The uplift resistance increases when placing a rockfill due to the increase in H/D that is caused by an addition of overburden pressure and not by an increase in the mobilized friction angle.

White et al. (2001) performed experiments using a mini-drum centrifuge to determine the pipe uplift mechanism and to measure the uplift force. The results showed that the uplift mechanism is a function of the soil density and the uplift resistance is associated with an inclined shearing surface. They concluded that vertical slip model does not reliably represent the failure mechanism. Therefore, White et al. (2001) presented a new solution to represent the failure mechanism for upheaval buckling of pipelines in sand through load-displacement curves based on their experimental results (Figure 1.6).

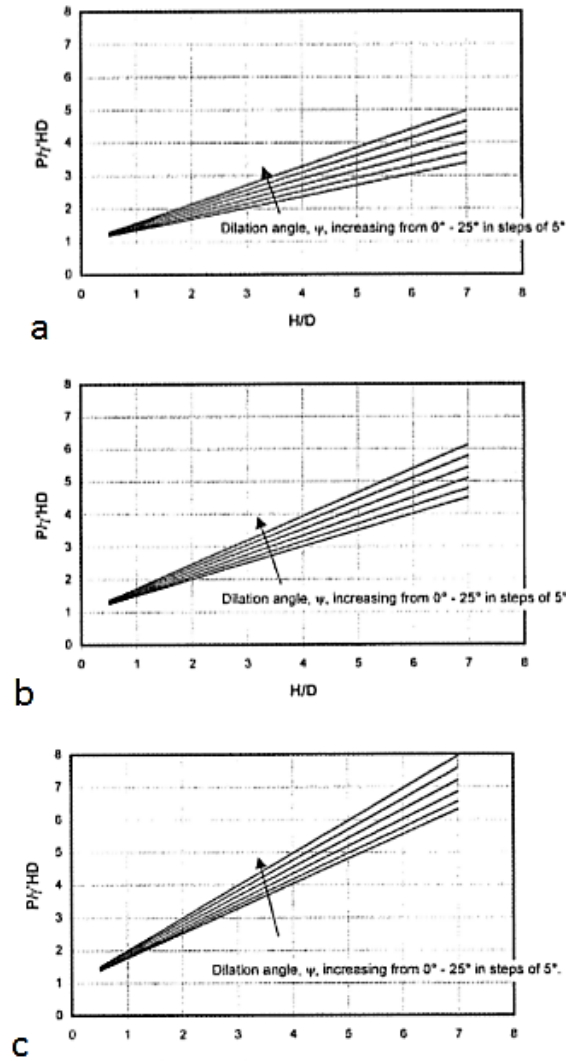


Figure 1.5 The normalized uplift resistance ($P/\gamma'HD$) versus the burial depth (H/D) for a) ID=0-20%, b) ID=20-50% and c) ID=50-80% (after White et al., 2001)

Bransby et al. (2001) investigated the soil resistance due to pipe uplift displacement using physical and centrifuge models for dry saturated sand and gravel. The authors studied the effects of the pipeline diameter and soil burial depth (H/D). The finite

element software SAGE-CRISP was then used to validate the experimental results. Bransby et al. (2001) showed that the deformation failure mechanism depended on the initial density of the soil, while the peak uplift resistance and the mobilization distance depend on the movement of the soil during “gap formation” (underneath the moving pipeline), and not on the failure mechanism. A flow around mechanism was observed after reaching the peak uplift resistance and a mobilized distance between 0.5 to 1%D.

Chin et al. (2006) conducted uplift centrifuge tests to study the uplift resistance of buried pipelines in cohesionless soils. The peak uplift resistance was found to increase with the increase in the soil cover to pipeline diameter (H/D) and is mobilized within small pipeline displacements. These uplift resistance values are higher in dense soil than in loose soil. Chin et al. (2006) compared their experimental results with the available analytical solutions. They found that not all available analytical models are reliable in predicting the uplift resistance of pipelines buried in cohesionless soil.

Gao et al. (2011) carried out large-scale model experiments to measure the pipeline uplift resistance. They showed that the soil can be modeled as ideal “elastic-plastic” model for $H/D > 5$ and as “elastic-softened” model for $H/D < 5$. Moreover, they showed that the capacity of the pipeline (uplift resistance) increases with the increase in the soil burial depth and decreases with the increase in the pipe initial imperfection.

Schupp et al. (2006) and Byrne et al. (2008, 2013) performed 2D and 3D tests in terms of plain strain, small-scale and large-scale testing for loose uniform sand from the North Sea to study the effects of upheaval buckling, pipe flotation and liquefaction. The pipeline uplift failure mechanisms were observed using particle image velocimetry by evaluating the velocities around the pipe. Schupp et al. (2006) studied the relation between

the soil burial depth (H/D), pipe diameter and pullout resistance for dry drained sand. They also investigated the relationship between the axial-load displacement response and soil cover depth. According to Shupp et al. (2006), a correlation exists between the load-displacement curves and the failure mechanisms, as shown in Figure 1.7 (images 1 to 6: deep flow failure, images 7 to 10: vertical slip model, images 11 to 13: near surface slip and flow mechanism). They noted that the uplift force increases with the increase in the pipeline diameter and soil cover depth.

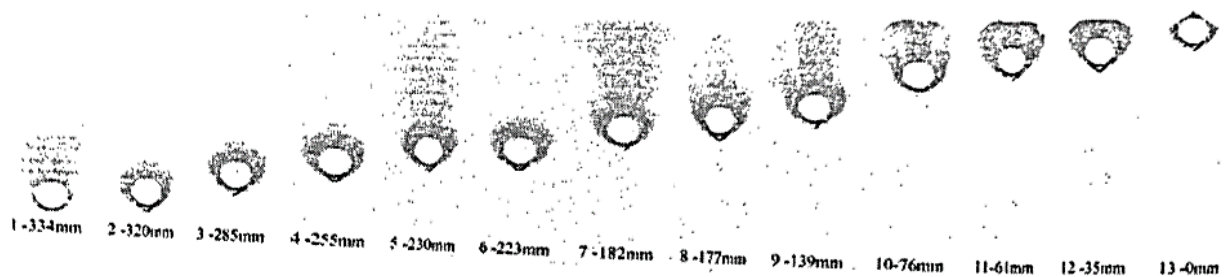


Figure 1.6 Correlation of pullout test results with different mechanisms ($D/D_0=2$) (after Schupp et al. 2006)

a. Effect of Pullout Rate

Byrne et al. (2008) carried out uplift tests for buried pipes, in dry and saturated sand under different pullout rates for different pipeline diameters and soil cover depths and determined the loads and associated displacements. For loose dry sand, the uplift load increases with the pipe upward displacement until it reaches a peak value then decreases in

a proportional manner. For the saturated sand, the uplift load shows a high dependency on the uplift rate. Slow rates give responses similar to the dry case and the fast rates give undrained responses that lead to loss of uplift resistance and risk of liquefaction. The model developed by Byrne et al. (2008) accounts for the dissipation of excess pore pressures during pipe pullout. Small and large-scale experiments were performed to show the relation between the buckling loads and the soil cover depth. Lower axial buckling forces were observed in the saturated case compared to the dry case.

Byrne et al. (2013) designed a pipeline testing apparatus to measure the force on the pipe and the excess pore water pressure around the pipe. The apparatus was pulled vertically at different rates in very loose saturated fine uniform sand (North Sea sand). They showed that the uplift resistance increases with the increase in the soil cover depth and the initial pore pressure depends on the initial velocity and on H/D . A simple analytical model (the vertical slip model modified as in Figure 1.8), which accounts for the dissipation of the excess pore water pressures around the pipe, was used to fit the experimental results.

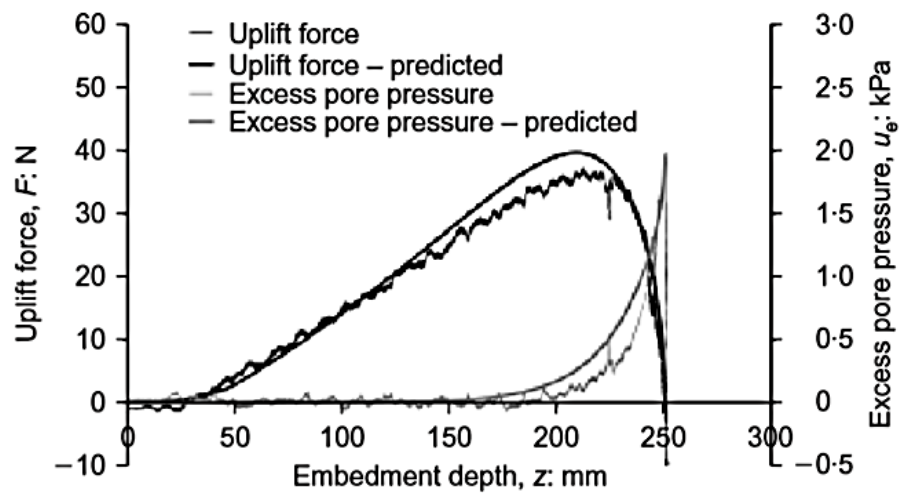


Figure 1.7 The modified vertical slip model used to predict experimental results (after Byrne et al., 2013)

Bransby and Ireland (2009) conducted physical and centrifuge pullout experiments to study the effects of the pullout rates on the peak uplift capacity and displacement in loose saturated sand. These rate effects depend on the normalized velocity. For the drained cases, the results were similar to previous studies. For the fast uplift displacement cases, partially drained soil responses were observed. The peak uplift resistance and displacement increase with the velocity (Figure 1.9). The relationship between the uplift capacity and normalized velocity depends on the soil relative density.

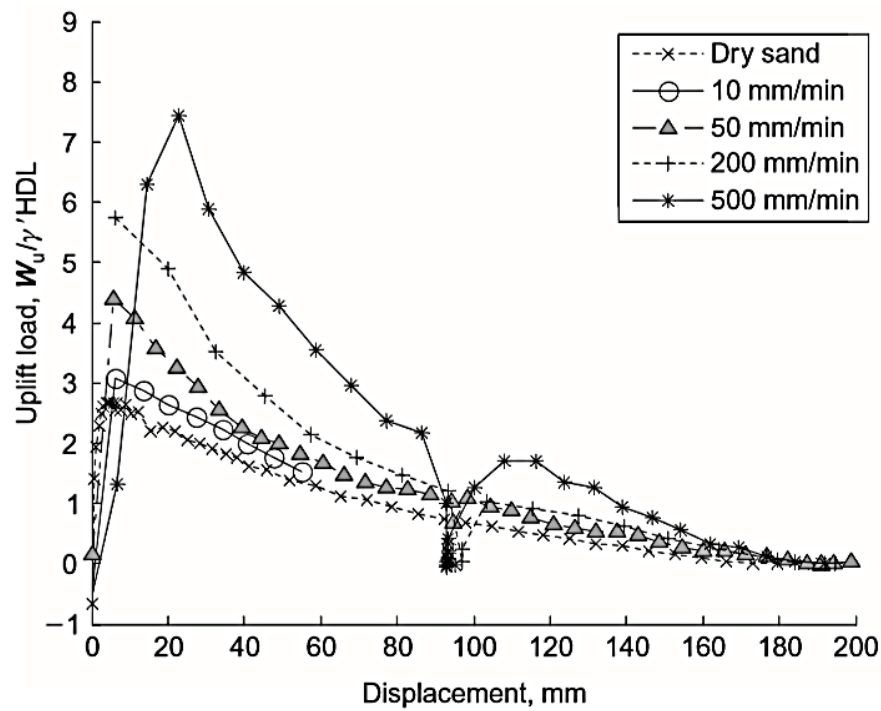


Figure 1.8 Load-displacement data for pipeline tests carried out at different velocities (saturated sand: $H/D=3$ and $D=0.048\text{m}$) (after Bransby et al.,2009)

b. Effect of Soil Particle Size

Stone (2006) studied the influence of the soil particle size on the mobilization of the soil uplift resistance in terms of the peak and residual uplift force and displacement. The results indicated that the finer the sand, the lower the peak uplift force and resistance. He interpreted the effects of the scale on the pullout centrifuge experiments on buried pipelines in sand. A transition zone exists between the failure mechanism that is related to the mobilized dilation being maximum at the tip of the shear band and zero at the critical state condition.

Cheuk et al. (2008) performed a model-scale experiment, a novel image-based deformation technique, to study the mobilization of the uplift resistance mechanism in silica sand. The soil movement was tracked by the image analysis technique that is based on particle image velocimetry (PIV) and combined with close range photogrammetric. The effects of particle size and soil density for the uplift response were observed. The results (Figure 1.10) showed that the uplift resistance is unaffected by the particle size for a given H/D while the width of the shear zone is strongly dependent on the grain size. The inclination of the shear zone is dependent on the soil density and dilatancy. In addition, the movement needed to mobilize the peak uplift resistance is independent of the grain size and density.

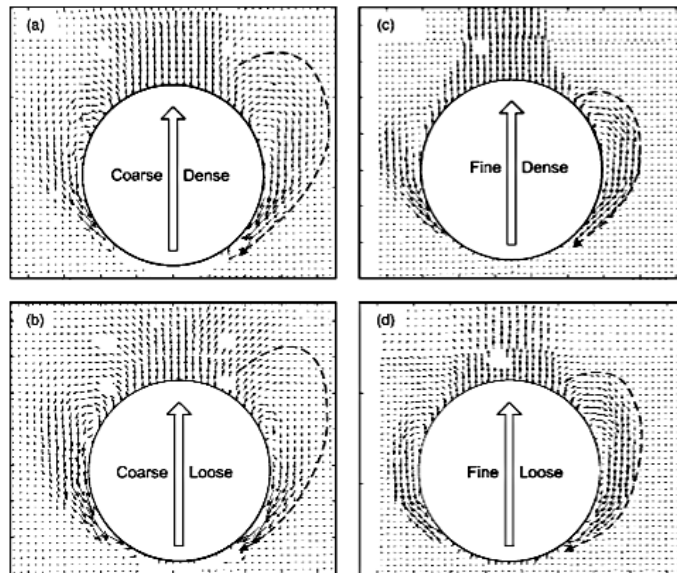


Figure 1.9 Flow around mechanism at a pipe displacement of $0.5D$ in a)dense coarse sand, b)dense fine sand, c)loose dense sand and d)loose fine sand (after Cheuk et al.,2008)

c. Mobilization Distance

Wang et al. (2012) carried out uplift experiments to study the mobilization distance for upheaval buckling for pipelines buried in sand and rock backfills for different soil burial depths ($H/D= 0.1$ to 6). The required pipeline distance to develop peak resistance is defined as the mobilization distance. Wang et al. (2012) obtained that the post-peak uplift force-displacement can be obtained from the residual uplift factor that depends on the critical friction angle. For shallow burial depths ($H \leq 0.6$), the mobilization distance increases linearly with the increase in H/D and may be higher than the values indicated by DNV (2007).

Robert and Thusyanthan (2014) explored this issue by conducting uplift experiments on submerged pipelines with different soil to cover heights of loose fine sands. They measured peak mobilization values and compared them with the values indicated by ASCE (2001) and DNV (2007). Robert and Thusuanthan (2014) showed that the measured peak mobilization values are higher than the recommended values by ASCE(2001) and DNV(2007) as shown in Figure 1.11.

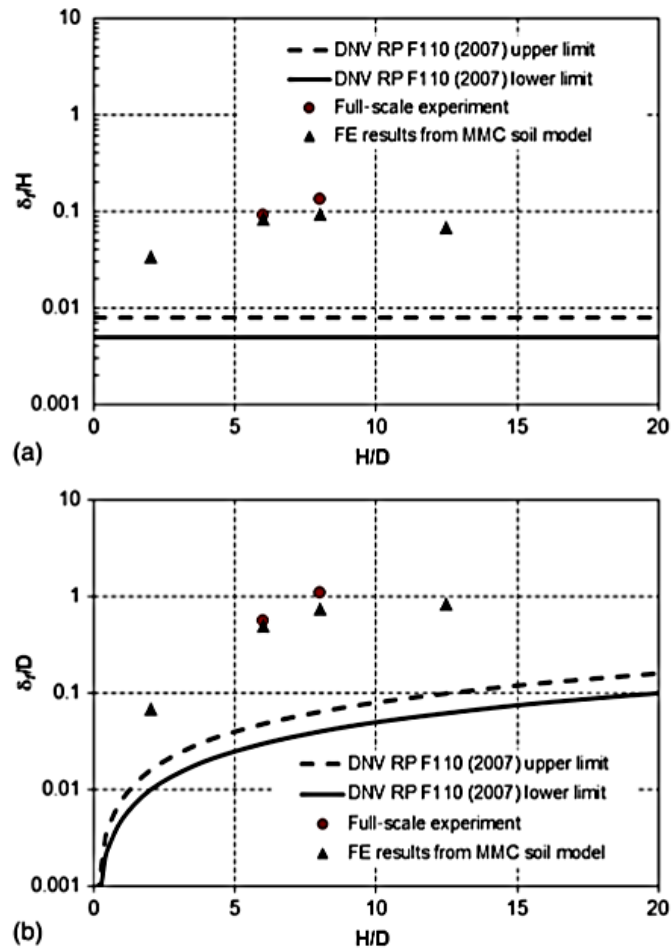


Figure 1.10 Summary of the parametric experimental and numerical study a) peak mobilization distance normalized by H and b) peak mobilization distance normalized by D (after Robert and Thusyanthan, 2014)

As a conclusion, it was established by a number of researchers who approached the problem from an experimental testing perspective that:

- The uplift resistance increases with the increase in the soil burial depth as presented by Schaminee et al. (1990), Ng and Springman (1994), Gao et al. (2011), Chin et al. (2006) and Schupp et al. (2006).
- The uplift resistance decreases with increasing initial pipeline imperfection amplitude as determined by Gao et al. (2011) and Schupp et al. (2006).
- The uplift resistance is a function of the soil density as presented by White et al. (2001).
- The deformation mechanism and kinematics depend on the initial soil density as demonstrated by Bransby et al., 2001.
- The effect of rate of pullout on the uplift resistance was examined by Byrne et al. (2008) and Bransby and Ireland (2009) who found that slow rates give responses similar to drained/dry cases and fast rates give undrained responses that lead to loss of uplift resistance and risk of liquefaction.
- The uplift resistance increases with the increase in the soil cover depth and the initial pore pressure depends on the initial velocity and on H/D as shown by Byrne et al. (2013) and Bransby and Ireland (2009).
- The relationship between the uplift capacity and the normalized velocity depends on the soil relative density as stated by Bransby and Ireland (2009).
- The mobilization distance depends on the movement of the soil during gap formation and not on the failure mechanism as presented by Bransby et al. (2001).
- Stone (2006) showed that the finer sand, the lower the peak uplift resistance while Cheuk et al. (2008) showed that the movement needed to mobilize the peak uplift resistance is independent of the grain size and density.
- Finally, Wang et al. (2012) and Robert and Thusyanthan (2014) showed that the measured peak mobilization values are higher than the recommended values by ASCE (2001) and DNV (2007), suggesting that these industry standards may be conservative.

3. Numerical Studies

Numerical studies on upheaval buckling of offshore pipelines allow researchers to explore complex scenarios which may not be properly captured by the simplified analytical solutions or too difficult to reproduce and test experimentally, and are intrinsically relatively fast and inexpensive solutions.

Buried subsea pipelines are affected by the strength and the stability of the soil surrounding them. This effect may be captured in the finite element models through proper modeling of the soil-pipe interaction. The first documented finite element work performed on pipe-soil interaction was by Lyons in 1973. Lyons (1973) found that the traditional Coulomb friction model can be used for lateral sliding on sand and cannot be used for the case of soft clay seabeds.

Since that earlier work, finite element tools have evolved considerably. Current standard finite element software such as Plaxis, Abaqus and Ansys are used today to study the upheaval buckling on offshore pipelines by considering the effects of non-linearity in steel, soil-pipe interaction and large displacements. Sun et al. (2011), Gao et al. (2011), Zeng et al. (2014), and Liu et al. (2015) used Abaqus to model the pipe using pipe-beam elements and the soil using spring models, to study the effect of upheaval buckling of offshore pipelines.

Sun et al. (2011) analyzed the upheaval buckling of a partially “Hot Pressure High Temperature” (HPHT) buried pipeline in clay, an example of an annulus flooded pipe-in-pipe (PIP) configuration. They studied the effects of the soil cover height, vertical prop size (initial pipeline vertical imperfection), soil resistance, and interaction and transition between the upheaval and the lateral response of the partially buried pipeline. Sun et al.

(2011) presented the latest techniques used for buckling behavior of partially buried pipeline under HPHT to help the industry follow a safer but less costly design. They focused on the two applications of partially buried pipelines: thermal insulation and pipeline walking. They found that burying sections of the HPHT pipeline when the soil cover depth is sufficient can regain the pipe cool-down time and decrease the risk of pipeline walking, noting however that attention must be given to the transition between the seabed and the buried sections.

Gao et al. (2011) used non-linear spring models that are based on large-scale model tests to simulate the soil behavior (sand) during the movement of a buried pipe that was simulated by a 2D beam element under thermal loading. They considered the effects of the pipe initial imperfection and soil cover depth and proposed empirical formulas to calculate the maximum friction force in the axial direction and soil uplift resistance for different embedment conditions. They found that to simulate uplift resistance, ideal “elastic-plastic” models can be used for $H/D > 5$ cases and “elastic-softened” models for $H/D \leq 5$ cases. Moreover, the uplift capacity of the pipeline increases with the increase in the soil cover depth and decreases with the increase in the magnitude of the initial imperfection presented in the pipeline.

Zeng et al. (2014) proposed new formulas that consider the initial imperfection of the pipeline to calculate the critical axial force of upheaval buckling of an imperfect pipeline. Pipelines, as beam element types with different imperfection amplitudes and shapes were simulated using Abaqus (Figure 1.12). The results have shown that the initial imperfection has a big effect on the critical axial force for upheaval buckling. A snap failure occurs with the presence of an initial imperfection. This snap decreases with the

degree of compaction of this imperfection and as its magnitude increases, the snap occurs at lower axial forces.



Figure 1.11 FE model of pipeline upheaval buckling (after Zeng et al., 2014)

Liu et al. (2015) performed uplift laboratory tests in order to obtain the nonlinear force-displacement relationships necessary for modeling the mobilization of the soil resistance (clay) due to pipeline movement. These relationships (Figure 1.14) were implemented in the finite element software Abaqus to model thermal upheaval buckling of buried pipelines with different initial imperfection amplitudes. The model geometry is shown in Figure 1.13. The experimental results were then compared with the numerical results that show that the capacity of the pipeline, under thermal loading increases with the increase in the soil cover depth and with the decrease in the magnitude of the pipeline initial imperfection (Figure 1.15).

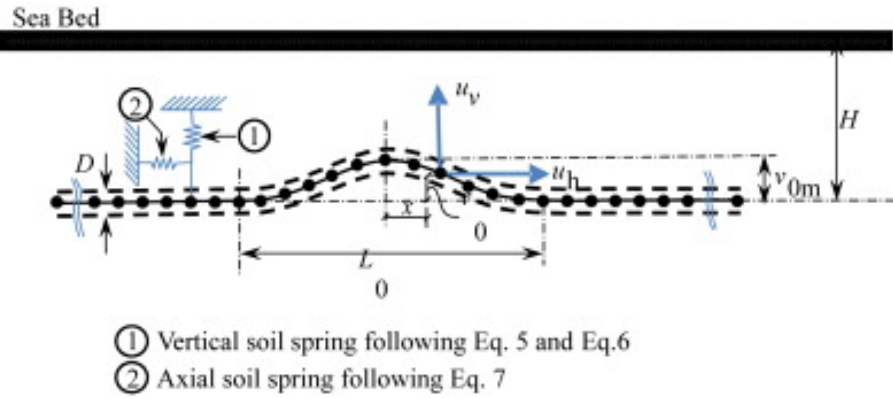


Figure 1.12 Model geometry and soil support idealization (after Liu et al., 2015)

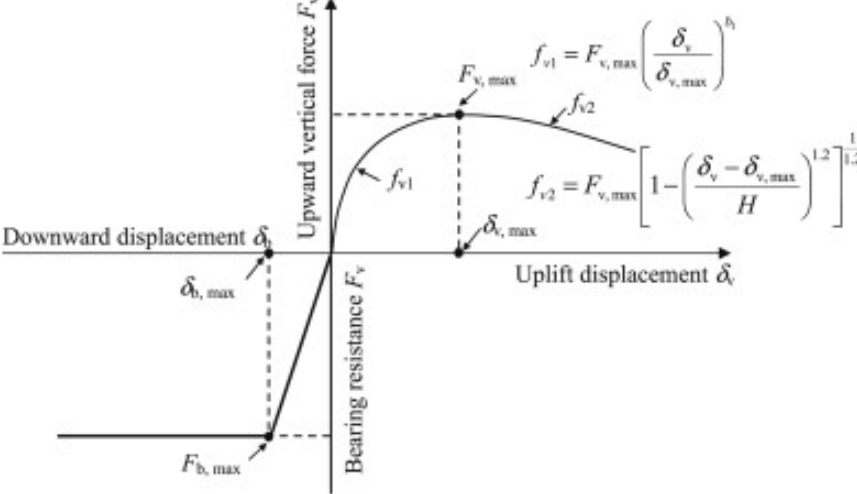


Figure 1.13 Nonlinear soil springs used to represent clay resistance on pipe uplift displacement (after Liu et al., 2015)

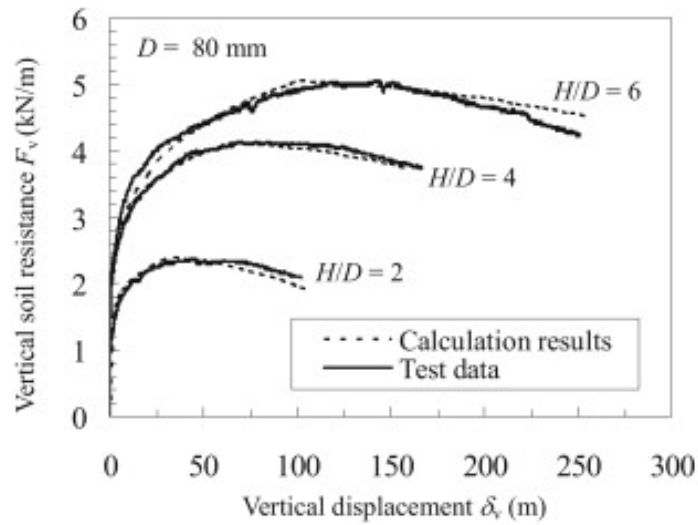


Figure 1.14 Comparison between experimental (test data) and numerical (calculation results) using the non-linear spring models (after Liu et al., 2015)

In addition to the work described above, plain strain models were developed using Plaxis and Abaqus to study the upheaval buckling of offshore pipelines. Vanden Berghe et al. (2005) studied the uplift mechanism of pipelines in very loose to loose sand in drained condition using Plaxis. They investigated the mechanism of uplift failure for the cases of dilative and contractive soils. They then compared the results obtained with a simplified uplift model. For the uplift resistance in dilative sand, their results showed that the finite element and the White method (White 2001) confirm a relation between the shearing mechanisms along planes angled at the dilation angle to the vertical planes. Uplift of the pipeline in loose sand is dominated by "local" failure and "flow around" mechanisms and in dense sand by a "wedge" failure mechanism that was first proposed by Shamminee et al., (1990).

Newson and Deljoui (2006) conducted a parametric study of upheaval buckling of offshore pipelines in clays using Plaxis. The purpose of their study was to calculate the upheaval buckling resistance of rough offshore pipelines in undrained conditions and to estimate the critical embedment depth and the effect of overburden. They studied the pullout force and the failure mechanisms by varying the soil self-weight, undrained shear strength and pipe embedment for fully bonded and breakaway cases. Their results presented in Figures 1.16 and 1.17, suggest that the uplift factor (the uplift resistance divided by the soil unit weight, pipe diameter and embedment depth $F/(\gamma'HD)$) increases with the increase in H/D and they are similar to plate anchors. The critical normalized embedment depths (H/D) for the transition from shallow to deep mechanisms is between 5 and 6. Moreover, for shallow embedment, the breakaway case displays a failure mechanism with the majority of the displacement "above the crown, ahead of the displacing pipeline" which is similar to the slip plane model (Schaminee et al, 1990). However, the bonded case displays a failure mechanism that is a combination of a vertical shear plane ahead of the pipeline and limited to the displacement of the soil around the pipeline. For deep embedment, the breakaway case shows a similar failure mechanism while the bonded case displays a "flow failure mechanism".

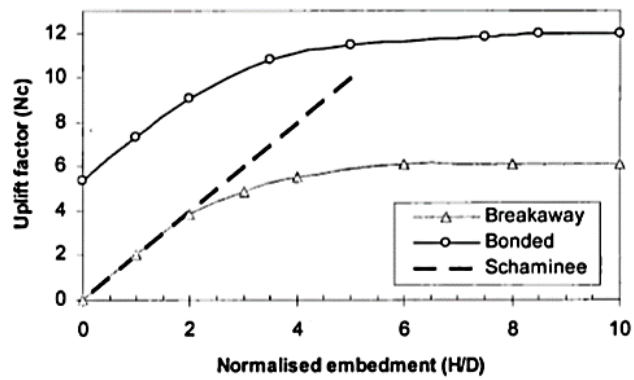


Figure 1.15 Normalized vertical force as a function of embedment ratio (after Newson and Deljoui, 2006)

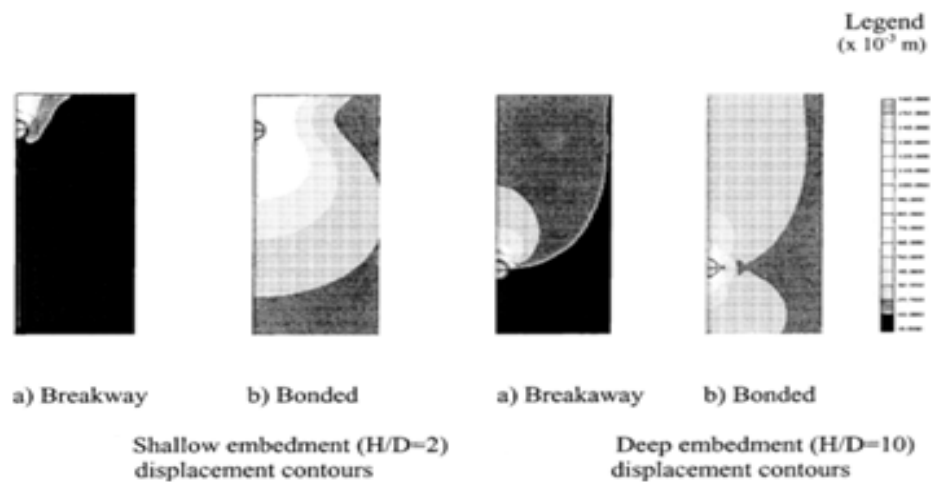


Figure 1.16 Shallow and deep embedment contours for breakaway and bonded cases (after Newson and Deljoui, 2006)

Liu et al. (2008, 2013) introduced an analytical solution and a finite element analysis model using Abaqus to study the effect of upheaval buckling on pipelines with initial imperfection (Figure 1.18). Their results have shown that pipelines with initial imperfection will most likely suffer from upheaval buckling and that the buckling temperature depends on the amplitude of the initial imperfection (Figure 1.19). The triggering temperature difference that causes upheaval increases with the increase in the soil cover depth, soil strength and friction between the pipeline and subsoil.

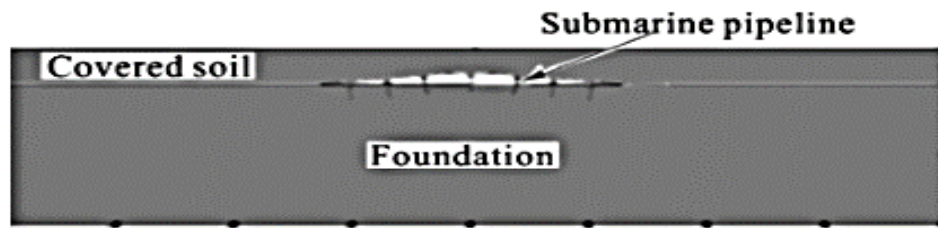


Figure 1.17 Plain strain finite element model for buried offshore pipeline (after Liu et al., 2013)

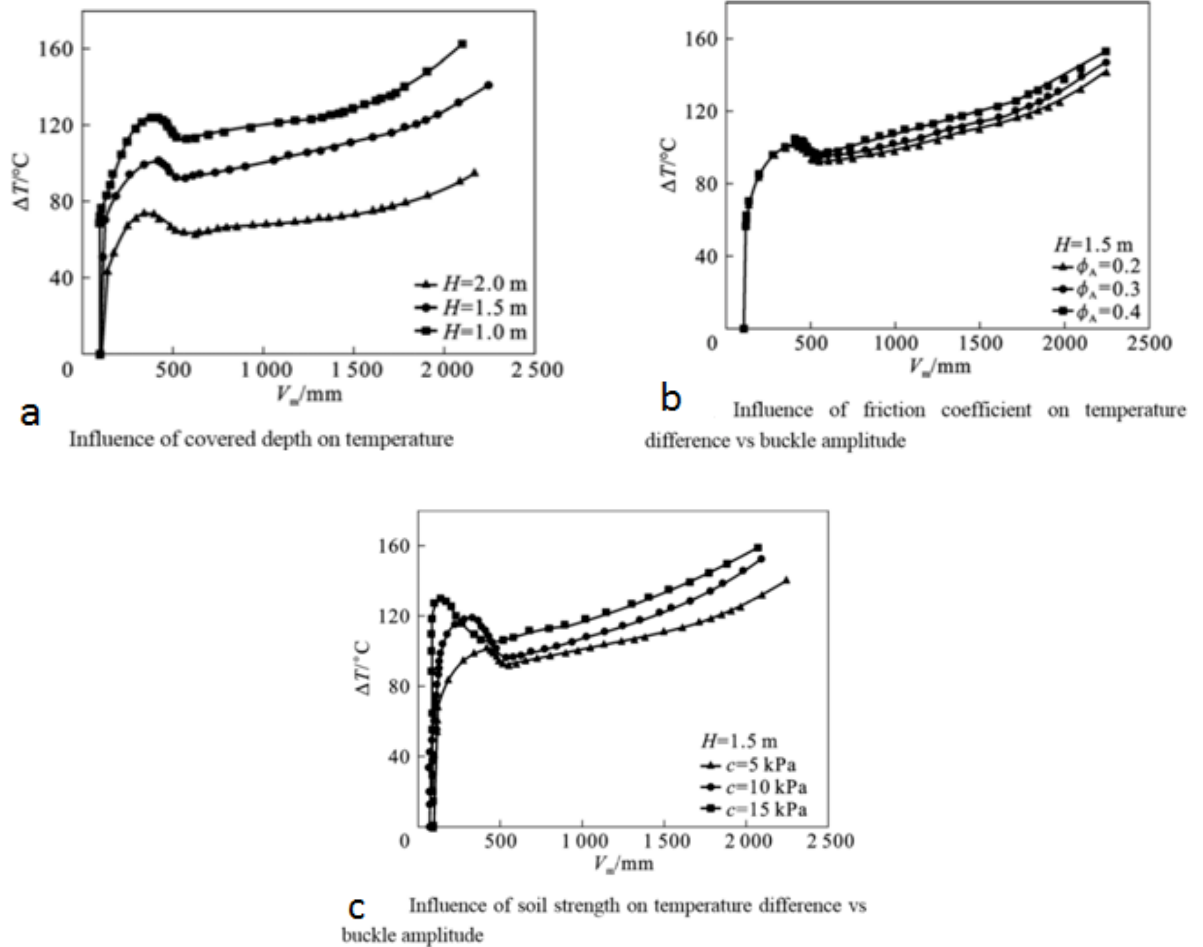


Figure 1.18 Influence of a) the soil cover depth, b) the friction coefficient and c) the soil strength on the temperature difference versus buckle amplitude (after Liu et al., 2013)

Robert and Thusyanthan (2014) performed a parametric study using Abaqus on buried offshore pipelines in loose and dense sand for different embedment soil depths and pipeline diameters (Figure 1.20). The peak uplift mobilization values obtained from the study are much greater than the recommended values by ASCE and DNV guidelines (Figure 1.21). The normalized soil embedment depth (H/D) and the soil relative density

affect these values. A new relationship to predict the peak uplift mobilization from the soil cover depth based on the soil relative density was presented.

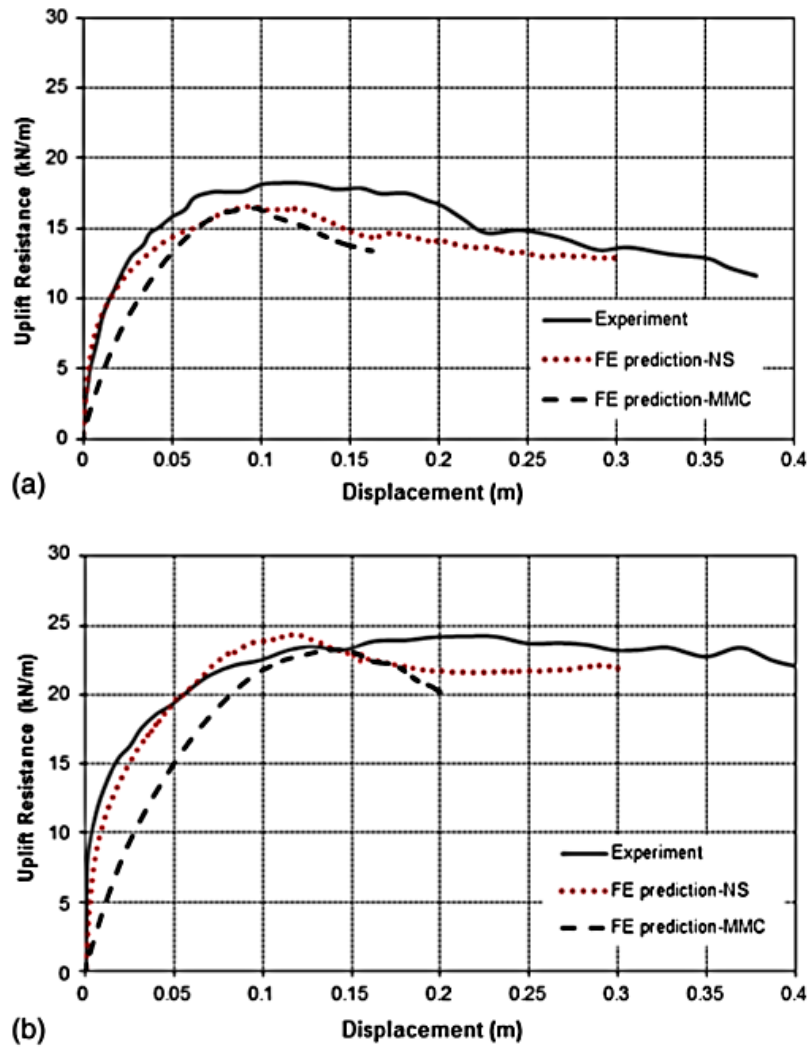


Figure 1.19 Finite element uplift resistance results compared with experimental results for a) $H/D=6$ and b) $H/D=8$ (after Robert and Thusyanthan, 2014)

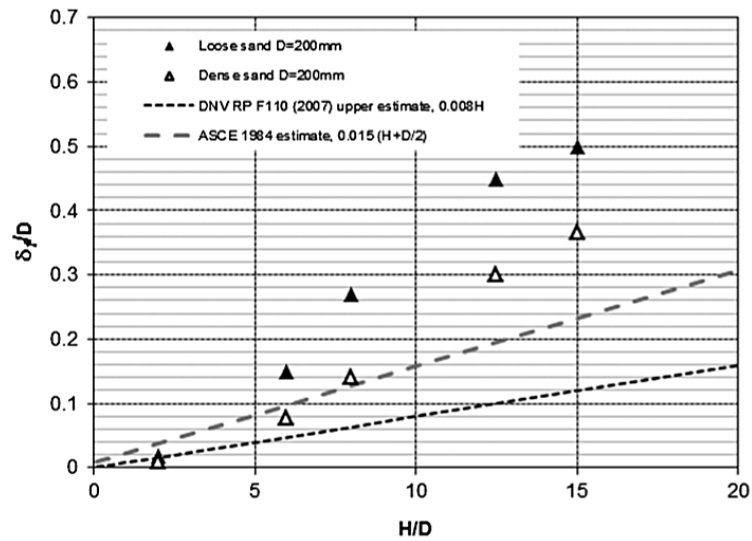


Figure 1.20 The dimensionless mobilization versus H/D for D=200mm for loose and dense sand compared with DNV and ASCE guidelines (after Robert and Thusyanthan, 2014)

Yimsiri et al. (2004) analyzed the peak uplift force and its transition from shallow to deep failure mechanism for upward and lateral pipe movement in sand for different embedment conditions using Abaqus and for two soil models: Modified Mohr-Coulomb and Nor-Sand (Figure 1.22). A design chart (Figure 1.23) was obtained for deep embedded pipelines based on the results of the finite element analysis that gave the critical embedment ratios and the corresponding peak forces for different peak friction angles (35°, 40° and 45°). This chart was based on a 200 kPa confining pressure with a relatively small diameter pipeline.

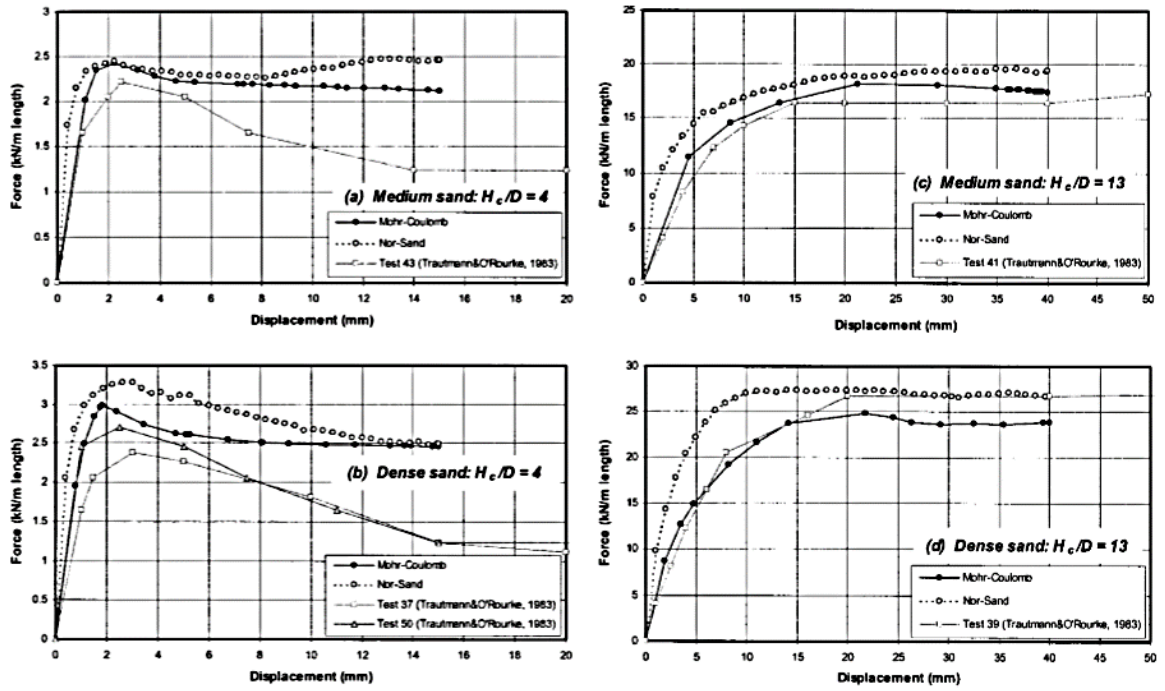


Figure 1.21 Finite element analysis results for upward pipeline movement a) medium sand, $H/D=4$, b) dense sand, $H/D=4$, c) medium sand, $H/D=13$ and d) dense sand, $H/D=13$ (after Yimsiri et al., 2004)

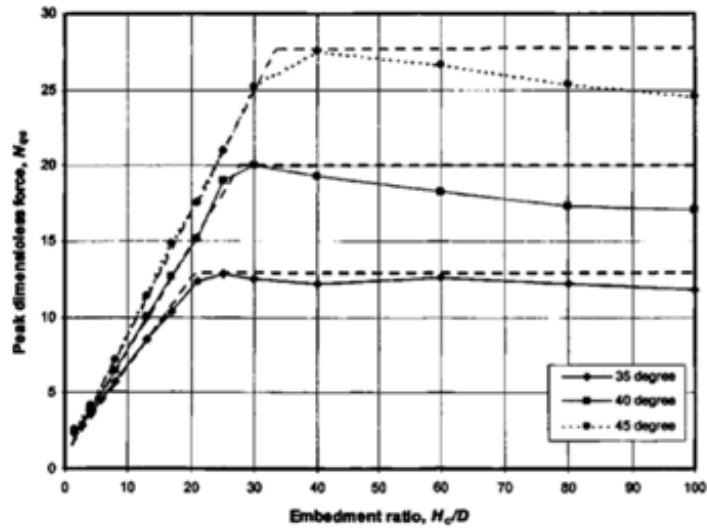


Figure 1.22 Design chart for upward pipe movement (after Yimsiri et al., 2004)

Liu et al. (2014) presented four different numerical simulation methods using Abaqus: 2D implicit, 2D explicit, 3D implicit and 3D explicit (Figures 1.24 and 1.25) to simulate global buckling of offshore pipelines under thermal loading. The results of the numerical simulations were compared to analytical solutions. The 2D implicit and the 2D explicit results are similar and those obtained from 2D implicit are very close to the analytical solutions. However, the 3D implicit and the 3D explicit solutions are similar but they are considerably different than the analytical solutions due to the fact that the 3D model considers the sinking of the pipeline in the seabed: the soil surrounding the pipeline provides additional resistance to global buckling (Figure 1.26 and 1.27). Liu et al. (2014) presented a new method to model the global buckling of offshore pipelines with initial imperfection using Abaqus.



Figure 1.23 2D finite element model (after Liu et al., 2014)

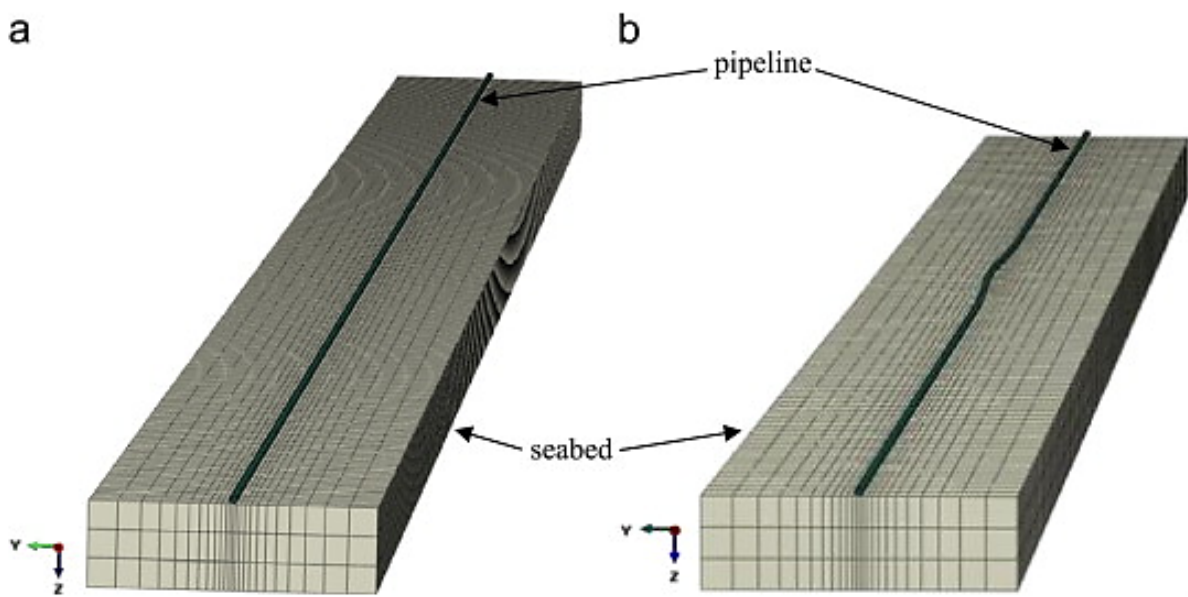


Figure 1.24 3D finite element model a) pipeline without initial imperfection and b) pipeline with initial imperfection (after Liu et al., 2014)

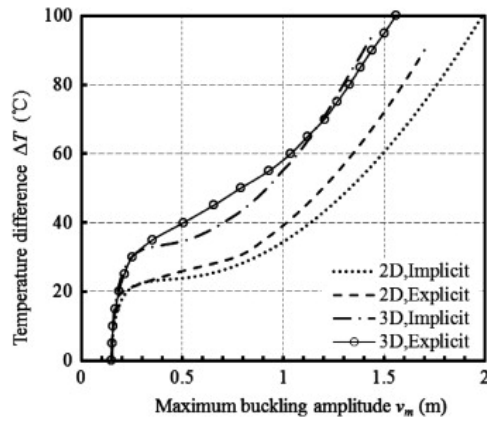


Figure 1.25 Midpoint pipeline buckling amplitude versus operational temperature difference for different models (after Liu et al., 2014)

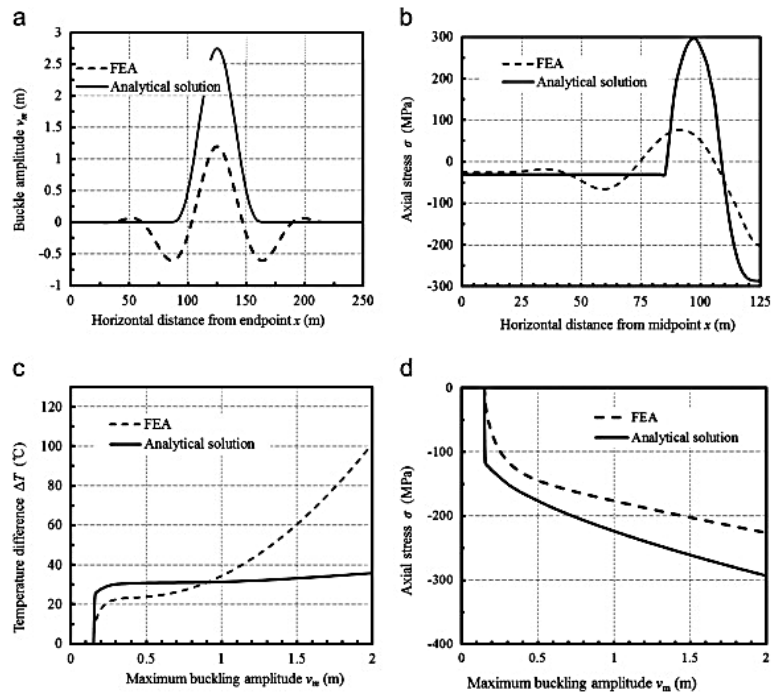


Figure 1.26 Comparison of finite element models and analytical solution a) lateral deformation, b) axial stress, c) maximum buckling amplitude versus temperature difference and d) maximum buckling amplitude versus axial stress (after Liu et al., 2014)

In summary and in reference to the numerical studies related to upheaval buckling in offshore pipelines, the following are relevant findings:

- Sun et al. (2011) found that burying sections of the pipeline with enough soil could decrease the risk of upheaval buckling and pipeline walking.
- Gao et al. (2011), Newson and Deljoui (2006) and Liu et al. (2015) stated that the uplift resistance increases with the increase in the soil burial depth and with the decrease in the pipeline initial imperfection amplitude.
- Robert and Thusyathan (2014) proved that the uplift resistance depends on the soil burial depth and soil relative density, and that these values are greater than those recommended by ASCE (2001) and DNV (2007).
- Liu et al. (2008, 2013) showed that the buckling temperature increases with the increase in the soil burial depth, soil strength and friction between the pipeline and the subsoil.
- Vanden Berghe et al. (2005) and Newson and Deljoui (2006) investigated the mechanisms of failure and found that a "local" failure mechanism occurs in loose sand and a "wedge" failure mechanism in dense sand.
- Zeng et al. (2014) proposed new formulas that consider the initial imperfection of the pipeline to calculate the critical axial force of upheaval buckling of an imperfect pipeline.
- Robert and Thusyanthan (2014) proposed new relationship to predict the peak uplift mobilization from the soil cover depth based on the soil relative density and Yimsiri et al. (2004) presented a design chart for deep embedded pipelines that gave the critical embedment ratios and the corresponding peak forces for different peak friction angles (35°, 40° and 45°).
- Finally, Liu et al. (2014) compared the results of four different numerical methods that simulate the global buckling of offshore pipelines under thermal loading using Abaqus and analytical solutions: 2D implicit, 2D explicit, 3D implicit and 3D explicit. The results of the 2D methods are similar to the

analytical solutions while the results of the 3D methods are different from the analytical solutions because 3D models consider the sinking of the pipeline in the seabed that provides additional resistance from the seabed to the pipeline.

C. SCOPE AND OBJECTIVES OF THE RESEARCH

1. Objectives of the Proposed Study

The first objective of the work presented in this thesis is to study the upheaval buckling behavior of a buried offshore pipeline by varying the soil burial depth, soil and pipeline properties and geometries using the finite element software Abaqus.

The second objective of this study is to propose a modified design approach for buried offshore pipelines based on the results obtained in the first phase of the work. The proposed study will bring a marked and significant improvement from previous studies reported in the literature through the modeling of the problem in its “true” 3D nature, and adopting elements which allow for the representation of the soil medium in its complex solid/pore fluid interaction and for the exploration of the effect of depth of water to the seabed.

2. Scope of work

The scope of work presented in this thesis was designed to achieve the above objectives includes the following:

- Use the comprehensive and thorough database of previous work presented in the earlier sections of this chapter, and the associated observations and results to design and execute a numerical modeling program using finite element analyses with the aim of investigating the upheaval failure mode of a buried pipeline in different soil densities (sand with fines). The parameters which will be varied will include but will not be limited to: the soil burial depth, soil state and properties and the pipeline properties and geometries.

- The results of the FE analyses will then be compared to the available analytical solutions.
- Based on the findings and comparisons with existing solutions, propose a buried pipeline design approach that would lead to a more reliable design of pipelines against upheaval-buckling modes of failure

3. Organization of the thesis

The thesis is composed of 5 chapters. Chapter 1 is the introductory chapter. It includes a general background of the topic, literature review that discusses the analytical, experimental and finite elements studies performed on upheaval buckling of offshore pipelines, as well as the thesis objectives and scope of work.

Chapter 2 presents and discusses the finite element problem: problem definition, element type, geometry, boundary conditions and mesh sensitivity analysis in addition to the pipe and soil constitutive models used in the software (Mohr Coulomb and Modified Mohr Coulomb).

The results and analysis are presented in chapter 3. This chapter starts with an overview of soil and pipe properties and geometries of all finite element studies performed. Then, after checking the effect of water depth, the effects of pipe properties and geometries (pipe diameter, embedment depth, pullout length, diameter to wall thickness ratio) are investigated for medium dense sand with fines then for different soil properties (cohesion and soil density). The finite element results are presented in terms of load displacement and buckling amplitude curves, maximum uplift soil resistances and normalized mobilization distances. The results are then compared to the analytical solutions presented in the literature.

A simplified approach is presented in chapter 4 to calculate the uplift soil resistance of a buried offshore pipeline and includes the effects of soil and pipe properties and geometries.

Finally chapter 5 presents the conclusions extracted from the thesis and recommends ideas for future work.

CHAPTER II

FINITE ELEMENT MODEL OF UPHEAVAL BUCKLING OF BURIED OFFSHORE PIPELINE

A. Software

3D Finite Element models were built to simulate the upheaval buckling of buried offshore pipeline using the commercial software Abaqus 6.13-4. The simulations were performed using large strain formulations while incorporating geometric nonlinearity. The NLGEOM option, available in Abaqus, considers the changes in soil and pipe geometries during the pipe uplift, maintains equilibrium during the analysis and makes sure large strains produced in and around the pipe are modeled correctly. The 3D models include the soil and the pipeline: the soil was modeled using eight node brick, trilinear displacement, trilinear pore pressure, reduced integration, hourglass control: C3D8RP element type with 89832 elements while the pipeline was modeled using eight node linear brick, reduced integration, hourglass control: C3D8R element type with 3534 elements.

B. Problem Definition

Figure 2.1 shows the geometry and the mesh of the finite element model used to simulate the upheaval buckling of buried offshore pipeline. Different elements were tested: linear and quadratic types with different model lengths: 10, 20, 50 and 100 m to ensure effective and conclusive results. Only a quarter of the problem was simulated due to symmetry. A comparison of the uplift resistance versus vertical displacement curves of the full model and its quarter is presented in figure 2.2 for the case involving a pipeline with a

diameter of x m, an embedment ratio of z , and a length of y m. The pipeline was assumed to be embedded in a “medium dense” sand layer and was uplifted along a central section that is 20% of the total length of the pipeline. The resulting uplift resistance versus normalized displacement curves for the full model and the quarter model are almost identical indicating that modeling the quarter of the 3D problem does not affect the accuracy of the results.

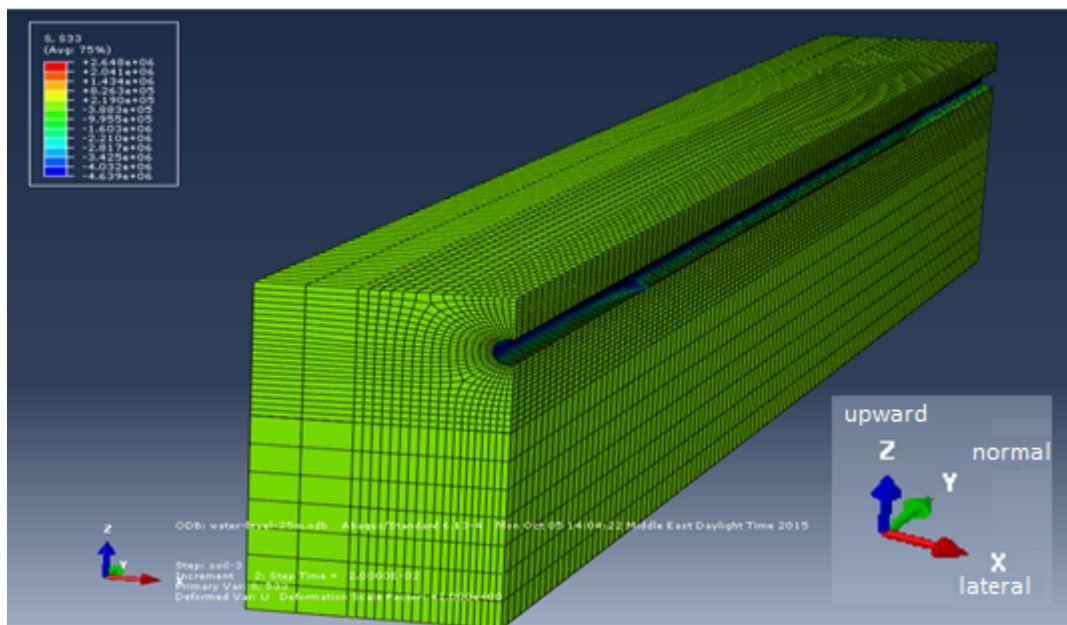


Figure 2.1 Geometry and model mesh distribution

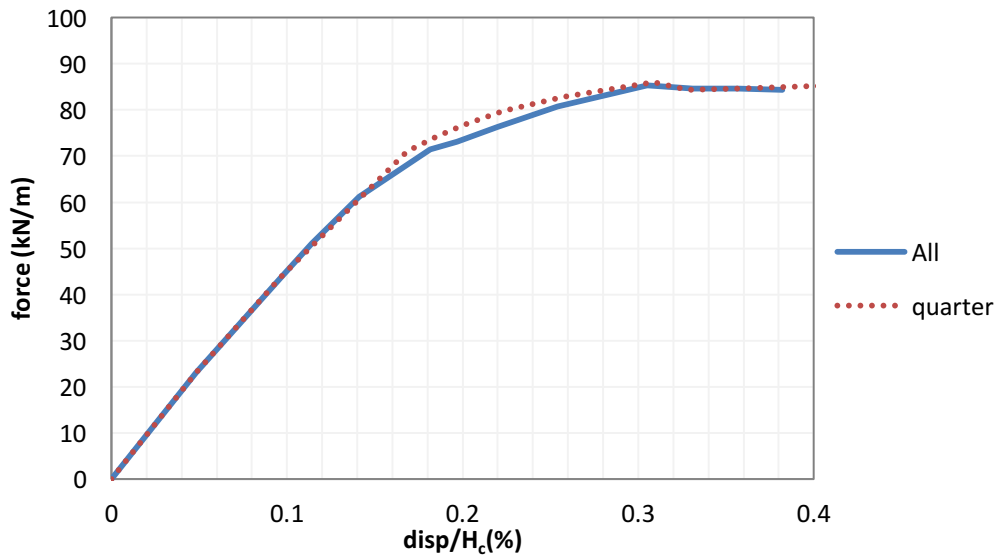


Figure 2.2 Load displacement curves of the full model and its quarter

In defining the boundary conditions, movement along the soil boundaries was "restrained axially": supported in the normal direction (the soil boundaries cannot move in the y direction) (Figure 2.1). For the pipeline boundaries two cases were considered. In the first case, the pipeline was restrained axially (the pipeline boundaries cannot move in the y direction) while in the second case, the pipeline was assumed to be fixed at the boundary (Figure 2.1). The sensitivity of the load displacement curves to the assumed boundary conditions is presented in Figure 2.3. Results indicate that both cases lead to similar responses. This could be attributed to the fact that the pipe is long and is pulled vertically along a section of limited length in the central section (20% of the length of the pipe in the cases shown in Figure 2.4). As a result, the "restrained axially" boundary condition was

adopted in the analyses conducted in this research study while allowing the pipe and soil wall boundaries to be free to move in the lateral and upward directions (Figure 2.1).

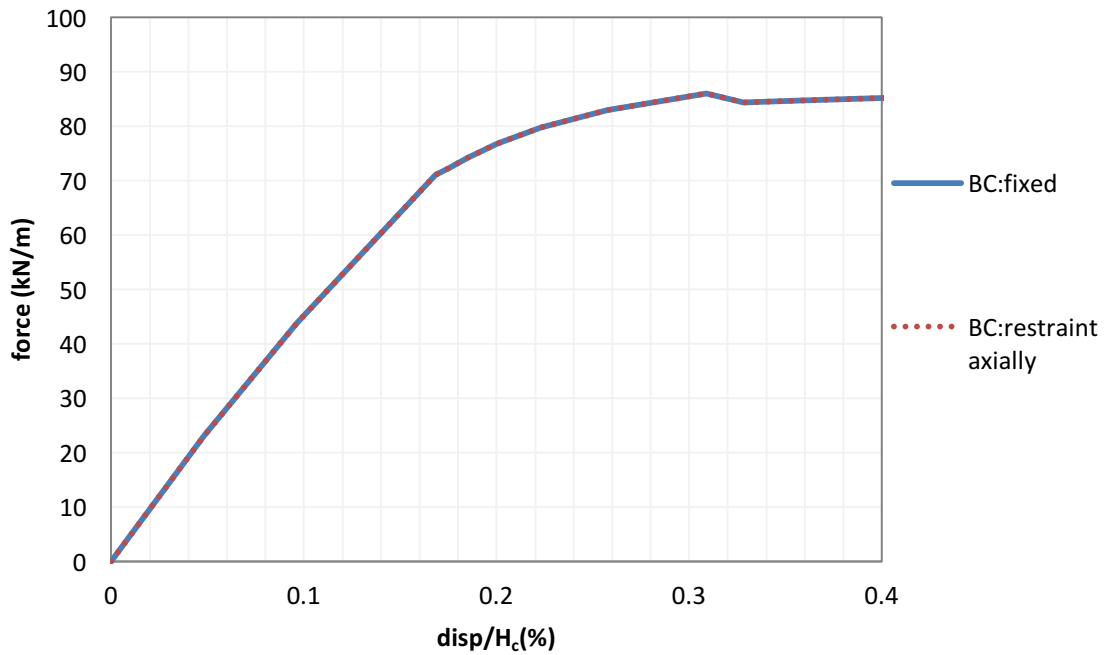


Figure 2.3 Load displacement curves of the pipe wall- fixed and restrained axially boundary conditions

Reduced integration elements in Abaqus use lower-order integration matrices than non-reduced elements. Therefore, the use of reduced integration elements reduces the simulation running time in 3D. However, this element, if used with hourglass control in first order elements (C3D8R), can cause severe distortions in stress or displacement analyses in Abaqus. To prevent this problem, a fine mesh should be used. Figure 2.4 shows

the difference in the load displacement curves between a reduced and a non-reduced mesh element type. The results match in the two curves. Given that the reduced mesh requires less computational time, it was adopted in the analyses conducted in this study.

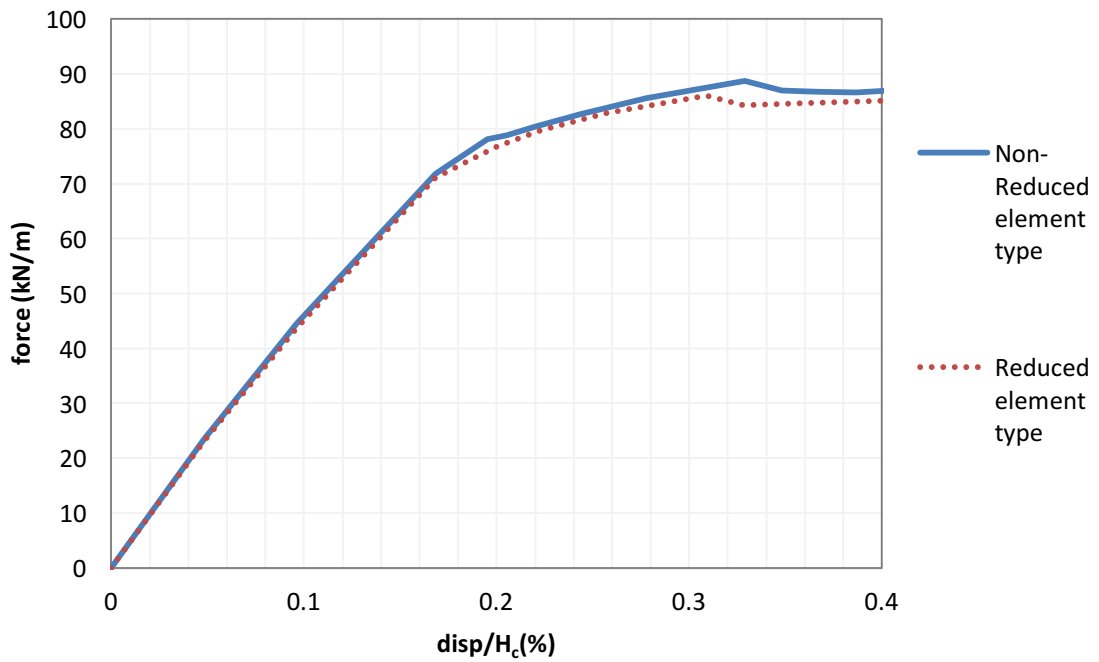


Figure 2.4 Load displacement curves of the reduced and non reduced element types

C. Constitutive Models

The interaction between the pipe and the soil was modeled using the Mohr-Coulomb failure model. The contact surface between the pipe and the soil is assumed to be stable as long as the frictional shear stress (τ) is less than the critical frictional shear stress

(τ_{crit}). Once $\tau > \tau_{crit}$, slipping along the interface occurs. The Mohr Coulomb failure model states that: $\tau_{all} = \mu \sigma'_n$ and $\mu = \tan \phi_\mu$ with $\phi_\mu = 0.5 \phi_{peak}$ of the soil.

Where μ : the interface friction coefficient (after Cheong, 2006 and Yimisri et al., 2004).

In Abaqus, the contact elements are created between the pipe and the soil in three directions. The first direction is along the dead weight of the pipeline and set as "hard contact" while the second and third directions are along the longitudinal and radial directions of the pipeline and exhibit a tangential contact behavior set as a "penalty" function equal to the interface friction coefficient.

The base case that is analyzed in this study involves soil that is characterized as medium dense sand with fines. To account for possible strain-softening in the stress-strain response of the soil, the sand was modeled using a Modified Mohr Coulomb model (MMC) that has the advantage of capturing the strain softening behavior of the soil when compared to the conventional elasto-plastic Mohr Coulomb model (MC). The MMC constitutive model can be programmed in Abaqus and has been widely used in previous studies involving FE modeling of pipelines in Abaqus. The MMC model requires a small set of parameters that can be obtained from conventional laboratory shear strength tests (ex. direct shear test or triaxial tests). These parameters include the peak friction angle, the dilation angle, and a pre-defined strain softening scheme (Robert and Saga, 2010). The softening behavior is generally modeled by a reduction of the mobilized friction and dilation angles with the increase in plastic deviatoric shear strain such that (after Robert and Thusyanthan , 2014):

$$\phi'_{\text{mob}} = \phi'_{\text{max}} - ((\phi'_{\text{max}} - \phi'_{\text{crit}}) / \gamma_f^p) \gamma_{\text{dev}}^p \text{ for } 0 \leq \gamma_{\text{dev}}^p \leq \gamma_f^p$$

$$\phi'_{\text{mob}} = \phi'_{\text{crit}} \text{ for } \gamma_{\text{dev}}^p > \gamma_f^p$$

$$\psi_{\text{mob}} = \psi_{\text{max}} (1 - \gamma_{\text{dev}}^p / \gamma_f^p) \text{ for } 0 \leq \gamma_{\text{dev}}^p \leq \gamma_f^p$$

$$\psi_{\text{mob}} = \psi_{\text{res}} \text{ for } \gamma_{\text{dev}}^p > \gamma_f^p$$

$$\text{and } \gamma_{\text{dev}}^p = \gamma_{\text{oct}} / \sqrt{2} = \sqrt{2}/3 \sqrt{(\epsilon_x - \epsilon_y)^2 + (\epsilon_x - \epsilon_z)^2 + (\epsilon_y - \epsilon_z)^2}$$

It should be noted that the elastic part of the stress-strain relationship in the MMC model is the same as that of the typical MC model. More importantly, a non-zero cohesive intercept was included in the constitutive model to reflect the presence of fines in the sandy soil.

Table 2.1 includes the soil and pipe properties and dimensions that were adopted in the base-case that was analyzed in this study. These parameters were also used as a basis for conducting the mesh sensitivity analysis. Many of the parameters shown in Table 2.1 will be varied in the following chapters of this thesis and their impact on the uplift resistance will be quantified.

Table 2.1 Soil and Pipe model parameters used in the Finite Element Analyses (FE)

	Soil Type	Medium Dense Sand with Fines
Soil Properties	E (MPa)	25
	ν	0.3
	Gs	2.6
	γ_d (kN/m ³)	15
	γ_{sat} (kN/m ³)	19
	e	0.7
	ϕ_{peak}°	40
	ϕ_{res}°	33
	ψ_{peak}°	8.75
	ψ_{res}°	0.1
	c (kPa)	10
	Water level (m)	100
	Soil Dimensions	Length (m)
Height (m)		10
Width (m)		10
Pipe/Steel Properties	E (GPa)	206
	ν	0.3
	ρ (kg/m ³)	7850
	σ_y (MPa)	448
Pipe Dimensions	D (mm)	800
	WT(mm)	27
	H/D	2

where:

ϕ'_{mob} = Mobilized friction angle (°)

ϕ'_{max} = Maximum friction angle (°)

ϕ'_{crit} = Critical friction angle (°)

ϕ_{peak} = Peak friction angle (°)

ϕ_{res} = Residual friction angle (°)

ψ_{mob} = Mobilized dilation angle (°)

ψ_{max} = Maximum dilation angle (°)

ψ_{res} = Residual dilation angle (°)
 ψ_{peak} = Peak dilation angle (°)
 ψ_{res} = Residual dilation angle(°)
 γ_{dev}^P = Plastic deviatoric shear strain
 γ_f^P = Shear strain at softening completion
 γ_{oct} = Octahedral strain
 ϵ = Principal strain
 E = Young Modulus (Pa)
 ν = Poisson's ratio
 G_s = Specific Gravity
 γ_d = Dry unit weight (kN/m³)
 γ_{sat} = Saturated unit weight(kN/m³)
 e = void ratio
 c = Cohesion (kPa)
 ρ = Density (kg/m³)
 σ_y = Yield stress (MPa)
 D = Outside pipe diameter (mm)
 WT = Wall thickness (mm)
 H = Depth to the top of the pipe (m)
 H/D = Embedment depth

The dilation angle was estimated based on: $\phi'_{peak} = \phi'_{crit} + 0.8\psi$ (after Bolton, 1986).

The strain softening behavior of the friction and dilation angles were integrated in Abaqus in a user subroutine USDFLD written in the programming language Fortran (Appendix A). This model was checked by running a triaxial test in Abaqus for medium dense sand with fines under 10 and 50 kPa confinement pressures. Figure 2.5 shows the undeformed and the deformed shape (bulging) of the soil model. The stress strain curves (figure 2.6) clearly

illustrate the softening of the soil model and the difference between the MC and MMC constitutive models. The Mohr Coulomb envelopes were drawn for the MC and MMC models at peak and residual states (figures 2.7 and 2.8).

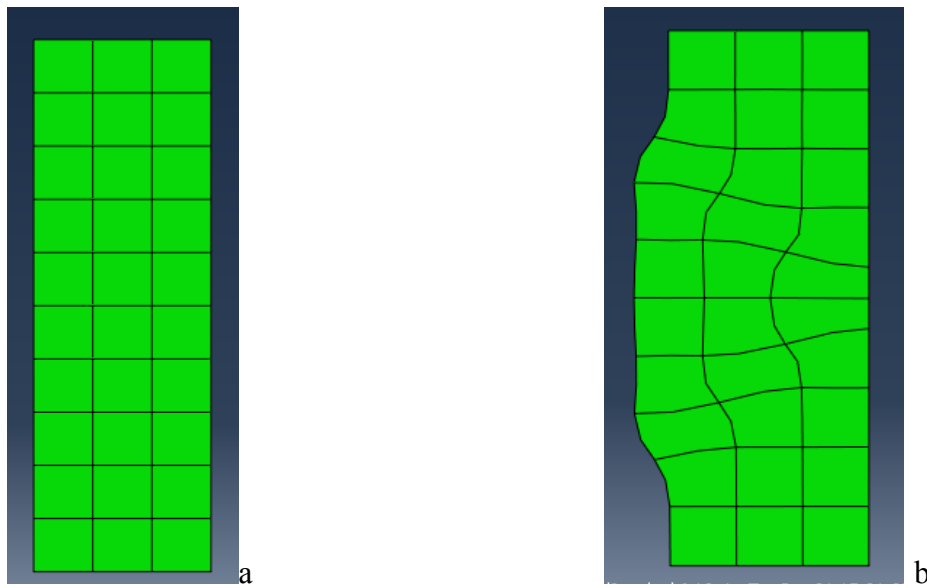


Figure 2.5 a) Undeformed and b) Deformed shape of Triaxial Test of MMC soil model

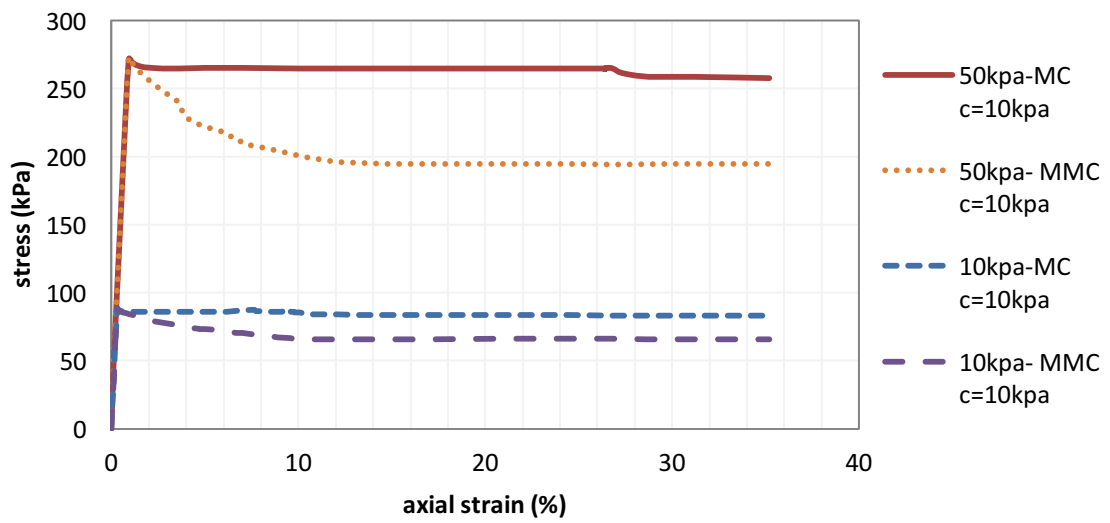


Figure 2.6 Vertical stress versus axial strain of MC and MMC triaxial test at 10 and 50 kPa confinement

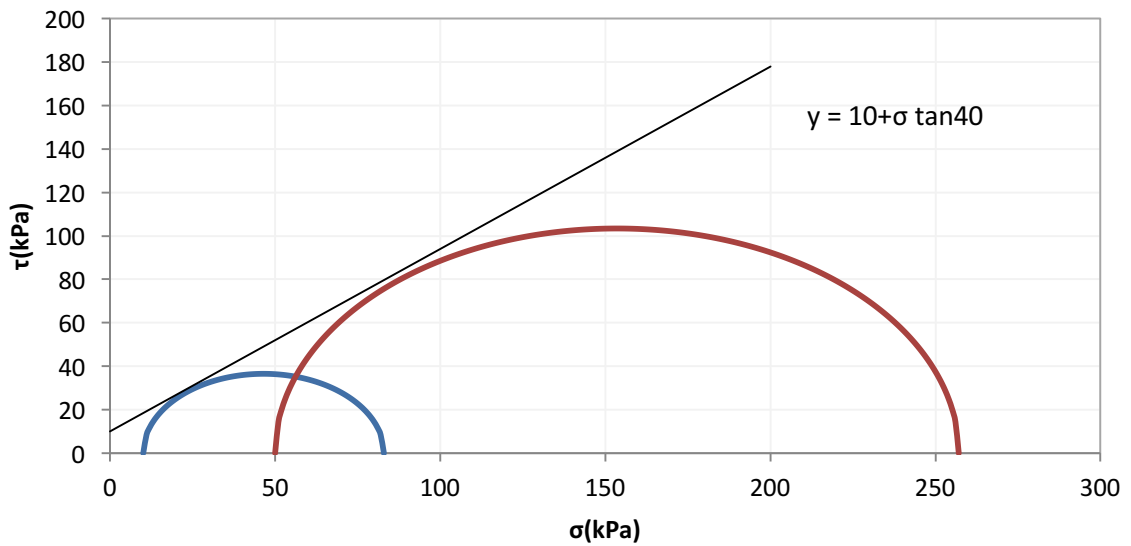


Figure 2.7 Mohr Coulomb Envelope for the medium dense sand with fines for the MC model and the MMC at peak states

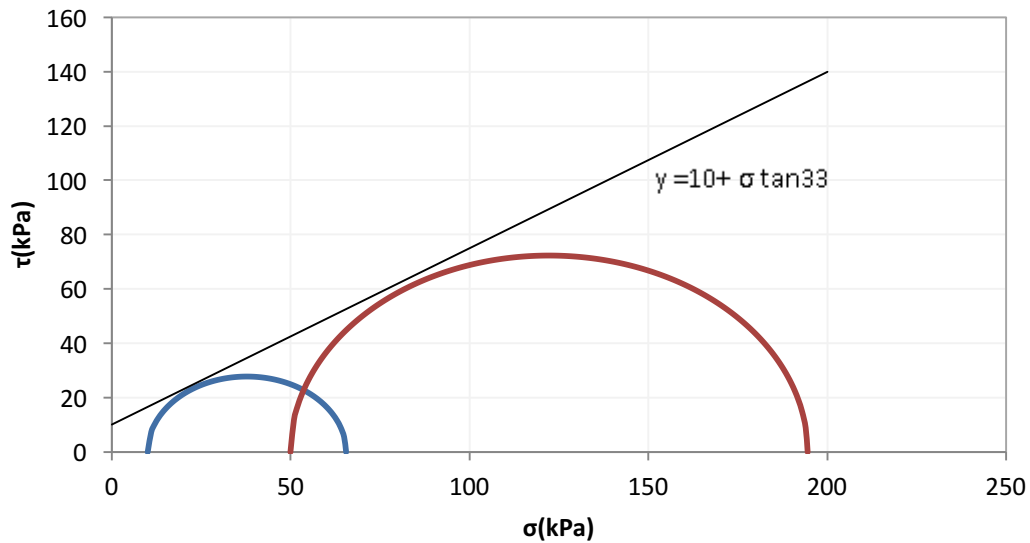


Figure 2.8 Mohr Coulomb Envelope for the medium dense sand with fines for the MMC model at residual states

D. Mesh Sensitivity Analysis

A mesh sensitivity analysis was performed in Abaqus to establish a mesh configuration that would yield accurate and stable results while minimizing the computational cost in the 3D finite element analysis. For this purpose, the finite element model was divided into 7 zones (A to F) as indicated in figure 2.9. For each zone, different meshing options with different element sizes (m) were investigated as indicated in Table 2.2. The different meshing alternatives were used to predict the variation of the uplift soil resistance with vertical deformation for the base case pipelines and soil properties that were presented in Table 2.1. For the mesh sensitivity analysis, a representative and realistic case that involves a pipeline with an embedment depth ratio of 2.0 was considered.

The results of the mesh sensitivity analysis are presented in figure 2.10 in the form of uplift resistance versus normalized displacement curves. Results indicate that the stress-displacement curves for the different mesh size configurations converged for options 4, 5 and 6. Since mesh option 4 required the least computational time compared to options 5 and 6 (24 hours running time on average), it was adopted as a basis for conducting the parametric analyses in the following chapter of this thesis.

Table 2.2 Mesh sensitivity analysis: mesh sizes sections and respective computational time

Element size (m)	A	B	C	D	E	F	Computational time (hours)
mesh-0	0.88	0.3	0.04	0.3	0.88	0.44	8
mesh-1	1.76	0.6	0.08	0.6	1.76	0.88	5
mesh-2	1.1	0.4	0.05	0.4	1.1	0.55	4
mesh-3	0.66	0.2	0.03	0.2	0.66	0.33	12
mesh-4	0.22	0.1	0.04	0.1	0.88	0.44	24
mesh-5	0.22	0.1	0.04	0.1	0.88	0.33	30
mesh-6	0.22	0.1	0.04	0.1	0.88	0.22	48

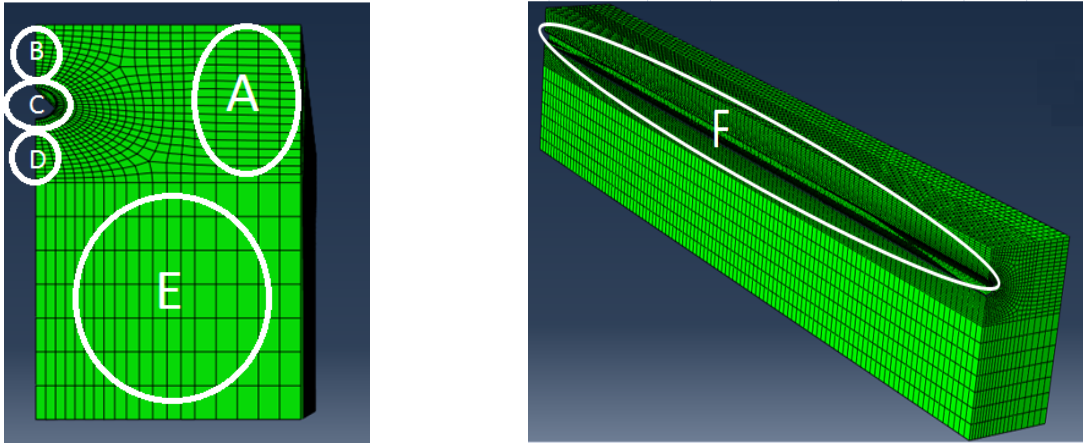


Figure 2.9 Different mesh sizes sections of the 3D finite element model

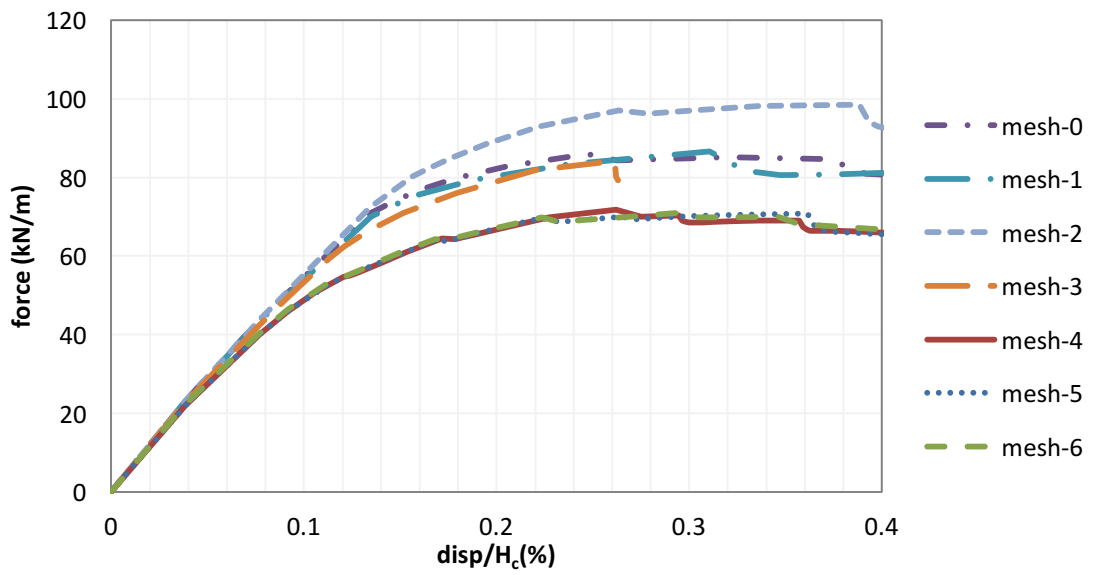


Figure 2.10 Load displacement curves of the mesh sensitivity analyses

CHAPTER III

RESULTS AND ANALYSIS

A. Overview of Analyses/Parametric Study

Offshore pipelines are used to transport oil and gas at high temperature and pressure. Axial forces formed under these conditions push the pipe to expand. The soil cover contributes to resisting this expansion. However, the interaction between the compressive forces with the soil along the pipe length may cause global buckling to occur. For buried pipelines, buckling occurs in the vertical direction: the direction of the least resistance (Figure 3.1).

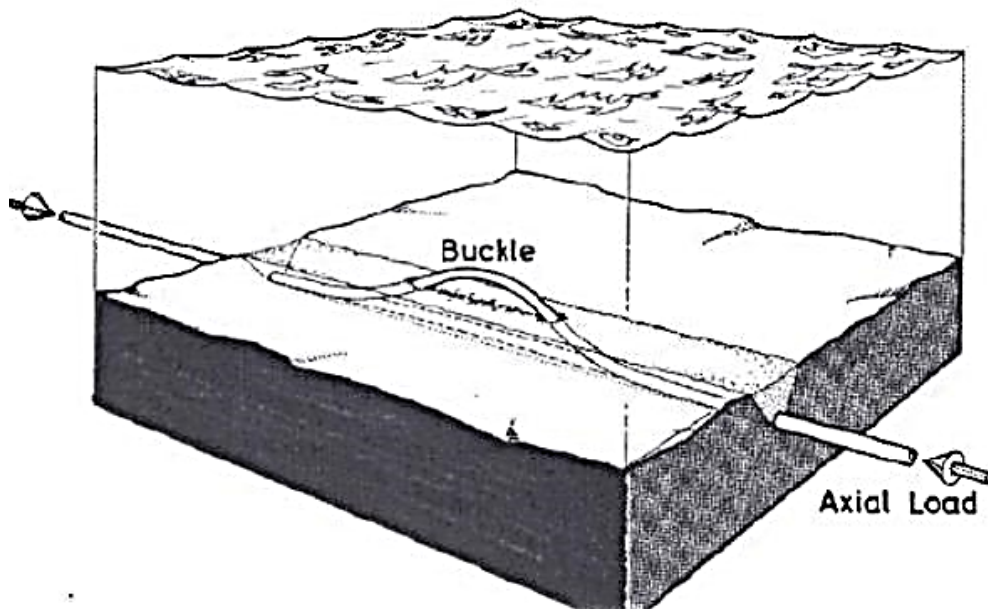


Figure 3.1 Upheaval buckling of an offshore pipeline (after Friis-Hansen, 2000)

In our effort to assess the soil resistance under “global buckling” conditions, displacement-controlled finite element modeling of the field conditions was adopted as detailed in Chapter II. The FEM analyses conducted can be grouped in three Cases/Groups. These will be referred to in the balance of this document as Group 1, 2 and 3, respectively. The analyses/studies were grouped in reference to the denseness/state of the seabed “Sands with fines”. As such, analyses in Group-1 involve Medium Dense seabed soil; whereas Groups 2 and 3 are concerned with Loose and Dense states, respectively.

In the models analyzed, a buried pipeline is displaced upward along a specific pullout section length (i.e. a portion of the total pipe length -L) and the force-displacement response is obtained. Using the same model setup and methodology, parametric studies were conducted to investigate the effects of pipe diameter (D), embedment depth ratio (H/D), pullout section length (%L) and soil apparent cohesion (c).

In the baseline model adopted, a mobilized/pulled-out section of 20% the original pipe length was used. Variations on this baseline condition, with different portions/lengths of the pipe being mobilized/pulled up are analyzed as part of the parametric study. In running the analyses, the pipe section length (20%L or other) was pulled up at the mid-length and with “forced uniform displacement” in the pulled-up section, until an upward displacement equal to $1\%H_c$ (H_c , is the depth from the top of seabed to centerline of the pipe at initial conditions). The total upward resistance obtained from the model was in units of force. In order to normalize with respect to length of pipe, that total force was then divided in the interpreted results presented herein by one of two lengths: Pullout Length (which corresponds to the length of the section forced upwards in the FEM analyses-e.g. 20% \times L) and/or the “Effective Length”. The effective length was defined as the portion of

the pipe that is “substantially” affected by uplifting of the forced pulled out length of pipe. As such, the effective length is larger than the pullout length. The effective length was defined as bounded by minimal pipe slopes: typical “cutoff slope” values of 0.0014 corresponding to an angle of 0.08° were used (Figure 3.2).

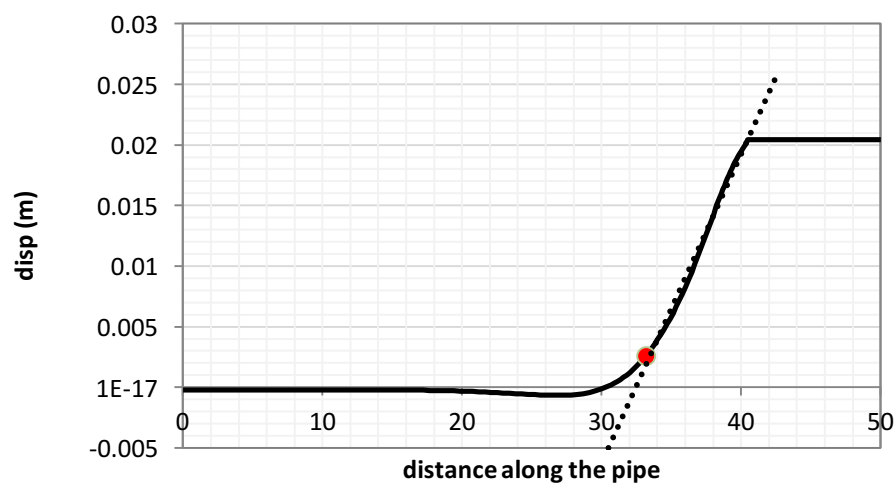


Figure 3.2 Pipeline effective length using "cutoff slope" value of 0.0014

In order to establish the mobilization distance (or upward displacement necessary to mobilize the maximum force, i.e. resistance) which may not be obvious particularly for cases where load-displacement curves exhibited continued, albeit mild increases in resistance with displacement (hardening behavior), the mobilization distance was deduced graphically based on the tangent intersection method. In this method, two tangential lines

are plotted along the initial and the “large displacement” portions of the load-displacement curve (Figure 3.3) respectively. The normalized displacement corresponding to the force (load) defined by the intersection point of these two lines was considered as the mobilization distance (Figure 3.3). Tables 3.1 to 3.4 summarize the finite element studies performed under different conditions.

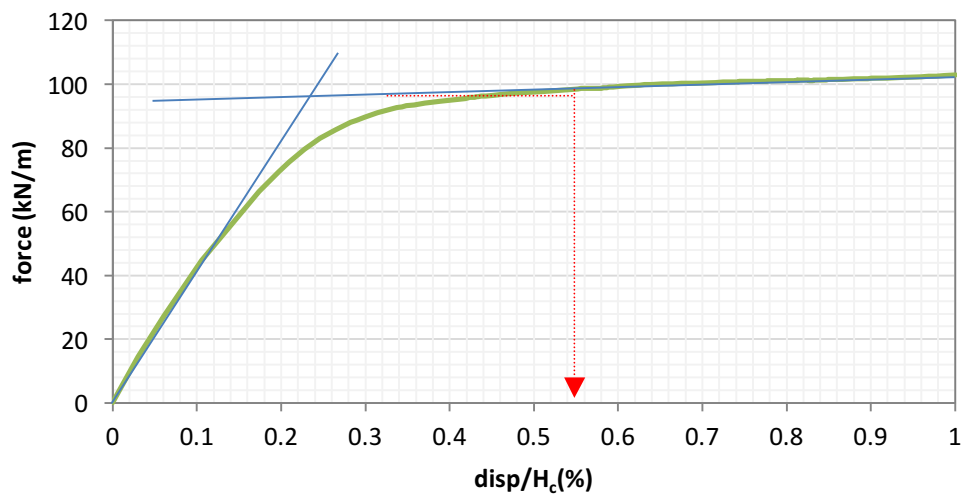


Figure 3.3 Normalized mobilization distance- tangent intersection method

Table 3.1 Medium Dense Sand with Fines simulation cases (GROUP-1)

	E (MPa)	γ_d (kN/m ³)	γ_{sat} (kN/m ³)	e	Φ_{peak} °	Ψ_{peak} °	c (kPa)	D (mm)	WT (mm)	D/ WT	H/ D	Water Level (m)	pullout section (%)	Length (m)		
Medium dense sand with fines (MD-F)	25	15	19	0.7	40	8.75	10	800	27	30	2	0	20	100	water level	
	25	15	19	0.7	40	8.75	10	800	27	30	3	50	20	100		Pipe diameter
	25	15	19	0.7	40	8.75	10	800	27	30	4	100	20	100		
	25	15	19	0.7	40	8.75	10	300	10	30	4	100	20	100	H/D	
	25	15	19	0.7	40	8.75	10	600	20	30	4	100	20	100		
	25	15	19	0.7	40	8.75	10	800	27	30	4	100	20	100		
	25	15	19	0.7	40	8.75	10	1000	33	30	4	100	20	100	Pullout section	
	25	15	19	0.7	40	8.75	10	800	27	30	0.75	100	20	100		
	25	15	19	0.7	40	8.75	10	800	27	30	1	100	20	100		
	25	15	19	0.7	40	8.75	10	800	27	30	1.5	100	20	100	Pullout section	
	25	15	19	0.7	40	8.75	10	800	27	30	2	100	20	100		
	25	15	19	0.7	40	8.75	10	800	27	30	3	100	20	100		
	25	15	19	0.7	40	8.75	10	800	27	30	4	100	20	100	Pullout section	
	25	15	19	0.7	40	8.75	10	800	27	30	4	100	10	100		
	25	15	19	0.7	40	8.75	10	800	27	30	4	100	20	100		
	25	15	19	0.7	40	8.75	10	800	27	30	4	100	30	100	Pullout section	
	25	15	19	0.7	40	8.75	10	800	27	30	4	100	50	100		
	25	15	19	0.7	40	8.75	10	800	27	30	4	100	75	100		
25	15	19	0.7	40	8.75	10	800	27	30	4	100	100	100	Pullout section		

NOTE: varied parameters indicated in red.

Table 3.2 Medium Dense Sand with Fines simulation cases (GROUP-1 Continued)

	E (MPa)	γ_d (kN/m ³)	γ_{sat} (kN/m ³)	e	ϕ_{peak} °	ψ_{peak} °	c (kPa)	D (mm)	WT (mm)	D/ WT	H/ D	water level (m)	pullout section (%)	length (m)	
Medium dense sand with fines (MD-F)	25	15	19	0.7	40	8.75	2	800	27	30	4	100	20	100	cohesion
	25	15	19	0.7	40	8.75	10	800	27	30	4	100	20	100	
	25	15	19	0.7	40	8.75	15	800	27	30	4	100	20	100	
	25	15	19	0.7	40	8.75	20	800	27	30	4	100	20	100	
	25	15	19	0.7	40	8.75	30	800	27	30	4	100	20	100	
	25	15	19	0.7	40	8.75	2	800	27	30	4	100	100	100	
	25	15	19	0.7	40	8.75	10	800	27	30	4	100	100	100	
	25	15	19	0.7	40	8.75	15	800	27	30	4	100	100	100	
	25	15	19	0.7	40	8.75	20	800	27	30	4	100	100	100	
	25	15	19	0.7	40	8.75	30	800	27	30	4	100	100	100	
Medium dense sand with fines (MD-F)	25	15	19	0.7	40	8.75	10	800	32	25	4	100	10	100	Pipe diameter to wall thickness ratio
	25	15	19	0.7	40	8.75	10	800	32	25	4	100	20	100	
	25	15	19	0.7	40	8.75	10	800	32	25	4	100	30	100	
	25	15	19	0.7	40	8.75	10	800	32	25	4	100	50	100	
	25	15	19	0.7	40	8.75	10	800	32	25	4	100	75	100	
	25	15	19	0.7	40	8.75	10	800	32	25	4	100	100	100	
	25	15	19	0.7	40	8.75	10	800	27	30	4	100	10	100	
	25	15	19	0.7	40	8.75	10	800	27	30	4	100	20	100	
	25	15	19	0.7	40	8.75	10	800	27	30	4	100	30	100	
	25	15	19	0.7	40	8.75	10	800	27	30	4	100	50	100	
	25	15	19	0.7	40	8.75	10	800	27	30	4	100	75	100	
	25	15	19	0.7	40	8.75	10	800	27	30	4	100	100	100	
	25	15	19	0.7	40	8.75	10	800	23	35	4	100	10	100	
	25	15	19	0.7	40	8.75	10	800	23	35	4	100	20	100	
	25	15	19	0.7	40	8.75	10	800	23	35	4	100	30	100	
	25	15	19	0.7	40	8.75	10	800	23	35	4	100	50	100	
25	15	19	0.7	40	8.75	10	800	23	35	4	100	75	100		
25	15	19	0.7	40	8.75	10	800	23	35	4	100	100	100		

NOTE: varied parameters indicated in red

Table 3.3 Loose Sand with Fines simulation cases (GROUP-2)

	E (MPa)	γ_d (kN/m ³)	γ_{sat} (kN/m ³)	e	ϕ_{peak} °	ψ_{peak} °	c (kPa)	D (mm)	WT (mm)	D/ WT	H/ D	water level (m)	Pullout Section (%)	length (m)		
Loose sand with fines (L-F)	10	13	18.6	0.96	35	2.750	10	300	10	30	4	100	20	100	Pipe diameter	
	10	13	18.6	0.96	35	2.750	10	600	20	30	4	100	20	100		
	10	13	18.6	0.96	35	2.750	10	800	27	30	4	100	20	100		
	10	13	18.6	0.96	35	2.750	10	800	27	30	1	100	20	100	H/D	
	10	13	18.6	0.96	35	2.750	10	800	27	30	2	100	20	100		
	10	13	18.6	0.96	35	2.750	10	800	27	30	3	100	20	100		
	10	13	18.6	0.96	35	2.750	10	800	27	30	4	100	20	100		
	10	13	18.6	0.96	35	2.750	10	800	27	30	4	100	20	100	Pullout section	
	10	13	18.6	0.96	35	2.750	10	800	27	30	4	100	50	100		
	10	13	18.6	0.96	35	2.750	10	800	27	30	4	100	75	100		
	10	13	18.6	0.96	35	2.750	10	800	27	30	4	100	100	100		
	10	13	18.6	0.96	35	2.750	2	800	27	30	4	100	20	100	cohesion	
	10	13	18.6	0.96	35	2.750	10	800	27	30	4	100	20	100		
	10	13	18.6	0.96	35	2.750	20	800	27	30	4	100	20	100		
	10	13	18.6	0.96	35	2.750	30	800	27	30	4	100	20	100		
	10	13	18.6	0.96	35	2.750	2	800	27	30	4	100	100	100		
	10	13	18.6	0.96	35	2.750	10	800	27	30	4	100	100	100		
	10	13	18.6	0.96	35	2.750	20	800	27	30	4	100	100	100		
10	13	18.6	0.96	35	2.750	30	800	27	30	4	100	100	100			

NOTE: varied parameters indicated in red

Table 3.4 Dense Sand with Fines simulation cases (GROUP-3)

	E (MPa)	γ_d (kN/m ³)	γ_{sat} (kN/m ³)	e	ϕ_{peak} °	ψ_{peak} °	c (kPa)	D (mm)	WT (mm)	D/ WT	H/ D	water level (m)	pullout section (%)	Length (m)	
Dense Sand with fines (D-F)	50	17	20	0.5	45	15	10	300	10	30	4	100	20	100	Pipe diameter
	50	17	20	0.5	45	15	10	600	20	30	4	100	20	100	
	50	17	20	0.5	45	15	10	800	27	30	4	100	20	100	
	50	17	20	0.5	45	15	10	800	27	30	1	100	20	100	H/D
	50	17	20	0.5	45	15	10	800	27	30	2	100	20	100	
	50	17	20	0.5	45	15	10	800	27	30	3	100	20	100	
	50	17	20	0.5	45	15	10	800	27	30	4	100	20	100	Pullout section
	50	17	20	0.5	45	15	10	800	27	30	4	100	20	100	
	50	17	20	0.5	45	15	10	800	27	30	4	100	50	100	
	50	17	20	0.5	45	15	10	800	27	30	4	100	75	100	
	50	17	20	0.5	45	15	10	800	27	30	4	100	100	100	cohesion
	50	17	20	0.5	45	15	2	800	27	30	4	100	20	100	
	50	17	20	0.5	45	15	10	800	27	30	4	100	20	100	
	50	17	20	0.5	45	15	20	800	27	30	4	100	20	100	
	50	17	20	0.5	45	15	30	800	27	30	4	100	20	100	
	50	17	20	0.5	45	15	2	800	27	30	4	100	100	100	
	50	17	20	0.5	45	15	10	800	27	30	4	100	100	100	
	50	17	20	0.5	45	15	20	800	27	30	4	100	100	100	
50	17	20	0.5	45	15	30	800	27	30	4	100	100	100		

NOTE: varied parameters indicated in red

B. Effect of Water Level

The importance/relevance of the depth of water to the seabed on the model and analyses was investigated. To that goal, the finite element model was run with three different scenarios of water levels (above seabed). The scenarios run were: Depth to seabed=0m (water table at the seabed), 50m and 100 m, respectively. All the models tested for these scenarios were based on pipeline with diameter equal to 0.8 m, buried at an embedment depth $H/D=2$ in a medium dense sand with fines. As shown in figures 3.4 and 3.5, the “buckling amplitudes” (upwards displacement of the pipeline) along the length of the pipe and the load displacement curves (the variation of the uplift force (kN/m) with the normalized pipe displacement (disp/H_c , %)) are almost identical for the water level scenarios. A depth of water of 100m was considered as representative of relatively shallow coastal waters in Lebanon and other areas in the world with operating offshore pipelines (ex. Bohai Gulf in China) and as such was adopted throughout the analyses run in this thesis. This does not constrain and/or diminish the applicability of the findings/recommendations reported given that the depth of water appears to have little to no effect on the results obtained, which is an expected outcome given that the initial effective stresses in the soil/subsurface are unchanged as water levels are varied.

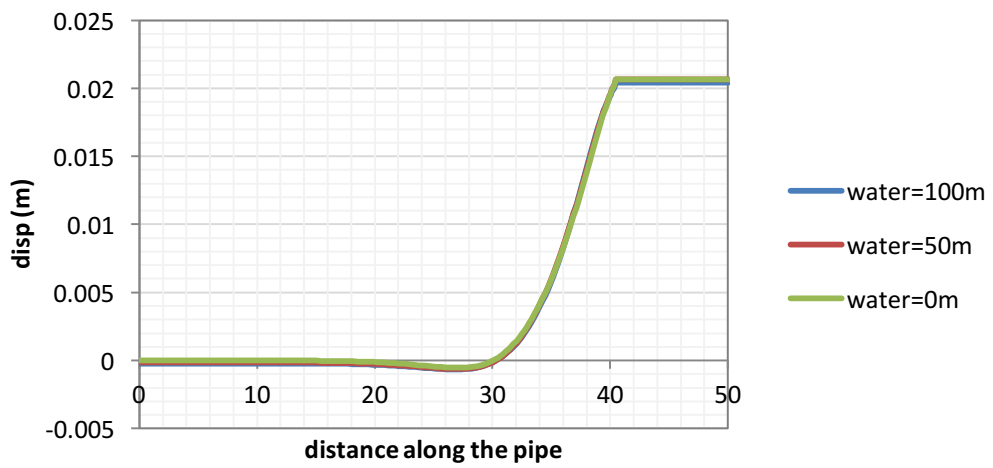


Figure 3.4 Pipeline buckling amplitude along the length of the pipe for different water levels

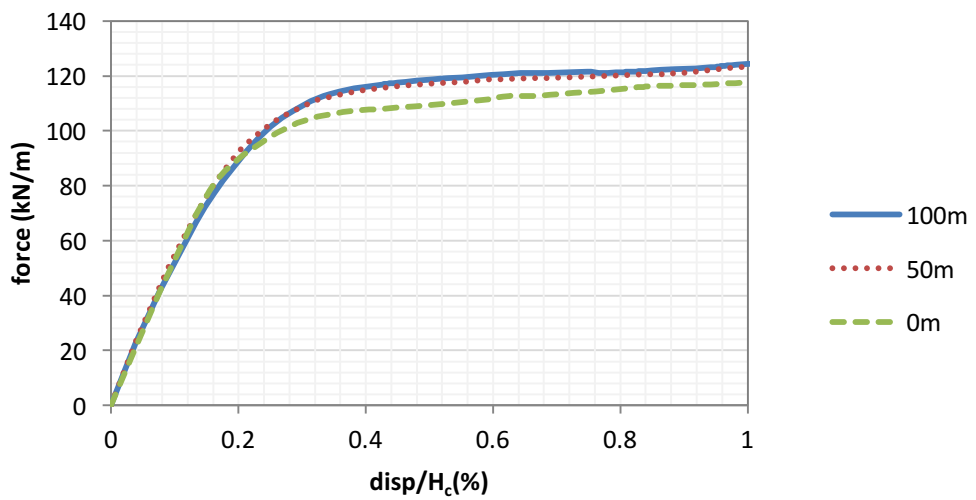


Figure 3.5 Load displacement curves- F (divided by L_p) versus $disp/H_c$ for different water levels

C. CASE-1 Medium Dense Sand with Fines

In analyzing the effects of the various parameters on the response of the pipeline (load-deformation) a baseline scenario is adopted with individual parameters varied around it, while maintaining all remaining factors constant. The baseline scenario involved the following:

- Pipe Diameter, $D=0.8\text{m}$
- Pipe Embedment $H/D=2$ (H =Distance from seabed to top of pipe)
- Cohesion associated with the fines present in the soil; $c=10\text{kPa}$
- Portion of pipeline pulled out at constant vertical displacement=20% of pipeline length.
- Pipeline wall thickness, t . Ratio of $D/t=30$

1. Effect of Pipeline Diameter, D

The load-displacement response was investigated for different pipeline diameters: 0.3 to 1 m. The cases analyzed with varying diameters maintained all other parameters in the baseline scenario constant. The effective lengths as defined earlier in this chapter were plotted on the buckling amplitude curves along the length of different pipe sizes (Figure 3.6). The effective length increases with the pipe diameter in a consistent/expected manner, thus validating the adopted slope method technique. As the pipe diameter increases, the uplift forces as well as the normalized mobilization distance increase (Table 3.5 and figures 3.6 to 3.9). The difference between the uplift force per m obtained by dividing the total resistance by either pullout or effective lengths respectively varies from 23 to 44%. The corresponding normalized mobilization distances increase from 0.37 to 0.64% H_c for $D=0.3$

to 1m, respectively. The results/variations obtained from the FE analyses indicating that the uplift resistance increases with the increase in the pipeline diameter are in line with those reported by Liu et al. (2013).

Table 3.5 Maximum uplift soil resistance and normalized mobilization distance-effect of pipe diameter-Medium Dense Sand with Fines

FE Results, Medium Dense Sand with Fines			Normalizing wrt Pullout Length	Normalizing wrt $L_{\text{effective}}$	L_{eff} (m)	disp/ H_c (%)
			Force (kN/m)			
D (m)	H/D=2, $L_p=20\%L$, c=10kPa	0.3	26.8	20.6	25.5	0.36
		0.6	73.4	48.9	29.7	0.40
		0.8	124.5	73.3	33.5	0.47
		1	185.2	102.9	37.4	0.64

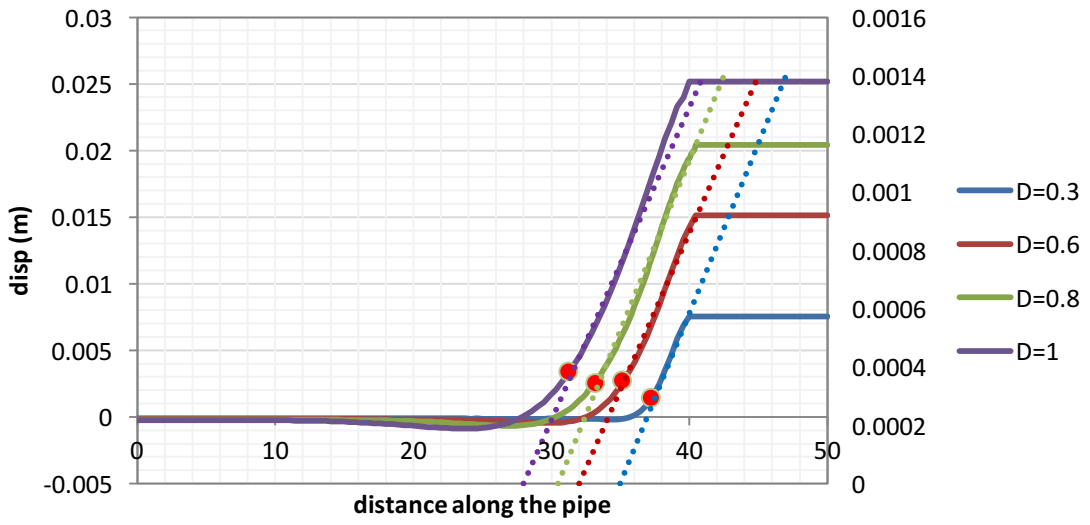


Figure 3.6 Pipeline buckling amplitude at 1% H_c upward pipeline displacement along the length of the pipe for different pipeline diameters-Medium Dense Sand with Fines

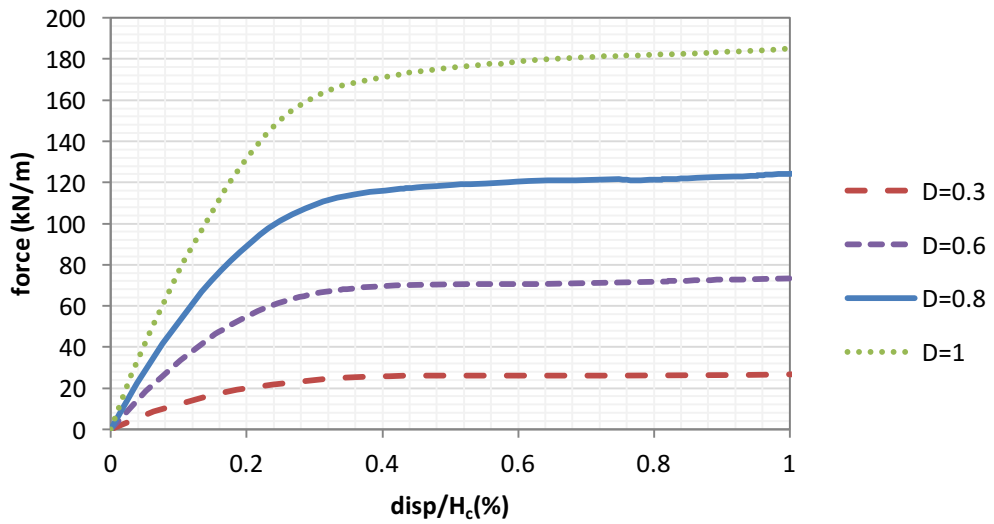


Figure 3.7 Load displacement curves- F (divided by L_p) versus $disp/H_c$ for different pipeline diameters-Medium Dense Sand with Fines

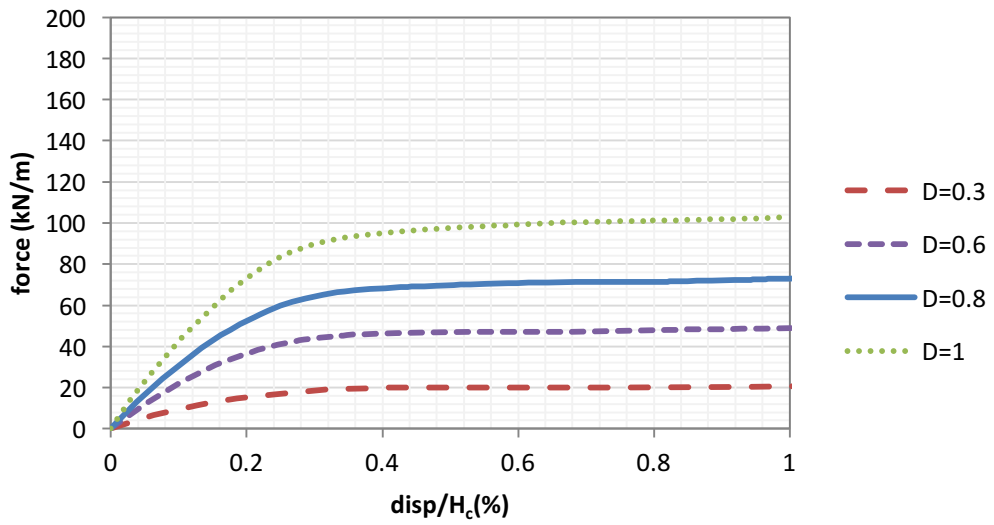


Figure 3.8 Load displacement curves- F (divided by L_{eff}) versus $disp/H_c$ for different pipeline diameters-Medium Dense Sand with Fines

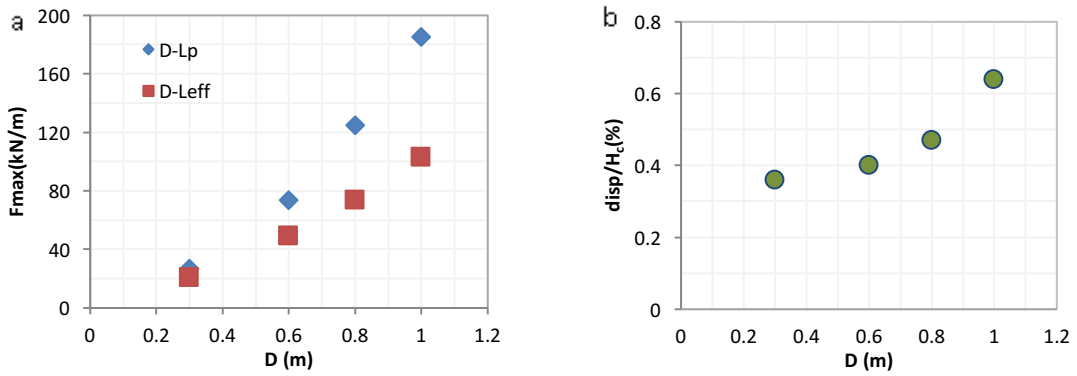


Figure 3.9 a) Maximum uplift resistance and b) maximum normalized mobilization distance for different pipe diameters -Medium Dense Sand with Fines

2. Effect of Embedment depth, H

The 0.8 m diameter pipeline was buried in shallow embedment depths with H/D varying from 0.75 to 4 in medium dense sand with fines that has 10 kPa cohesion value. The effective lengths were plotted on the buckling amplitude curves along the length of different embedment depths (Figure 3.10). The embedment depth does not affect the effective length that varies by about 5% between the different cases. As the embedment depth increases, the effect of soil resistance (block weight and shearing resistance along uplifted soil block boundaries) increases resulting in an increase in uplift resistance values and normalized mobilization distances (Table 3.6 and Figures 3.10 to 3.13). The effect of pipeline embedment depth was explored by a number of researchers such as Schaminee et al. (1990), Ng and Springman (1994), Chin et al. (2006), Newson and Deljoui (2006), Schupp et al. (2006), Bransby and Ireland (2009), Gao et al. (2011), Sun et al. (2011), Byrne et al. (2013), Robert and Thusyathan (2014) and Liu et al. (2015). These studies showed that the uplift resistance increases with the soil the burial depth as was confirmed/found in the FE results from our analyses. The difference between the uplift resistance divided by pullout and effective lengths increases with the embedment depth from 29 to 44% for H/D=0.75 to 4, respectively.

DNV (2007) states that for medium dense sand, the mobilization distance is between 0.5 to 0.8%H and is independent of the soil burial depth. However, as discussed by Chin et al. (2006) and shown in our FE results, the normalized mobilization distance is a function of the embedment depth: it increases from 0.38 to 0.80% H_c (0.63 to 0.9%H) for H/D=0.75 to 4.

Table 3.6 Maximum uplift soil resistance and normalized mobilization distance -effect of embedment depth-Medium Dense Sand with Fines

FE Results, Medium Dense Sand with Fines			Normalizing wrt Pullout Length	Normalizing wrt $L_{\text{effective}}$	L_{eff} (m)	disp/ H_c (%)
			force (kN/m)			
H/D	D=0.8m, $L_p=20\%L$, c=10 kPa	0.75	63.0	45.0	28.1	0.38
		1	74.3	49.6	30.8	0.40
		1.5	99.4	60.2	33.3	0.47
		2	124.5	73.3	33.5	0.50
		3	180.8	103.3	34.7	0.65
		4	263.8	146.5	35.8	0.80

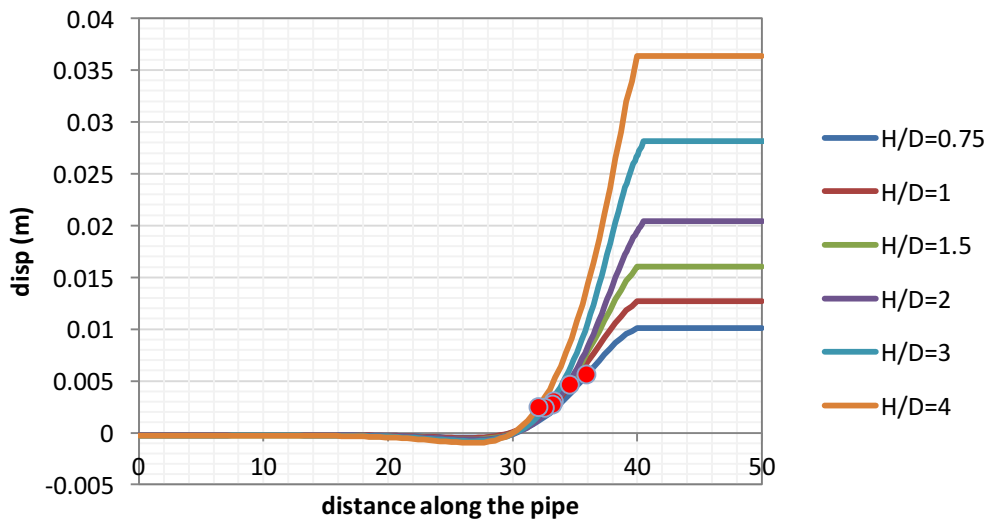


Figure 3.10 Pipeline buckling amplitude at $1\%H_c$ upward pipeline displacement along the length of the pipe for different embedment depths-Medium Dense Sand with Fines

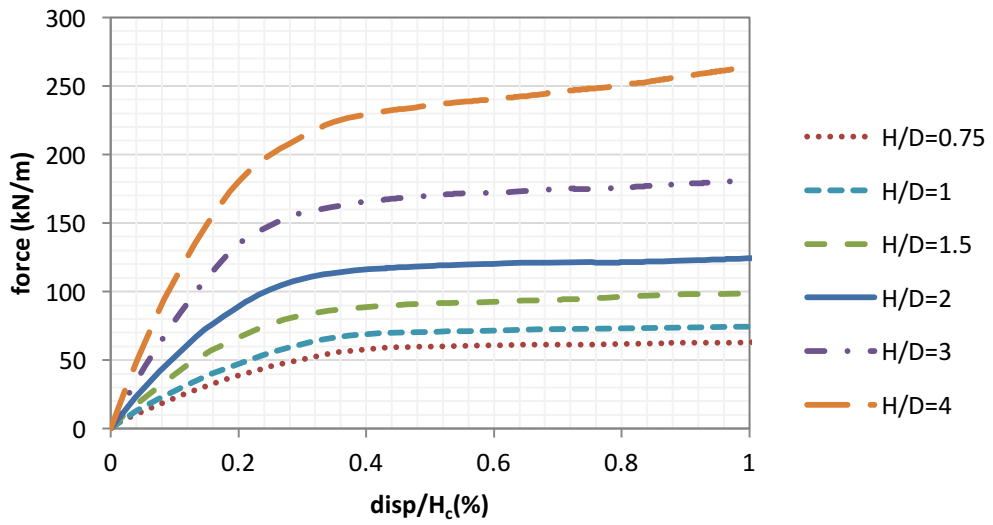


Figure 3.11 Load displacement curves- F (divided by L_p) versus disp/H_c for different embedment depths (H/D) -Medium Dense Sand with Fines

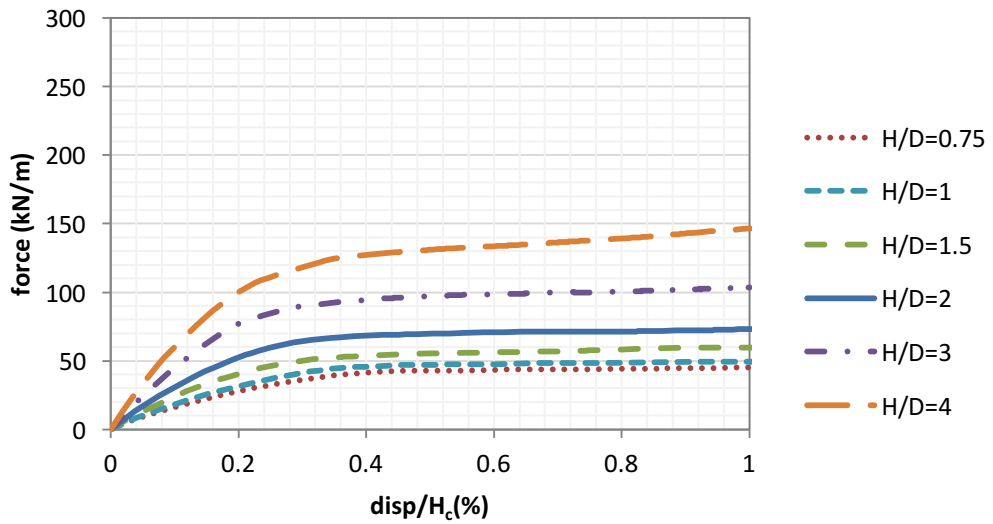


Figure 3.12 Load displacement curves- F (divided by L_{eff}) versus disp/H_c for different embedment depths (H/D) -Medium Dense Sand with Fines

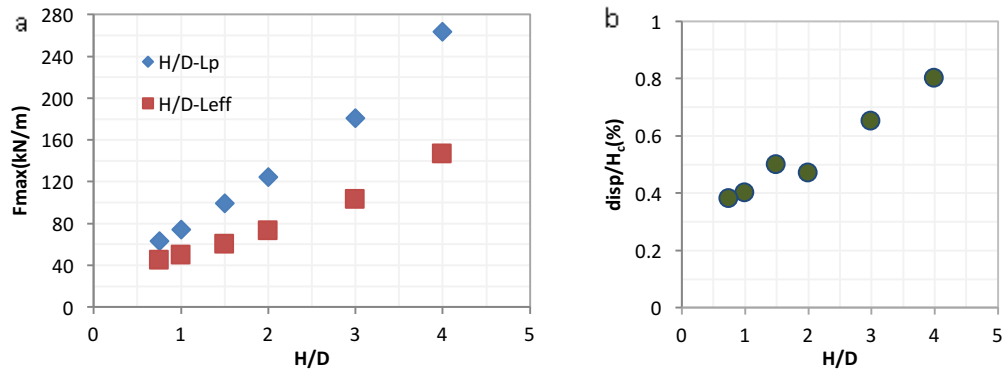


Figure 3.13 a) Maximum uplift resistance and b) maximum normalized mobilization distance for different embedment depths -Medium Dense Sand with Fines

3. Effect of Pullout length, L_p

Laboratory and/or real-scale experimental studies typically involve pulling out the entire pipe length ($L_p=L$) to simulate plain strain conditions. In reality, given its relative slenderness (large length to diameter) the pipe does not buckle/deform in a plain strain manner. The true value of modeling the problem in 3D and not 2D is that such 3D analyses allow us to vary the portions/lengths of the pipe being pulled upwards. 3D models allow sinking of the pipe in the seabed and providing additional resistance to global buckling (Liu et al. 2014).

In the work presented in this thesis pipeline sections varying between 10% and 75% of the total length were pulled up. The results obtained were compared with the 100% pullout cases that capture/model plain strain conditions. Figure 3.14 shows the buckling amplitude along the length of the pipe with the effective lengths for different pullout cases. The difference between the uplift resistance divided by pullout and effective lengths decreases with the increase in pullout section length: 58 to 17% for pullout sections of 10 to 75% respectively (Table 3.7). At high displacements, as the pullout length increases, the uplift force divided by L_p decreases (figure 3.15) while the uplift force divided by L_{eff} is no longer affected (figure 3.16). This provides additional validation of the method adopted to calculate the effective length. The maximum uplift resistances are obtained at lower normalized mobilization distances for both strain hardening and strain softening curves. For strain hardening curves (pullout sections <50%), the maximum uplift resistances are obtained at normalized mobilization distances equal to 0.7 to 0.46% H_c for 10 to 30% pullout sections, while for strain softening curves (pullout sections >50%), they are obtained at normalized mobilization distances equal to 0.46 to 0.35% H_c for 50 to 100%

pullout sections. At 10 to 50% pullout sections, the soil elements fail one after the other resulting in a strain hardening behavior, while for pullout sections greater than 50%, the soil elements fail together resulting in a strain softening behavior.

Table 3.7 Maximum uplift soil resistance and normalized mobilization distance -effect of pullout length-Medium Dense Sand with Fines

FE Results, Medium Dense Sand with Fines			Normalizing wrt Pullout Length	Normalizing wrt $L_{\text{effective}}$	L_{eff} (m)	disp/ H_c (%)
			force (kN/m)			
Pullout section (%)	H/D=2, D=0.8m, $L_p=x\%L$	10	176.4	73.5	24	0.70
		20	124.5	73.3	33.5	0.47
		30	106.6	71.1	44.9	0.46
		50	93.6	73.2	64	0.46
		75	88.4	73.6	90.2	0.38
		100	78.6	78.6	100	0.35

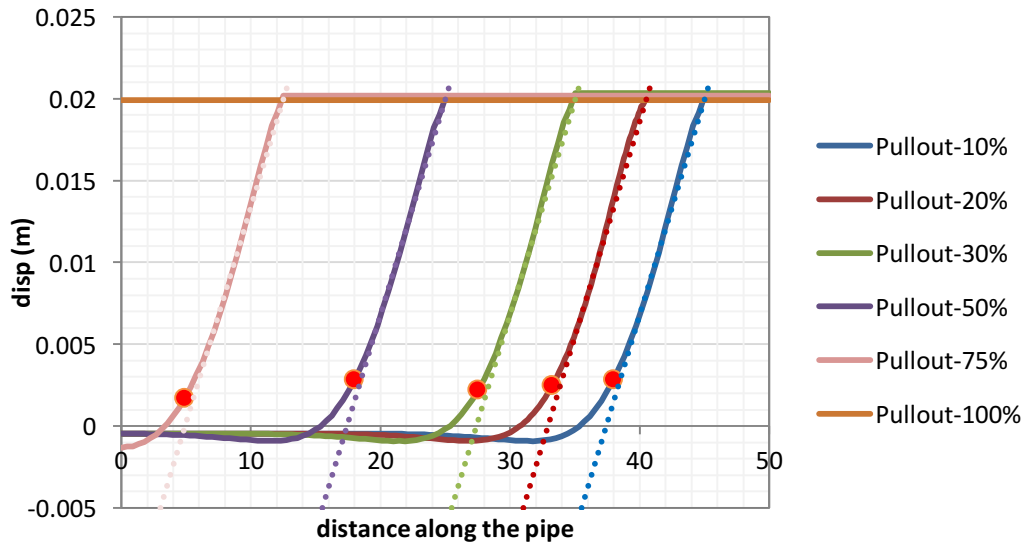


Figure 3.14 Pipeline buckling amplitude at 1% H_c upward pipeline displacement along the length of the pipe for different pullout lengths (% L) -Medium Dense Sand with Fines

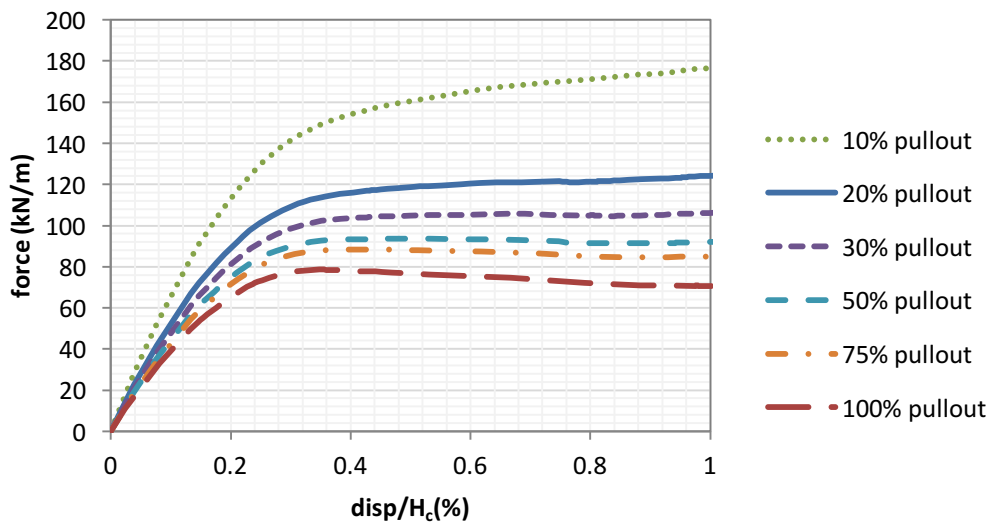


Figure 3.15 Load displacement curves- F (divided by L_p) versus $disp/H_c$ for different pullout lengths-Medium Dense Sand with Fines

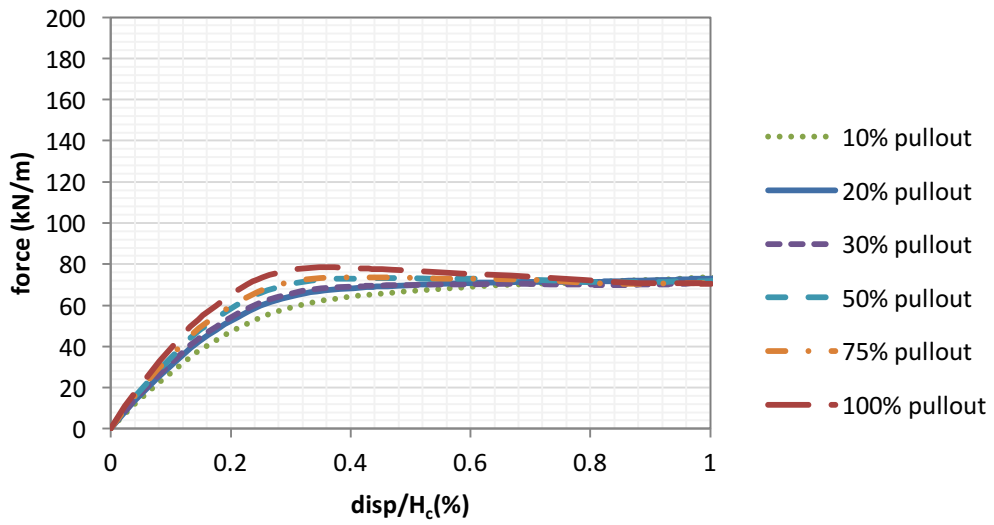


Figure 3.16 Load displacement curves- F (divided by L_{eff}) versus $disp/H_c$ for different pullout lengths-Medium Dense Sand with Fines

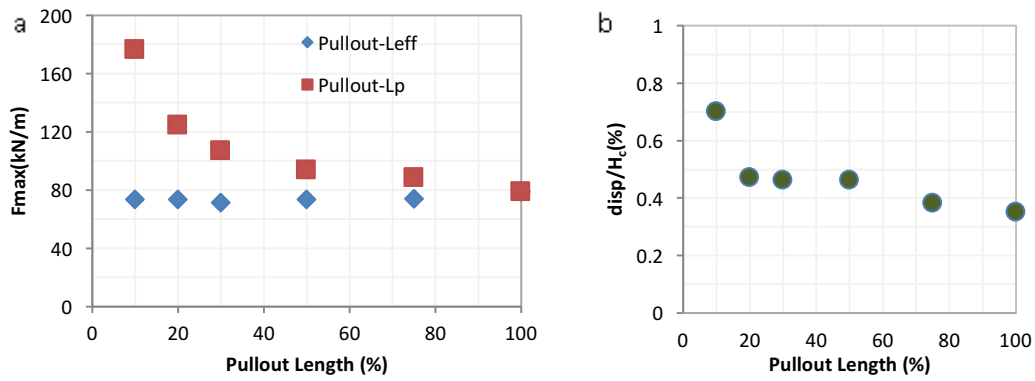


Figure 3.17 Maximum uplift resistance and b) maximum normalized mobilization distance for different pullout lengths -Medium Dense Sand with Fines

4. Effect of Pipeline Diameter to Wall Thickness Ratio, D/t

The effect of diameter to wall thickness ratio (D/t) was investigated for 0.8m diameter pipes embedded in medium dense sand with fines with 10 kPa cohesion and at an embedment depth ratio H/D of 2. The baseline case and all previous simulations were performed at a $D/t=30$.

In practice, the wall thickness design criteria for a high pressure high temperature pipeline depends on limiting hoop stress due to internal pressure and hydrostatic collapse and buckle propagation due to external pressure. The minimum wall thickness should be greater than the design wall thickness from the above criteria. DNV (2007) recommends a diameter to wall thickness ratio (D/t) between 15 and 45 with a minimum wall thickness of 12 mm. Thus, typical D/t values of 25, 30 and 40 were examined for the 0.8m diameter pipeline. Table 3.8 presents the pipe stiffness for different diameter sizes and D/t ratios. As shown in figure 3.18, the D/t ratio (in the practical/realistic range explored) does not affect the effective length. The load displacement curves show that for medium dense sand with fines, the uplift resistance (whether divided by L_p or L_{eff}) is slightly affected by the D/t ratio for different pullout lengths with 1 to 5% difference for D/t equal to 25 to 40. Moreover, D/t does not affect the difference between the uplift resistance divided by pullout and effective lengths that decreases with the increase in pullout section length from 58 to 17% for pullout sections of 10 to 75%, respectively. Furthermore, D/t slightly affects the normalized mobilization distance that varies between 1 and 10% for D/t equal to 25 to 40 (figures 3.19 to 3.21). Therefore, it can be concluded that within the range of values tests, D/t has a minimal influence on the pipe uplift resistance, normalized mobilization distance and effective length.

Table 3.8 Pipe stiffness for different diameter sizes and diameter to wall thickness ratios

E(GPa)	D/WT	WT (m)	D _o (m)	D _i (m)	EI(10 ⁹ * N.m ²)
206	25	0.032	0.8	0.736	1.175
		0.024	0.6	0.552	0.372
		0.012	0.3	0.276	0.023
	30	0.027	0.8	0.747	0.999
		0.020	0.6	0.56	0.316
		0.010	0.3	0.28	0.020
	40	0.020	0.8	0.76	0.768
		0.015	0.6	0.57	0.243
		0.008	0.3	0.285	0.015

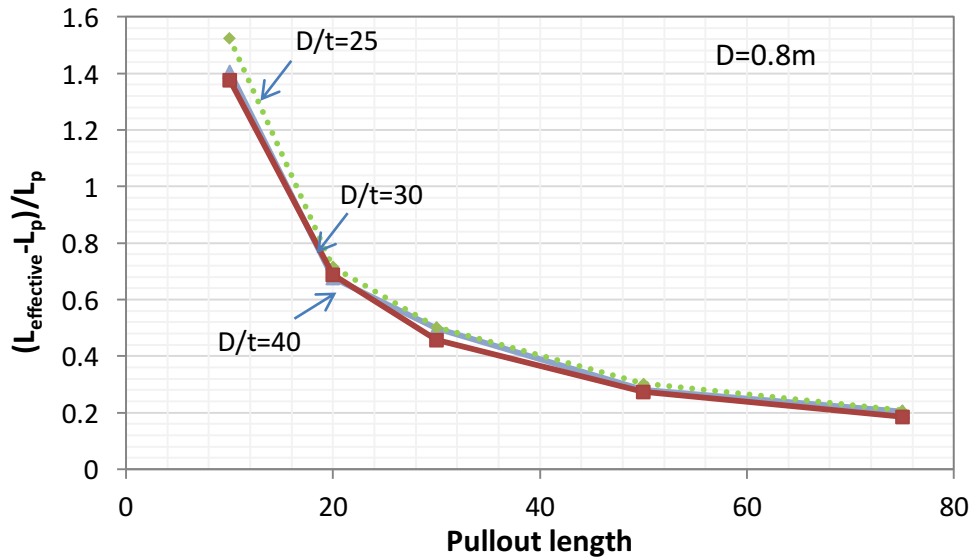
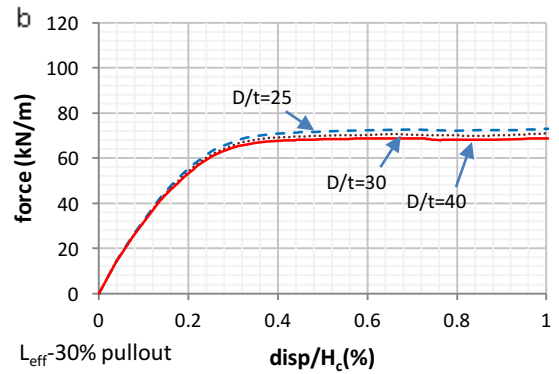
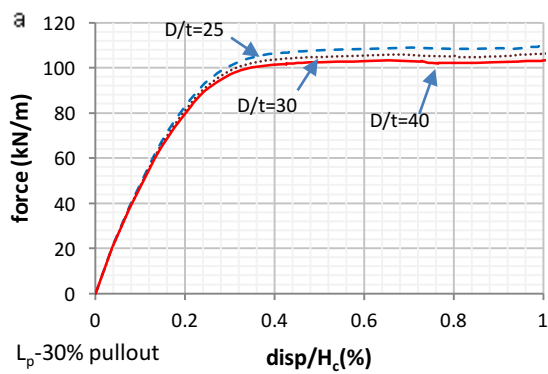
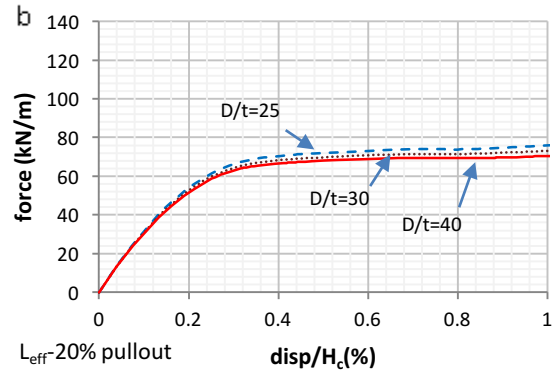
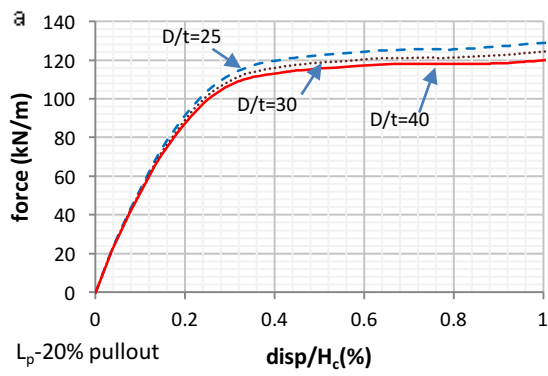
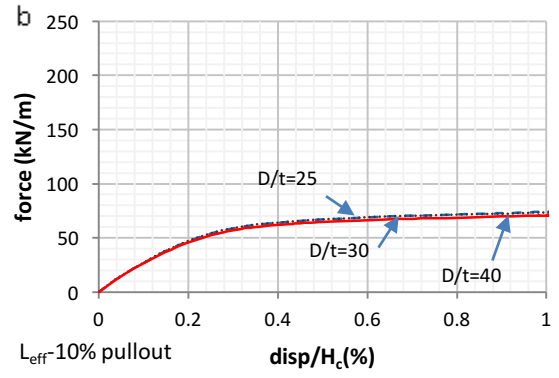
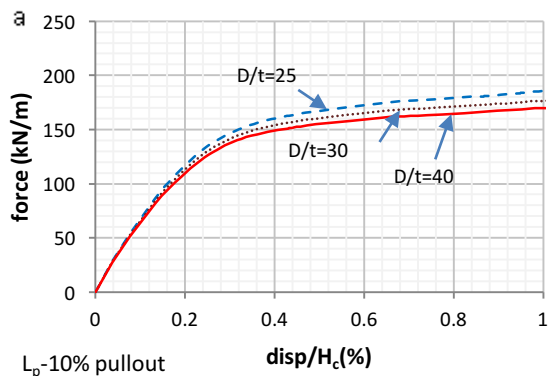


Figure 3.18 Variation of the relative change in effective length $(L_{\text{eff}} - L_p) / L_p$ for different pullout lengths at different diameter to wall thickness ratios –Medium Dense Sand with Fines



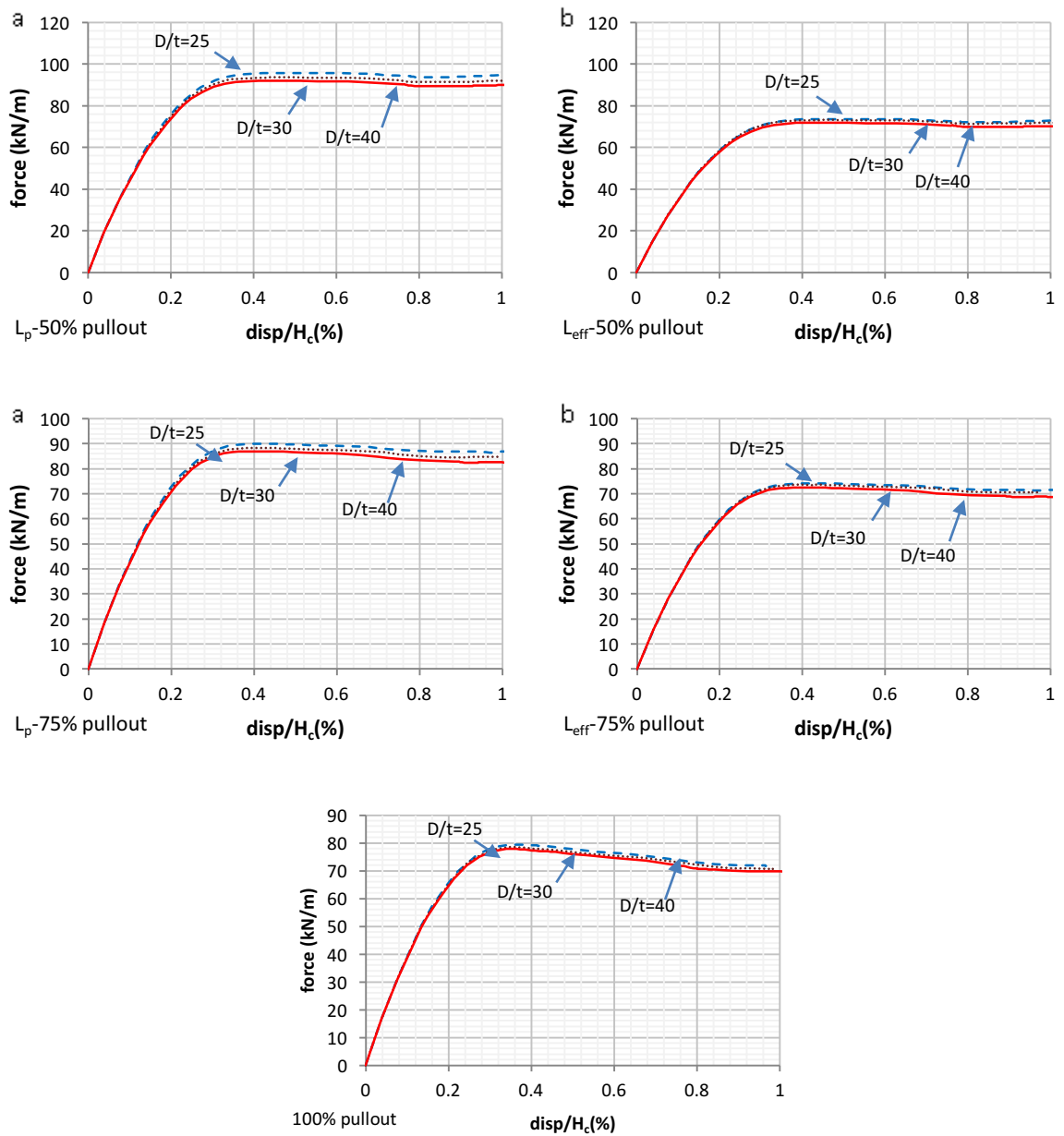


Figure 3.19 Load displacement curves- a) F divided by L_p and b) F divided by L_{eff} versus $disp/H_c$ for different pullout lengths at different diameter to wall thickness ratios-Medium Dense Sand with Fines

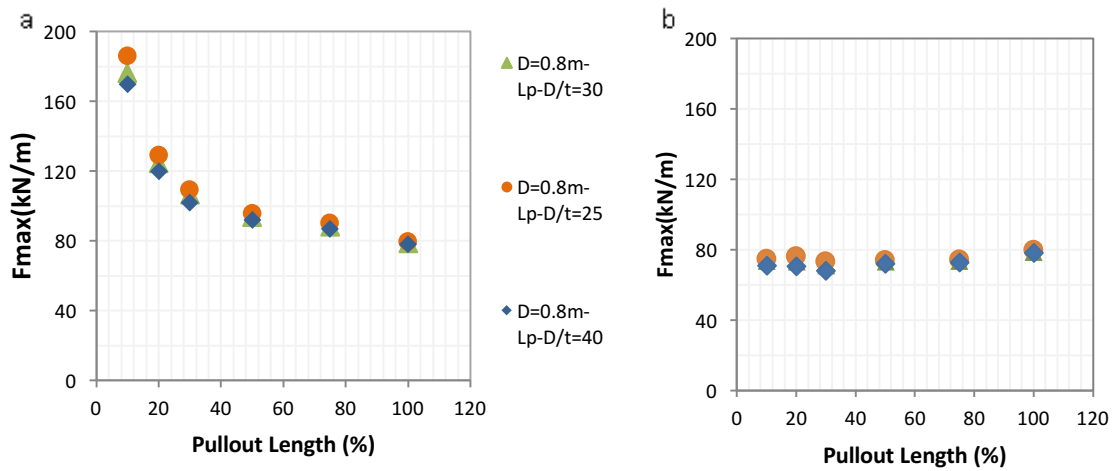


Figure 3.20 Maximum uplift resistance: a) F divided by L_p and b) F divided by L_{eff} versus pullout lengths at different diameter to wall thickness ratios-Medium Dense Sand with Fines

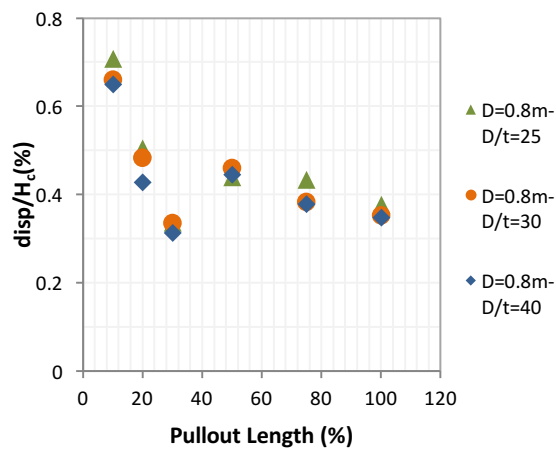


Figure 3.21 Maximum normalized mobilization distance for different pullout lengths at different diameter to wall thickness ratios-Medium Dense Sand with Fines

D. Effect of Soil Properties

1. Effect of Soil Cohesion, c

Offshore seabed deposits vary in composition and state of denseness throughout the globe. Whereas earlier studies have predominantly associated offshore pipelines with embedment soils that are characterized as “clean Sands”, the documented presence of various percentages of fines in the Lebanese offshore seabed sediments and at other locations suggests that it would be of value to attempt to incorporate the effect of apparent soil “cohesion” in the evaluation of uplift resistance. This is all the more significant given the shallow depths of embedment and associated low confining stresses, which render the effect of cohesion, even for low values of c , relatively significant.

To study the effect of soil cohesion, different c values ranging from 2 to 30 kPa were used as variants on the baseline scenario (0.8 m diameter pipeline, $D/t=30$, embedded at $H/D=2$ and pulled at its middle by 20% and 100% pullout sections). Neither the buckling amplitude at max load, nor the effective length is affected by the increase in soil cohesion (Figure 3.22). The pipe uplift resistance as well as the mobilization distance increase with the soil cohesion (Table 3.9 and figures 3.23 to 3.26). This is clearly shown in the uplift resistances divided by the effective length and 100% pullout cases that intersect at high displacements. The contribution of the cohesion component is usually governed by their undrained behavior (Schaminee et al 1990). According to Schaminee and his co-workers, the cohesion component increases the soil strength by $2.H_c.c_u$, as is demonstrated in the analytical solution section included at the end of this chapter, and causes the pipe to displace more to reach the peak uplift resistance.

Table 3.9 Maximum uplift soil resistance and normalized mobilization distance -effect of soil cohesion-Medium Dense Sand with Fines

FE Results, Medium Dense Sand			Normalizing wrt Pullout Length	Normalizing wrt $L_{\text{effective}}$	Normalizing wrt Pipe Length	L_{eff} (m)	Normalizing wrt $L_{\text{effective}}$
			force (kN/m)				
c (kPa)	H/D=2, D=0.8m, $L_p=20\%L$	2	84.9	48.5	48.6	34.5	0.36
		10	124.5	73.3	78.6	33.5	0.47
		15	150.0	90.9	97.5	33.3	0.48
		20	180.1	109.2	116.5	33.1	0.65
		30	237.2	143.7	155.3	33.0	0.76

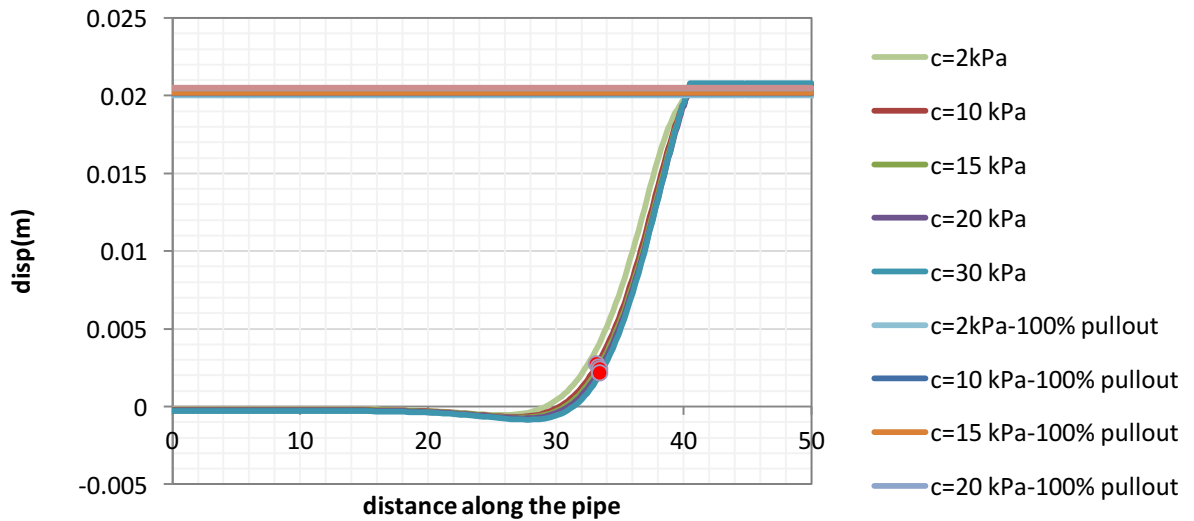


Figure 3.22 Pipeline buckling amplitude at $1\%H_c$ upward pipeline displacement along the length of the pipe for different soil cohesion values-Medium Dense Sand with Fines

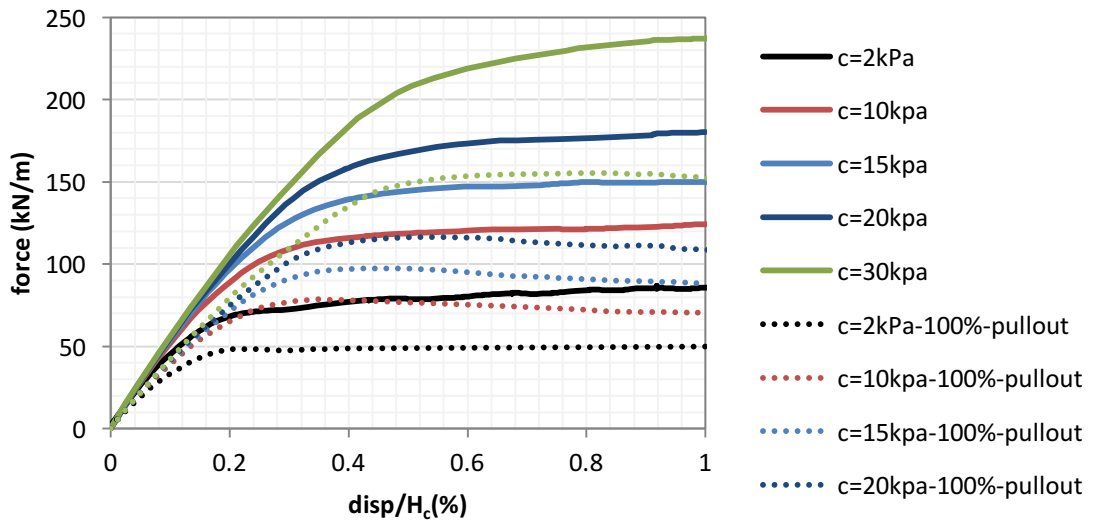


Figure 3.23 Load displacement curves- F (divided by L_p) versus $disp/H_c$ for different soil cohesion values and pullout lengths-Medium Dense Sand with Fines

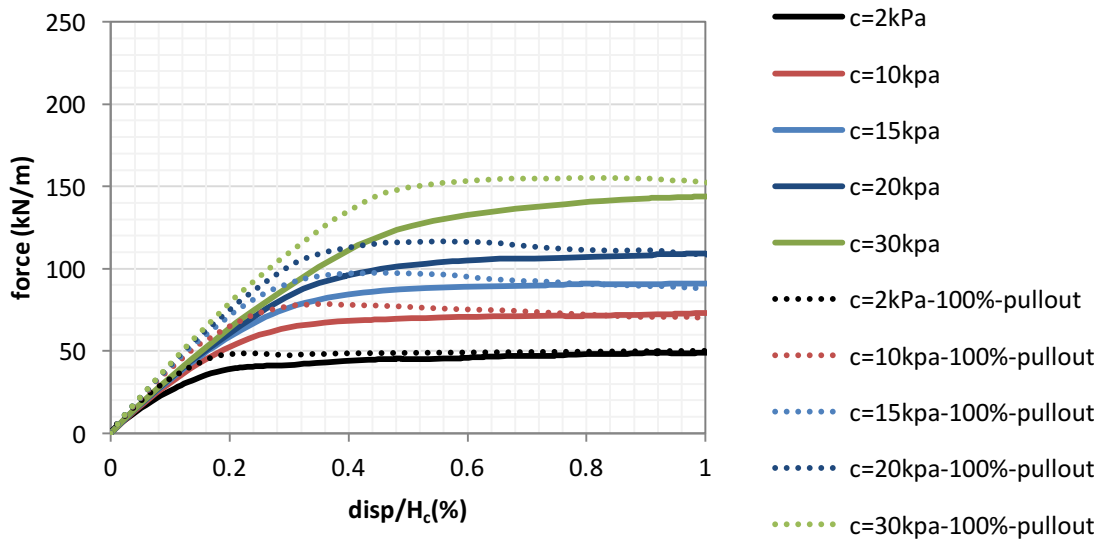


Figure 3.24 Load displacement curves- F (divided by L_{eff}) versus $disp/H_c$ for different soil cohesion values and pullout lengths-Medium Dense Sand with Fines

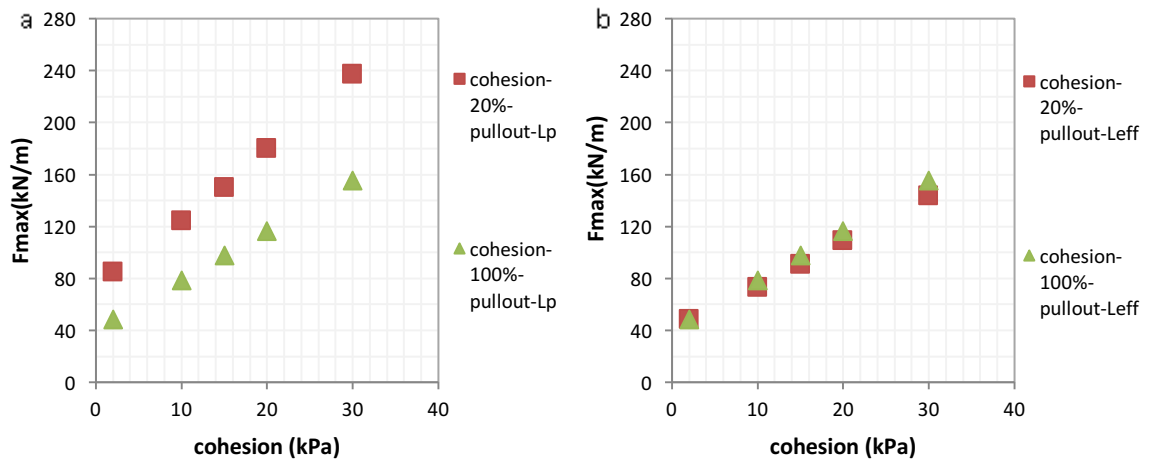


Figure 3.25 Maximum uplift resistance: a) F divided by L_p and b) F divided by L_{eff} versus pullout lengths at different soil cohesion values-Medium Dense Sand with Fines

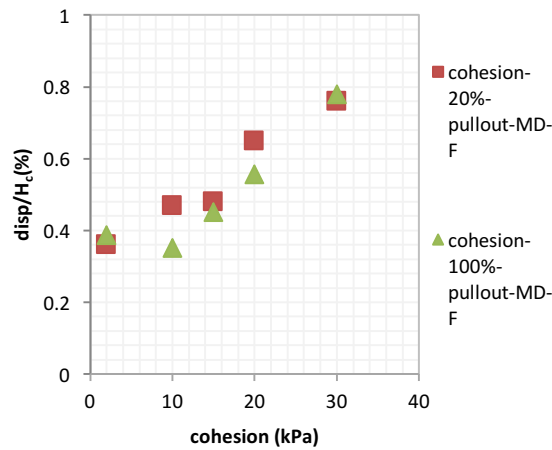


Figure 3.26 Maximum normalized mobilization distance for different pullout lengths at different soil cohesion values-Medium Dense Sand with Fines

2. Effect of Soil Denseness

Pipeline uplift simulations were conducted on loose, medium dense and dense sand with fines (effective unit weight γ' equal to 8.8, 9.2 and 10.2 kN/m³ and ϕ_{peak} 35, 40 and 45° respectively) for different pipe diameters, embedment depths, pullout sections and soil cohesion values as described in part A of this chapter: Overview (Tables 3.10 to 7).

As the pipe diameter increases, an increase in soil denseness enhances the uplift resistance values. The uplift resistance is almost the same at $D=0.3\text{m}$ with 1% difference between the different soil density cases: at an embedment depth ratio H/D of 2 and with the use of this small diameter, a local failure occurs diminishing the importance of the soil denseness contribution. The maximum uplift resistance as well as the difference between the uplift resistance between the different soil denseness cases increases with the pipe diameter: 1 to 13 % between loose and medium dense and between medium dense and dense cases for $D=0.3$ to 0.8m, respectively. The increase in soil denseness reduces the normalized mobilization distance required to achieve the maximum uplift resistance by an average of 50% between loose and medium dense cases and 50 to 15% between medium dense and dense cases for 20% pullout lengths (Figures 3.27 and 3.31)

Moreover, the increase in soil density for different embedment depths is manifested by the decrease in pipe normalized mobilization distance and small enhancement in the uplift soil resistance. As the embedment depth increases, the soil density contribution to the mobilization distance decreases from 50 to 12% for H/D equal 1 to 4 while to the uplift resistance it increases from 10 to 30% from loose to medium dense and from 5 to 12% for medium dense to dense cases (Figures 3.28 and 3.32).

The small increase in soil density that allows the grains to go from loose to medium or dense state increases the uplift resistance by about 10% for the different pullout lengths. Furthermore, soil density does not change the effective length methodology that leads to the soil uplift resistance normalization (with 10% margin difference) at large strains. However, the soil denseness decreases the normalized distance by 15% for the strain hardening curves and 50% for the strain softening curves (Figures 3.29 and 3.33).

As for the effect of soil cohesion in the various cases of soil denseness states, the denser soils enhance cohesion contribution to the uplift resistance. This enhancement is clearly shown between loose and medium dense cases by an increase of 20% and between medium dense and dense cases by an increase of 10%. The difference between the uplift resistance values divided by the effective length and 100% cases is about 10% for medium dense and dense cases and 20% for loose cases. As for the normalized mobilization distance, it increases with the soil cohesion and decreases with the soil density (Figures 3.30 and 3.34).

The effect of soil density on upheaval buckling of offshore pipelines was studied by several researchers. Stone (2006), White et al. (2001) and Robert and Thusyathan (2014) showed that the uplift resistance is a function of the soil density. Bransby et al. (2001), Vanden Berghe et al. (2005) and Newson and Deljoui (2006) proved that deformation mechanism depends on the soil density; the uplift mechanism is dominated by "local" failure and "flow around" mechanism in loose sand and by "wedge" failure mechanism in dense sand. As for the mobilization distance, Bransby et al. (2001) and Cheuk et al. (2008) showed that the movement needed to mobilize the peak uplift resistance is independent of the grain size and density.

At large strains in drained behavior and for the same confining pressure, the displacement of the pipe in loose soil causes a decrease in the void ratio: the soil particles compress, the pipe needs a force higher than the loose soil resistance to displace till it reaches mobilization distance. However, in medium dense and dense soil, the displacement of the pipe causes compression then dilation of soil particles, the void ratio increases allowing movement of soil grains; the pipe needs a force higher than medium dense and dense soil resistance and also higher than loose soil resistance to displace few millimeters before it reaches mobilization distance. This phenomenon is actually related to the Modified Mohr Coulomb soil model used in the finite element that is based on strain softening response. The peak soil resistance comes from the peak friction angle. The peak friction angle increases with soil density (ϕ is equal to 35, 40 and 45° for loose, medium dense and dense sand with fines respectively). Medium dense and dense soils strains soften, they dilate after the pipe displaces few millimeters allowing the load displacement curve to reach a peak at a small normalized mobilization distance. However, loose soils strains harden, they compress: thus, the increasing in soil resistance with the pipe displacement requires a lot of displacement for soil particles to reach critical state (when the load displacement curve becomes constant). Therefore, as demonstrated by the finite element results, the increase in soil density (going from loose to dense soil) increases the uplift resistance and decreases the normalized mobilization distance. Peak uplift resistance is higher in denser soils due to the effect of densification that increases the internal friction angle and soil density.

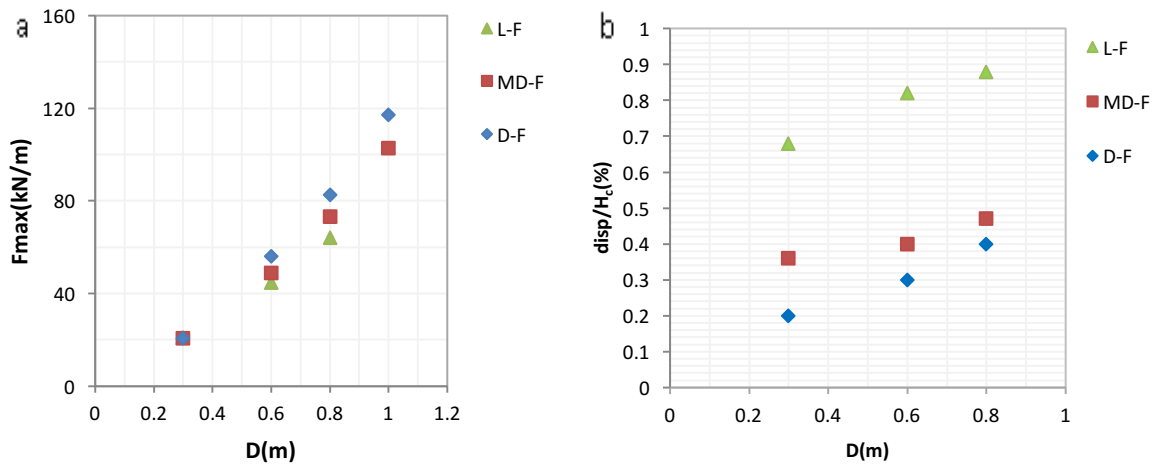


Figure 3.27 a) Maximum uplift resistance and b) mobilization distance for loose, medium dense and dense sand with fines for different pipe diameters

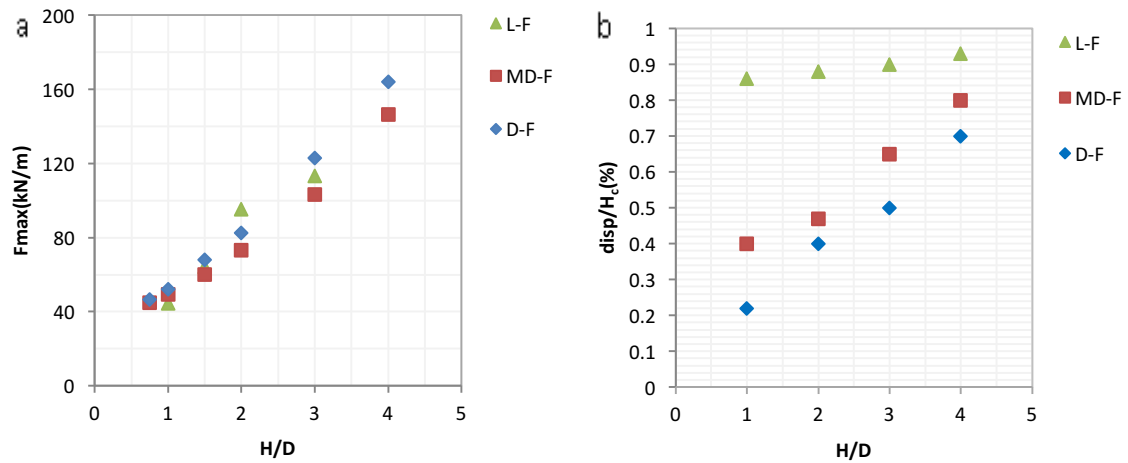


Figure 3.28 a) Maximum uplift resistance and b) mobilization distance for loose, medium dense and dense sand with fines for different embedment depths

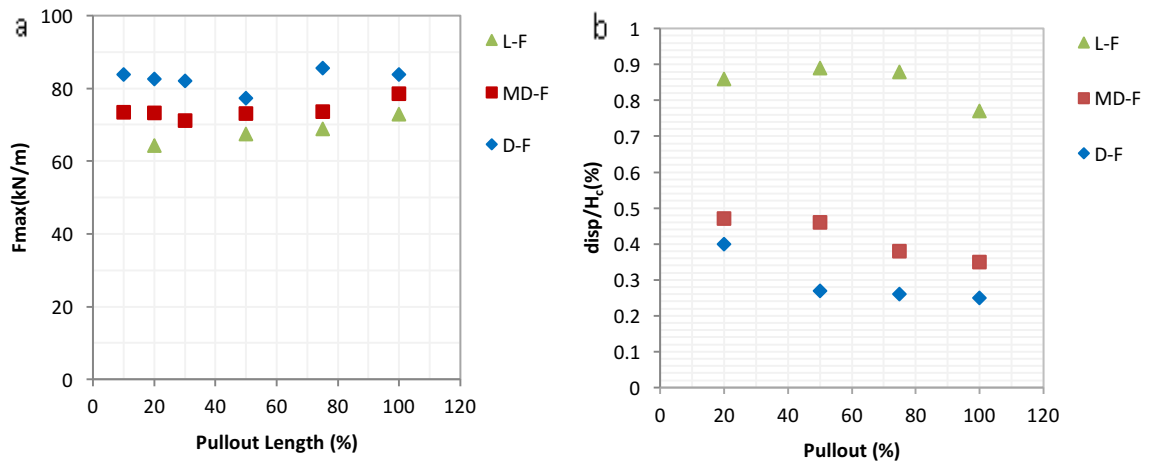


Figure 3.29 a) Maximum uplift resistance and b) mobilization distance for loose, medium dense and dense sand with fines for different pullout lengths

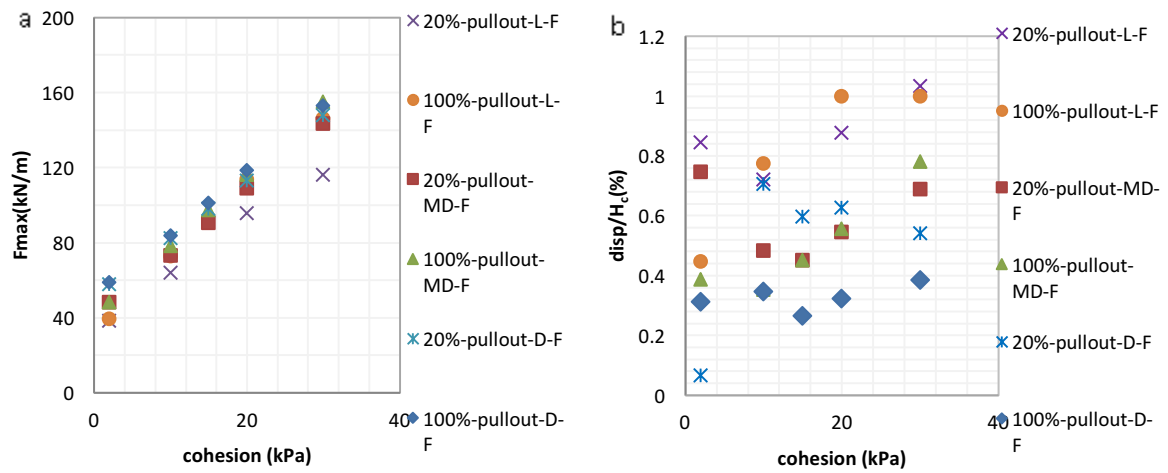


Figure 3.30 a) Maximum uplift resistance and b) mobilization distance for loose, medium dense and dense sand with fines for different soil cohesion

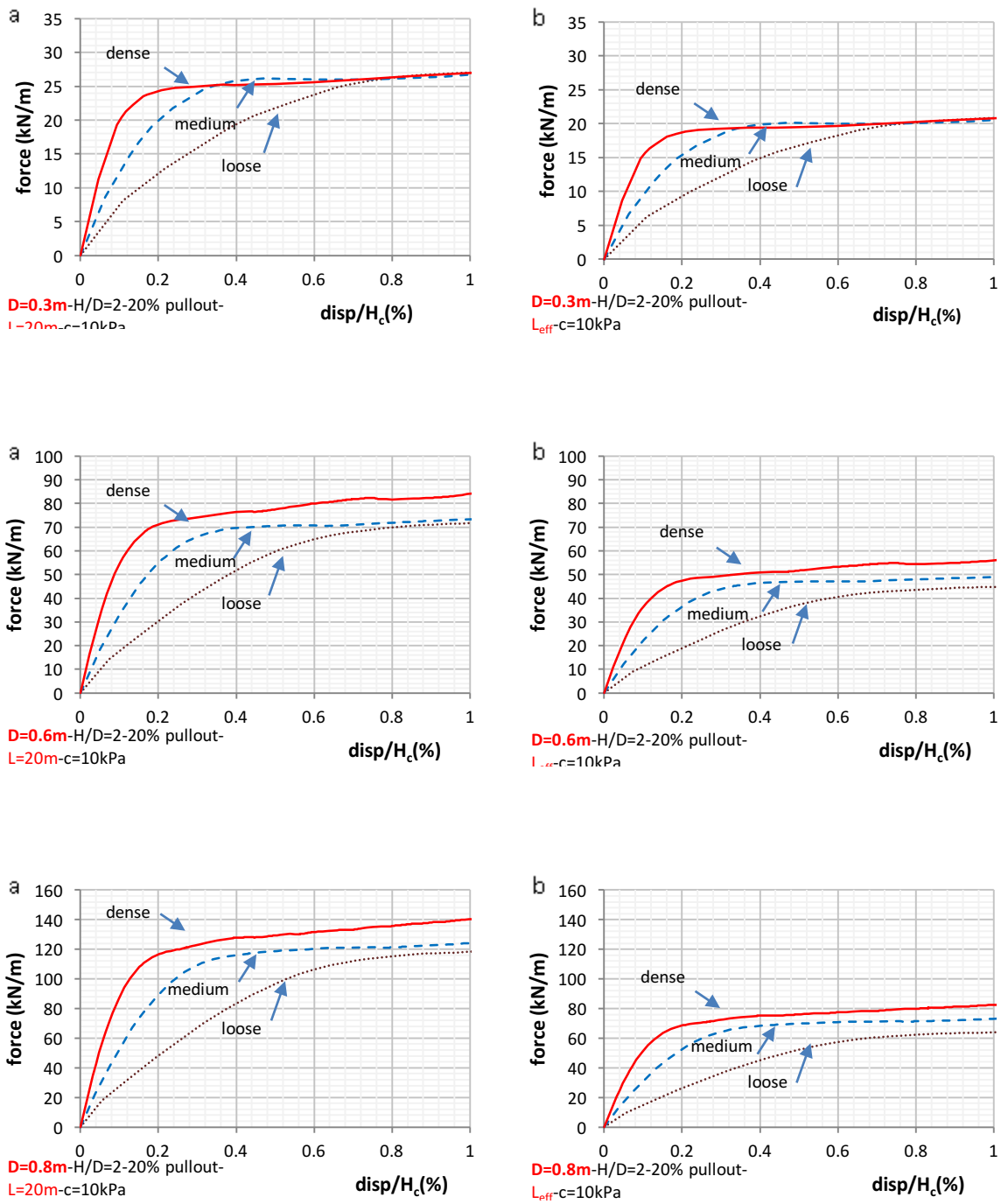
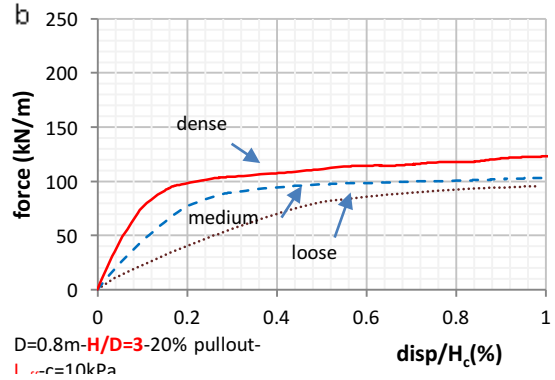
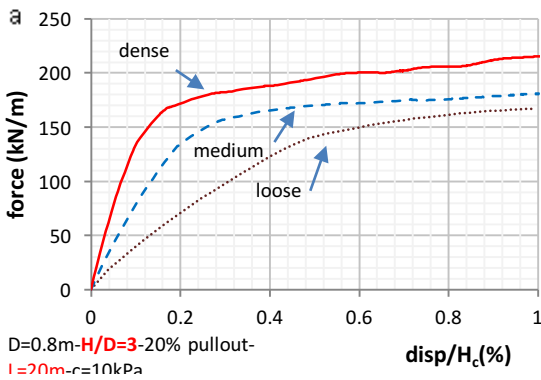
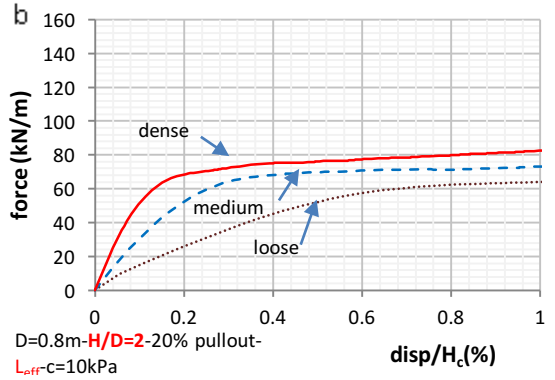
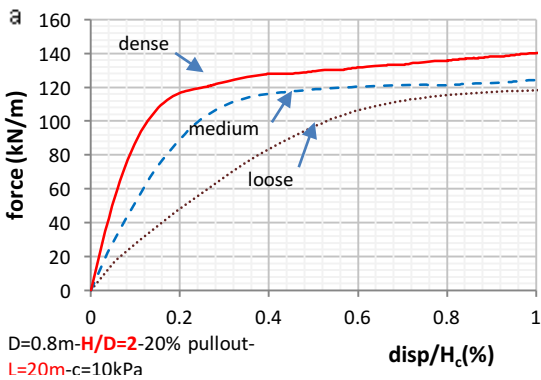
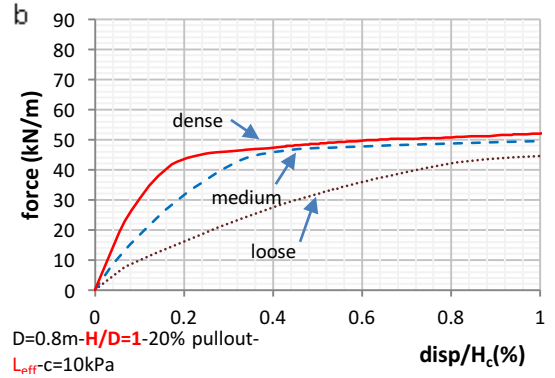
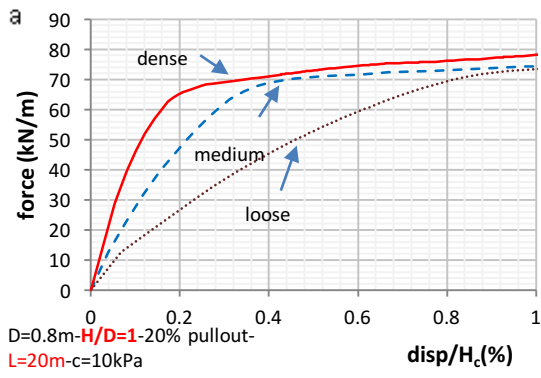


Figure 3.31 Load displacement curves F versus $disp/H_c$ for loose, medium and dense sand with fines for different pipe diameters



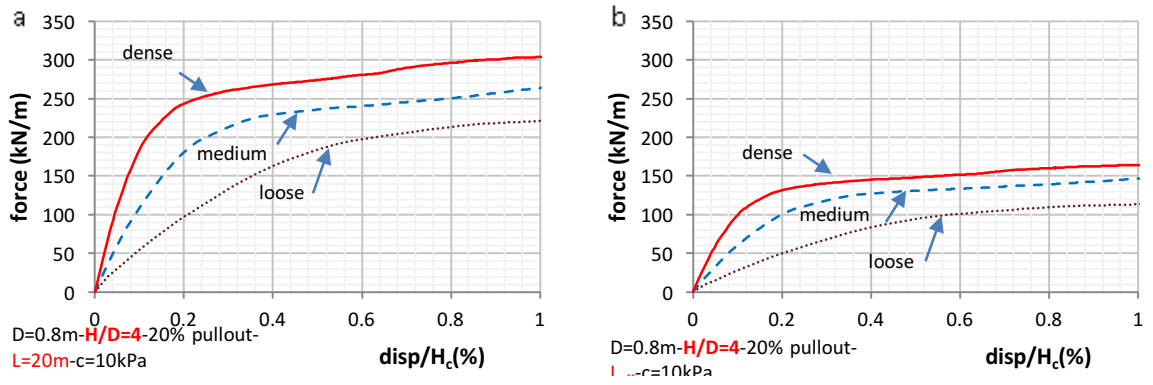
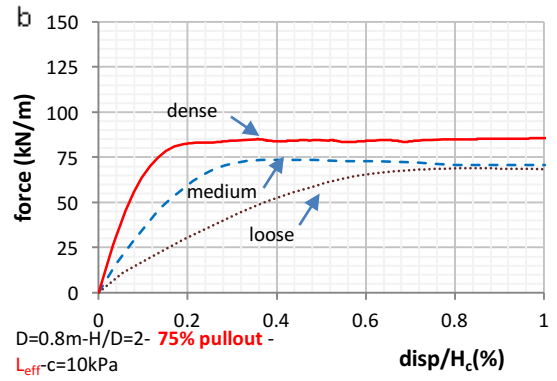
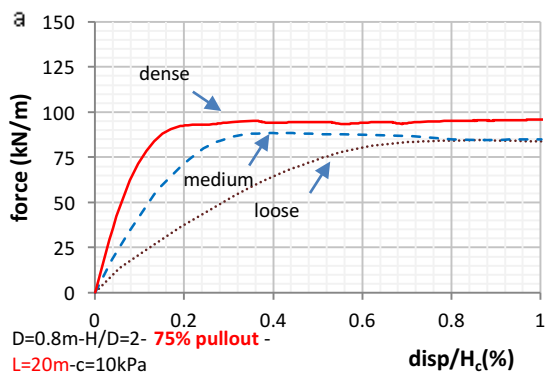
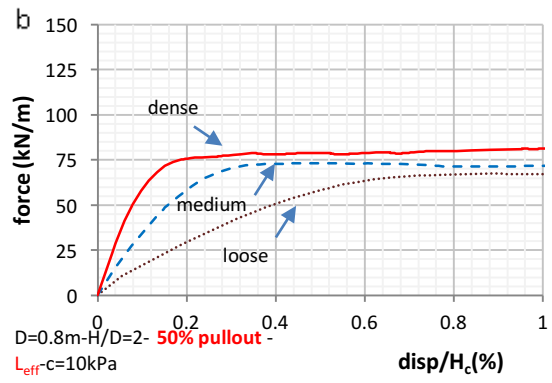
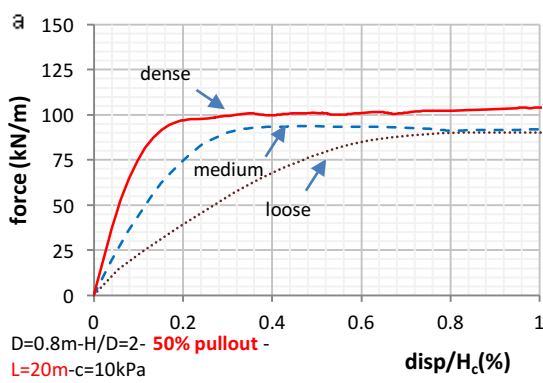
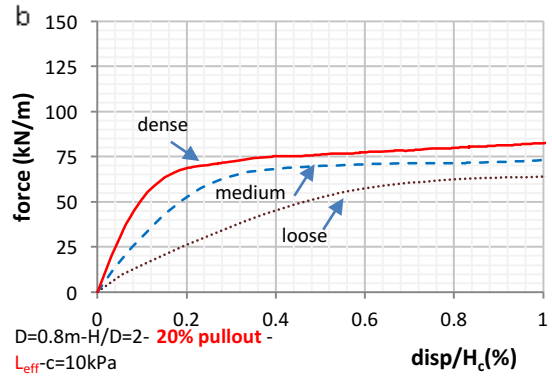
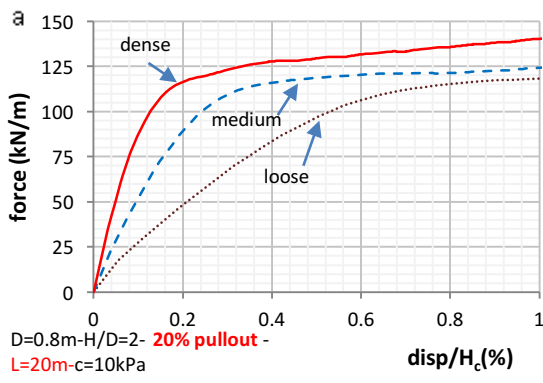


Figure 3.32 Load displacement curves F versus $disp/H_c$ for loose, medium dense and dense sand with fines for different embedment depths



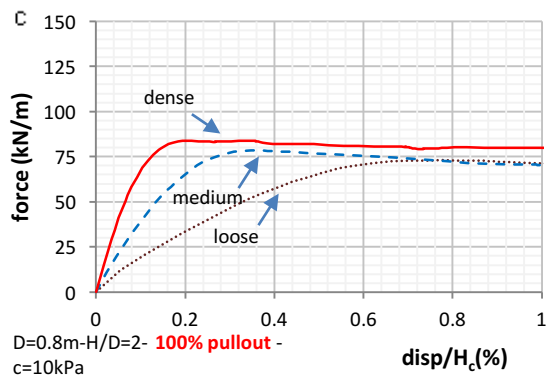
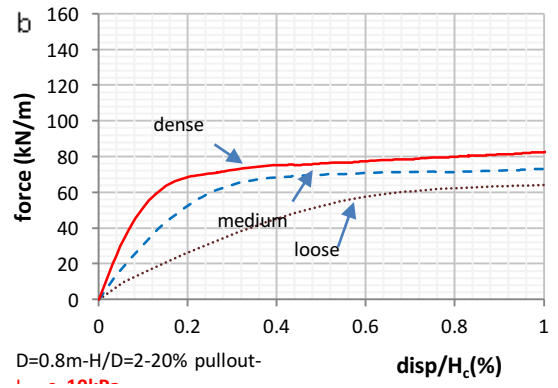
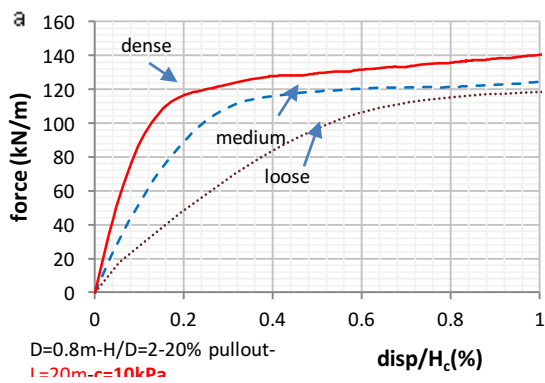
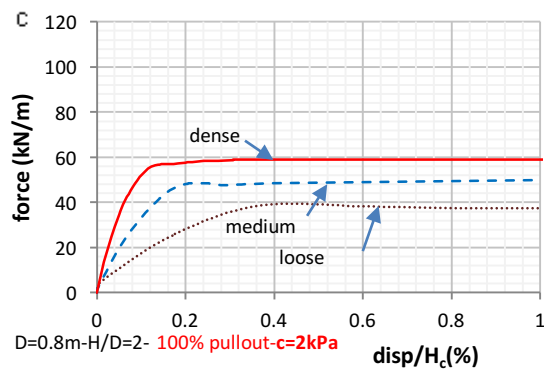
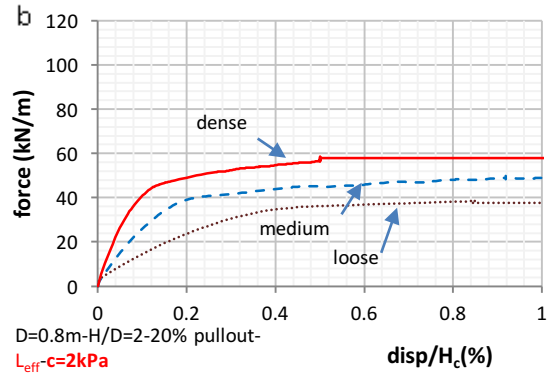
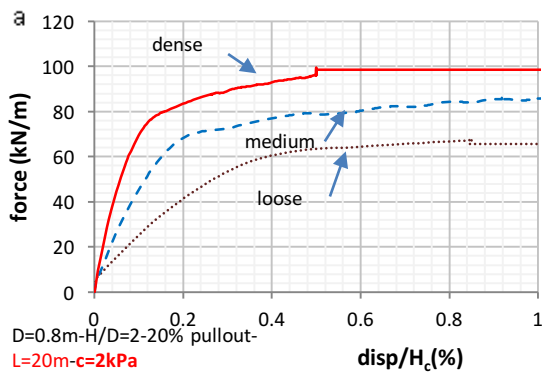
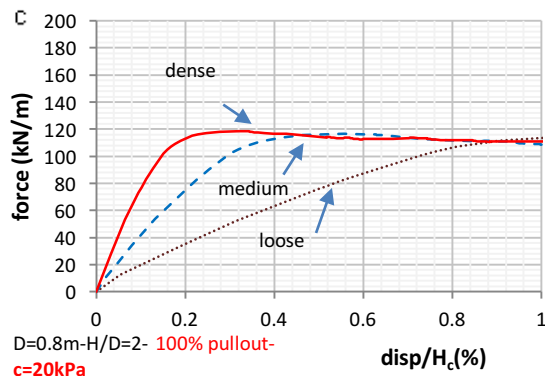
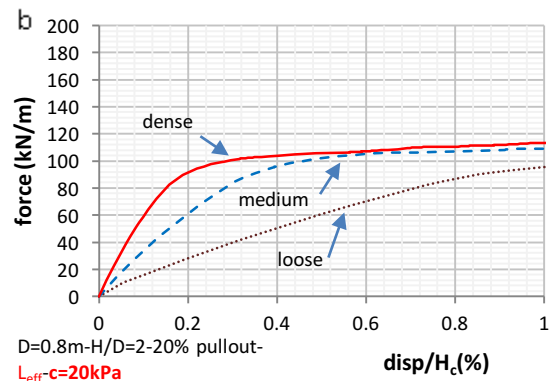
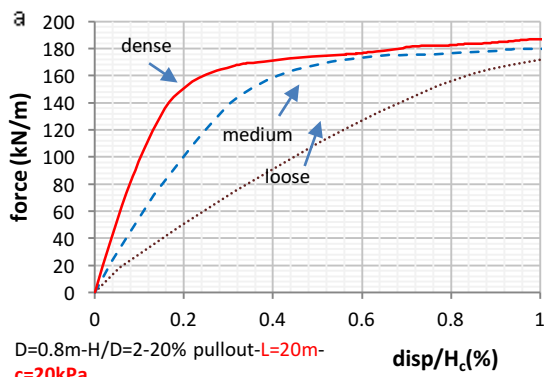
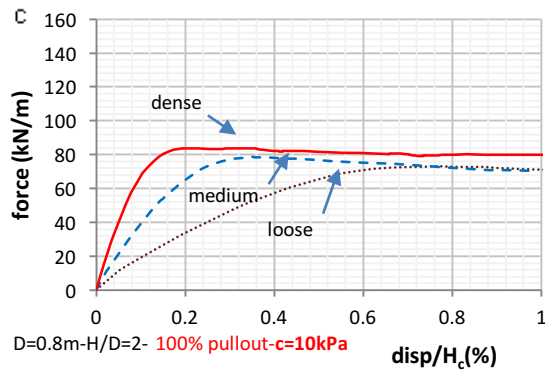


Figure 3.33 Load displacement curves F versus $disp/H_c$ for loose, medium dense and dense sand with fines for different pullout lengths





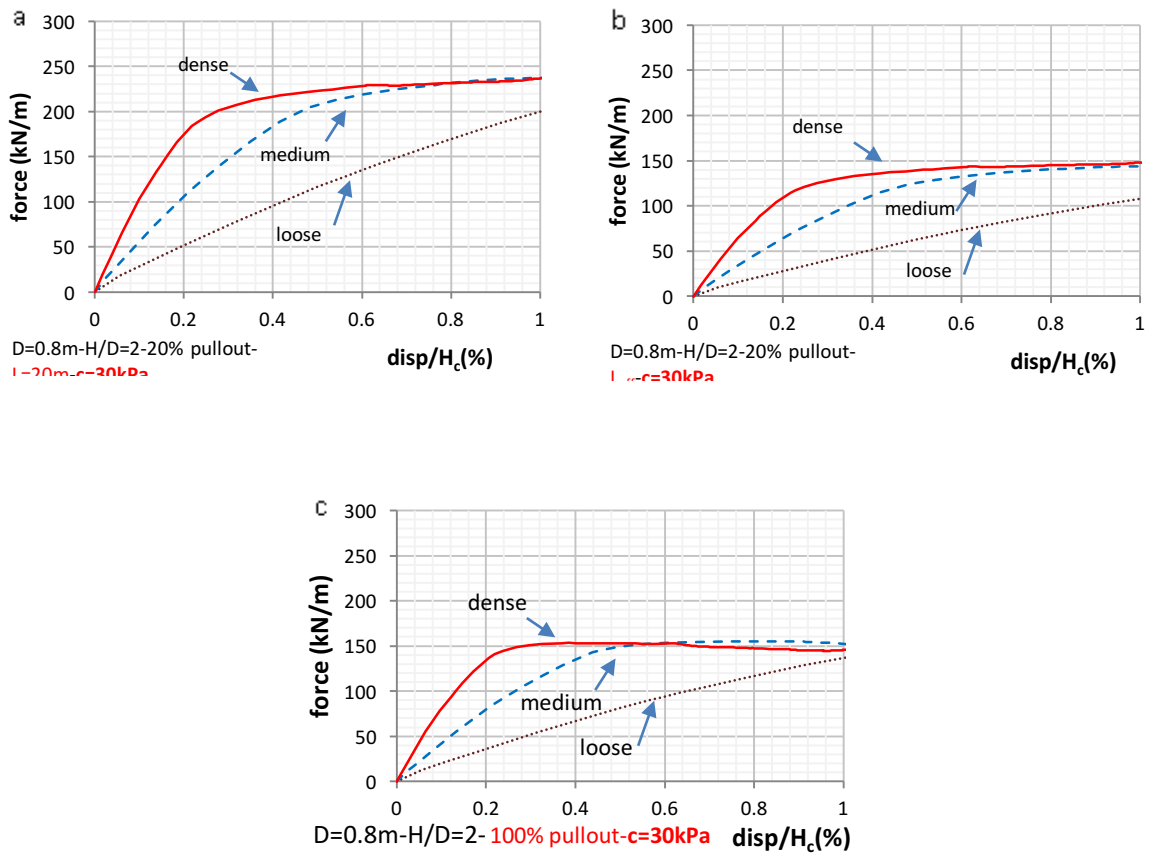


Figure 3.34 Load displacement curves F versus $disp/H_c$ for loose, medium dense and dense sand with fines for different soil cohesion and pullout lengths

E. Analytical Solutions

As presented earlier in Chapter I section A Analytical Studies, the soil uplift resistance against upheaval can be derived from two models: Vertical Slip Model and Sliding Block with Inclined Failure Surfaces (Figure 3.35). Moreover, the DNV (DET NORSKE VERITAS) practice describes this uplift resistance in the buried pipe design procedure.

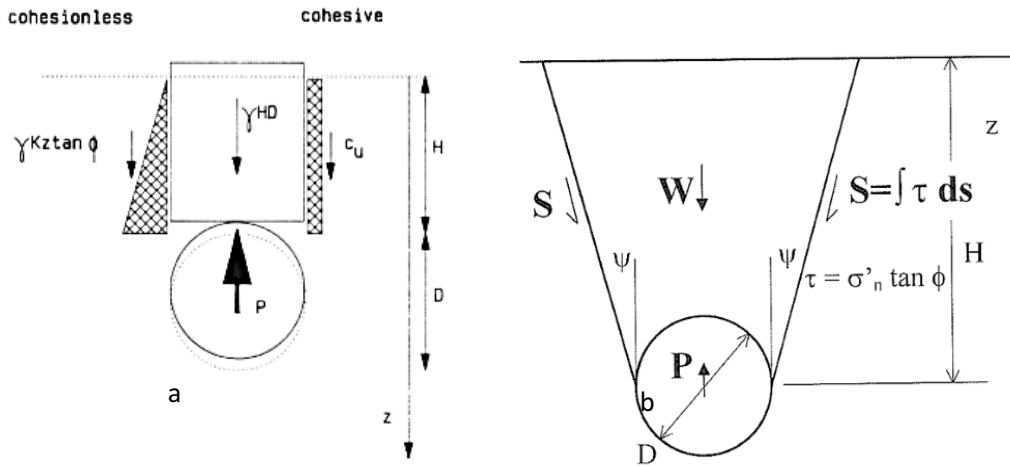


Figure 3.35 a) Vertical slip model (after Schaminee et al. (1990)) and b) Sliding block mechanism with shear planes at ψ to the vertical (after White et al. (2001))

The 100% pullout length cases corresponding to plain strain conditions were first compared with the analytical solutions. In order to allow for a proper comparison the cases analyzed numerically (FEM) in which the soil type adopted was a sand with fines type (with both friction and cohesion components of shearing resistance), the individual

analytical models which presented equations based on either cohesionless or cohesive soils were “merged” to produce “compounded hybrid solutions” which accounted for both (section 1 to 3 of this part) As shown in Figures 3.36 to 3.39, for the first set of analytical solutions, namely the Vertical Slip Model, Schaminee et al. (1990) and Palmer et al. (1990) do not appear to capture the results obtained from the FE analyses. The average bias factor corresponding to the ratio of “measured” (FE) over predicted (Analytical Models) results is around 1.4 to 2.1 for loose cases and 1.5 to 2 for medium dense and dense cases, respectively. The results obtained using the Bransby et al. (2002) solution are close to the FE results with an average bias factor of 1.17 for loose cases and 1.25 for medium dense and dense cases. For the second set of analytical solutions, DNV, DNV, max (2007) results are almost identical to the FE results with an average bias factor of 1.07 for all soil density cases. For the third set of analytical solutions, Sliding Block with Inclined Failure Surfaces, no solution is presented for cohesive soil. Thus, $2c_u(H+D/2)$ (or $2c_uH_c$) (per Bransby et al., 2002 and DNV, max, 2007) were added to the cohesionless equations to account for the cohesion component. White et al. (2001) combined equation results are very close to the FE results with an average bias factor of 1.08, 1.12 and 1.14 while Ng and Springman (1994) and Vermeer and Sutjiadi (1985) present upper bound solutions with average bias factors of 0.89 and 0.94, 0.92 and 0.97 and 0.93 and 0.99 for loose, medium dense and dense soil respectively. Since different pullout lengths load displacement curves when used with effective lengths intersect at large strains with 100% pullout cases that capture plain strain conditions, the analytical solutions were later compared with the corresponding FE parametric studies results.

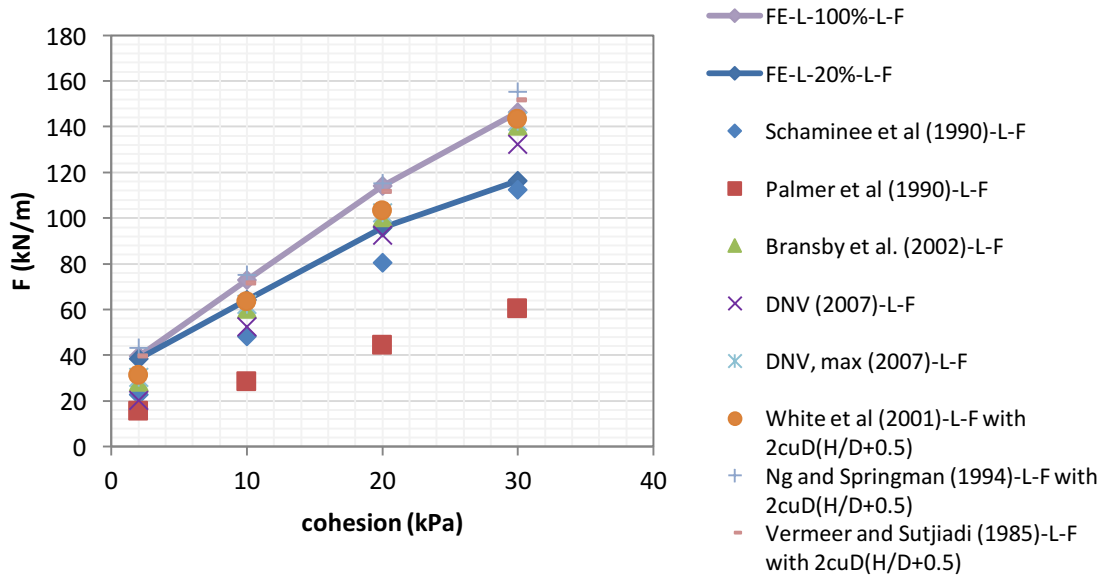


Figure 3.36 Uplift soil resistance versus Soil Cohesion for Loose Sand with Fines- 100% pullout length FE results and Analytical Solutions

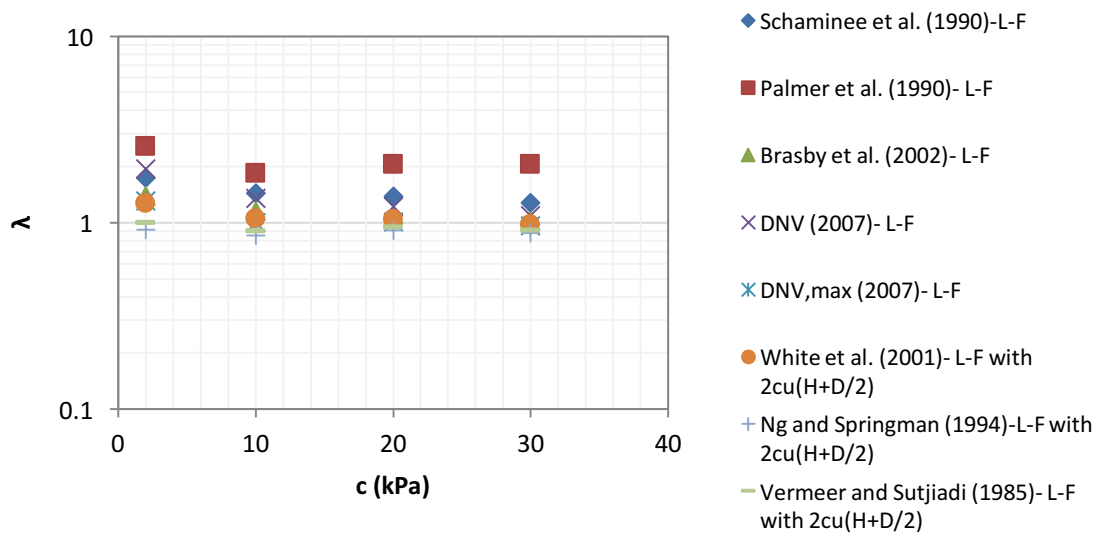


Figure 3.37 Bias Factor versus soil cohesion Analytical Solutions-Loose Sand with Fines

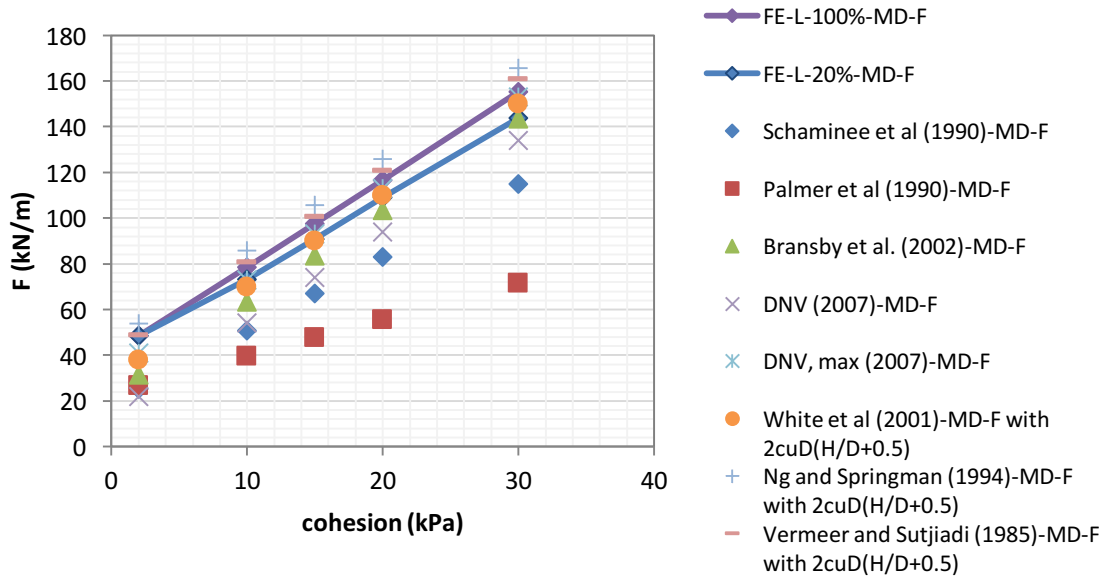


Figure 3.38 Uplift soil resistance versus Soil Cohesion for Medium Dense Sand with Fines- 100% pullout length FE results and Analytical Solutions

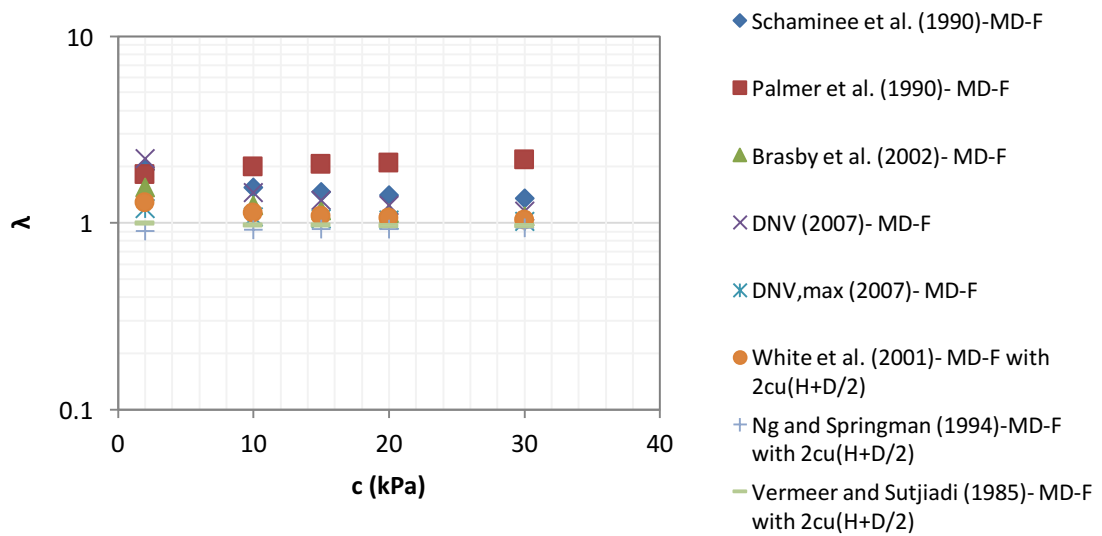


Figure 3.39 Bias Factor versus soil cohesion Analytical Solutions-Medium Dense Sand with Fines

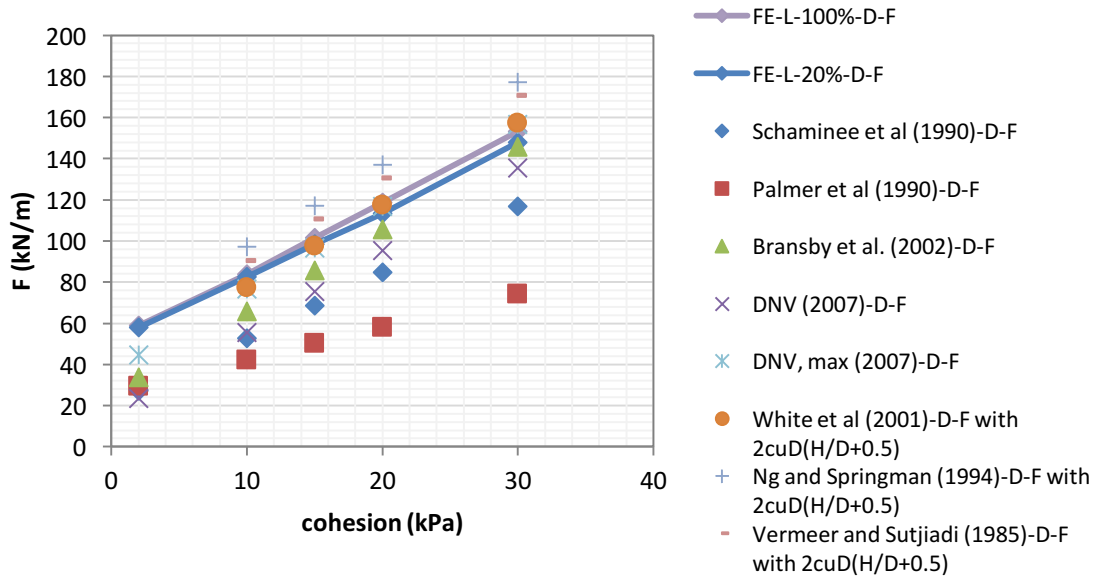


Figure 3.40 Uplift soil resistance versus Soil Cohesion for Dense Sand with Fines- 100% pullout length FE results and Analytical Solutions

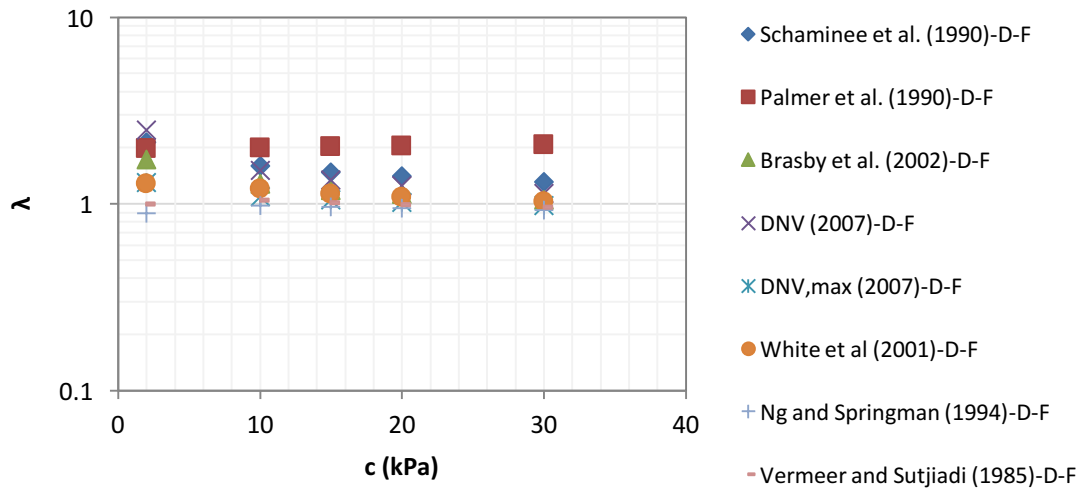


Figure 3.41 Bias Factor versus soil cohesion Analytical Solutions- Dense Sand with Fines

1. Vertical Slip Models

The maximum uplift resistance provided by the soil against upheaval buckling corresponds to the dead weight of the soil above the pipe along with the amount of friction being mobilized for cohesionless soil and the undrained behavior for cohesive soil. Several researchers derived this model:

- Schaminee et al. (1990)
 - Cohesionless soil: $F = \gamma'HD + H^2\gamma'K\tan\phi$
 - Cohesive soil: $F = \gamma'HD + 2Hc_u$

- Palmer et al. (1990)
 - Cohesionless soil: $F = \gamma'HD + f\gamma'H^2$
 - Cohesive soil: $F = c_u D \min[3, H/D]$

- Branby et al. (2002)
 - Cohesionless soil: $F = \gamma'HD[1 + 0.1D/H + K_o\tan\phi(H/D)(1 + D/(2H))^2]$
 - Cohesive soil: $F = \gamma'HD[1 + 0.1D/H + 2c_u/(\gamma'H)(H/D + 0.5)]$

The FE uplift resistances divided by effective lengths results were drawn as bounds in Figures 3.42 to 3.45. These figures present the variation of the uplift soil resistance with the pipe diameter, embedment depth, pullout section and soil cohesion for loose, medium dense and dense sand with fines (L-F, MD-F and D-F) Vertical Slip Model analytical solutions. The variation of the bias factor: ratio of measured (FE) over predicted (Analytical Solution) plots are presented in Appendix D. The results show that Bransby et al. (2002) combined solutions are the closest to FE bounds corresponding to the uplift

resistance divided by the effective length and confirming the 100% pullout cases (corresponding to plain strain conditions). However, the average bias factor for the uplift resistance divided by the effective lengths decrease from 1.17, 1.23 for the 100% cases to around 1.05, 1.18 for loose and medium dense cases and remains equal to 1.27 for dense cases. As for Schaminee et al. (1990) and Palmer et al. (1990) combined solutions, they are still far from the FE bound with average bias factors between 1.3 and 2.47 for all soil densities.

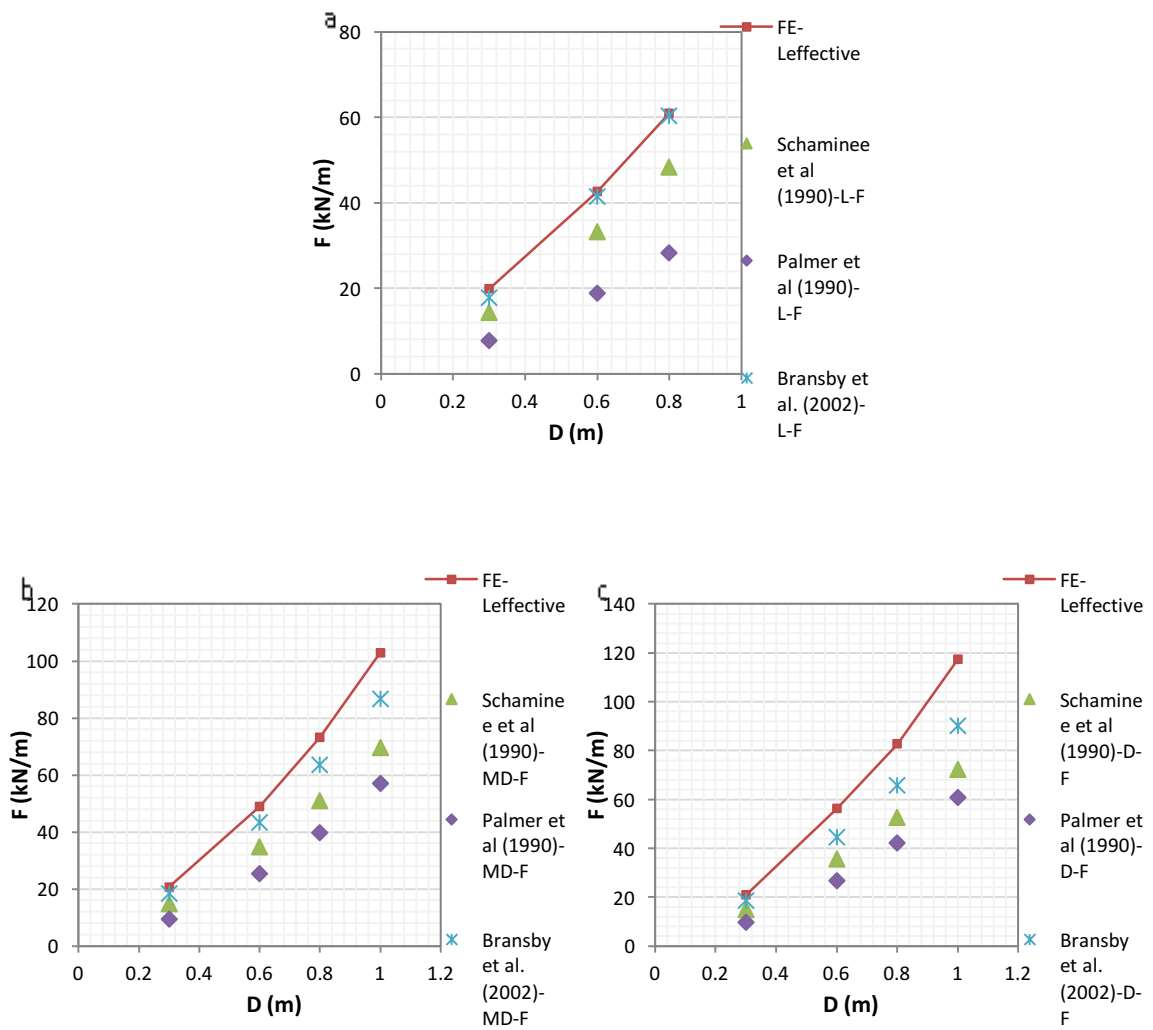


Figure 3.42 Uplift soil resistance versus pipe diameter a) Loose b) Medium Dense and c) Dense sand with Fines- FE and Vertical Slip Model Analytical Solutions

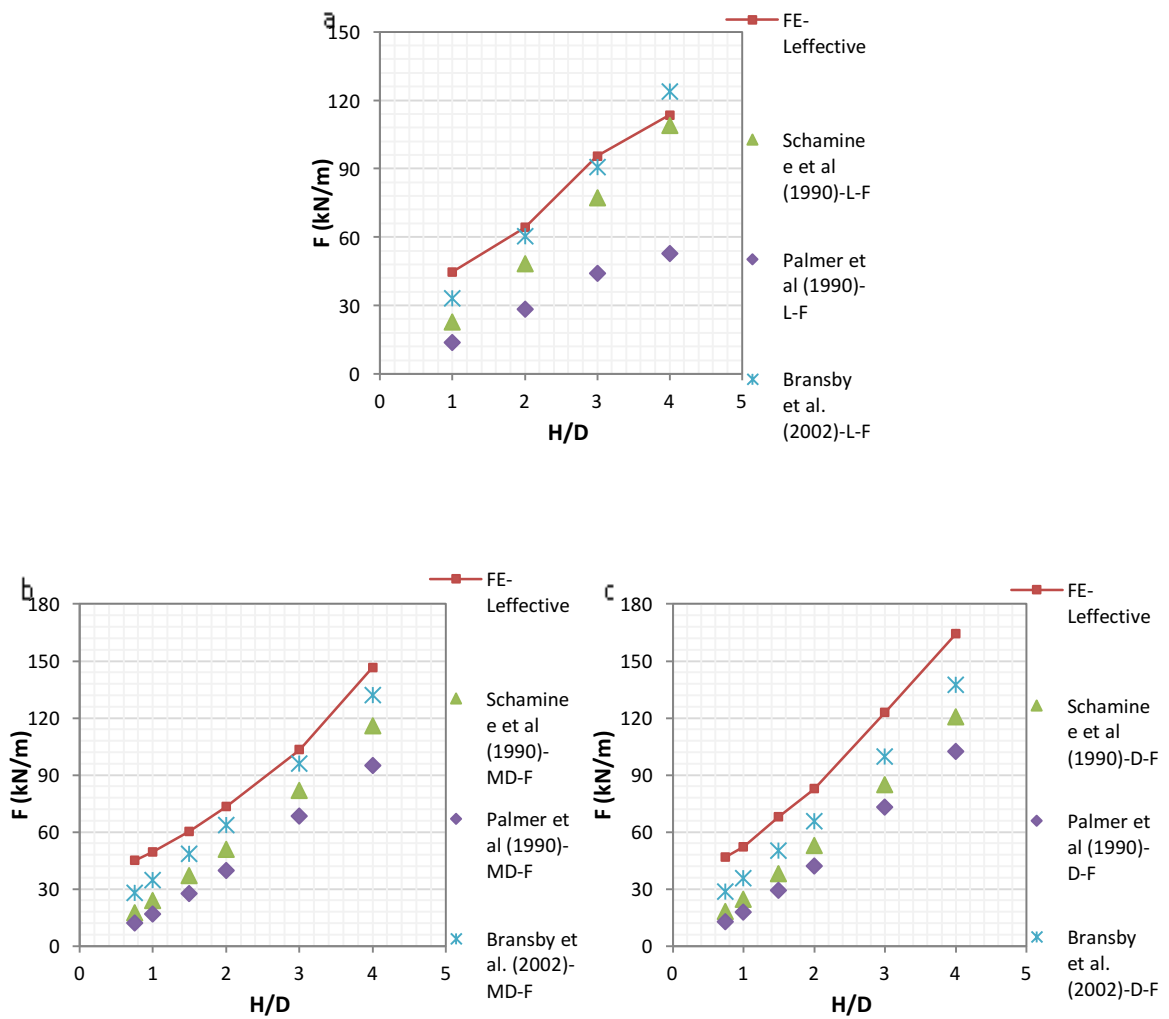


Figure 3.43 Uplift soil resistance versus embedment depth a) Loose b) Medium Dense and c) Dense sand with Fines - FE and Vertical Slip Model Analytical Solutions

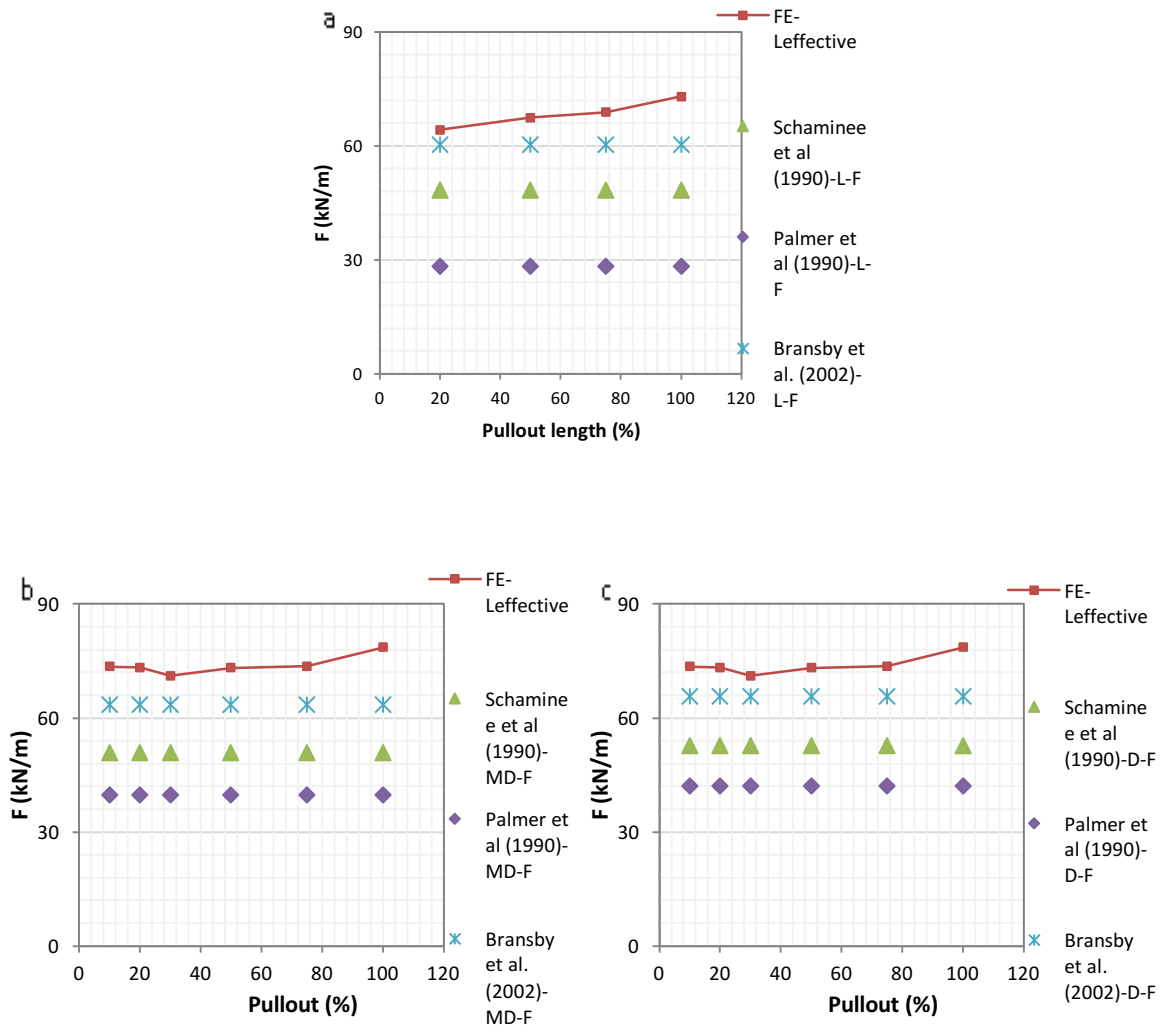


Figure 3.44 Uplift soil resistance versus pullout length a) Loose b) Medium Dense and c) Dense sand with Fines - FE and Vertical Slip Model Analytical Solutions

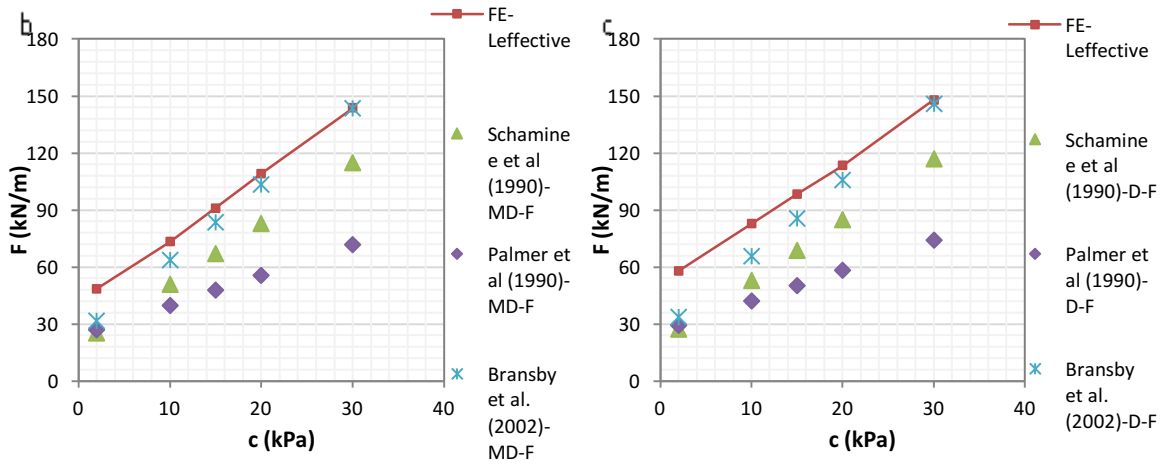
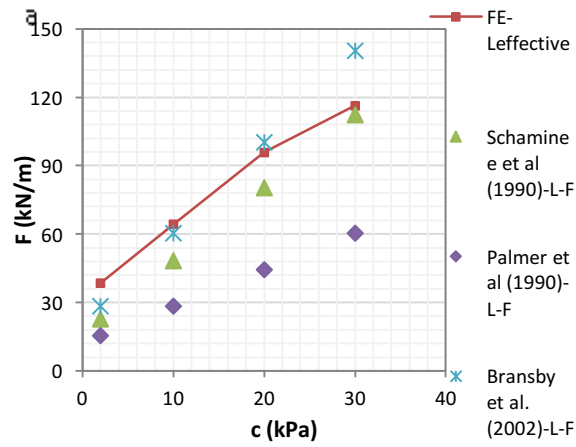


Figure 3.45 Uplift soil resistance versus soil cohesion a) Loose b) Medium Dense and c) Dense sand with Fines - FE and Vertical Slip Model Analytical Solutions

2. DNV

DNV (DET NORSKE VERITAS) presents a design procedure for buried pipelines to remain in place for a given probability of failure in the DNV-RP-F110 "Global Buckling of Submarine Pipelines" in October 2007 recommended practice. Buried pipelines, under a given temperature and pressure, are exposed to compressive axial forces that lead the pipe to displace in the vertical direction if the soil cover does not provide enough resistance.

Pipelines are buried to avoid global buckling. Global buckling or shallow wedge failure is a failure mode described by soil material displaced upward forming soil heave at the seabed surface. For shallow pipe embedment depths ($H_c/D < 4.5$), the maximum soil resistance, presented by global soil failure, is described by the vertical slip model that includes the weight of the soil column above the pipeline.

For cohesionless soil, a tri-linear model in section B.3.2 in DNV-RP-F110 (2007) presents the uplift soil resistance. This upward resistance (including the shear and the weight) increases until the pipeline reaches the mobilization distance:

- Cohesionless soil: $F = \gamma'HD[1 + (0.5 - \pi/8)D/H + f_p/(\gamma'HD)(H + D/2)^2]$

However, this model does not present the full force-displacement relation for a large-displacement pipeline. The full relation is described in the expression in section B.3.3 in the current practice: model for uplift resistance and load-displacement curve that considers the weight of the soil above the pipe and the soil friction component:

- DNV, max (2007), Cohesionless soil: $F = (\gamma'H_cD)(1 + fH_c/D)$ with $f = K \tan \phi$
 - For loose sand, $K = k_o = 1 - \sin \phi$
 - For medium and dense sand, $K = K_p$, $f = \tan \phi / \sqrt{(1 + \tan^2 \phi) - \tan \phi \sqrt{1 + r}}^2$ with $r = -1$.

The maximum uplift resistance is mobilized at a vertical uplift resistance between 0.5-1%H and independent of the embedment depth ratio H/D.

For cohesive soil, two failure modes are presented in section B.4 of the DNV-RP-F110 (2007) practice: local and global (Figure 3.46). In a local failure mode, soil is displaced around and beneath the pipeline and depends on the shear strength at the corresponding pipe depth while in a global failure mode, a soil wedge is formed above the pipe extending to the seabed surface and depends on soil weight and shear resistance. In drained conditions, the uplift resistance is equal to the cohesionless soil cover resistance. However, in undrained conditions, the uplift resistance depends on undrained shear strength of the trench material. For small embedment depths ($H_c/D < 4.5$), the maximum soil resistance is related to global soil failure. Thus, the uplift resistance in cohesive soil for global shallow shear failure mode described in section B.4.3.2 in the DNV-RP-F110 (2007) practice is:

- Cohesive soil: $F = \gamma'HD + \gamma'D^2(0.5 - \pi/2) + 2c_u(H + D/2)$.

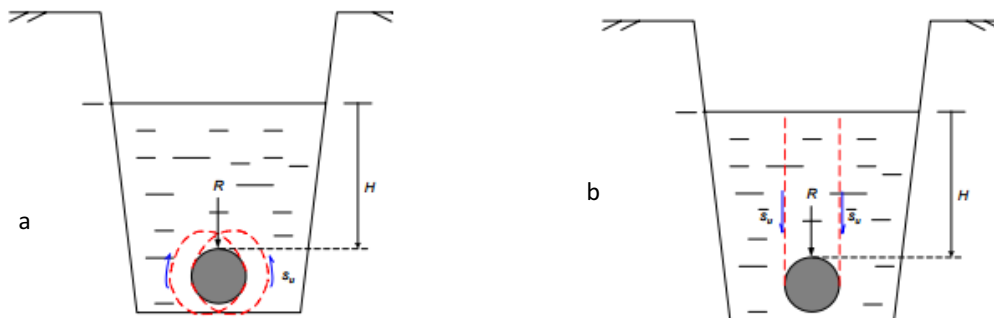


Figure 3.46 a) Local and b) Global soil failure modes

The DNV and DNV, max design equations were combined with the cohesive soil for global shallow shear failure mode design equation to describe loose, medium dense and dense with fines type (L-F, MD-F, D-F); the extra component is equal to $2c_u(H+D/2)$. The FE uplift resistances divided by effective pipe lengths results were drawn as bounds in Figures 3.47 to 3.50. These figures present the variation of the uplift soil resistance with the pipe diameter, embedment depth, pullout section and soil cohesion for combined DNV design equations. The variations of the uplift resistance bias factors for loose, medium dense and dense sand with fines are presented in Appendix D. The combined DNV, max solution is closer to the FE bound with average bias factor of around 1.03 for loose and medium dense sand and around 1.09 for dense sand than DNV (2007) combined solution confirming the 100% pullout cases with average bias factors between 1.047 to 1.6 for all soil densities.

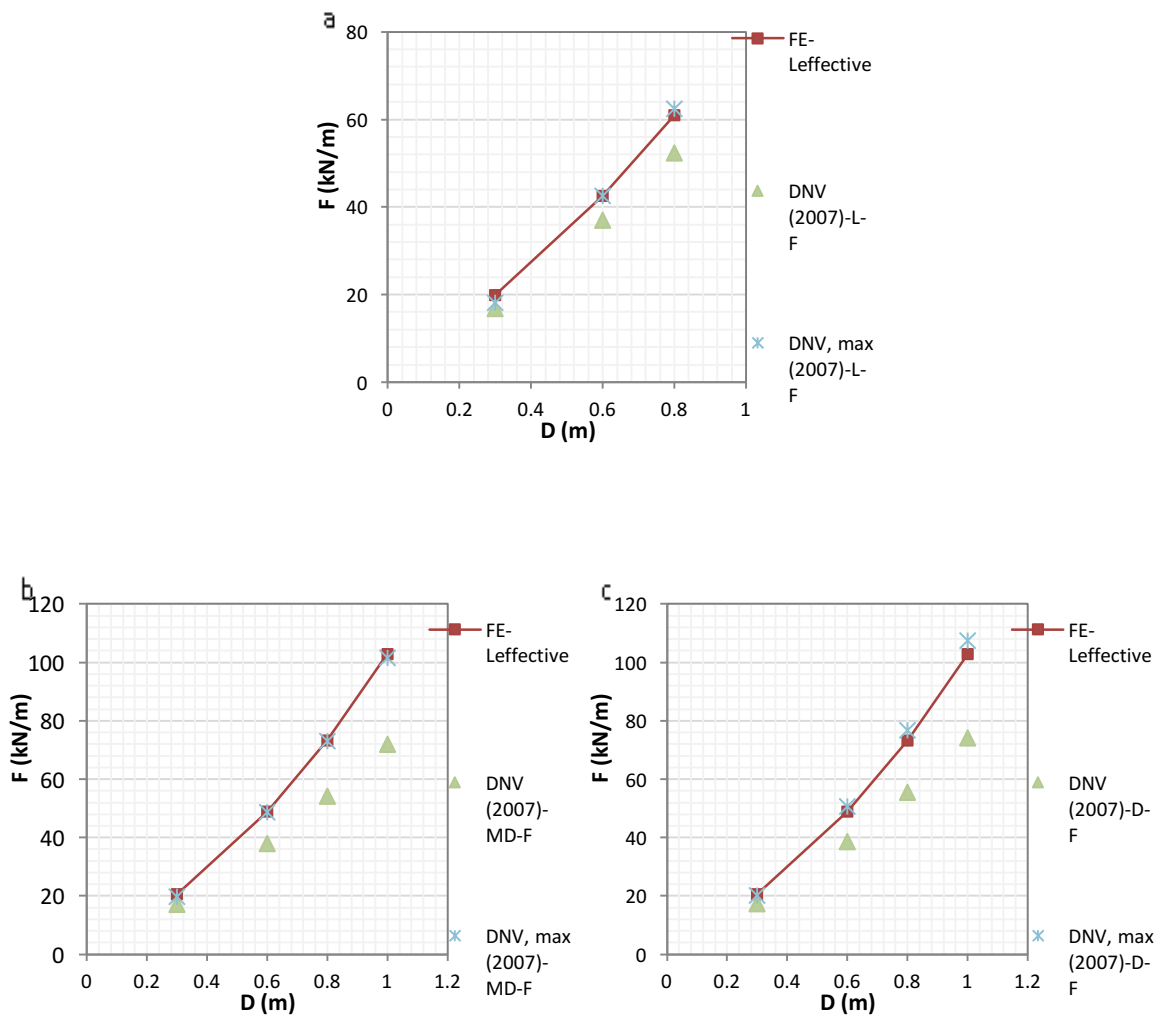


Figure 3.47 Uplift soil resistance versus pipe diameter a) Loose b) Medium Dense and c) Dense sand with Fines - FE and DNV Analytical Solutions

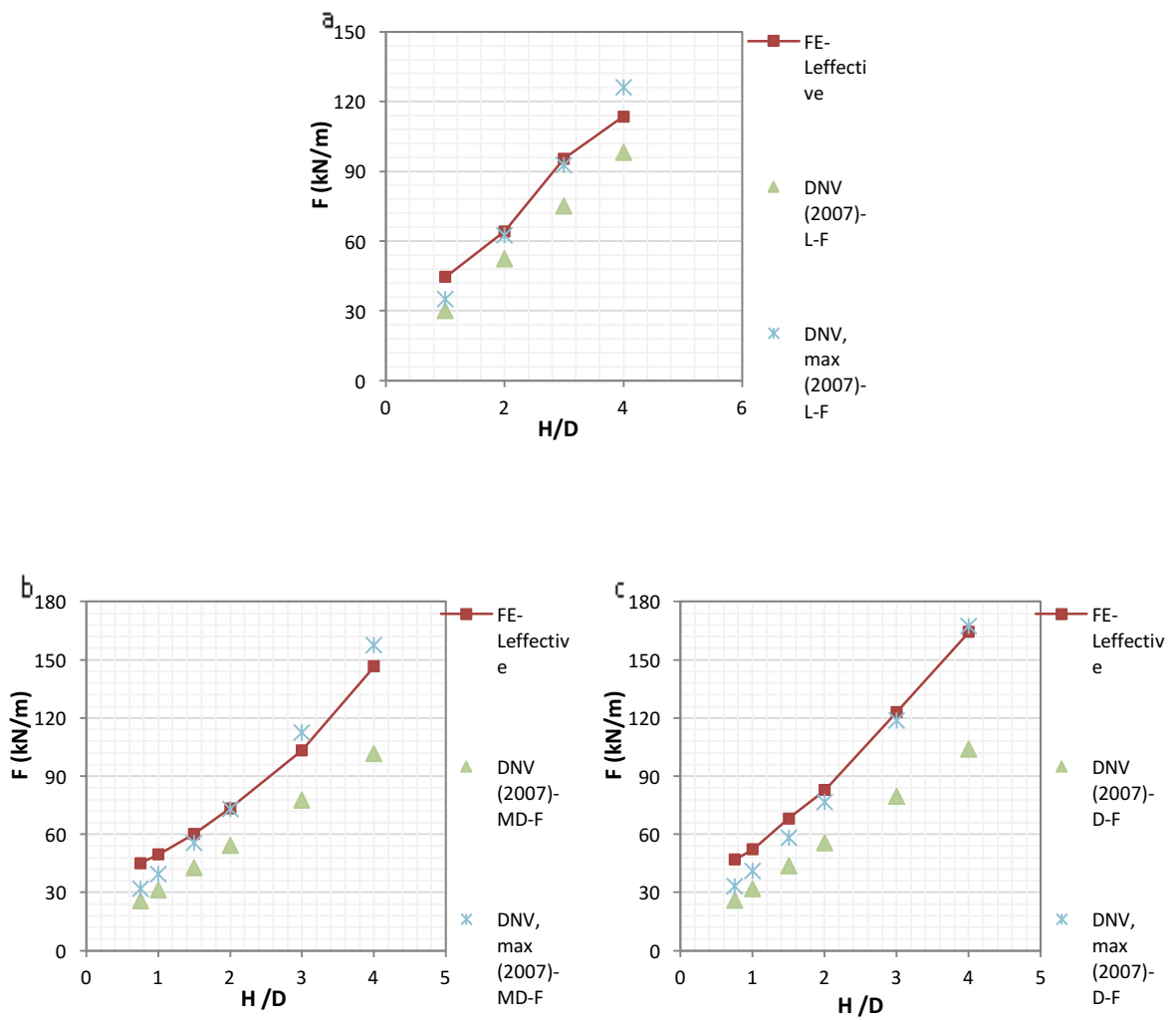


Figure 3.48 Uplift soil resistance versus embedment depth a) Loose b) Medium Dense and c) Dense sand with Fines - FE and DNV Analytical Solutions

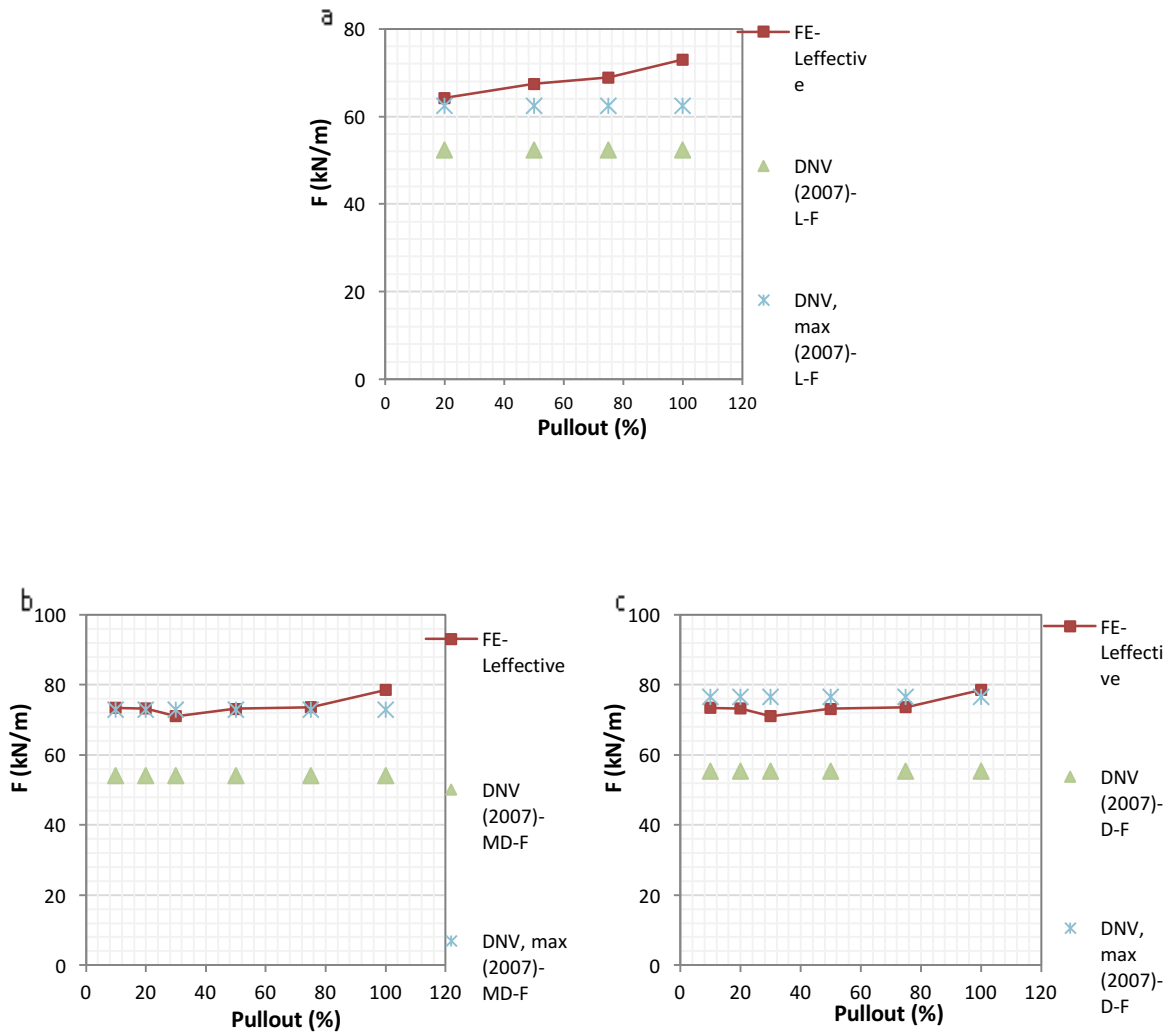


Figure 3.49 Uplift soil resistance versus pullout length a) Loose b) Medium Dense and c) Dense sand with Fines - FE and DNV Analytical Solutions

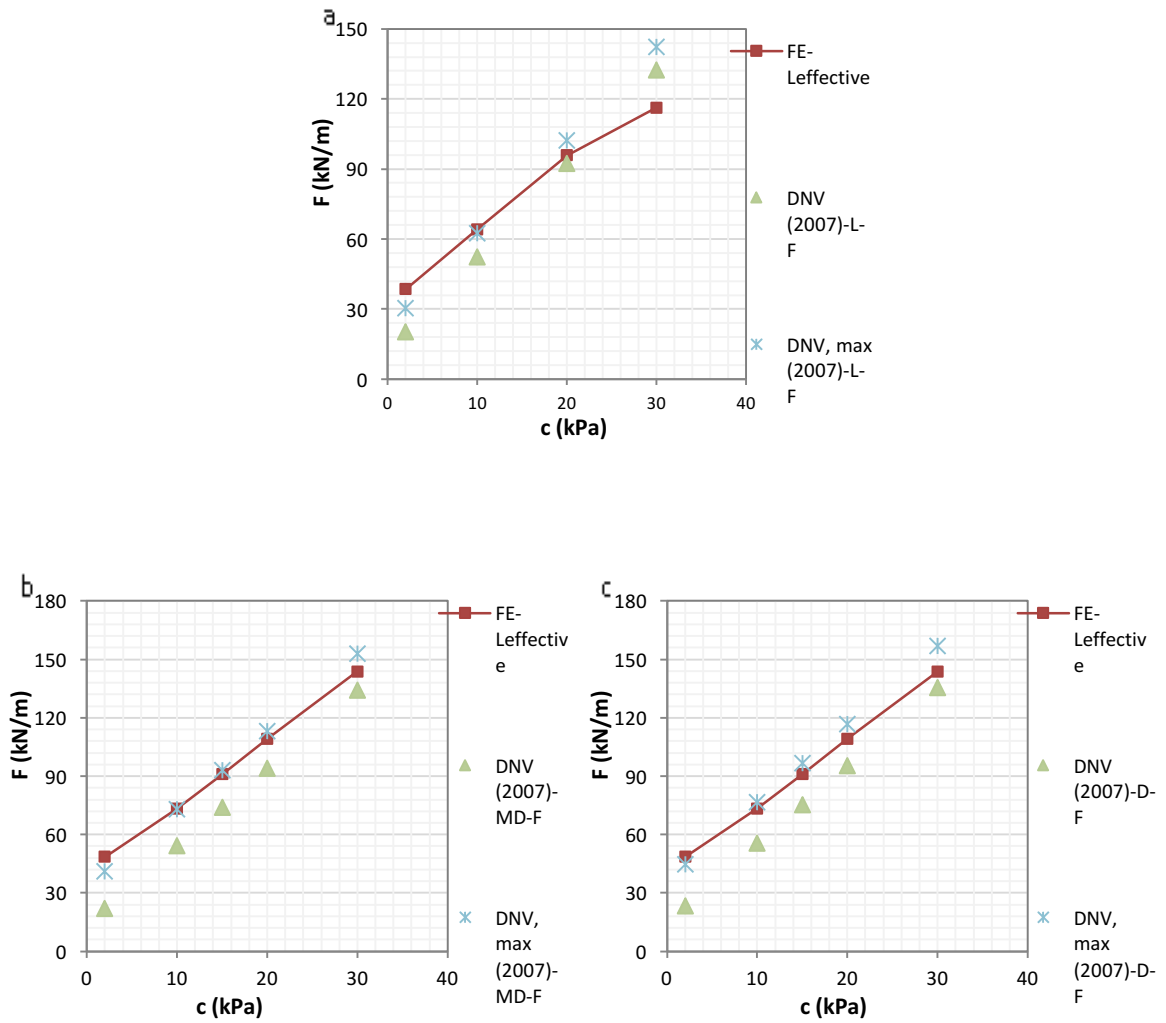


Figure 3.50 Uplift soil resistance versus soil cohesion a) Loose b) Medium Dense and c) Dense sand with Fines - FE and DNV Analytical Solutions

3. Sliding Block with Inclined Failure Surfaces

The difference between the Vertical Slip model and the Sliding Block with Inclined Failure Surface is that the shearing plane is inclined at an angle equal to the dilation angle to the vertical. This difference is illustrated by the addition of the soil weight and the change in length and normal stress on the shear plane. Several researchers derived this model:

- White et al. (2001)
 - $F = \gamma'HD + \gamma'H^2 \tan \psi + \gamma'H^2 (\tan \phi_{\text{peak}} - \tan \psi) [(1 + K_o)/2 - (1 - K_o)(\cos 2\psi)/2]$
- Ng and Sprigman (1994)
 - Cohesionless soil: $F = \gamma'HD + H^2 \gamma' \tan \phi_{\text{max}}$
- Vermeer and Sutjiadi (1985)
 - Cohesionless soil: $F = \gamma'HD + H^2 \gamma' \tan \phi_{\text{max}} \cos \phi_{\text{crit}}$

It was shown in the last two sections the importance of the cohesion component in the uplift soil resistance against upheaval for sand with fines. To account for the undrained soil behavior, the extra components corresponding to the soil cohesion in the Analytical Solutions were added to the Sliding Block Models:

- $2Hc_u$ (per Schaminee et al. (1990)) (Figures in Appendix C)
- $c_u D \min(3, H/D)$ (per Palmer et al. (1990)) (Figures in Appendix C)
- $c_u D (H/D + 0.5)$ (per Bransby et al. (2002) and DNV_{,max} (2007)) (Figures 3.52 to 3.55)

The variations of the uplift resistance bias factors for loose, medium dense and dense sand with fines are presented in Appendix D. A significant increase in the uplift

resistances is illustrated by the use of the cohesion component. The most considerable improvement is the addition of $2H_c c_u$ for White et al. (2001) solution: the combined results fall along the FE bound corresponding to the uplift resistance divided by the effective length and with average bias factors of 1.05 for all soil densities. Ng and Sprigman (1994) and Vermeer and Sutjiadi (1985) combined solutions fall above the FE bounds presenting upper bound solutions and confirming the 100% pullout length cases with average bias factors between 0.87 and 0.95 for all soil densities. (Figures 3.52 to 3.55). Thus, combined White et al. (2001) and $2H_c c_u$ model is the closest to the FE results. The FE model is best described as Sliding Block with Inclined Failure Surface model as shown in figure 3.51.

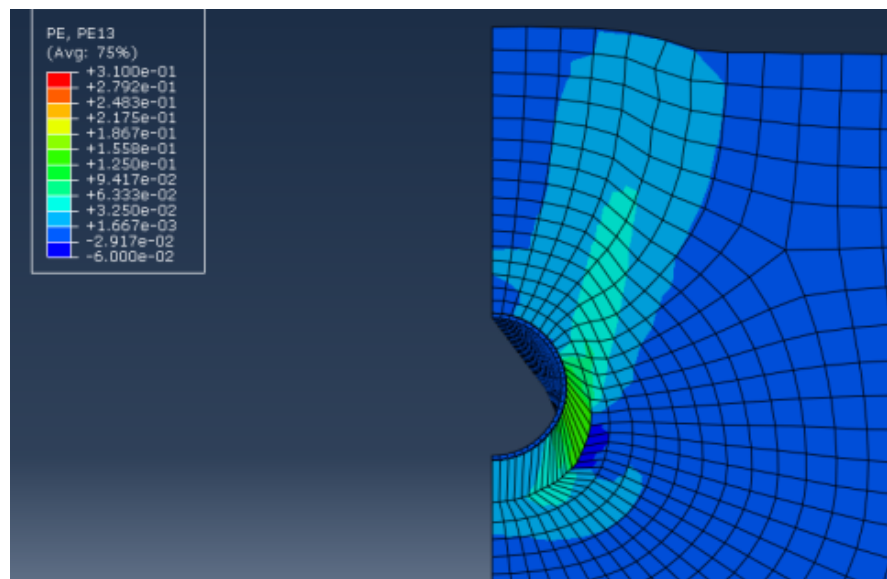


Figure 3.51 Shear strain plot

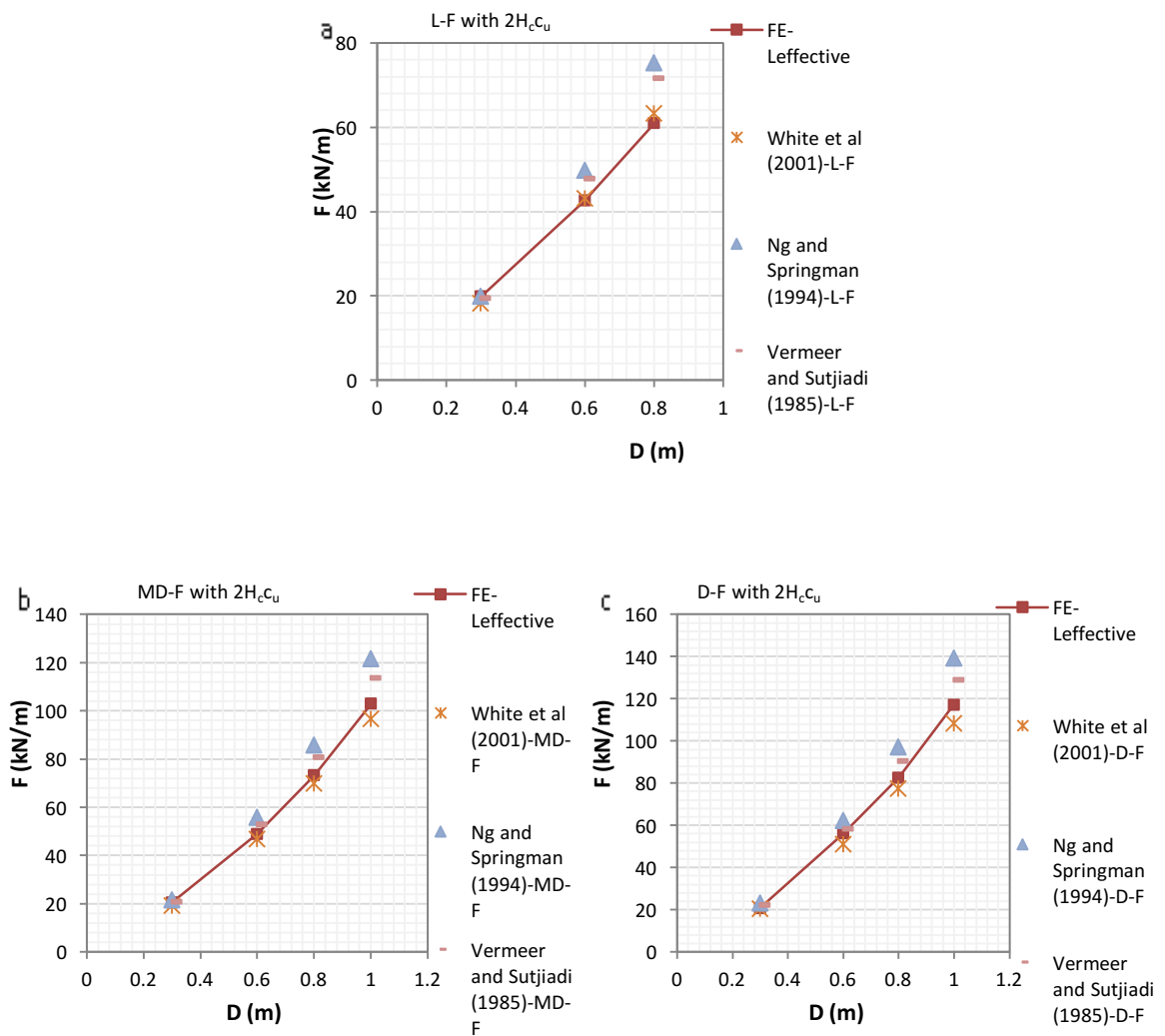


Figure 3.52 Uplift soil resistance versus pipe diameter a) Loose b) Medium Dense and c) Dense sand with Fines - FE and Inclined Failure Surface Analytical Solutions

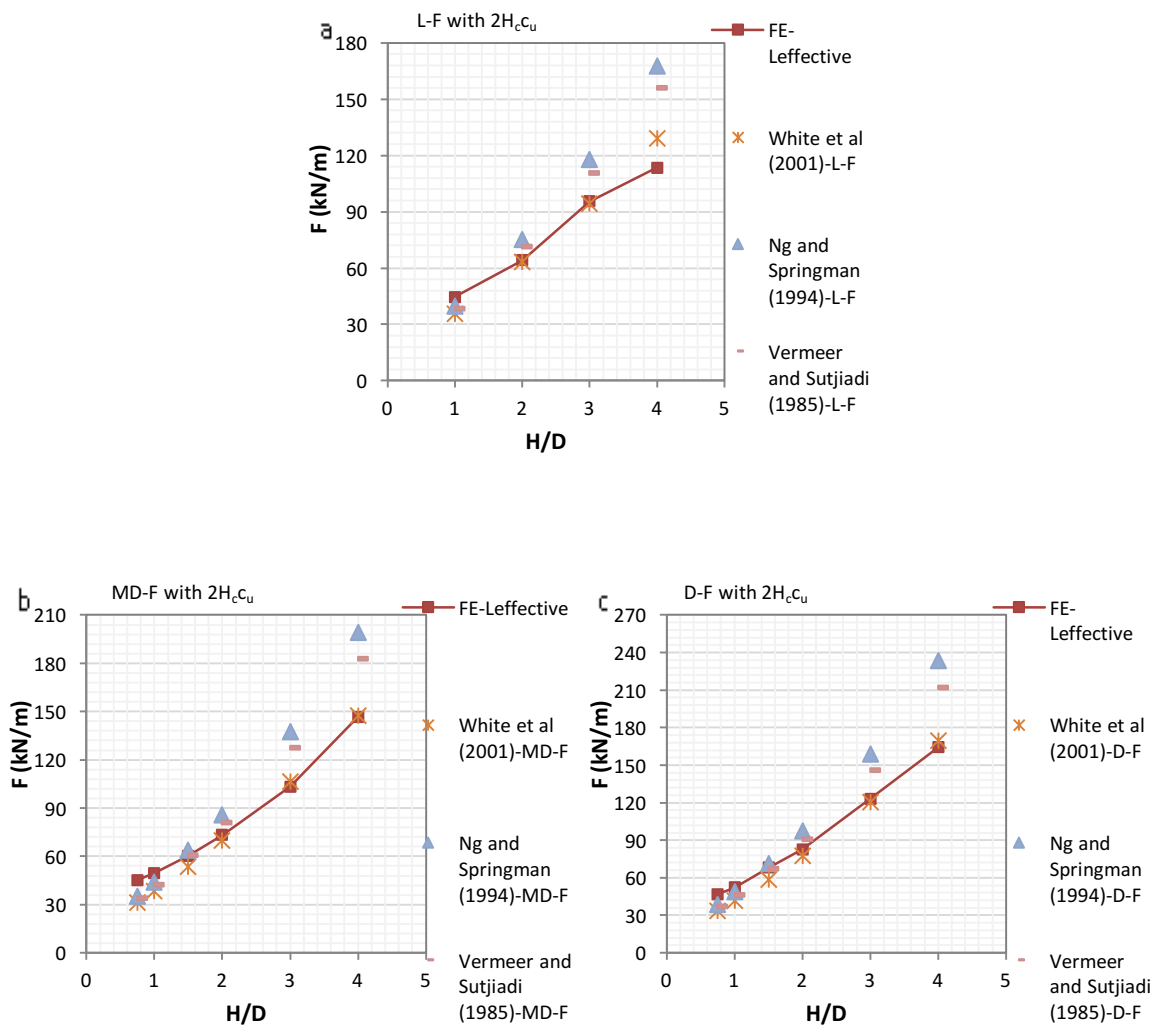


Figure 3.53 Uplift soil resistance versus Embedment Depth a) Loose b) Medium Dense and c) Dense sand with Fines - FE and Inclined Failure Surface Analytical Solutions

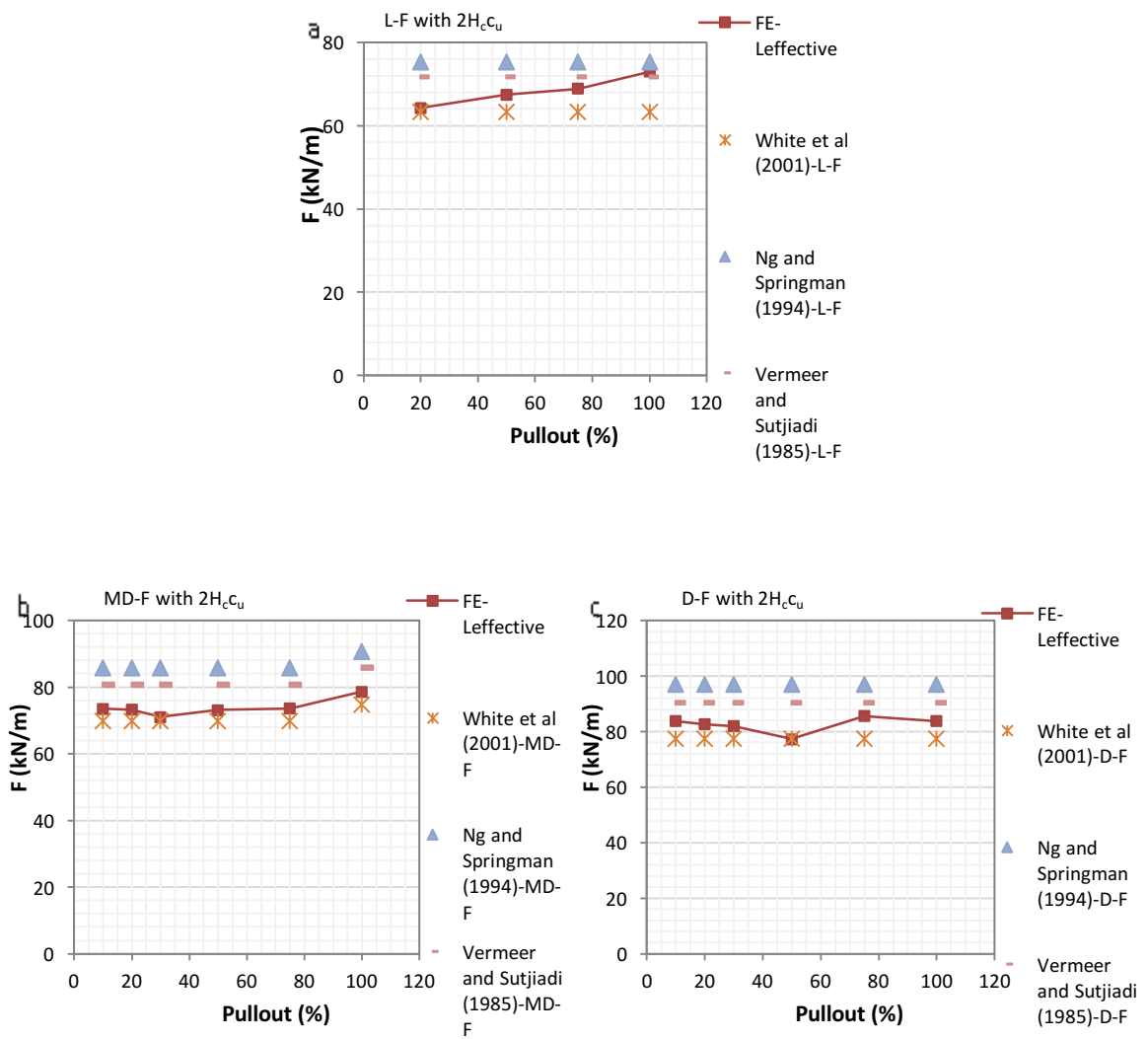


Figure 3.54 Uplift soil resistance versus pullout length a) Loose b) Medium Dense and c) Dense sand with Fines - FE and Inclined Failure Surface Analytical Solutions

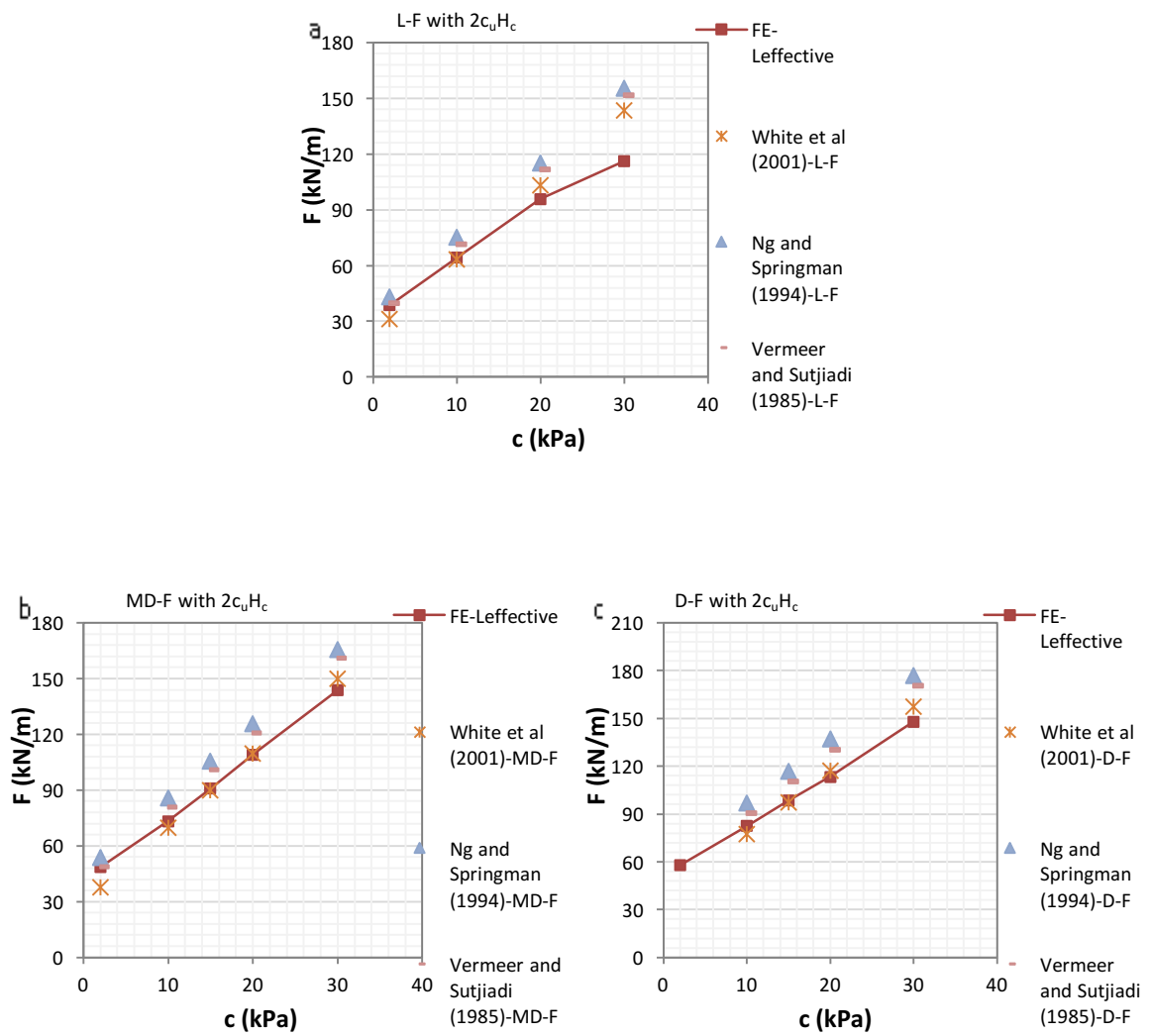


Figure 3.55 Uplift soil resistance versus soil cohesion a) Loose b) Medium Dense and c) Dense sand with Fines - FE and Inclined Failure Surface Analytical Solutions

CHAPTER IV

SIMPLIFIED APPROACH TO CALCULATE THE UPLIFT RESISTANCE

A. Empirical Approach

Based on the finite element simulations, a simplified approach to calculate the uplift resistance is presented. This approach consists of calculating the maximum uplift resistance for different soil densities (loose: $\gamma' 8.8 \text{ kN/m}^3$, $\phi_{\text{peak}} 35^\circ$, medium dense: $\gamma' 9.2 \text{ kN/m}^3$, $\phi_{\text{peak}} 40^\circ$ and dense: $\gamma' 10.2 \text{ kN/m}^3$, $\phi_{\text{peak}} 45^\circ$ sand with fines) based on the normalized uplift resistance $[F/(c.D)]$. The normalized uplift resistance allowing to obtain the resistance for different embedment depths for 0.8m diameter pipeline pulled at its middle by 20% pullout length with 10 kPa soil cohesion value is corrected for pipeline diameter, pullout length and soil cohesion value. The normalized uplift resistance as well as the pipeline diameter, pullout length and soil cohesion correction coefficient equations were obtained by exponential, linear and power regression of the finite element results as presented in figure 4.1.

The maximum uplift resistance can be calculated as follow:

$$F_{\text{max}} = (F_u * C_D * C_{PL} * C_C) * c * D$$

Where: F_{max} = maximum uplift resistance (kN/m)

F_u = normalized uplift resistance = $F/(cD)$

F = uplift resistance (kN/m)

c = soil cohesion value (kPa)

D = pipeline diameter (m)

PL = pullout length (%)

H/D = pipe embedment depth or soil cover depth

C_D = diameter correction coefficient

C_{PL} = pullout length correction coefficient

C_c = soil cohesion correction coefficient

For Loose sand with fines (L-F):

$$F_u = 4.1e^{0.315H/D} \text{ for } D=0.8\text{m, } 20\% \text{ pullout length, } c=10 \text{ kPa}$$

$$C_D = 0.26*D + 0.79$$

$$C_{PL} = 0.002(PL) + 0.96$$

$$C_c = 5c^{-0.67}$$

For Medium dense sand with fines (MD-F):

$$F_u = 4.35e^{0.36H/D} \text{ for } D=0.8\text{m, } 20\% \text{ pullout length, } c=10 \text{ kPa}$$

$$C_D = 0.53*D + 0.58$$

$$C_{PL} = 0.001(PL) + 0.96$$

$$C_c = 5c^{-0.67}$$

For Dense Sand with fines (D-F):

$$F_u = 4.65e^{0.37H/D} \text{ for } D=0.8\text{m, } 20\% \text{ pullout length, } c=10 \text{ kPa}$$

$$C_D = 0.65*D + 0.49$$

$$C_{PL} = 1$$

$$C_c = 5c^{-0.67}$$

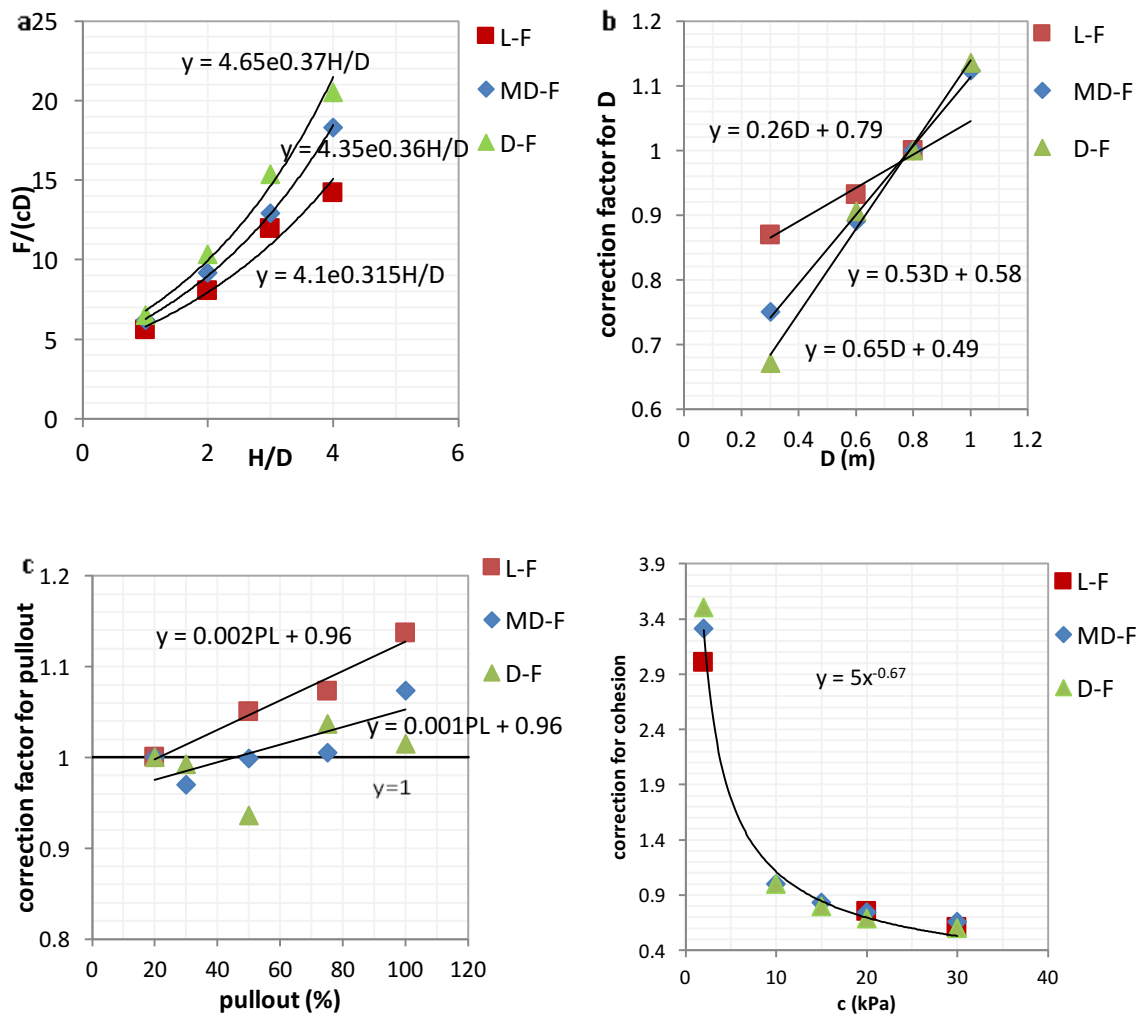


Figure 4.1 Variation of a) normalized uplift resistance exponential regression for different embedment depths, b) pipeline diameter linear regression correction coefficient, c) pullout length linear regression correction coefficient and d) soil cohesion power regression correction coefficient

B. Example

The maximum uplift resistance for 0.6m diameter pipeline embedded in medium dense sand with fines ($\gamma' 9.2 \text{ kN/m}^3$, $\phi_{\text{peak}} 40^\circ$) with 20 kPa cohesion value at $H/D=1$ is

equal to $F_{\text{max}} = (F_u * C_D * C_{PL} * C_C) * c * D$

$$F_u = 4.35e^{0.36H/D} \text{ for } D=0.8\text{m, } 20\% \text{ pullout length, } c=10 \text{ kPa}$$

$$\text{Then, } F_u = 4.35e^{0.36H/D} = 4.35e^{0.36*1} = 6.23498$$

$$C_D = 0.53 * D + 0.58 = 0.53 * 0.6 + 0.58 = 0.898$$

$$C_{PL} = 0.001(PL) + 0.96 = 0.001 * 50 + 0.96 = 1.01$$

$$C_c = 5c^{-0.67} = 5 * (20)^{-0.67} = 0.672$$

$$F_{\text{max}} = (F_u * C_D * C_{PL} * C_C) * c * D = (6.23498 * 0.898 * 1.01 * 0.672) * 20 * 0.6$$

$$F_{\text{max}} = 45.6 = 46 \text{ kN/m}$$

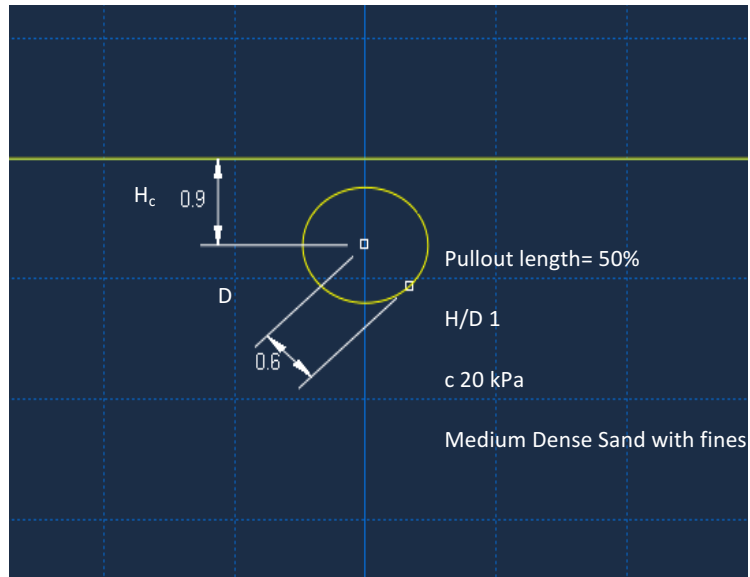


Figure 4.2 Example

C. Simplified Approach Validation

To check the suggested simplified approach, q-q plots of the measured (finite element) versus predicted (empirical and analytical solutions) uplift resistances were plotted for loose, medium dense and dense sand with fines (Figures 4.3, 4.5 and 4.7). The analytical solutions plotted are the solutions found in part E of chapter III as the closest to the finite element results: Bransby et al. (2002), DNV,max (2007) and White et al. (2001) with $2H_c c_u$ combined solutions (sand with fines). The bias factors (measured over predicted resistance) were also plotted for the different analytical solutions and empirical approach versus the pipe diameter, embedment depth, pullout length and soil cohesion value for loose, medium dense and dense sand with fines (Figures 4.4, 4.6 and 4.8). The results show that the empirical approach is a bit conservative yet it presents a consistency and stability in the results for the different parameters for different soil densities.

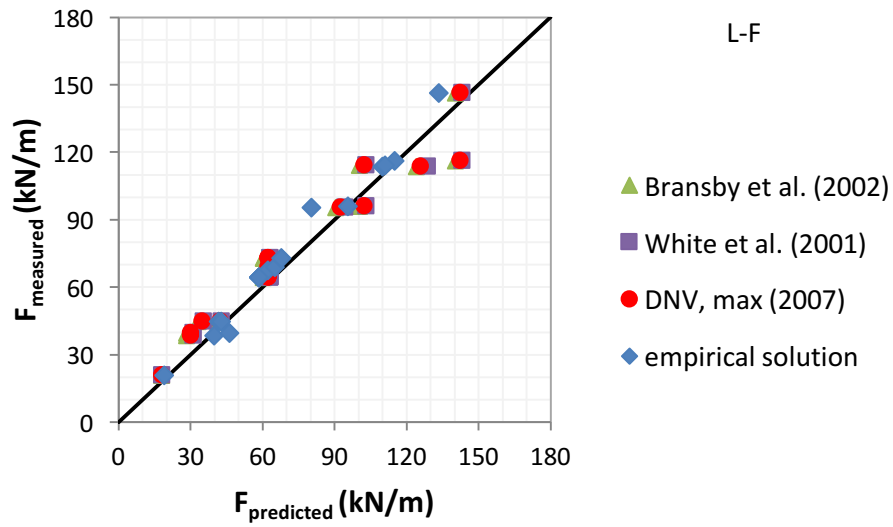


Figure 4.3 Variation of the measured (FE results) with the predicted uplift resistance for analytical and empirical solutions- Loose sand with fines

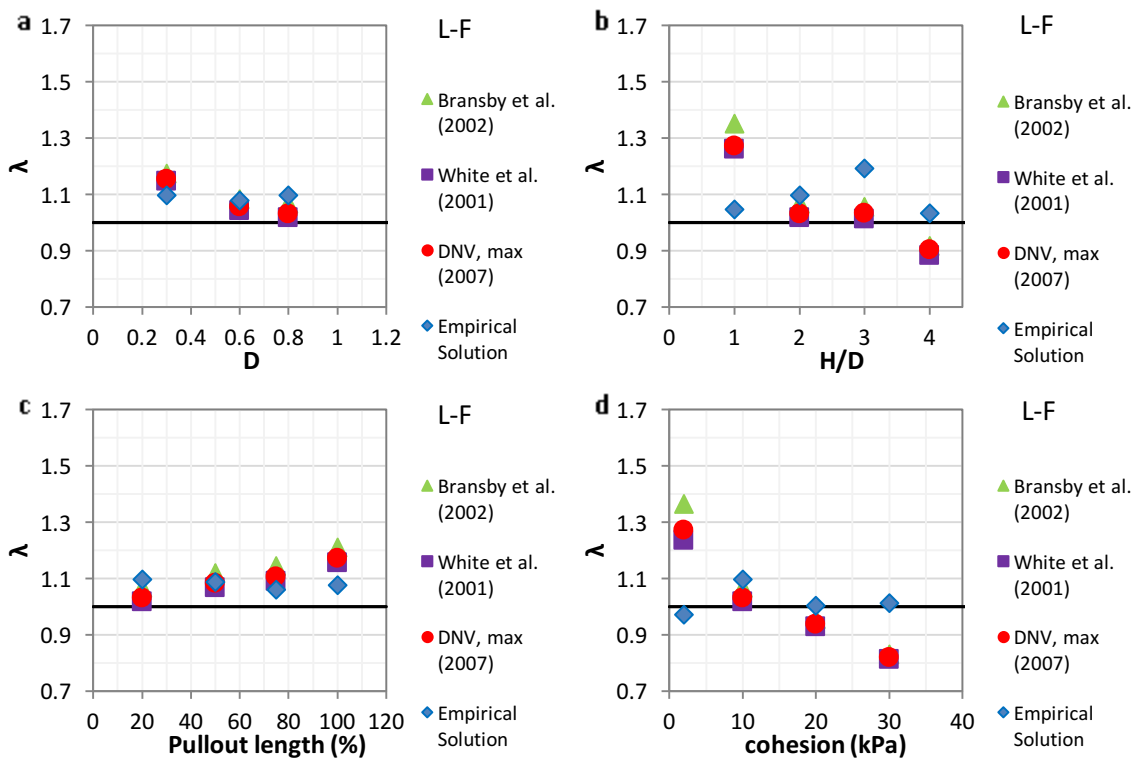


Figure 4.4 Variation of the bias factor with a) pipe diameter, b) embedment depth c) pullout length and d) soil cohesion for analytical and empirical solutions- Loose sand with fines

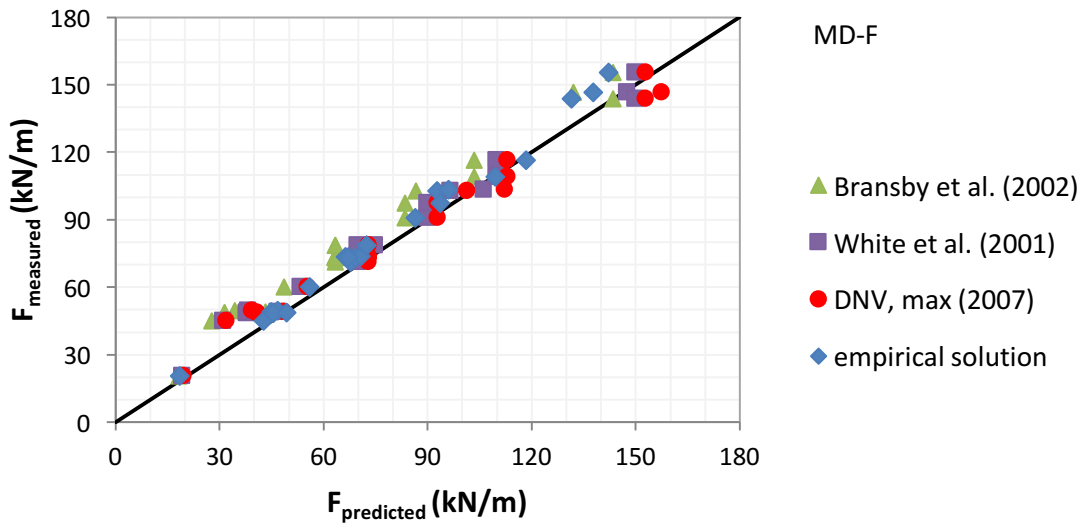


Figure 4.5 Variation of the measured (FE results) with the predicted uplift resistance for analytical and empirical solutions- Medium dense sand with fines

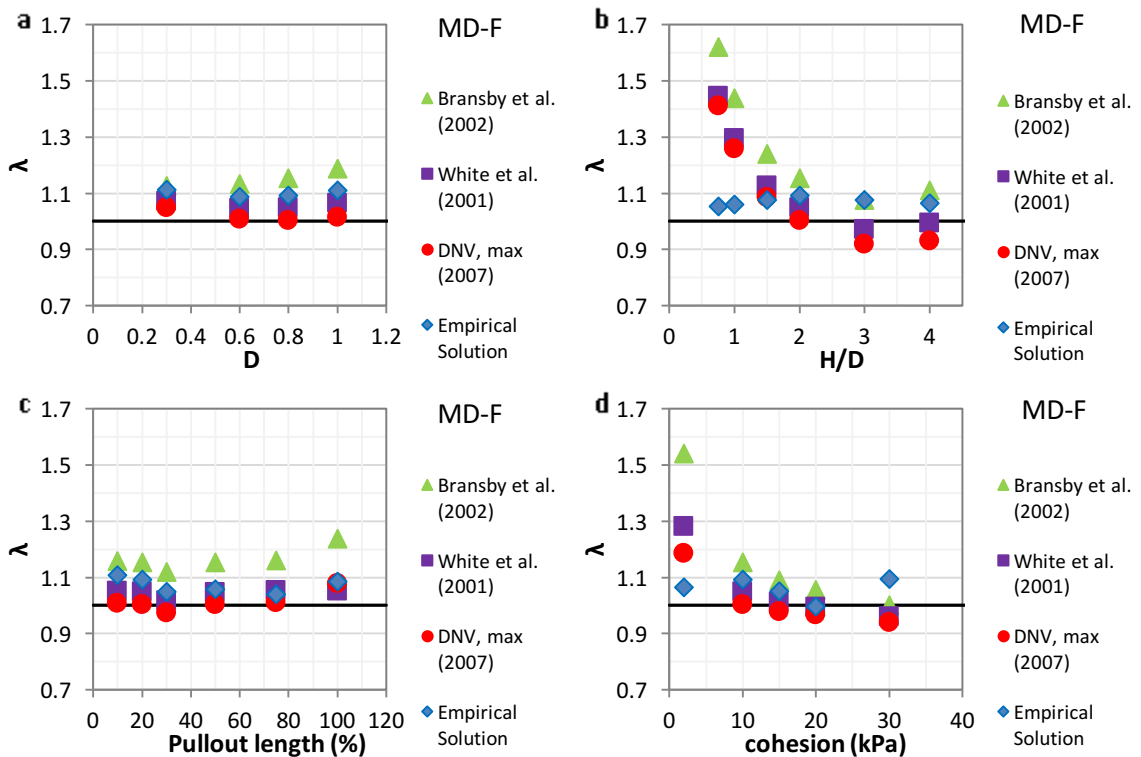


Figure 4.6 Variation of the bias factor with a) pipe diameter, b) embedment depth c) pullout length and d) soil cohesion for analytical and empirical solutions-Medium dense with fines

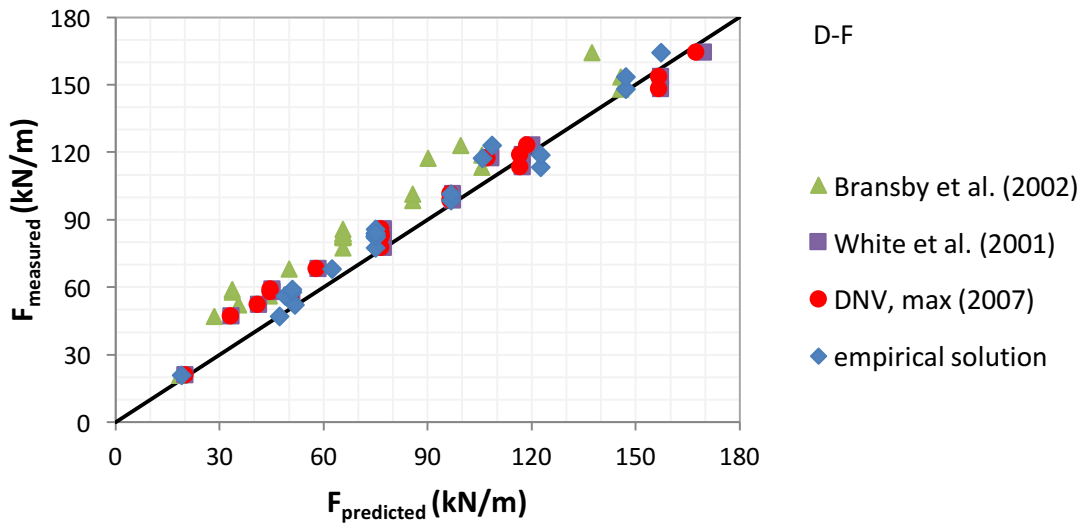


Figure 4.7 Variation of the measured (FE results) with the predicted uplift resistance for analytical and empirical solutions- Dense sand with fines

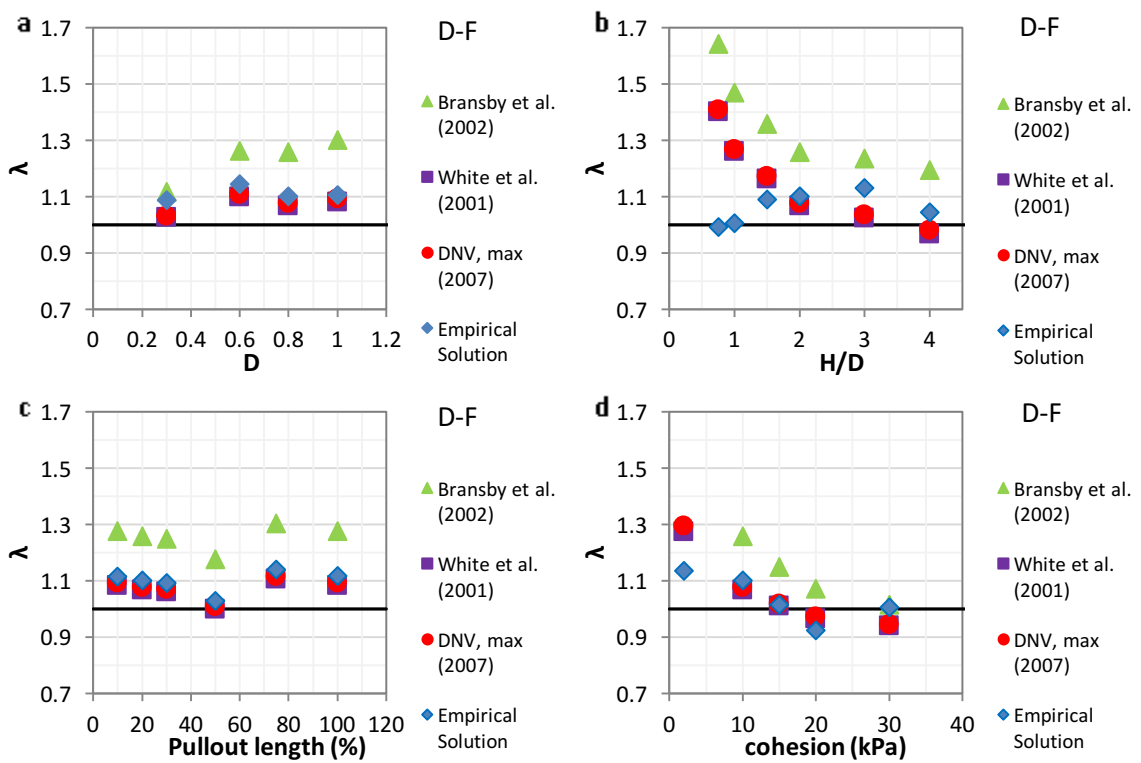


Figure 4.8 Variation of the bias factor with a) pipe diameter, b) embedment depth c) pullout length and d) soil cohesion for analytical and empirical solutions-Dense sand with fines

CHAPTER V

CONCLUSIONS AND RECOMMENDATIONS

Offshore pipelines transporting oil and gas placed on the seabed or buried in a trench are susceptible to global buckling that can be compared to a bar in compression. High pressure high temperature pipelines are typical candidates to global buckling. When the pipelines are put into operation, the internal temperature and pressure inside the pipeline increase, the pipeline walls start expanding. This expansion is resisted by the constrained pipeline; axial forces inside the pipeline are created. The pipeline will try to retrieve these stresses by buckling. However, buckling occurs in the direction of the least resistance. As a result, if the pipeline is placed on the seabed, buckling occurs in the lateral direction while if placed in a trench, buckling occurs in the vertical direction. Soil provides the buried pipeline with enough resistance. If the stresses inside the pipeline exceed the resistance provided by the soil, upheaval buckling occurs. Although global buckling is a load not a failure response, it can lead to failures such as local buckling, bending moments, large plastic deformations, fracture, fatigue, etc. It is very important to avoid upheaval buckling of a buried pipeline: if a buried pipeline undergoes upheaval buckling and breaks through the soil cover, additional failures may occur such as rupture that results in severe environment and economical damages.

Several researchers considered this problem since the 1970s especially after the offshore buckling incidents occurred in the North Sea in the 1980s. The soil uplift resistance against upheaval can be derived from two models: Vertical Slip Model presented

by Schaminee et al. (1990), Palmer et al. (1990) and Bransby et al. (2002) and Sliding Block with Inclined Failure Surfaces presented by White et al. (2001), Ng and Springman (1994) and Vermeer and Sutjiadi (1985). The DNV (DET NORSKE VERITAS) practice describes this uplift resistance in the buried pipe design procedure and provides uplift resistance analytical solutions. Uplift or pullout physical model and centrifuge experiments of buried pipelines were performed since 1990 by Schaminee et al. (1990), Ng and Springman (1994), White et al. (2001), Bransby et al. (2001), Gao et al. (2011), Chin et al. (2006), and Schupp et al. (2006). The effect of pullout rates was considered by Byrne et al. (2008 and 2013) and Bransby and Ireland (2009). The mobilization distance was discussed by Bransby et al. (2001), Stone (2006), Cheuk et al. (2008), Wang et al. (2012) and Robert and Thusyanthan (2014). As for the mechanism of failure, it was explained by Ng and Springman (1994), Bransby et al. (2001), White et al. (2001), Schupp et al. (2006), Stone (2006), Cheuk et al. (2008) and Byrne et al. (2008 and 2013). Standard finite element software such as Plaxis, Abaqus and Ansys are used to study the upheaval buckling of pipelines. Sun et al. (2011), Gao et al. (2011), Zeng et al. (2014), and Liu et al. (2015) used Abaqus to model the pipe by pipe-beam elements and the soil by spring models. Vanden Berghe et al. (2005), Newson and Deljoui (2006), Liu et al. (2008, 2013), Robert and Thusyanthan (2014) and Yimisri et al. (2004) modeled the buried pipeline in plain strain condition while Liu et al. (2014) presented four different numerical simulation methods using Abaqus: 2D implicit, 2D explicit, 3D implicit and 3D explicit to simulate global buckling of offshore pipelines under thermal loading.

To simulate the upheaval buckling of a buried offshore pipeline, 3D displacement-controlled finite element models were performed using the commercial software Abaqus.

Researchers consider upheaval buckling behavior as plain strain problem. In reality, the pipeline does not buckle in a plain strain manner. 3D models allow sinking of the pipeline in the seabed that provides additional resistance to global buckling. Pipeline buried in sand with fines at 100m depth with different soil densities (loose, medium dense and dense) was examined for the effects of pipeline diameter, embedment depth ratio, pullout length and soil apparent cohesion. The 3D models consisted of the soil and pipeline: the soil was modeled using eight node brick, trilinear displacement, trilinear pore pressure, reduced integration, hourglass control: C3D8RP element type while the pipeline was modeled using eight node linear brick, reduced integration, hourglass control: C3D8R element type. A quarter of the problem was simulated due to symmetry and the restrained axially boundary condition was adopted in the analyses; the pipe and soil wall boundaries were set free to move in lateral and upward directions. The pipeline was modeled using typical Mohr Coulomb model (MC) while the soil was modeled using Modified Mohr Coulomb model (MMC) that captures the material's strain softening behavior. The softening behavior is in terms of the reduction of the mobilized friction and dilation angles with the increase in plastic deviatoric shear strain. The interaction between the pipe and the soil was modeled based on Mohr Coulomb failure model.

Force displacement responses were obtained from the displacement control finite element models. The pipeline was pulled at the middle with “forced uniform displacement” in the pulled-up section till $1\%H_c$ upward displacement (H_c is the depth to the centreline of the pipeline). Using the same model setup and methodology, parametric studies were performed for loose, medium dense and dense sand with fines for the effects of different pipeline diameters D (0.3 to 1m), embedment depth ratios H/D (0.75 to 4), pullout section

lengths L_p (10 to 100%) and soil apparent cohesion values c (2 to 30 kPa). The pullout section was defined as a middle portion of the total pipe length ($L_p = \%L$). The upward resistance was divided in the analysis by two lengths: pullout and effective. The effective length was defined as bounded by minimal pipe slopes: typical “cutoff slope” values of 0.0014 corresponding to an angle of 0.08° . For strain hardening curves, the mobilization distance was deduced graphically based on the tangent intersection method. This method plots two tangential lines along the initial and the latter portions of the load displacement curve (large displacement portion of the curve). The normalized displacement of the load corresponding to the intersection point of these two lines was considered as the mobilization distance.

The results show that:

- The increase in pipe diameter increases the uplift soil resistance, normalized mobilization distance and pipeline effective length.
- The embedment depth does not affect the effective length but it increases the uplift resistance. The normalized mobilization distance depends on the burial depth unlike the DNV approach that states that the mobilization distance is between 0.5 to 0.8%H for loose to dense sand and independent of soil cover depth.
- The use of the effective length normalizes the pipeline load displacement curves at high displacement (at $1\%H_c$). The increase in pullout length increases the effective length and changes the pipeline load displacement behavior from strain hardening to strain softening while decreasing the normalized mobilization distance.
- Workable and typical diameter to wall thickness ratios (D/t 25 to 40) slightly affect the uplift soil resistance, normalized mobilization distance and pipeline effective length.

- The soil cohesion component presented in the sand does not affect the pipeline effective length but it increases the uplift soil resistance by about $2H_c c_u$ and causes the pipeline to displace more to reach the peak resistance due to the increase in the contact area between the soil elements.
- The uplift resistance, the normalized mobilization distance as well as the deformation mechanism are function of the soil density. Loose sands are disposed to local failure while medium dense and dense sand to wedge failure. The uplift resistance increases while the normalized mobilization distance decreases with the increase in soil density due to the effect of densification that increases the peak soil friction angle and soil unit weight.
- For the Vertical Slip model that assumes that the uplift soil resistance corresponds to the dead weight of the soil above the pipe along with the amount of friction being mobilized for cohesionless soil and the undrained behavior for cohesive soil, Branby et al. (2002) combined solution was the closest to the finite element results with average bias factors around 1.05 to 1.27 for loose to dense sand with fines.
- For the Sliding Block with Inclined Failure Surfaces model that consider the shearing plane inclined at angle equal to the dilation angle to the vertical and results in an addition of soil weight and change in length and normal stress on the shear plane, White et al. (2001) cohesionless soil equation combined with $2H_c c_u$ solution was the closest to the finite element results with average bias factors around 1.05 for loose to dense sand with fines.
- For the DNV (DET NORSKE VERITAS) practice, DNV, max design equation that describes the maximum soil resistance by the vertical slip model that includes the weight of the soil column above the pipeline combined with the cohesive soil for global shallow shear failure mode was the closest to the finite element results with average bias factors between 1.03 and 1.09 for loose to dense sand with fines.

Based on the finite element results, a simplified approach was presented to calculate the uplift soil resistance for different soil densities (loose, medium dense and dense sand with fines) and considered the pipe embedment depth, diameter, pullout length and soil apparent cohesion value. This approach compared to the finite element results and analytical solutions showed consistency and stability in the results.

For future work, different burial length along the pipeline route may be investigated to decrease the upheaval buckling risk and burial costs. Also, the effect of different trenching methods on decreasing the soil strength thus the uplift soil resistance can be studied.

REFERENCES

1. Anand, S. and Agarwal, S.L. (1981). "Field and Laboratory Studies for Evaluating Submarine Pipeline Frictional Resistance." *Journal of Energy Resources Technology*, 103(3), 250-254.
2. ASCE. (1984). "Guidelines for the Seismic Design Of Oil and Gas Pipeline Systems." Committee on Gas and Liquid Fuel Lifelines of the ASCE Technical Council on Lifeline Earthquake Engineering, Reston, VA.
3. ASCE. (2001). "Guidelines for the Design of Buried Steel Pipe." American Lifelines Alliance, ASCE, New York.
4. Ballet, J. P. and Hobbs, R. E. (1992). "Asymmetric Effects of Prop Imperfections On The Upheaval Buckling Of Pipelines." *Journal of Thin-Walled Structures*, ELSEVIER, 13(5), 355–373.
5. Bolton, M.D. (1986). "The Strength and Dilatancy Of Sands." *Geotechnique*, 36(1), 65–78.
6. Bouwkamp, J. G. and Stephen, R. M. (1973). "Large Diameter Pipe under Combined Loading." *Journal of Transportation. Engineering.*, 99(3), 521–536.
7. Bransby, M. F. and Ireland, J. (2009). "Rate Effects During Pipeline Upheaval Buckling in Sand." *Proceeding of The Institution of Civil Engineers*, 162, No. 5, 247–256.
8. Bransby, M.F, Newson, T.A., Brunning, P., 2002, The Upheaval Capacity of Pipelines in Jetted Clay Backfill, *International Journal of Offshore and Polar*, Vol. 12 Issue 4, pp280- 287.

9. Bransby, M.F., Newson, T.A., Brunning, P. and Davies, M.C.R. (2001). "Numerical and Centrifuge Modeling of the Upheaval Resistance of Buried Pipelines." Proceeding of the 20th International Conference on Offshore Mechanics and Arctic Engineering, Rio De Janeiro, Brazil, OMAE2001/PIPE-4118
10. Byrne, B. W., Schupp, J., Martin, C. M., Oliphant, J., Maconochie, A. and Cathie, D. N. (2008). "Experimental Modelling of the Unburial Behaviour of Pipelines." Proceeding Of Offshore Technology Conference, Houston, TX, Paper OTC 19573.
11. Byrne, B.W., Schupp, J., Martin, C.M., Maconochie, A., Oliphant, J. and Cathie, D. (2013). "Uplift of Shallowly Buried Pipe Sections in Saturated very Loose Sand." *Geotechnique* 63, No.5, 382-390
12. Cheuk, C.Y., Take, W.A., Bolton, M.D. and Oliviera, J.R.M.S. (2006). "Soil Restraint on Buckling Oil and Gas Pipelines Buried in Lumpy Clay Fill." *Journal of Engineering Structures, ScienceDirect*, 29(2007) 973-982
13. Cheuk, C.Y., White, D.J. and Bolton, M.D. (2008). "Uplift Mechanism of Pipes Buried in Sand." *Journal of Geotechnical and Environmental Engineering, ASCE*, 2008.134:154-163
14. Chin, E.L., Craig, W.H. and Cruickshank, M. (2006). "Uplift Resistance of Pipelines Buried in Cohesionless Soil." Proceeding of the 6th International Conference On Physical Modelling in Geotechnics. Ng, Zhang and Wang, Eds, Vol.1, Taylor and Francis Group, London, 723-728
15. Croll, J.G.A.(1997). "A Simplified Model of Upheaval Thermal Buckling Of Subsea Pipelines." *Journal of Thin-Walled Structures, ELSEVIER*, 29(1-4), 59-78.

16. Dean E.T.R. (2010) *Offshore Geotechnical Engineering - Principles and Practice*, Thomas Telford, Reston, VA, U.S.A., 520 p.
17. Det Norske Veritas (DNV). (2007). "Global Buckling of Submarine Pipelines- Structural Design Due To High Temperature High Pressure." RP-F110, Oslo, Norway.
18. Friis-Hansen, A., 2000, *Bayesian Networks as a Decision Support Tool in Marine Applications*, Doctoral Thesis, Department of Naval Architecture and Offshore Engineering, Technical University of Denmark, 184 pp.
19. Gao F., Yan, S. , Yang B. and Luo C., 2010, "Steady Flow-Induced Instability of a Partially Embedded Pipeline: Pipe-Soil Interaction Mechanism", *Journal of Ocean Engineering*, ELSEVIER, 38(2011) 934-942
20. GAO, X., LIU, R. and YAN, S., (2011). "Model Test Based Soil Spring Model and Application in Pipeline Thermal Buckling Analysis." *China Ocean Engineering*. Vol. 25, No.3, Pp.507-518
21. Gerwick B.C. (2007) *Construction of marine and offshore structures*. CRC Press, New York, 795 p.
22. Gresnigt, M. and Van Foeken, R. J. (2001). "Local Buckling Of UOE and Seamless Steel Pipes." *International Offshore and Polar Engineering Conference*, The International Society Of Offshore and Polar Engineers, California, Vol. 2, 131–142.
23. Guijt, J. (1990). "Upheaval Buckling of Offshore Pipeline: Overview and Introduction." *Proceeding Of The 22nd Annual Offshore Technology Conference*, Offshore Technology Conference, Richardson, TX, 573–578.

24. Guo, L., Liu, R. and Yan, S. (2013). "Global Buckling Behavior of Submarine Unburied Pipelines Under Thermal Stress." Journal of Central South University Press and Springer-Verlag Berlin Heidelberg 2013, Springer, 20:2054-2065,
25. Hobbs, R. E. (1981). "Pipeline Buckling Caused By Axial Loads." Journal of Construction Steel Resources, ELSEVIER, 1(2), 2–10.
26. Hobbs, R. E. (1984). "In-Service Buckling of Heated Pipelines." Journal of Transportation Engineering, ASCE, 110(2), 175–189.
27. Hunt, G. W. and Blackmore, A. (1997). "Homoclinic and Heteroclinic Solutions Of Upheaval Buckling." Phil. Trans. R. Soc. Lon., 355(4), 2185–2195.
28. Ivanovic A. and Oliphant J. (2013). "Uplift Mobilisation Resistance Of Subsea Pipelines In Loose Sand." Geotechnique (2014) 217-222
29. Jukes, P., Eltaher, A. and Sun, J. (2009). "The Latest Developments in The Design and Simulation of Deepwater Subsea Oil and Gas Pipelines using FEA." Proceeding Of The 3rd ISOPE International Deep-Ocean Technology Symp.: Deepwater Challenge, IDOT-2009, International Society Of Offshore and Polar Engineers, Cupertino, CA, 70–82.
30. Liu R., Basu P. and Xiong H. (2015). "Laboratory Tests and Thermal Buckling Analysis for Pipes Buried In Bohai Soft Clay", Journal of Marine Structures, ELSEVIER, 43 (2015) 44-60
31. Liu R., Xiong H., Wu X. and Yan S. (2014). "Numerical studies on global buckling of subsea pipelines", Journal of Ocean Engineering, ELSEVIER, 78 (2014) 62-7

32. Liu, J. X., Zhang, H. M., Meng, Q. R. and Zhang, H. (2008). "Study Examines Causes Of Upheaval Buckling In Shallow Subsea PIP Lines." *Journal of Oil and Gas*, 106(6), 53–57.
33. Liu, R. and Yan, S. (2013). "Brief History of Upheaval Buckling Studies For Subsea Buried Pipeline." *Journal of Pipeline Systems Engineering and Practice*, ASCE, 2013.4:170-183
34. Liu, R., Liu, W., Wu, X. and Yan, S. (2014). "Global Lateral Buckling Analysis of Idealized Subsea Pipelines." *Journal of Central South University Press And Springer-Verlag Berlin Heidelberg 2014*, Springer , 21:416-427
35. Liu, R., Wang, W. and Yan, S. (2013)." Finite Element Analysis on Thermal Upheaval Buckling Of Submarine Burial Pipelines with Initial Imperfections." *Journal of Central South University Press And Springer-Verlag Berlin Heidelberg 2013*, Springer, 20:236-245
36. Liu, R., Wang, W. G., and Yan, S. W. (2012). "Engineering Measures for Preventing Upheaval Buckling Of Buried Submarine Pipelines." *Applied Mathematics and. Mechanics*, Springer, 36(6), 781–796.
37. Liu, R., Yan, S. and Wu, X. (2013). "Model Test Studies on Soil Restraint to Pipeline Buried in Bohai Soft Clay." *Journal of Pipeline Systems Engineering And Practice*, ASCE, 2013.4:49-56,
38. Liu, R., Yan, S. W., and Wu, X. L. (2013). "Model Test Studies on Soil Restraint to Pipeline Buried In Bohai Soft Clay." *Journal of Pipeline System Engineering. Practice*, ASCE, 4(1), 49–56.

39. Lyons, C. G. (1973). "Soil Resistance to Lateral Sliding of Marine Pipelines." Proceeding Of The 5th Offshore Technology Conference, Offshore Technology Conference, Richardson, TX, 479–484.
40. Maltby, T. C., and Calladine, C. R. (1995b). "An Investigation into Upheaval Buckling of Buried Pipelines—II. Theory And Analysis Of Experimental Observations." *Int. J. Mech. Sci.*, 37(9), 965–983.
41. Maltby, T.C. and Calladine, C.R. (1995a). "An Investigation into Upheaval Buckling of Buried Pipelines—I. Experimental Apparatus and Some Observations." *Int. J. Mech. Sci.*, 37(9), 943–963.
42. Newson, T.A. and Deljoui, P. (2006). "Finite Element Modelling Of Upheaval Buckling Of Buried Offshore Pipelines In Clayey Soils." Proceedings of The Geoshanghai 2006 Conference On Soil and Rock Behavior And Modelling, ASCE
43. Ng, C. W. W. and Springman, S.M. (1994). "Uplift Resistance Of Buried Pipelines In Granular Materials." *Centrifuge 94*, Leung, Lee and Tan, Eds., 753-758
44. Nielsen, N. J. R., Lyngberg, B. and Pedersen, P. T. (1990). "Upheaval Buckling Failures of Insulated Burial Pipelines—A Case Story." Proceeding Of The 22nd Annual Offshore Technology Conference, Offshore Technology Conference, Richardson, TX, 581–592.
45. Nielsen, N. J. R., Pedersen, P. T., Grundy, A. K. and Lyngberg, B. S. (1990). "New Design Criteria of Upheaval Creep Of Buried Sub-Sea Pipelines." *Journal of Offshore Mechanics and Arctic Engineering*, ASME, 112(4), 290–296.
46. Nielsen, N-J-R. and Lyngberg B., Maersk Olie and Gas AS, and Pedersen, P.T.(1990). "Upheaval Buckling Failures of Insulated Buried Pipelines." Technical

University of Denmark, OTC 6488, 22nd Annual Offshore Technology Conf., OTC, Houston, TX

47. Palmer, A. C. and Baldry, J. A. S. (1974). "Lateral Buckling of Axially Compressed Pipelines." *Journal of Petroleum Technology*, Springer, 26, 1283–1284.
48. Palmer, A. C., Ellinas, C. P., Richards, D. M. and Guijt, J. (1990). "Design of Submarine Pipelines Against Upheaval Buckling." *Proceeding of The 22nd Offshore Technology Conference*, Offshore Technology Conference, Richardson, TX, 540–550
49. Palmer, A.C., White, D.J., Baumgard, A.J., Bolton, Barefoot, A.F., Finch, M.Powell, T, Faranski, A.S. and Baldry, A.S. (2003). "Uplift Resistance Of Buried Submarine Pipelines: Comparison Between Centrifuge Modeling and Full-Scale Test" *Geotechnique* 53(10):877-883
50. Reddy, B. D. (1979). "An Experimental Study of the Plastic Buckling of Circular Cylinders in Pure Bending." *International Journal Of Solids Structures*, ELSEVIER, 15(9), 669–683.
51. Robert, D.J. and Thusyanthan, N.I. (2014). "Numerical and Experimental Study of Uplift Mobilization of Buried Pipelines in Sands." *Journal of Pipeline Systems Engineering and Practice*, ASCE, 2014.04014009(10)
52. Schaminee, P. E. L., Zorn, N. F. and Schotman, G. J. M. (1990). "Soil Response For Pipeline Upheaval Buckling Analyses: Full-Scale Laboratory Tests and Modeling." OTC 6486, 22nd Annual Offshore Technology Conf., OTC, Houston, TX, 563–572
53. Schupp, J., Byrne, B. W., Martin, C. M., Oliphant, J., Maconochie, A. & Cathie, D. (2006). "Pipeline Unburial Behaviour In Loose Sand.", *Proceeding Of The 25th*

- International Conference Of Offshore Mechanical Arctic Engineering, Hamburg,
Paper OMAE2006-92542
54. Sherman, D. R. (1976). "Tests of Circular Steel Tubes in Bending." *Journal Of Struct. Div.*, 102(ST11), 2181–2195.
55. Stone, K.J.L. and Newson, T.A. (2006). "Uplift Resistance Of Buried Pipelines: An Investigation of Scale Effects In Model Tests." *Proceeding Of The 6th Int. Conf. On Physical Modelling In Geotechnic*, Ng, Zhang and Wang, Eds, Vol. 1, Taylor & Francis Group, London, 741-746
56. Sun, J. and Jukes, P. (2011). "Upheaval Buckling Analysis of Partially Buried Pipeline Subjected To High Pressure and High Temperature." *Proceedings of The ASME 2011 30th International Conference On Ocean, Offshore and Arctic Engineering*, ASME, OMAE2011-49498
57. Taylor, N. and Tran, V. (1993). "Prop-Imperfection Subsea Pipeline Buckling." *Marine Structures*, ELSEVIER, 6(4), 325–358.
58. Taylor, N. and Tran, V. (1996). "Experimental and Theoretical Studies In Subsea Pipeline Buckling." *Marine Structures*, ELSEVIER, 9(2), 211–257.
59. Tian Y., Cassidy M.J. and Gaudin C. (2010). "Advancing Pipe-Soil Interaction Models in Calcareous Sand", *Applied Ocean Research*, ELSEVIER, 32(2010) 284-297
60. Valle-Moline, C., Alamilla-Lopez, J. , Najjar, S. and Silve-Gonzalez, F. (2012). "Reliability Analyses of Clay-Embedded Offshore Pipelines Under Vertical Buckling Considering Lower-Bound Pipe-Soil Capacity." *Proceeding of the ASME*

31st International Conference on Offshore Mechanics and Arctic Engineering, ASME, OMAE2012-83546

61. Vanden Berghe, J. F., Cathie, D. and Ballard, J. C. (2005) "Pipeline Uplift Mechanisms using Finite Element Analysis." Proceedings of The 16th International Conference of Soil Mechanics and Foundation Engineering, Millpress Science Publishers, Fugro Engineers SA, Brussels, Belgium, 1801–1804
62. Wang, J. Haigh. S., Forrest, G. and Thusyanthan, N. (2012) "Mobilization Distance For Upheaval Buckling Of Shallowly Buried Pipelines." Journal of Pipeline System Engineering Practice, ASCE, 101.1061/(ASCE)PS.1949-12040000099.106-114
63. Wang, J., Eltahir, A., Jukes, P., Sun, J. and Wang, F. S. (2009). "Latest Developments in Upheaval Buckling Analysis for Buried Pipelines." Proceeding of The International Offshore and Polar Engineering Conference, The International Society Of Offshore and Polar Engineers (ISOPE), California, 594–602.
64. White, D. J., Barefoot, A. J. and Bolton, M. D. (2001). "Centrifuge Modelling of Upheaval Buckling in Sand." International Journal of Physical Modelling Geotechnical, 2(1), 19–28.
65. Yimsiri, S., Soga, K., Yoshizaki, K., Dasari, G. R. and O'Rourke, T. D. (2004). "Lateral and Upward Soil-Pipeline Interactions In Sand For Deep Embedment Conditions." Journal Of Geotechnical and Geoenvironmental Engineering, ASCE, 10.1061/ (ASCE)1090-0241(2004)130:8(830), 830–842.
66. Zeng, X., Duan, M. and Che, X. (2014)." Critical Upheaval Buckling Forces of Imperfect Pipelines." Journal of Applied Ocean Research, ELSEVIER 45(2014) 33-39

APPENDIX A
USDFLD CODE (SOFTENING OF THE FRICTION AND
DILATION ANGLES OF MMC)

```
subroutine usdfld(field,statev,pnewdt,direct,t,celent,time,dtime,  
  
1 cmname,orname,nfield,nstatv,noel,npt,layer,kspt,kstep,kinc,  
  
2 ndi,nshr,coord,jmac,jmtyp,matlayo,laccflg)  
  
include 'aba_param.inc'  
  
character*80 cmname,orname  
  
character*8 flgray(15)  
  
dimension field(nfield),statev(nstatv),direct(3,3),t(3,3),time(2),  
  
& coord(*),jmac(*),jmtyp(*)  
  
dimension array(15),jarray(15)  
  
call getvrm('PEP',array,jarray,flgray,jrcd,  
  
&jmac, jmtyp, matlayo, laccflg)  
  
field(1)=((2**0.5)/3)*sqrt((array(1)-array(2))**2+(array(2)-array(3))**2+(array(3)-  
array(1))**2)
```

If error, write comment to .DAT file:

```
IF(JRCD.NE.0)THEN

WRITE(6,*) 'REQUEST ERROR IN USDFLD FOR ELEMENT NUMBER ',

& NOEL,'INTEGRATION POINT NUMBER ',NPT

ENDIF

return

end
```

APPENDIX B

LOAD DISPLACEMENT CURVES

A. Loose Sand with Fines

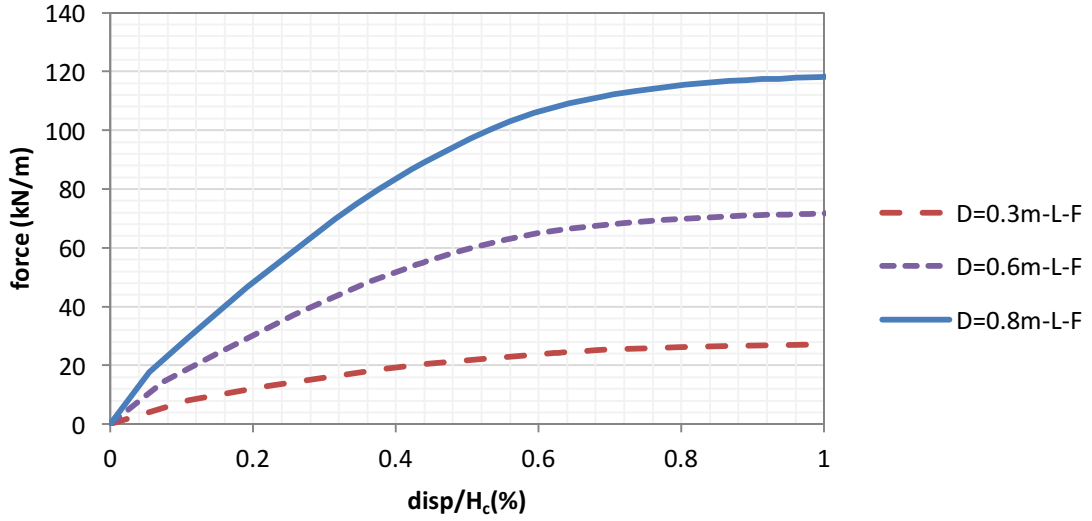


Figure B. 1 Load displacement curves- F (divided by L_p) versus $disp/H_c$ for different pipe diameters-L-F

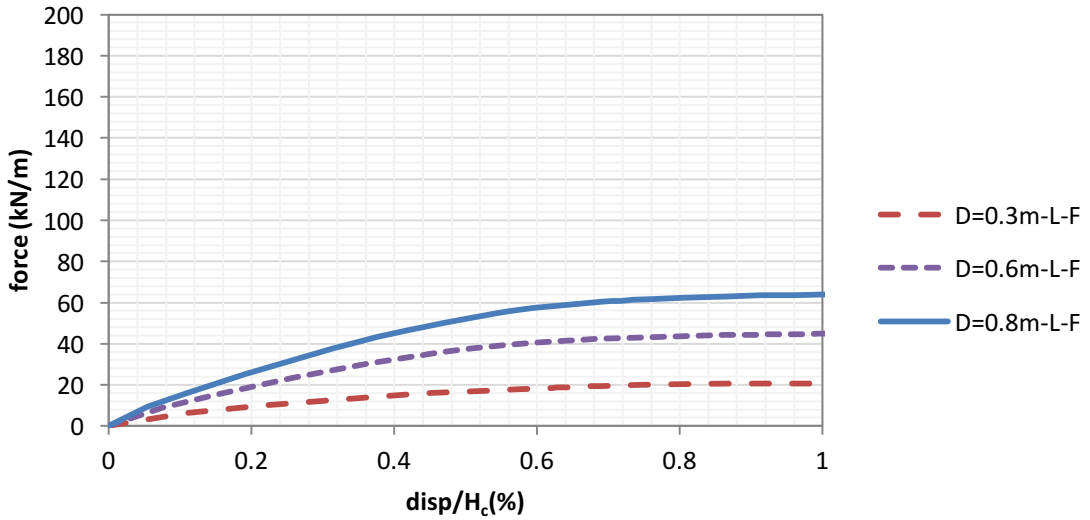


Figure B. 2 Load displacement curves- F (divided by L_{eff}) versus $disp/H_c$ for different pipe diameters-L-F

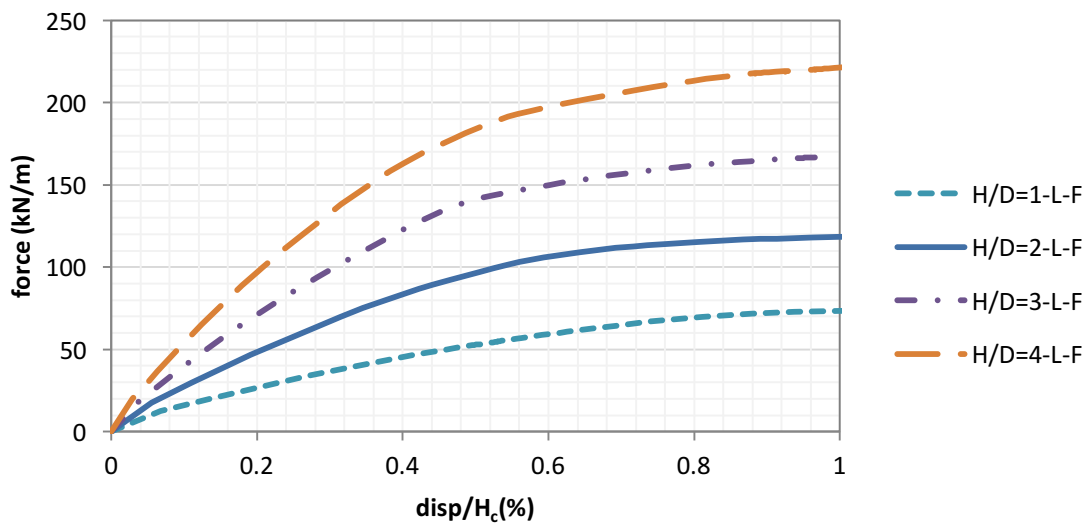


Figure B. 3 Load displacement curves- F (divided by L_p) versus disp/H_c for different embedment depths-L-F

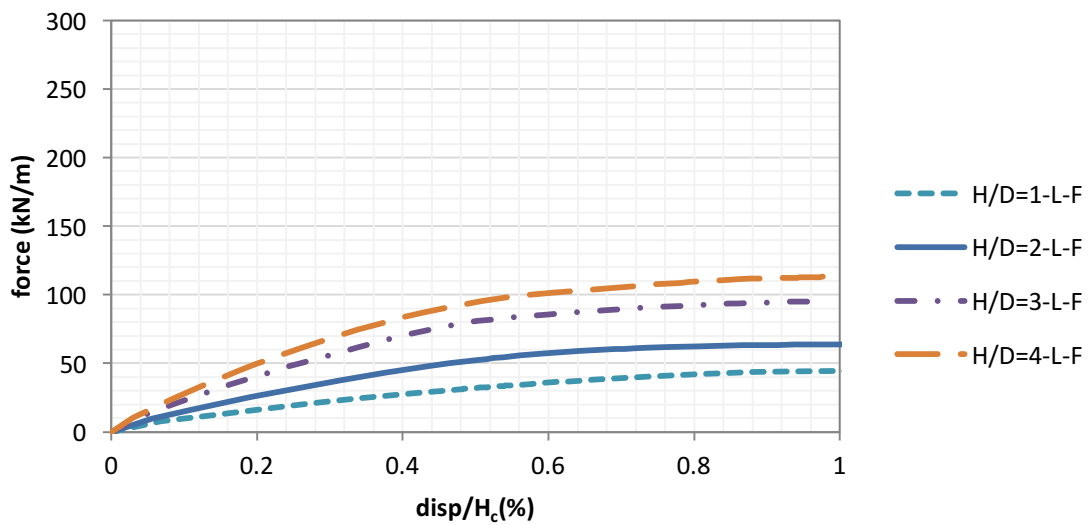


Figure B. 4 Load displacement curves- F (divided by L_{eff}) versus disp/H_c for different embedment depths-L-F

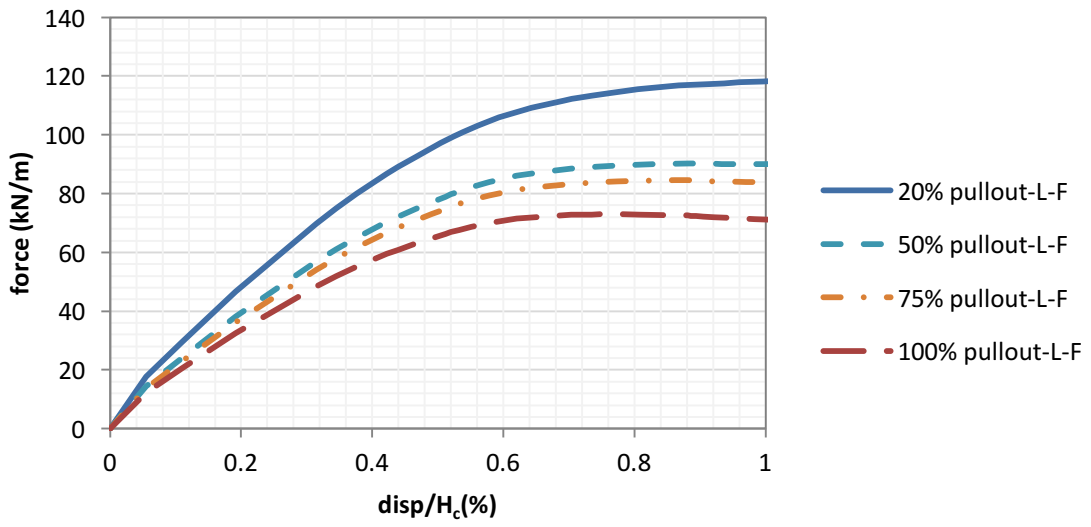


Figure B. 5 Load displacement curves- F (divided by L_p) versus $disp/H_c$ for different pullout lengths-L-F

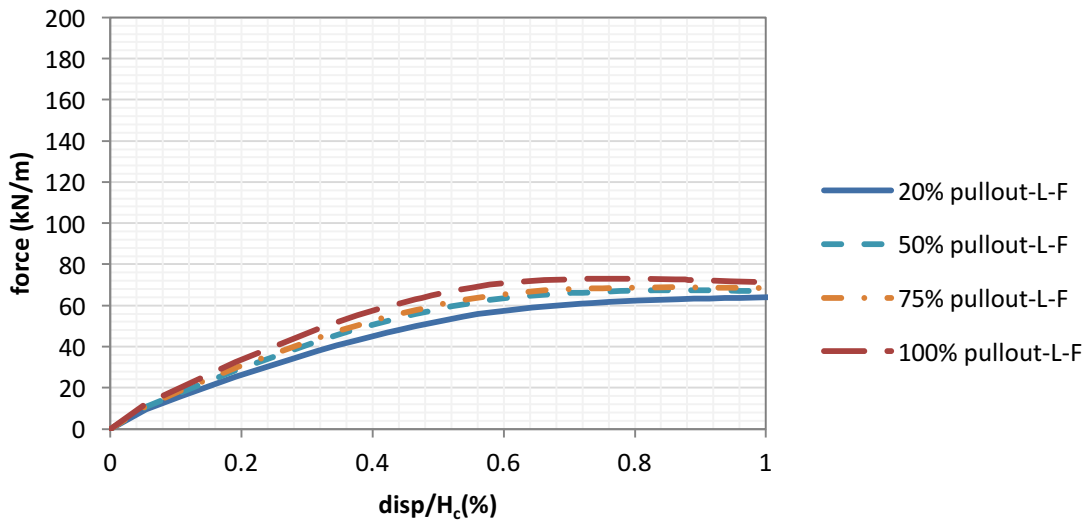


Figure B. 6 Load displacement curves- F (divided by L_{eff}) versus $disp/H_c$ for different pullout lengths-L-F

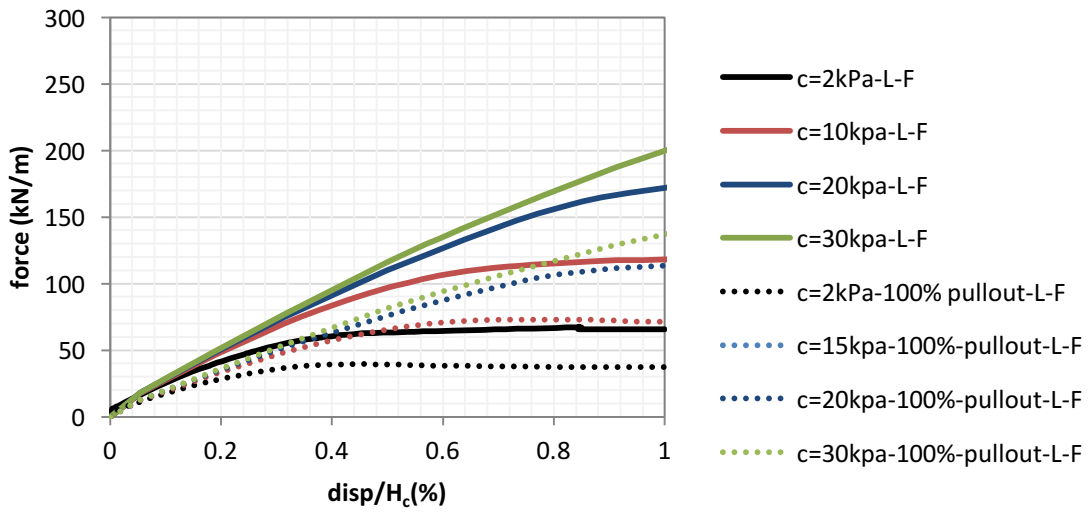


Figure B. 7 Load displacement curves- F (divided by L_p) versus $disp/H_c$ for different soil cohesion and pullout lengths- $L-F$

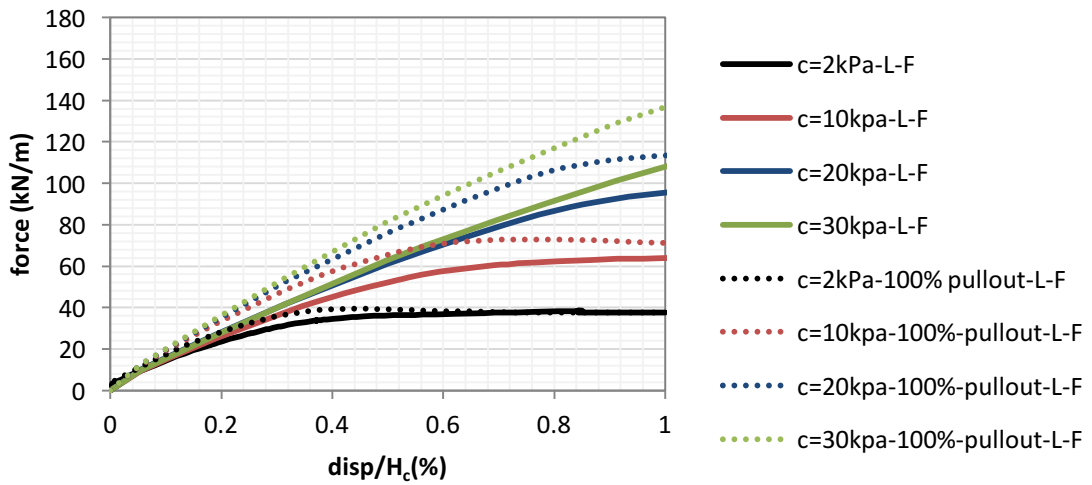


Figure B. 8 Load displacement curves- F (divided by L_{eff}) versus $disp/H_c$ for different soil cohesion and pullout lengths- $L-F$

B. Medium Dense Sand with Fines

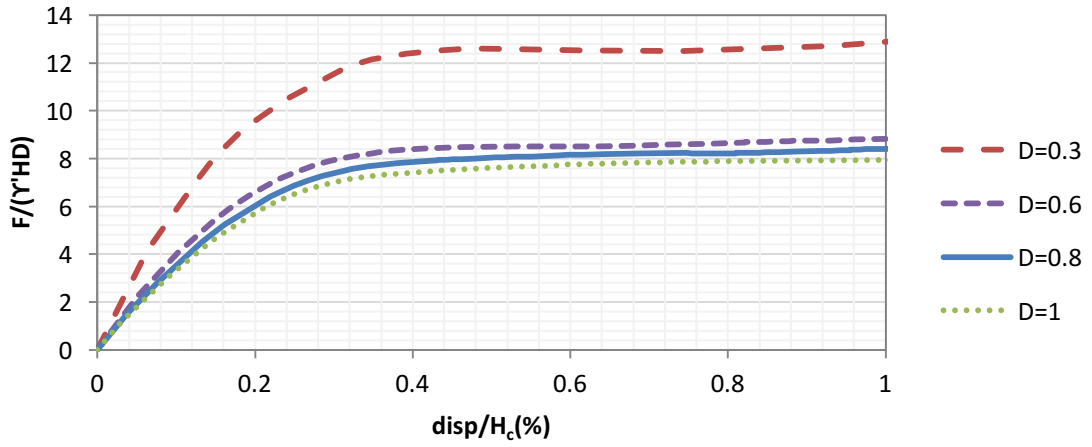


Figure B. 9 Normalized uplift force- $F/(Y'HD)$ (divided by L_p) versus $disp/H_c$ for different pipeline diameters-MD-F

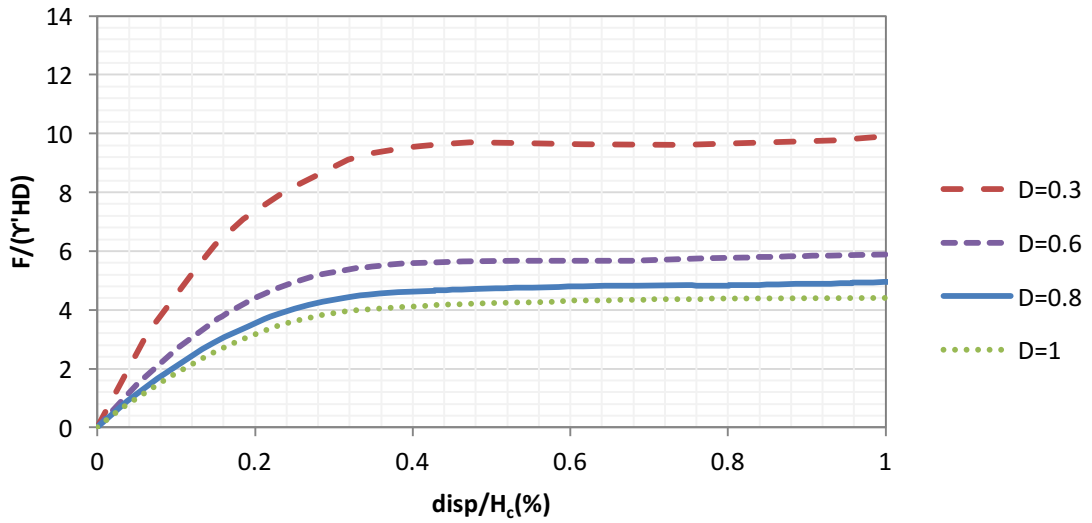


Figure B. 10 Normalized uplift force- $F/(Y'HD)$ (divided by L_{eff}) versus $disp/H_c$ for different pipeline diameters-MD-F

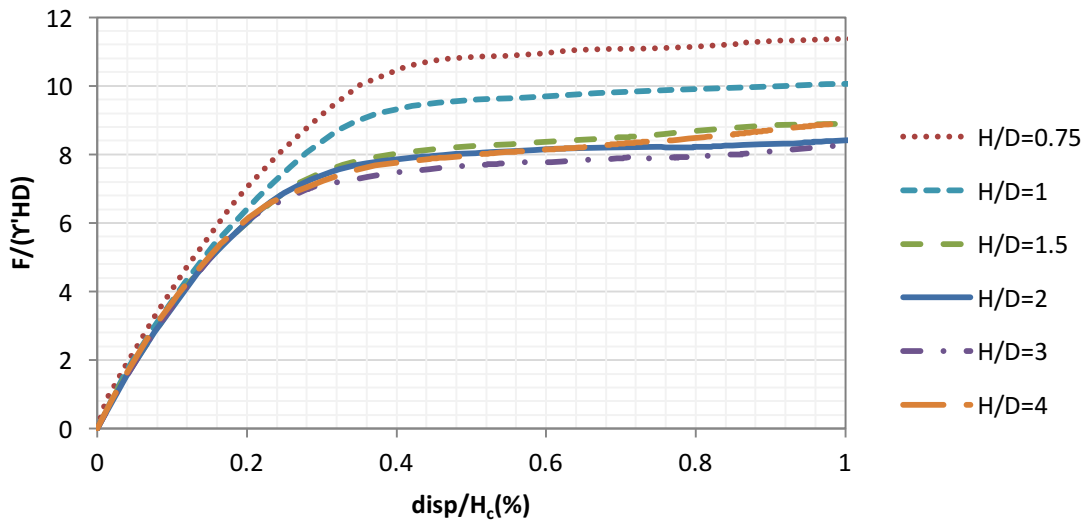


Figure B. 11 Normalized uplift force- $F/(\gamma'HD)$ (divided by L_p) versus $disp/H_c$ for different embedment depths (H/D) -MD-F

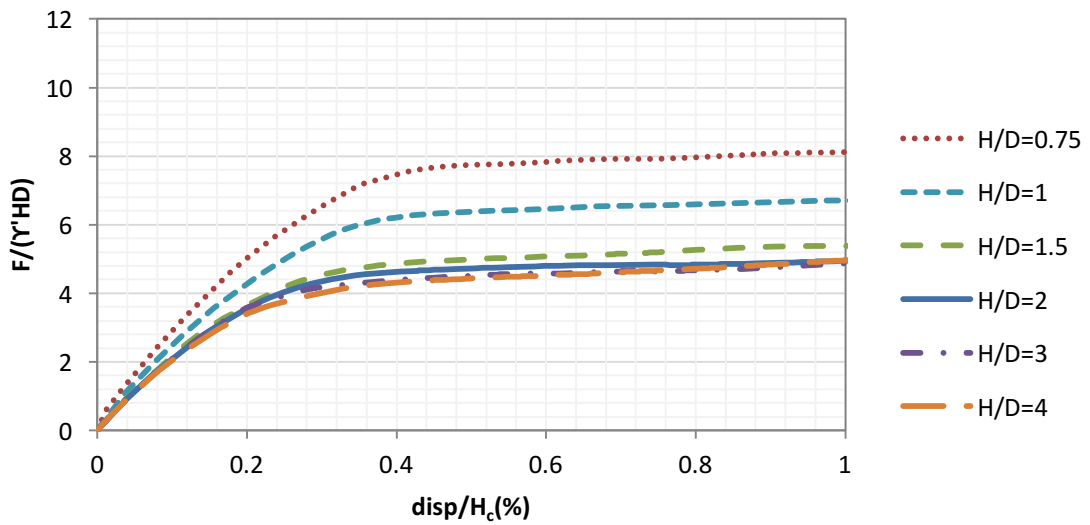


Figure B. 12 Normalized uplift force- $F/(\gamma'HD)$ (divided by L_{eff}) versus $disp/H_c$ for different embedment depths (H/D) -MD-F

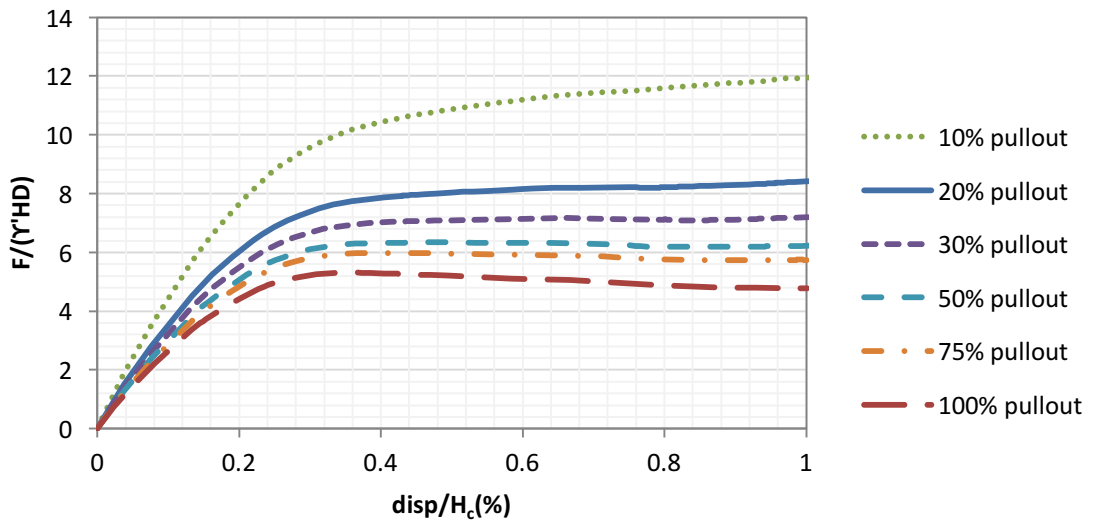


Figure B. 13 Normalized uplift force- $F/(Y'HD)$ (divided by L_p) versus $disp/H_c$ for different pullout lengths-MD-F

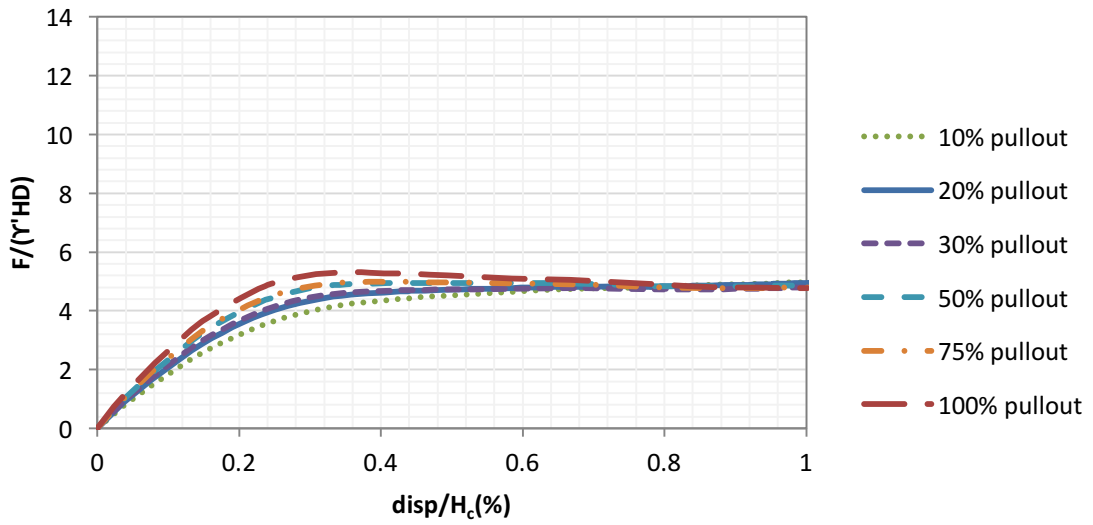


Figure B. 14 Normalized uplift force- $F/(Y'HD)$ (divided by L_{eff}) versus $disp/H_c$ for different pullout lengths-MD-F

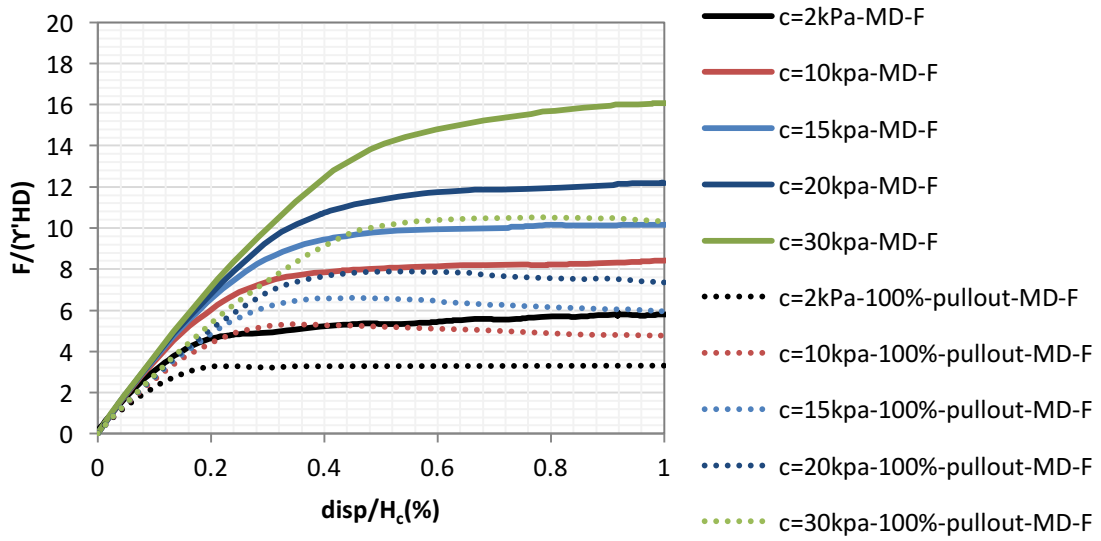


Figure B. 15 Normalized uplift force- $F/(\gamma'HD)$ (divided by L_p) versus $disp/H_c$ for different soil cohesion values and pullout lengths-MD-F

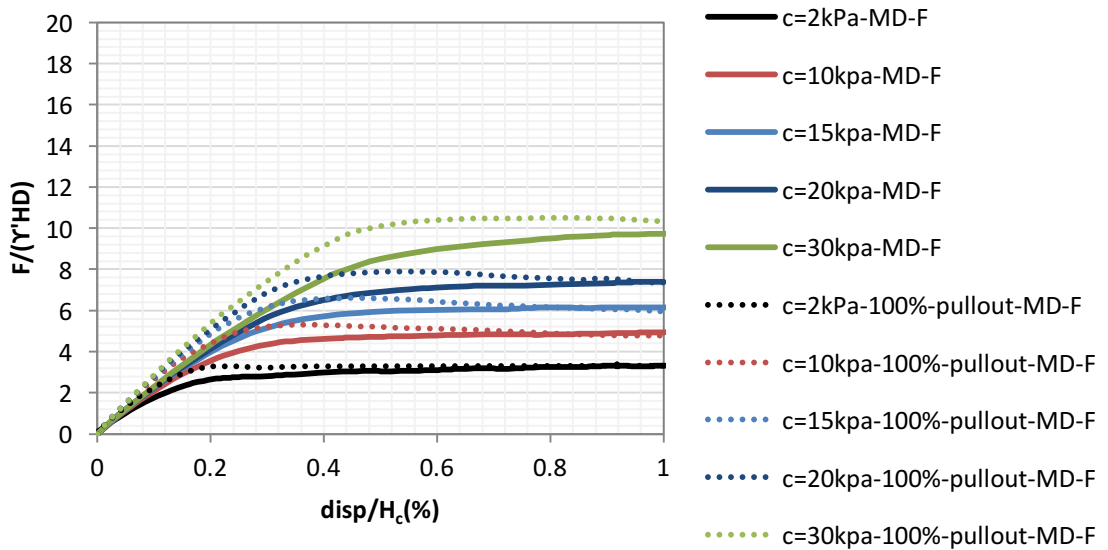


Figure B. 16 Normalized uplift force- $F/(\gamma'HD)$ (divided by L_{eff}) versus $disp/H_c$ for different soil cohesion values and pullout lengths-MD-F

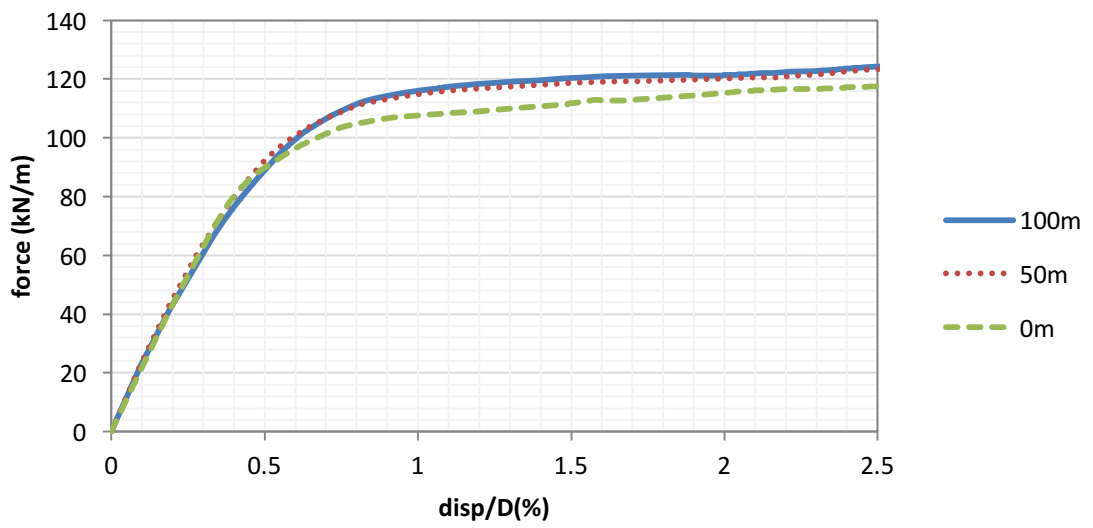


Figure B. 17 Load displacement curves- F (divided by L_p) versus $disp/D$ for different water levels-MD-F

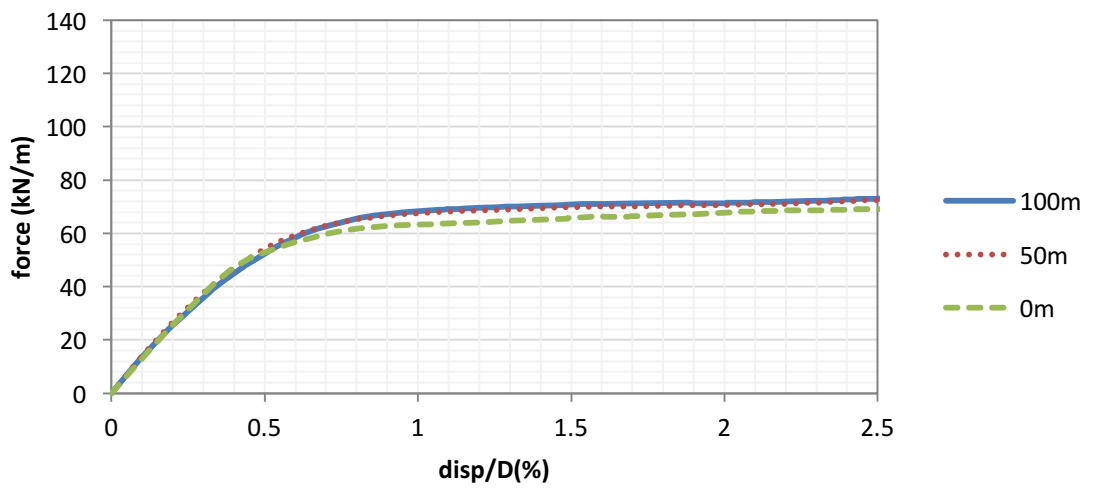


Figure B. 18 Load displacement curves- F (divided by L_{eff}) versus $disp/D$ for different water levels-MD-F

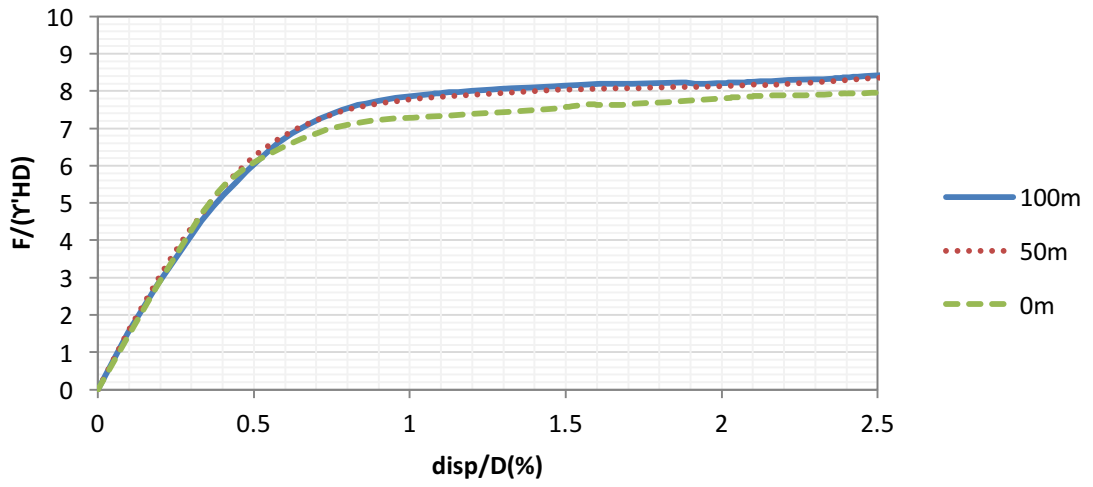


Figure B. 19 Normalized uplift force- $F/(\gamma'HD)$ (divided by L_p) versus $disp/D$ for different water levels-MD-F

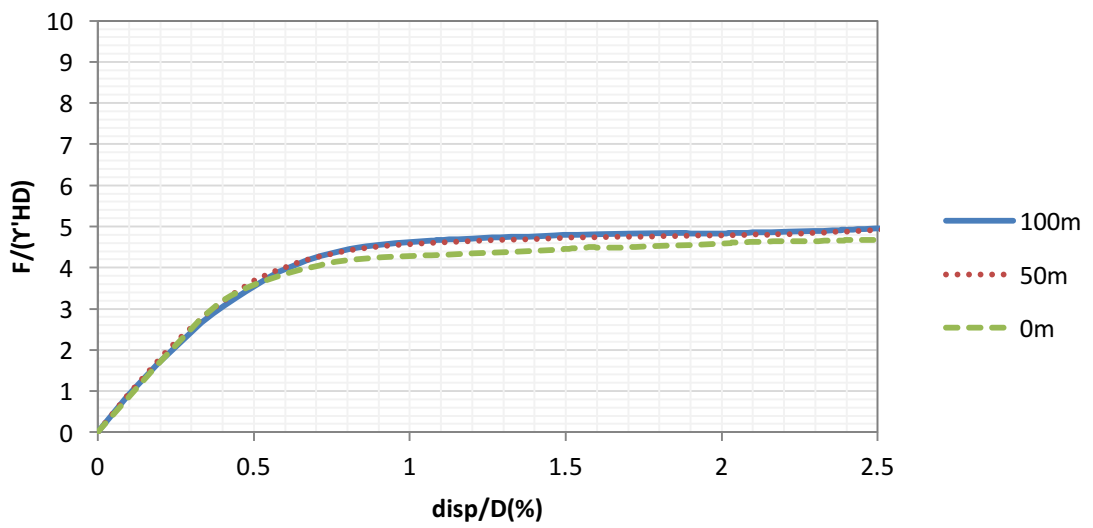


Figure B. 20 Normalized uplift force- $F/(\gamma'HD)$ (divided by L_{eff}) versus $disp/D$ for different water levels-MD-F

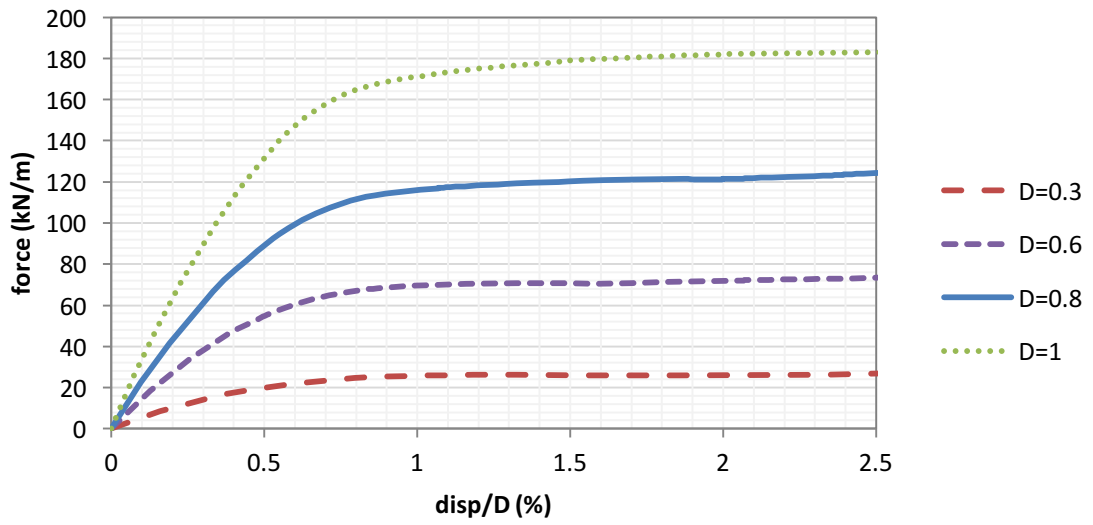


Figure B. 21 Load displacement curves- F (divided by L_p) versus disp/D for different pipeline diameters-MD-F

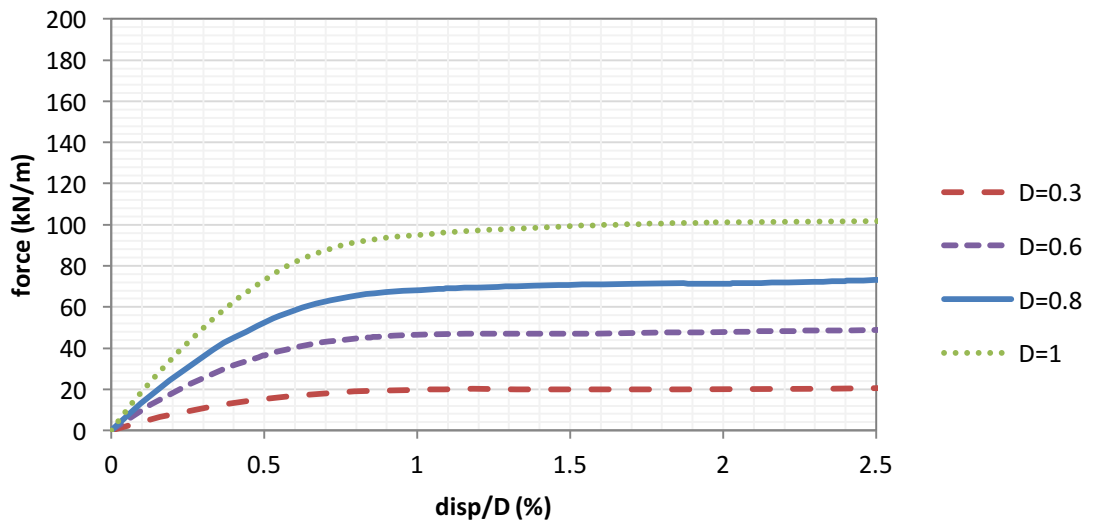


Figure B. 22 Load displacement curves- F (divided by L_{eff}) versus disp/D for different pipeline diameters-MD-F

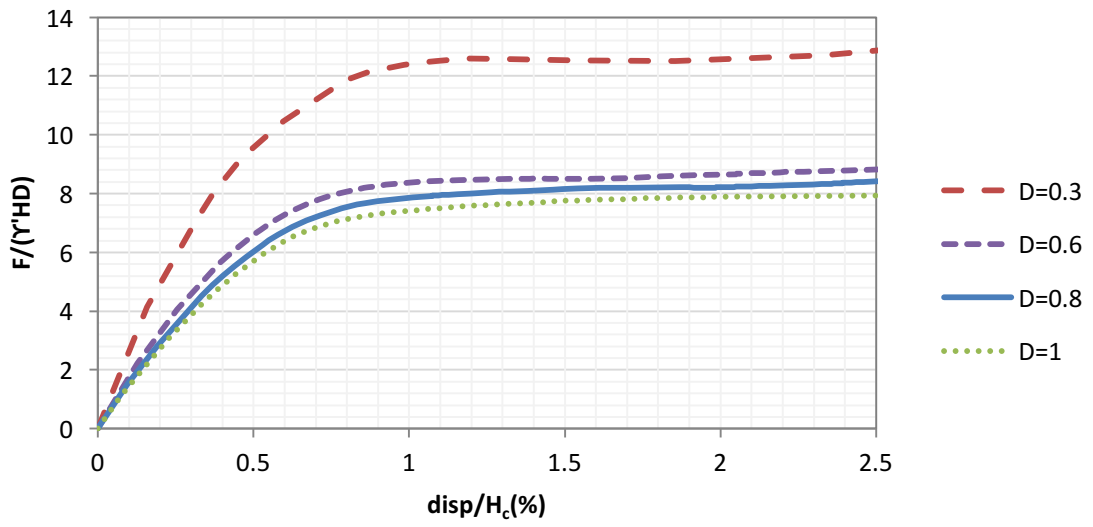


Figure B. 23 Normalized uplift force- $F/(\gamma'HD)$ (divided by L_p) versus $disp/H_c$ for different pipeline diameters -MD-F

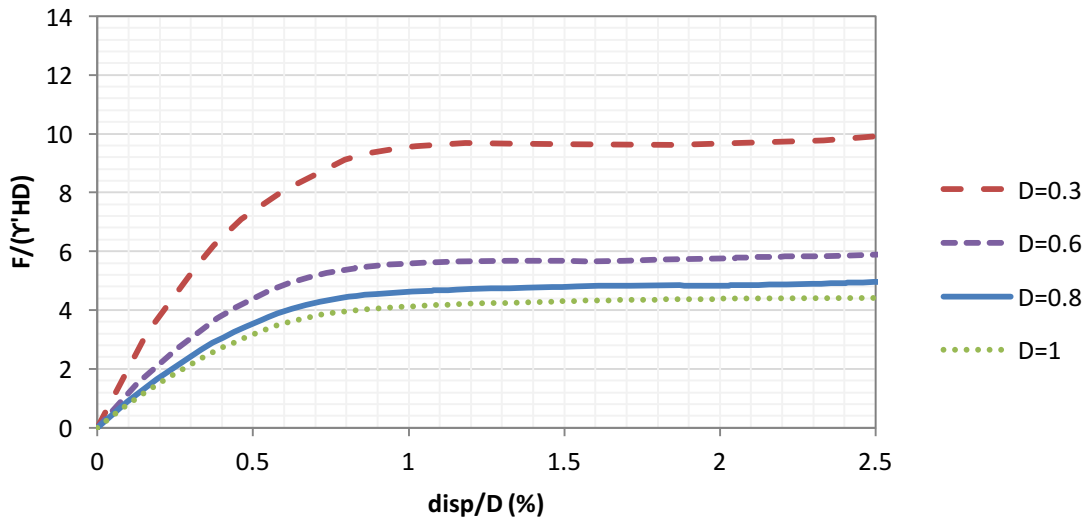


Figure B. 24 Normalized uplift force- $F/(\gamma'HD)$ (divided by L_{eff}) versus $disp/H_c$ for different pipeline diameters -MD-F

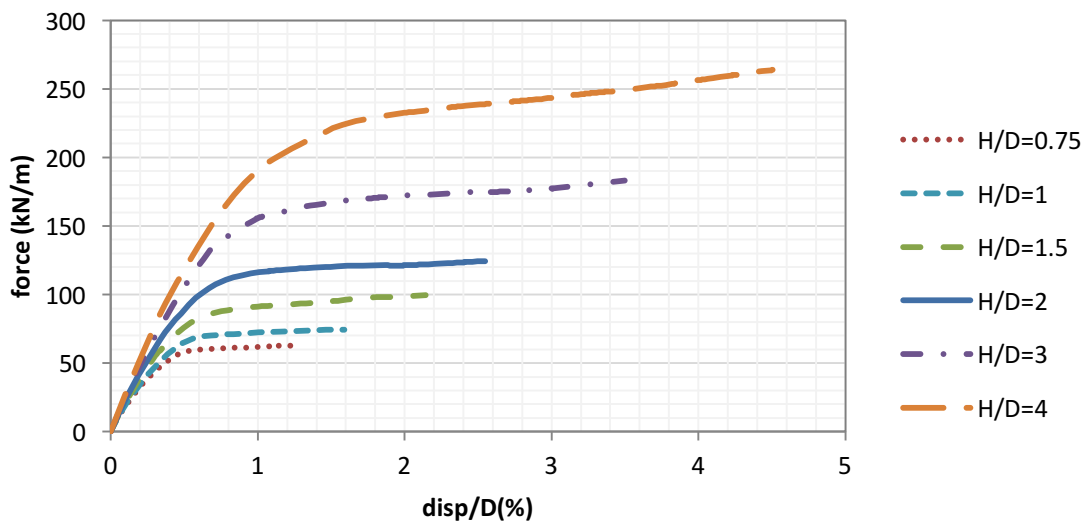


Figure B. 25 Load displacement curves- F (divided by L_p) versus $disp/D$ for different embedment depths -MD-F

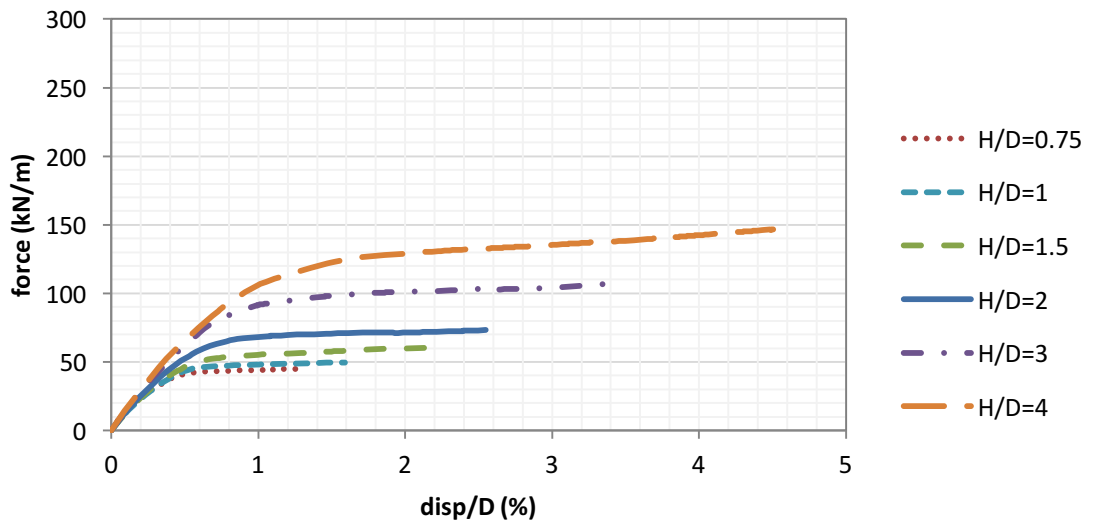


Figure B. 26 Load displacement curves- F (divided by L_{eff}) versus $disp/D$ for different embedment depths-MD-F

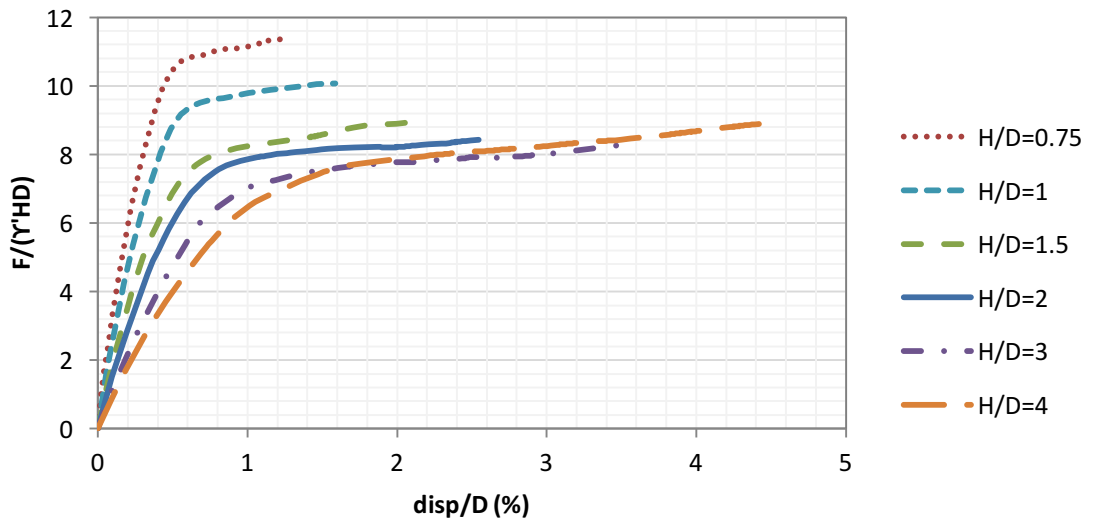


Figure B. 27 Normalized uplift force- $F/(\gamma'HD)$ (divided by L_p) versus $disp/D$ for different embedment depths -MD-F

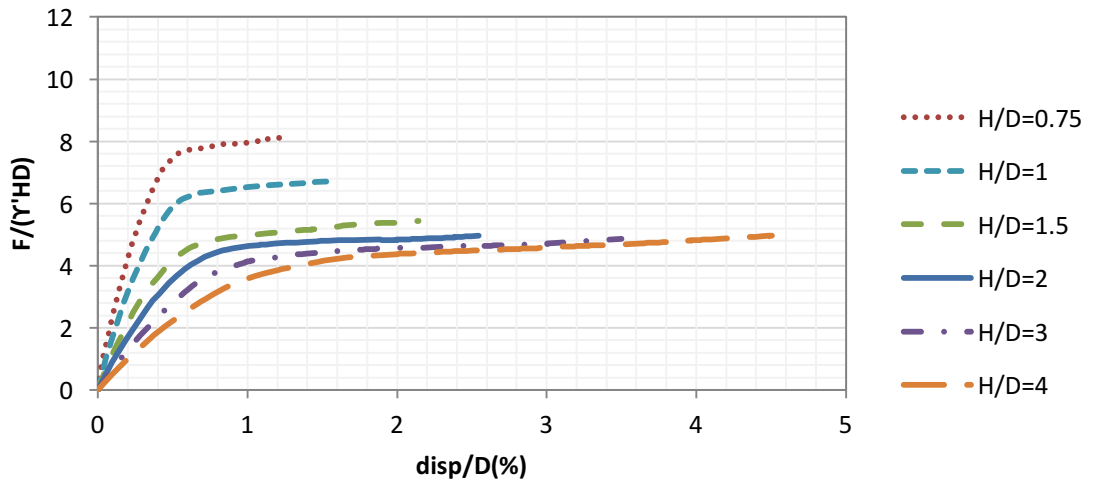


Figure B. 28 Normalized uplift force- $F/(\gamma'HD)$ (divided by L_{eff}) versus $disp/D$ for different embedment depths -MD-F

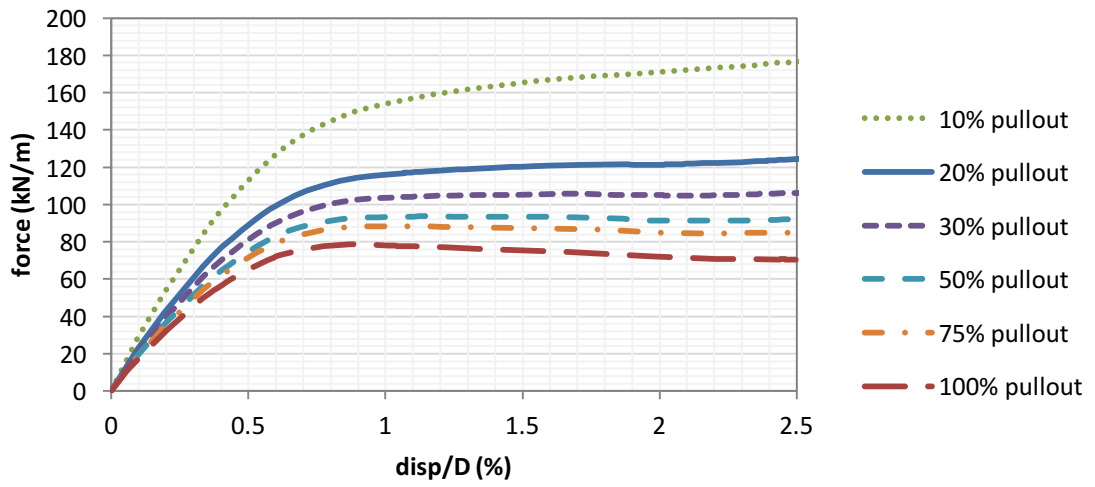


Figure B. 29 Load displacement curves- F (divided by L_{eff}) versus $disp/D$ for different pullout lengths-MD-F

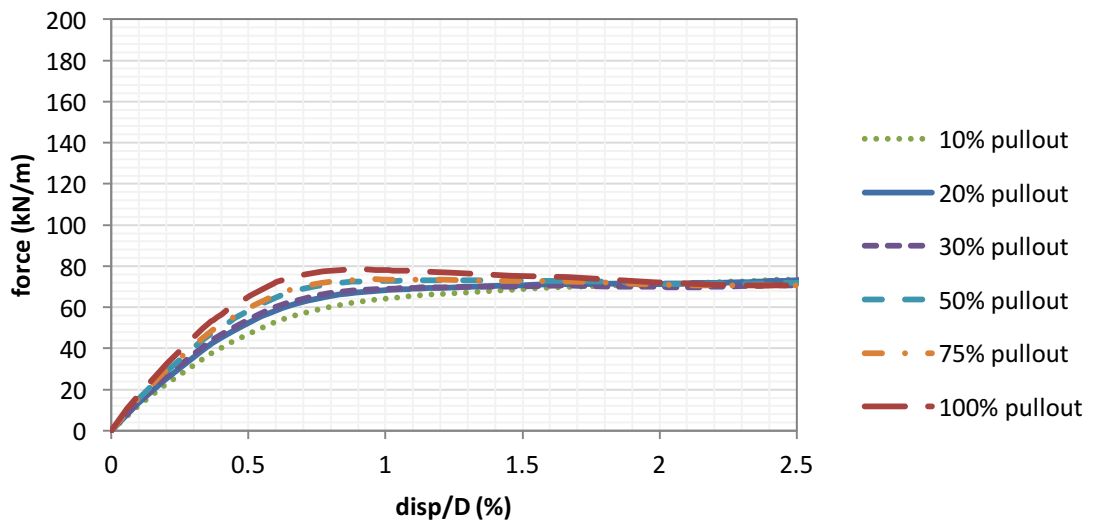


Figure B. 30 Load displacement curves- F (divided by L_{eff}) versus $disp/D$ for different pullout lengths-MD-F

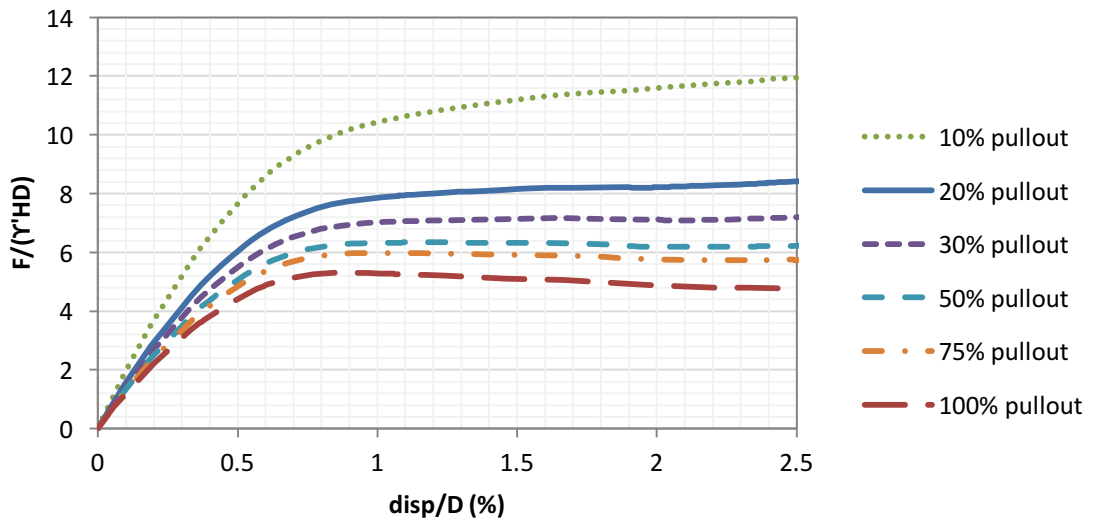


Figure B. 31 Normalized uplift force- $F/(Y'HD)$ (divided by L_p) versus $disp/D$ for different pullout lengths-MD-F

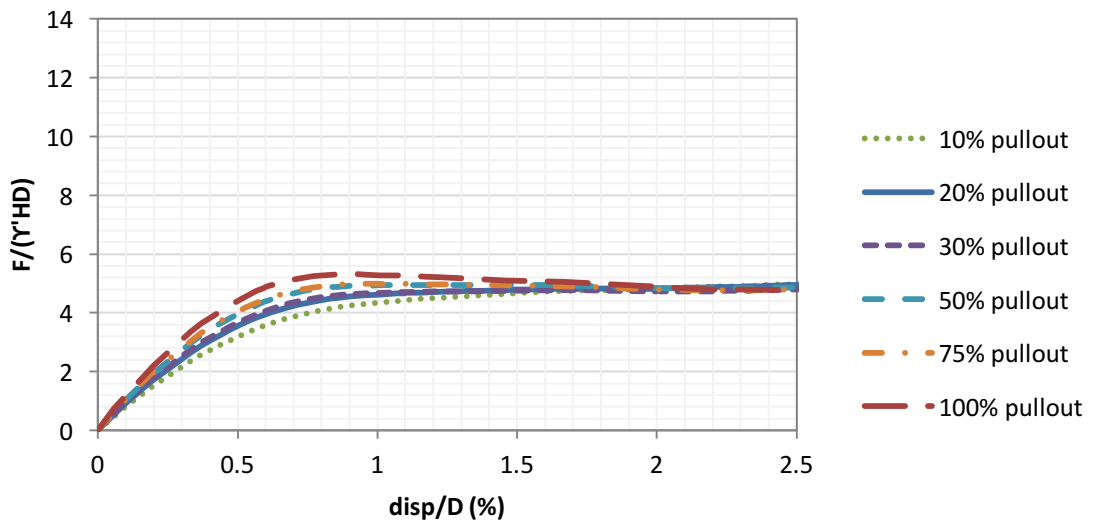


Figure B. 32 Normalized uplift force- $F/(Y'HD)$ (divided by L_{eff}) versus $disp/D$ for different pullout lengths-MD-F

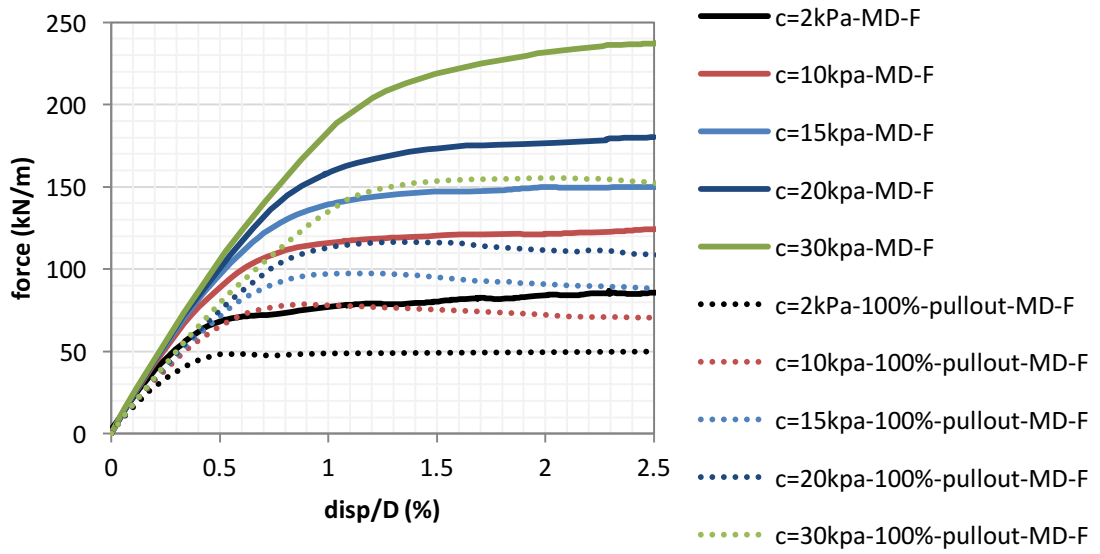


Figure B. 33 Load displacement curves- F (divided by L_p) versus $disp/D$ for different soil cohesion values and pullout lengths-MD-F

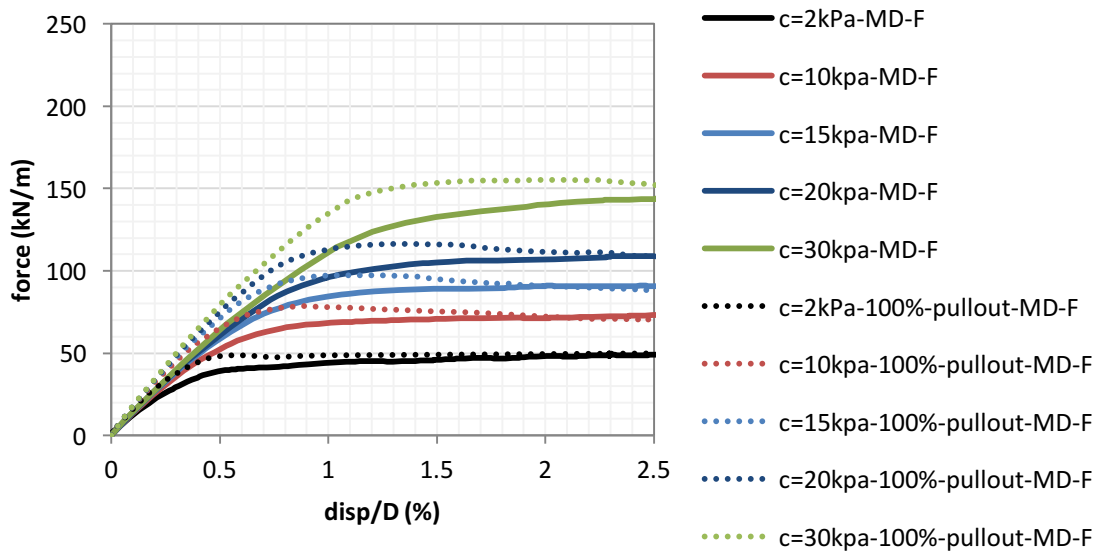


Figure B. 34 Load displacement curves- F (divided by L_{eff}) versus $disp/D$ for different soil cohesion values and pullout lengths-MD-F

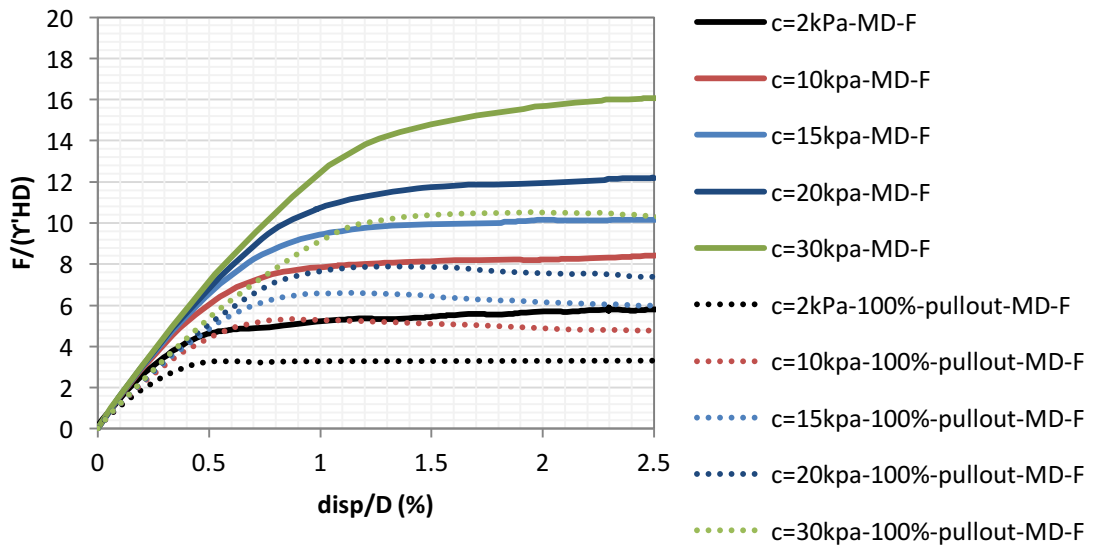


Figure B. 35 Normalized uplift force- $F/(\gamma'HD)$ (divided by L_p) versus $disp/D$ for different soil cohesion values and pullout lengths-MD-F

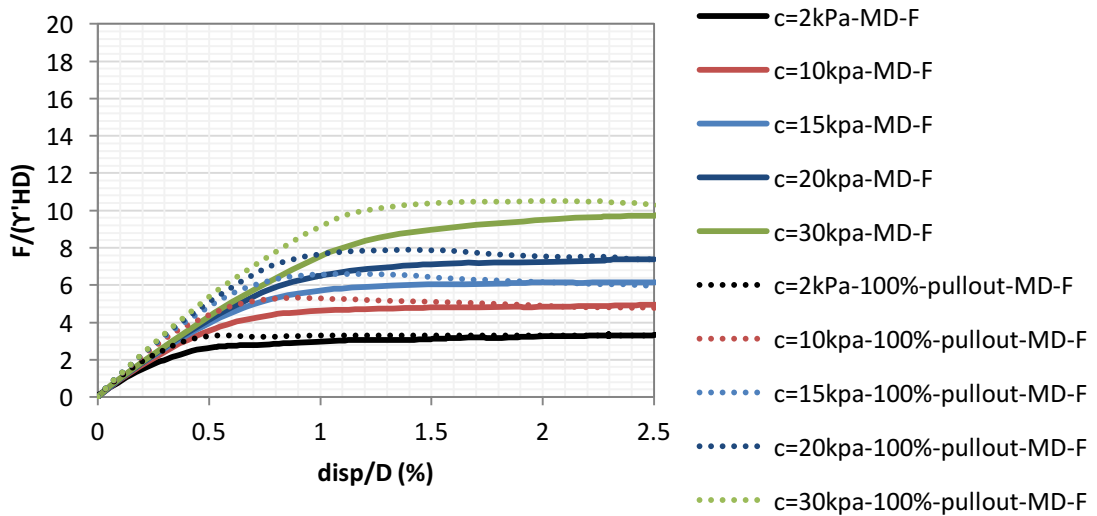


Figure B. 36 Normalized uplift force- $F/(\gamma'HD)$ (divided by L_{eff}) versus $disp/D$ for different soil cohesion values and pullout lengths-MD-F

B. Dense Sand with Fines

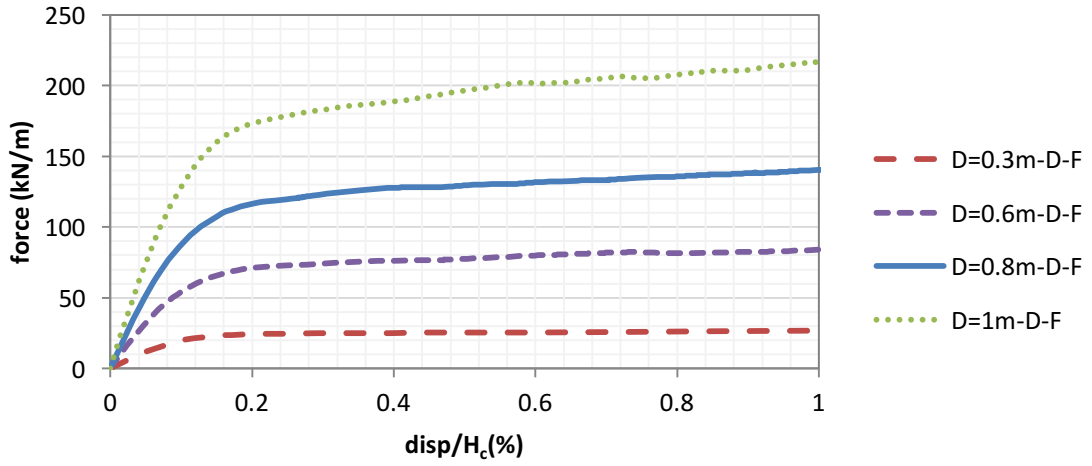


Figure B. 37 Load displacement curves- F (divided by L_p) versus $disp/H_c$ for different pipe diameters-D-F

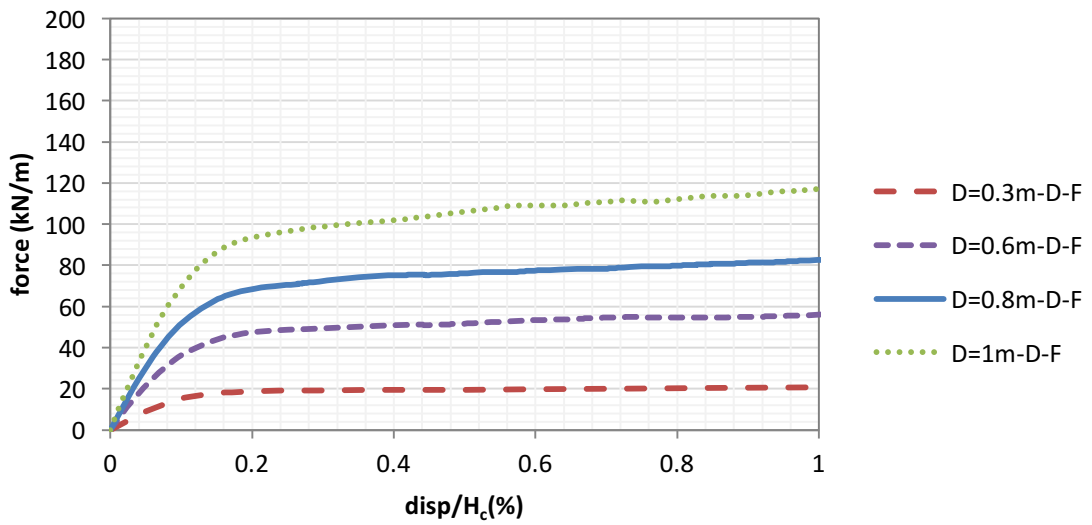


Figure B. 38 Load displacement curves- F (divided by L_{eff}) versus $disp/H_c$ for different pipe diameters-D-F

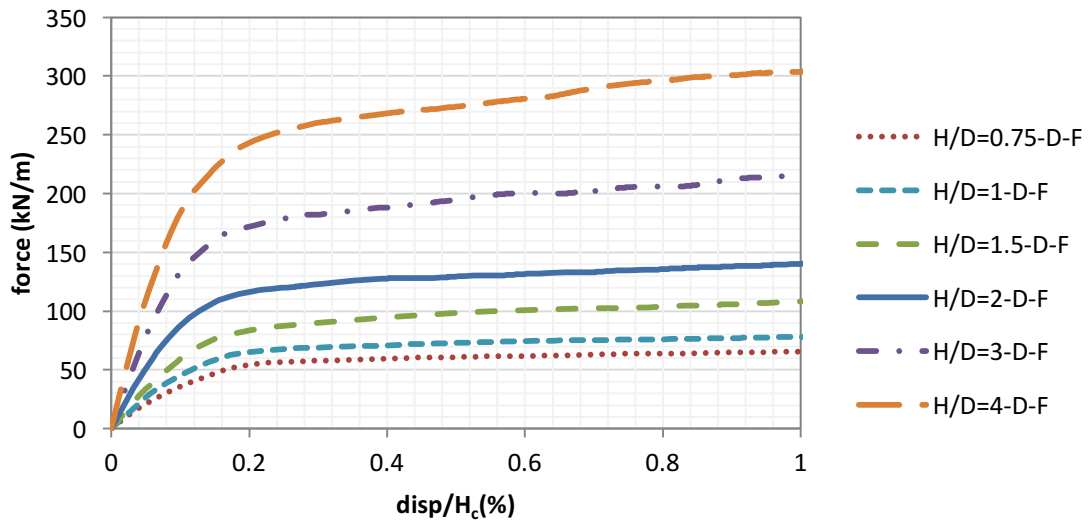


Figure B. 39 Load displacement curves- F (divided by L_p) versus $disp/H_c$ for different embedment depths-D-F

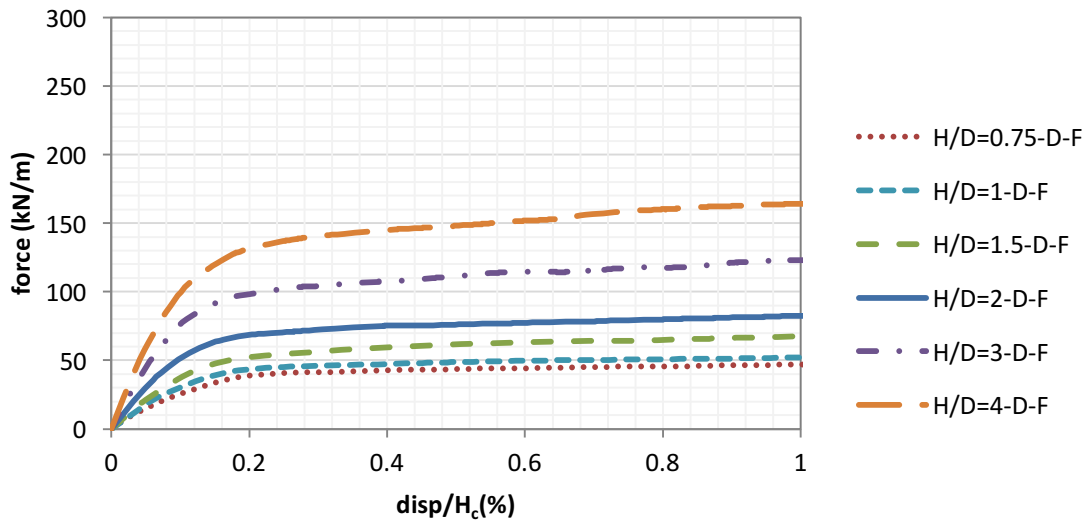


Figure B. 40 Load displacement curves- F (divided by L_{eff}) versus $disp/H_c$ for different embedment depths-D-F

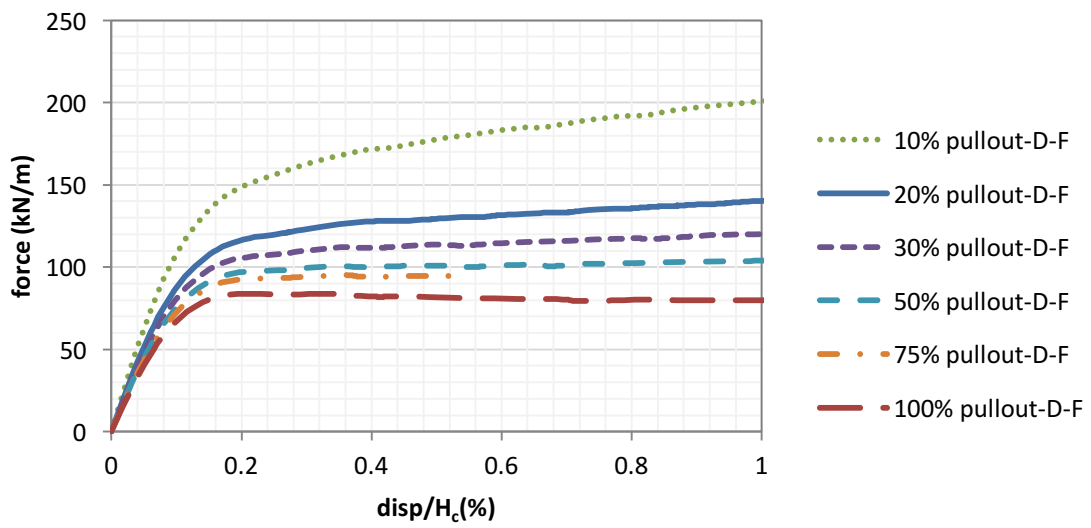


Figure B. 41 Load displacement curves- F (divided by L_p) versus $disp/H_c$ for different pullout lengths-D-F

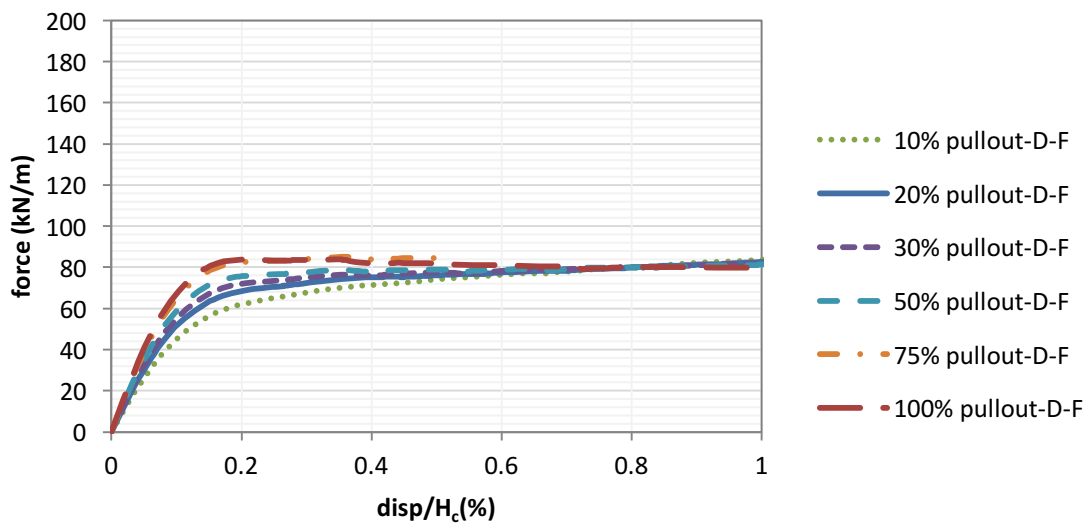


Figure B. 42 Load displacement curves- F (divided by L_{eff}) versus $disp/H_c$ for different pullout lengths-D-F

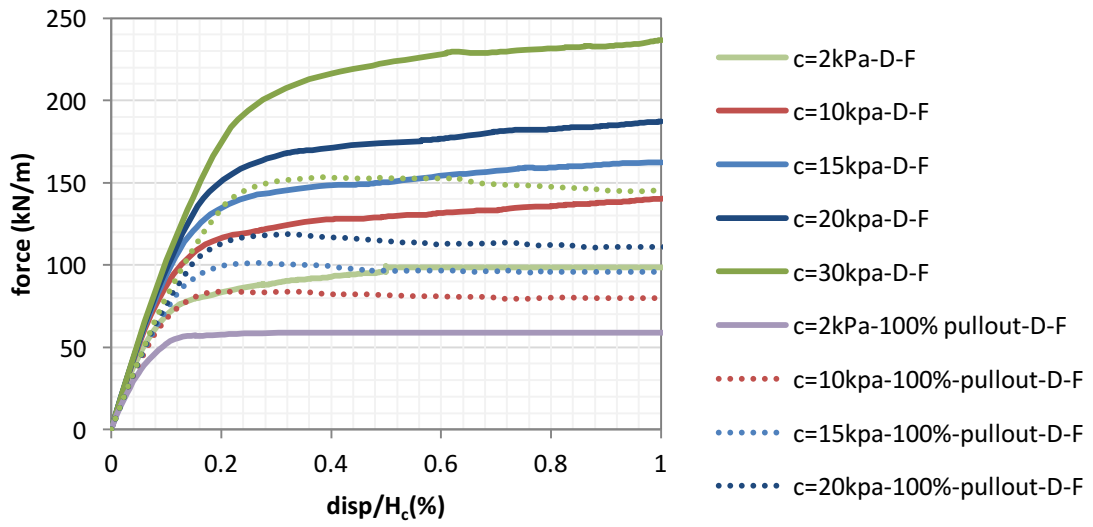


Figure B. 43 Load displacement curves- F (divided by L_p) versus $disp/H_c$ for different soil cohesion and pullout lengths-D-F

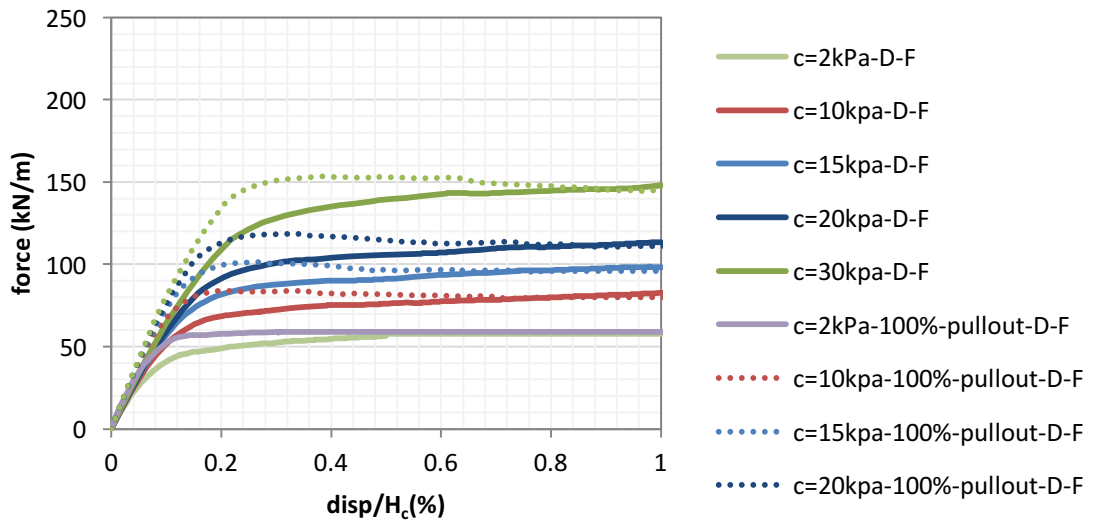


Figure B. 44 Load displacement curves- F (divided by L_{eff}) versus $disp/H_c$ for different soil cohesion and pullout lengths-D-F

APPENDIX C

MEDIUM DENSE SAND WITH FINES SLIDING BLOCK WITH INCLINED FAILURE SURFACES ANALYTICAL SOLUTIONS

A. Loose Sand with Fines

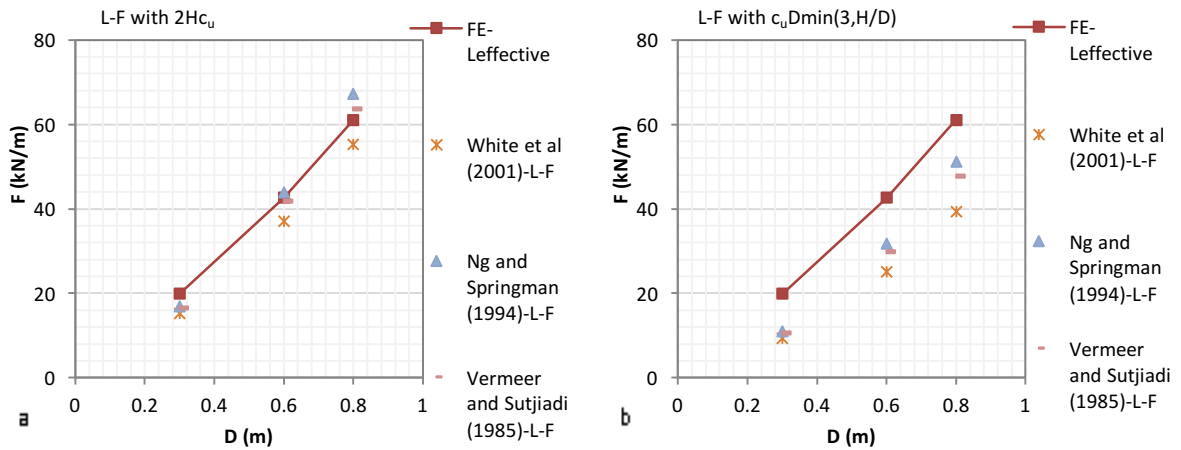


Figure C. 1 Uplift soil resistance versus pipe diameter - FE and Inclined Failure Surface Analytical Solutions with a) $2Hc_u$ and b) $c_u D \min(3, H/D)$ -Loose Sand with Fines

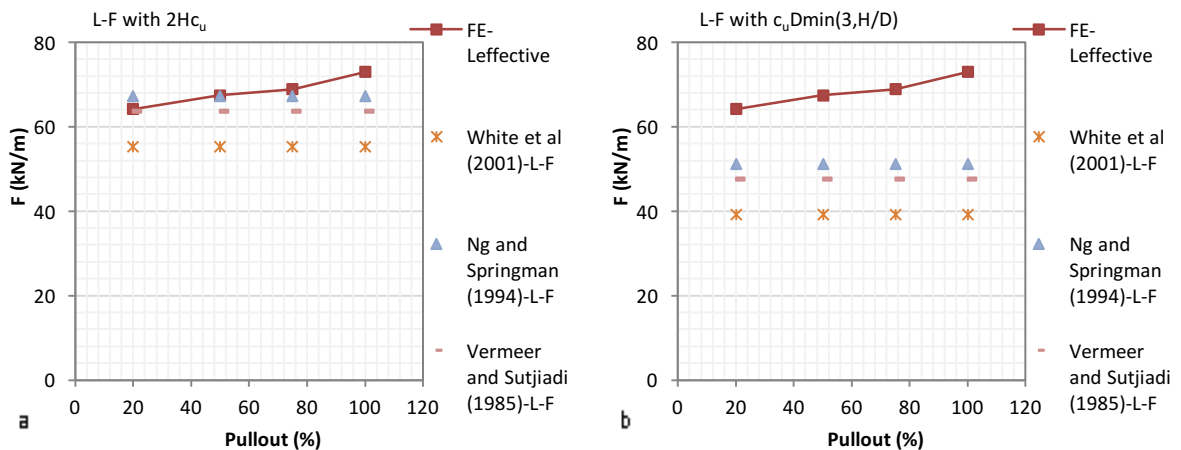


Figure C. 2 Uplift soil resistance versus pullout length - FE and Inclined Failure Surface Analytical Solutions with a) $2Hc_u$ and b) $c_u D \min(3, H/D)$ -Loose Sand with Fines

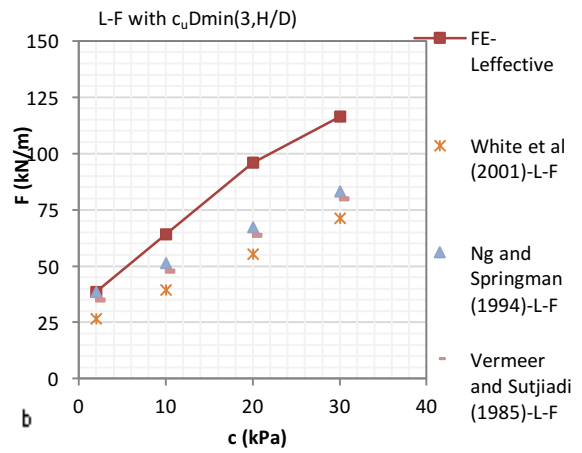
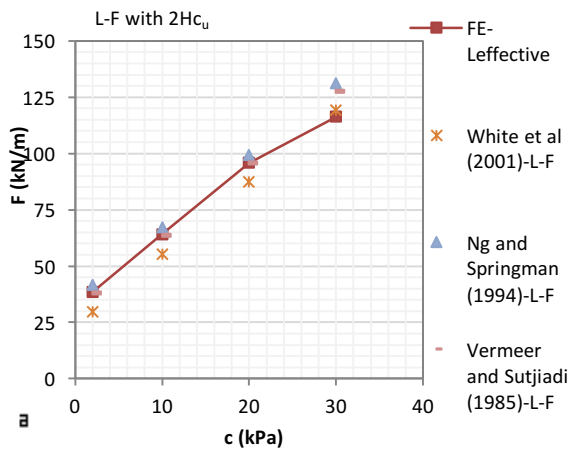


Figure C. 3 Uplift soil resistance versus soil cohesion- FE and Inclined Failure Surface Analytical Solutions with a) $2Hc_u$ and b) $c_u D_{min}(3,H/D)$ -Loose Sand with Fines

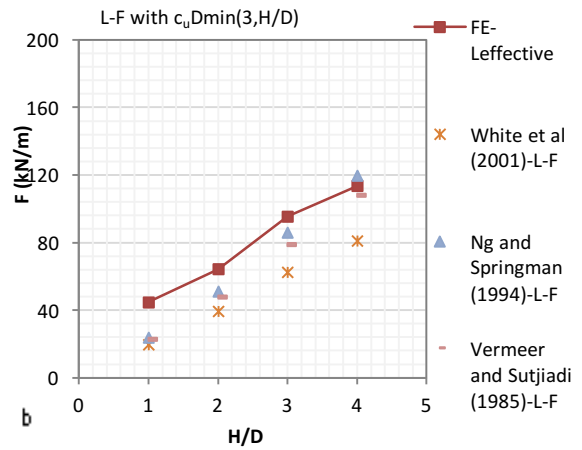
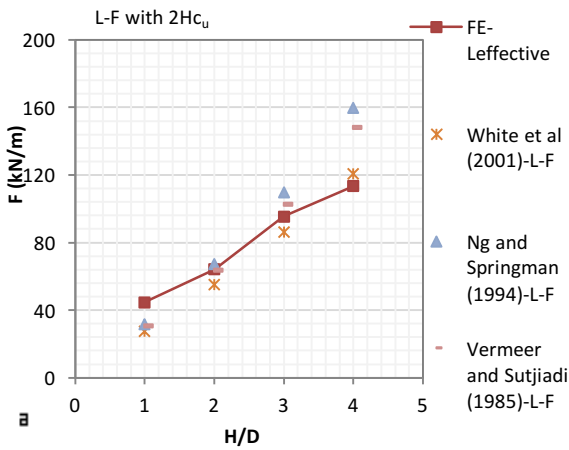


Figure C. 4 Uplift soil resistance versus embedment depth - FE and Inclined Failure Surface Analytical Solutions with a) $2Hc_u$ and b) $c_u D_{min}(3,H/D)$ -Loose Sand with Fines

B. Medium Dense Sand with Fines

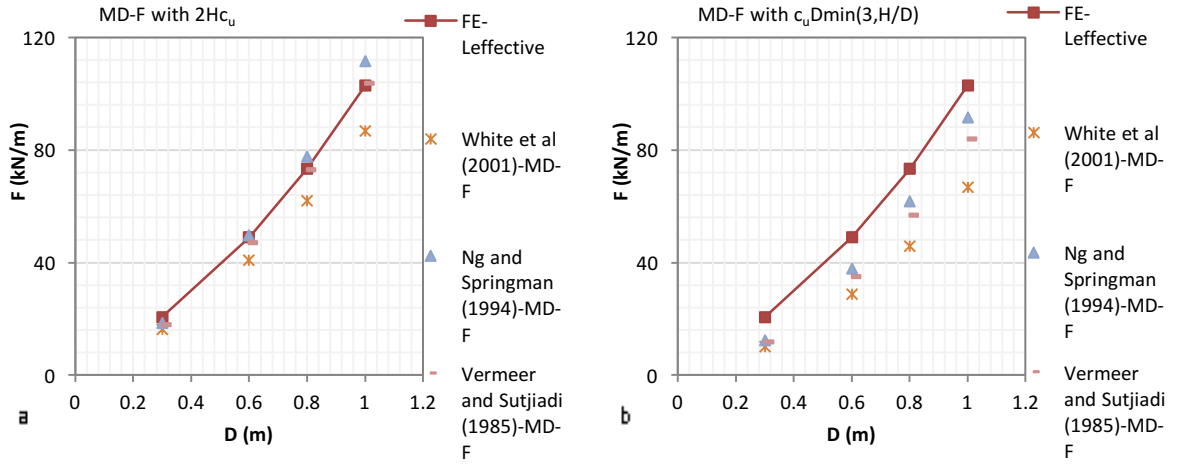


Figure C. 5 Uplift soil resistance versus pipe diameter - FE and Inclined Failure Surface Analytical Solutions with a) $2Hc_u$ and b) $c_u Dmin(3,H/D)$ -Medium Dense Sand with Fines

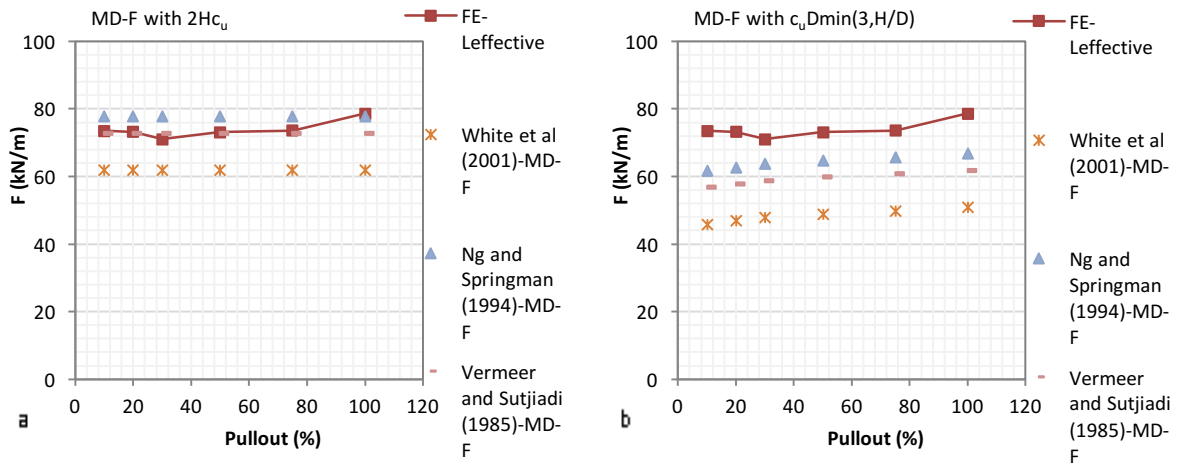


Figure C. 6 Uplift soil resistance versus pullout length - FE and Inclined Failure Surface Analytical Solutions with a) $2Hc_u$ and b) $c_u Dmin(3,H/D)$ -Medium Dense Sand with Fines

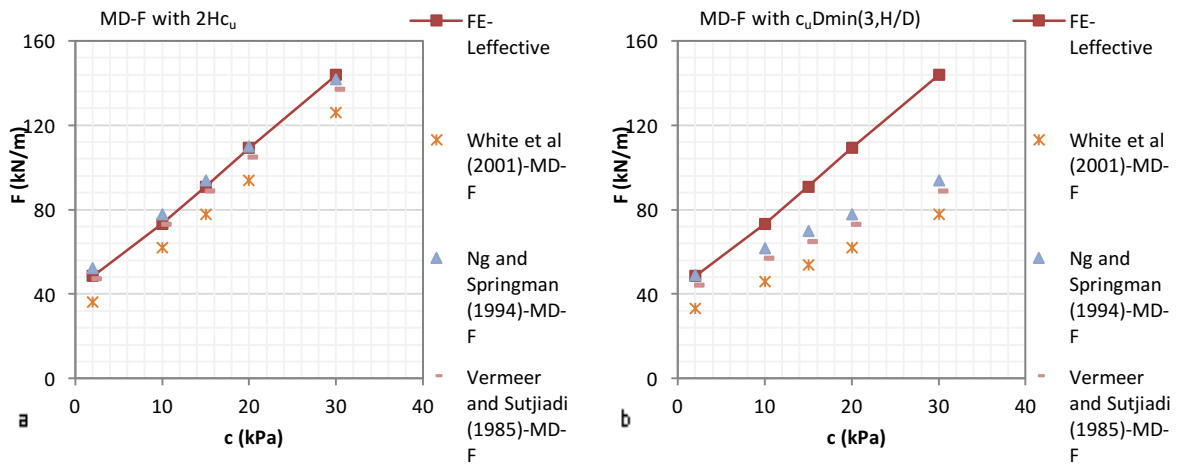


Figure C. 7 Uplift soil resistance versus soil cohesion- FE and Inclined Failure Surface Analytical Solutions with a) $2Hc_u$ and b) $c_u D_{min}(3,H/D)$ -Medium Dense Sand with Fines

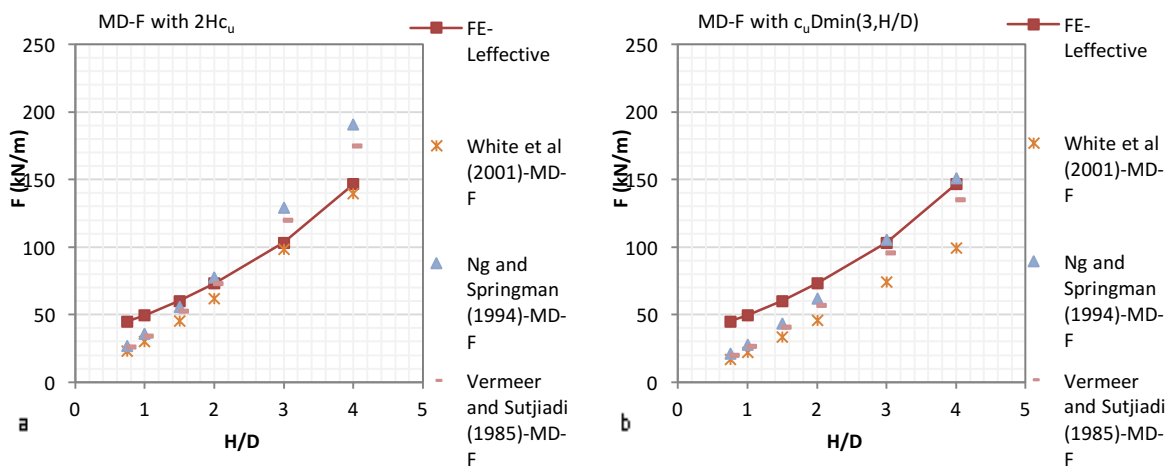


Figure C. 8 Uplift soil resistance versus embedment depth- FE and Inclined Failure Surface Analytical Solutions with a) $2Hc_u$ and b) $c_u D_{min}(3,H/D)$ -Medium Dense Sand with Fines

C. Dense Sand with Fines

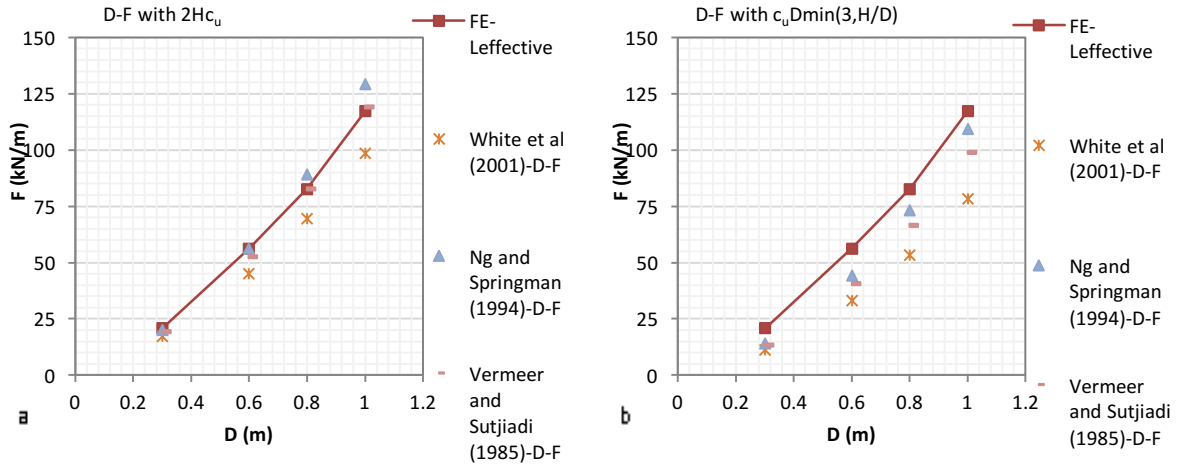


Figure C. 9 Uplift soil resistance versus pipe diameter - FE and Inclined Failure Surface Analytical Solutions with a) $2Hc_u$ and b) $c_u D_{min}(3,H/D)$ - Dense Sand with Fines

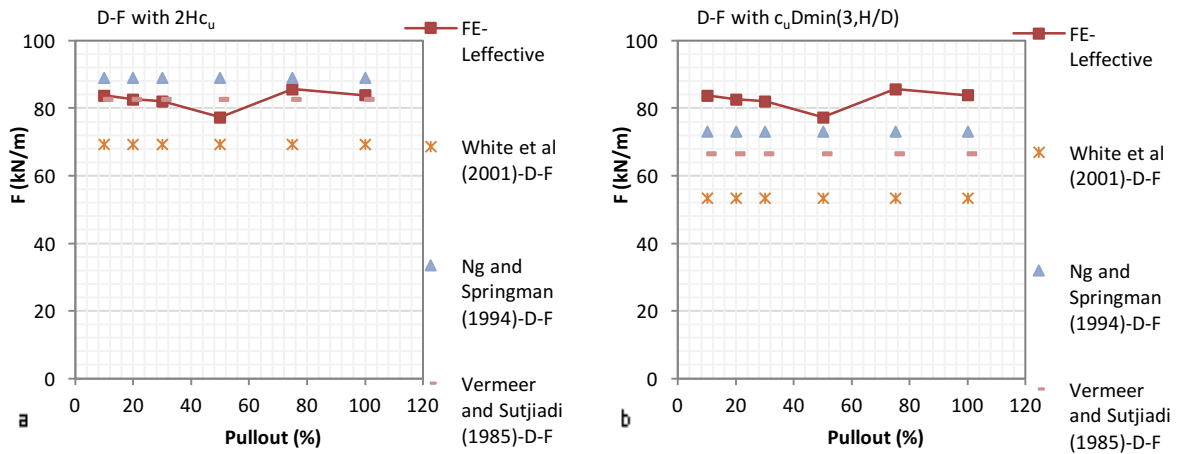


Figure C. 10 Uplift soil resistance versus pullout length - FE and Inclined Failure Surface Analytical Solutions with a) $2Hc_u$ and b) $c_u D_{min}(3,H/D)$ - Dense Sand with Fines

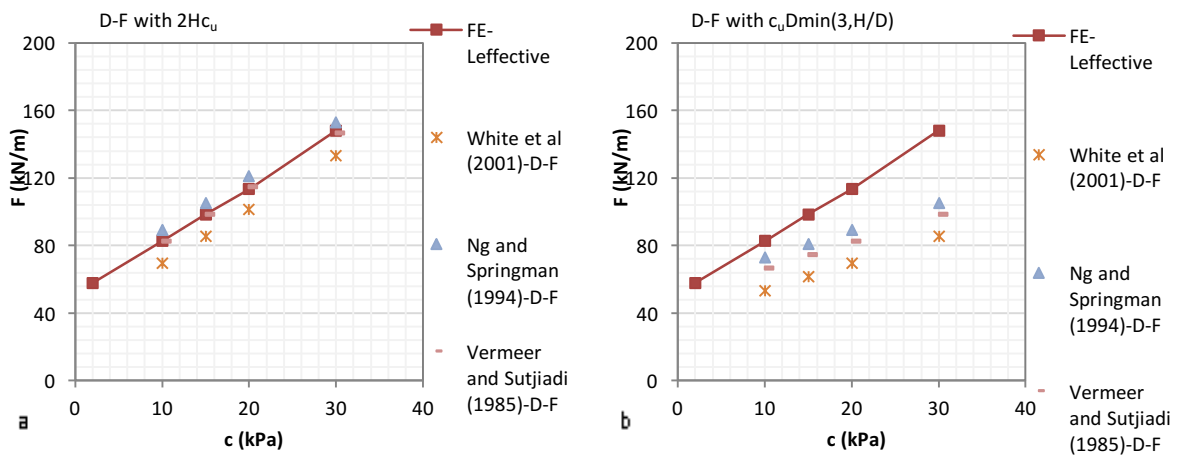


Figure C. 11 Uplift soil resistance versus soil cohesion - FE and Inclined Failure Surface Analytical Solutions with a) $2Hc_u$ and b) $c_u Dmin(3,H/D)$ - Dense Sand with Fines

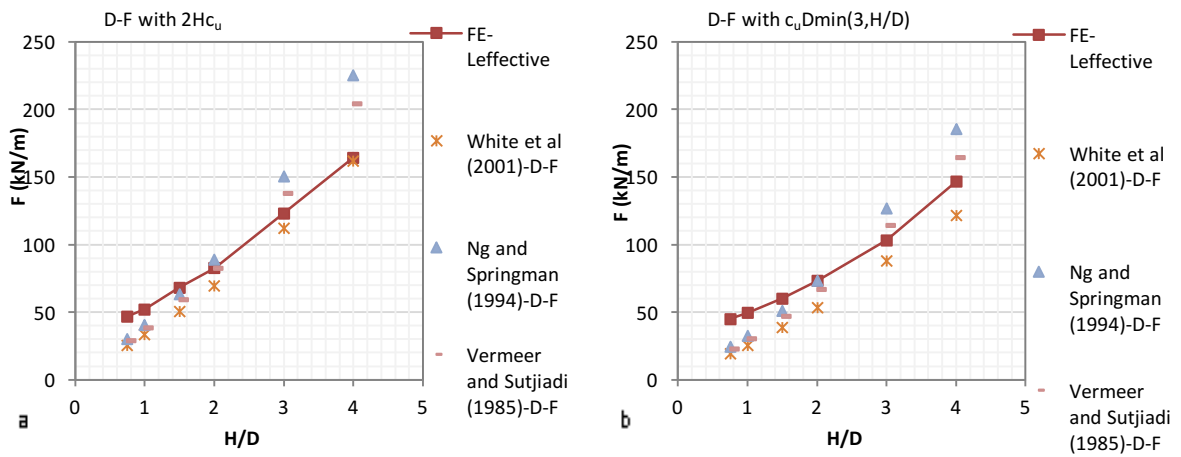


Figure C. 12 Uplift soil resistance versus embedment depth - FE and Inclined Failure Surface Analytical Solutions with a) $2Hc_u$ and b) $c_u Dmin(3,H/D)$ - Dense Sand with Fines

APPENDIX D

VARIATION OF THE BIAS FACTOR FOR DIFFERENT ANALYTICAL SOLUTIONS

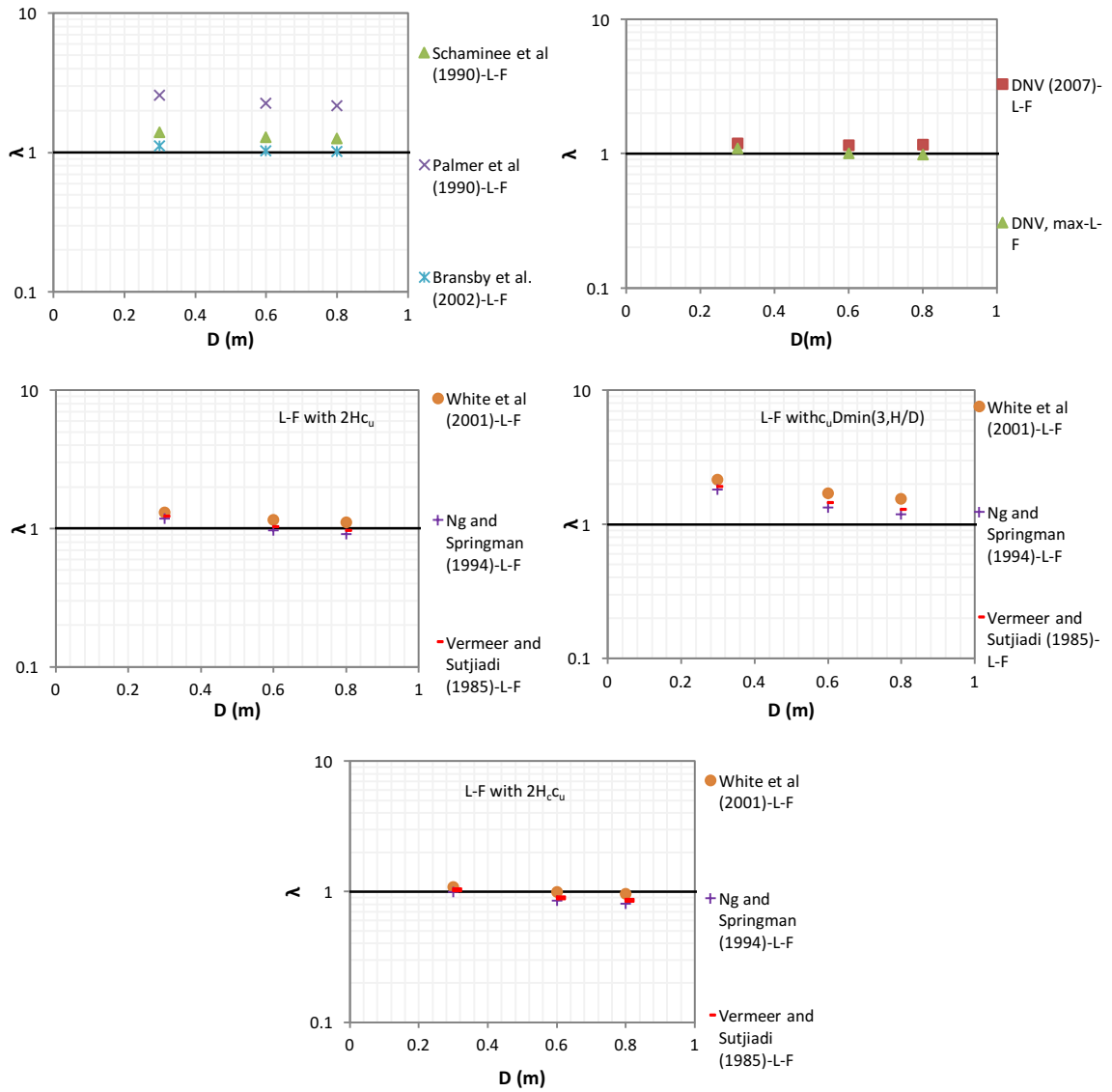


Figure D. 1 Bias Factor versus pipe diameter- Loose Sand with Fines

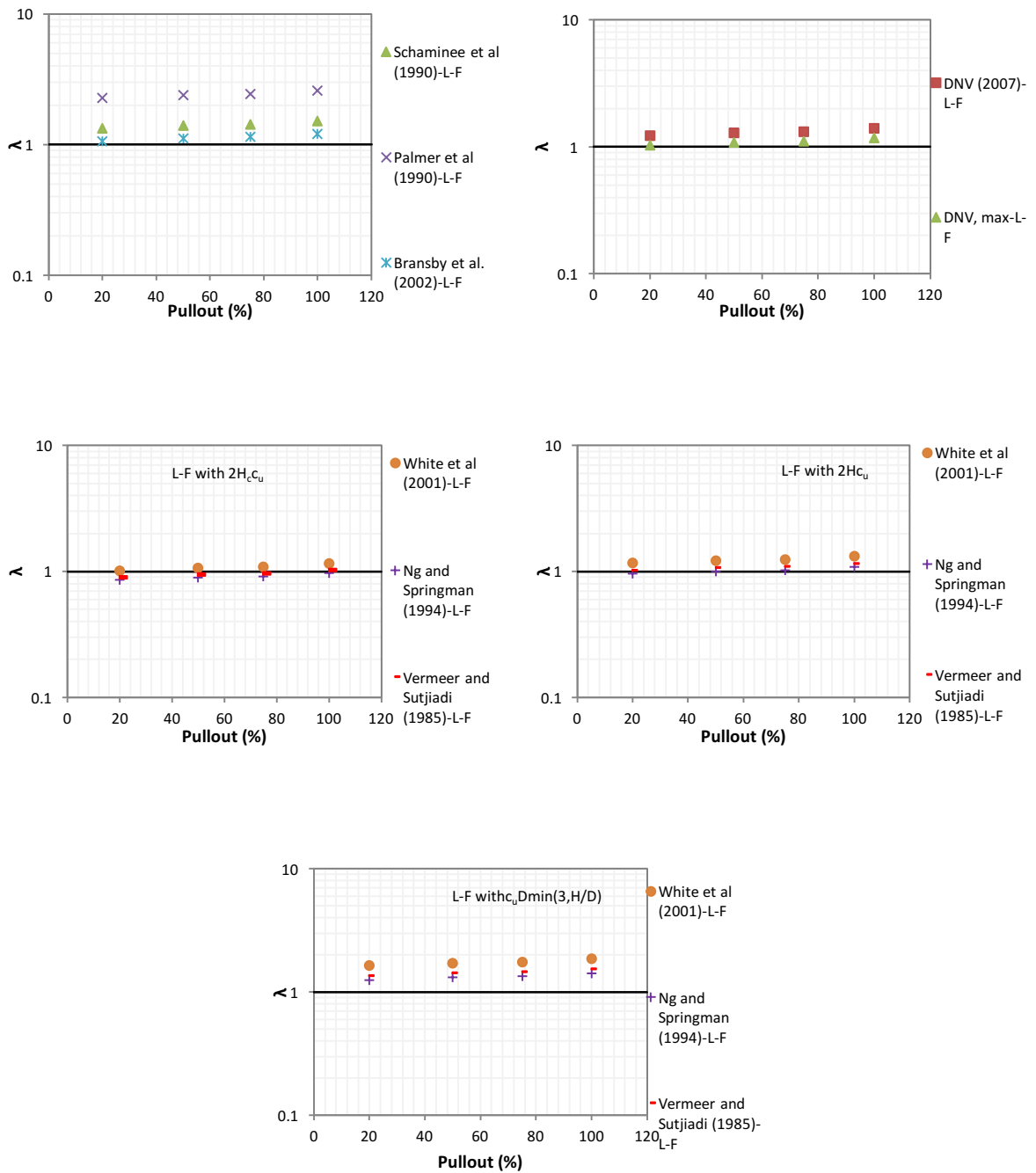


Figure D. 2 Bias Factor versus pullout length- Loose Sand with Fines

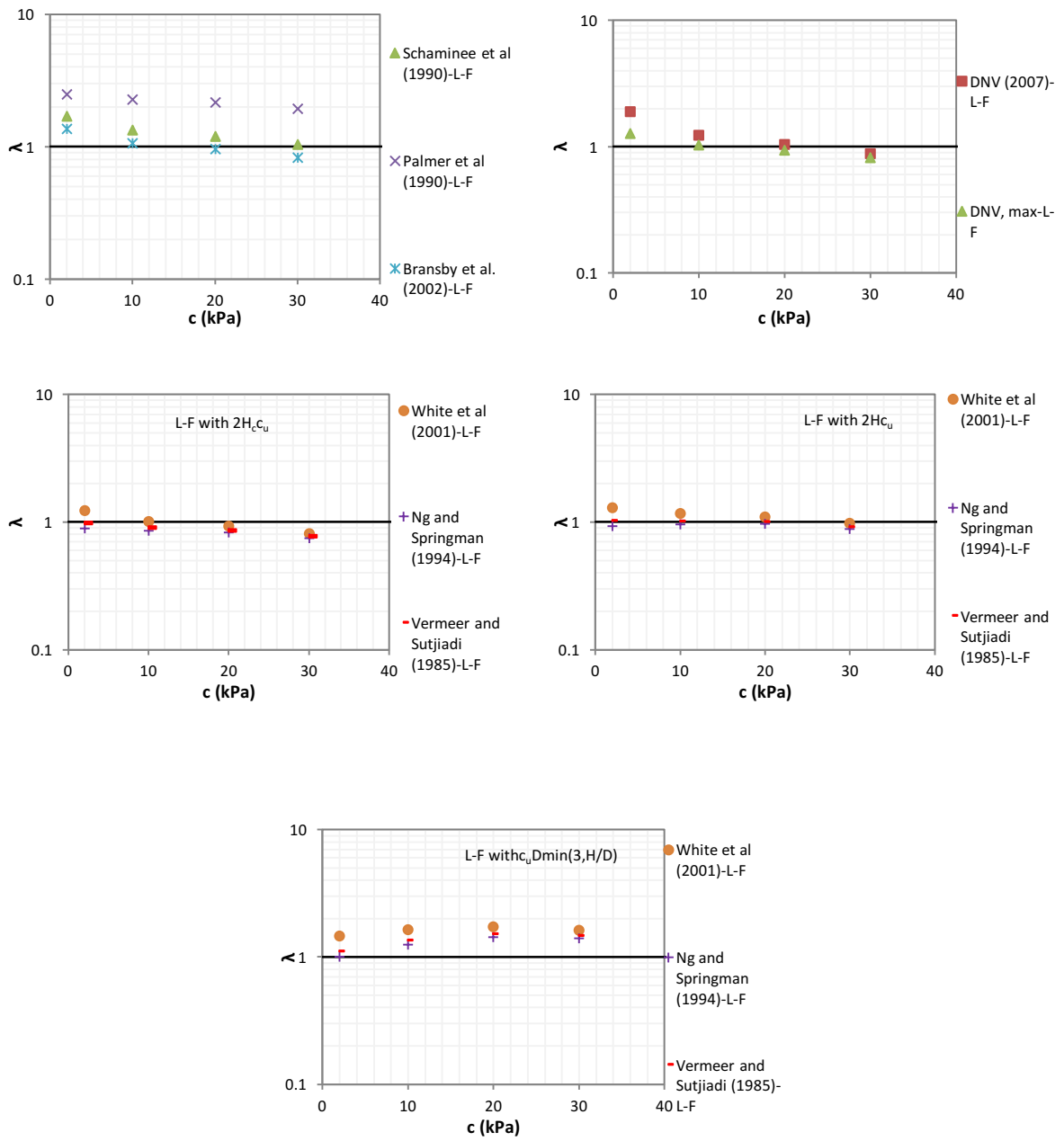


Figure D. 3 Bias Factor versus soil cohesion- Loose Sand with Fines

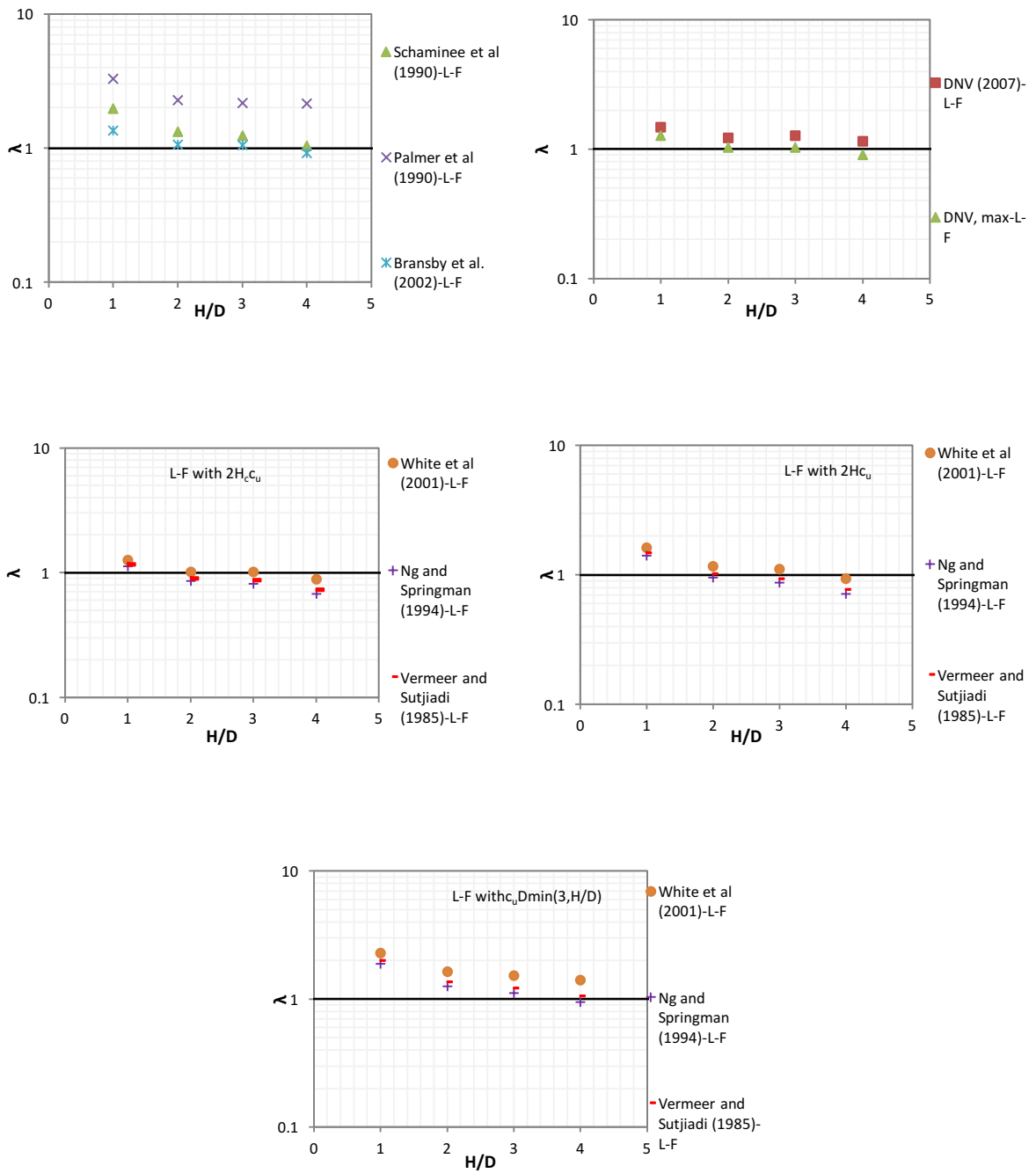


Figure D. 4 Bias Factor versus embedment depth- Loose Sand with Fines

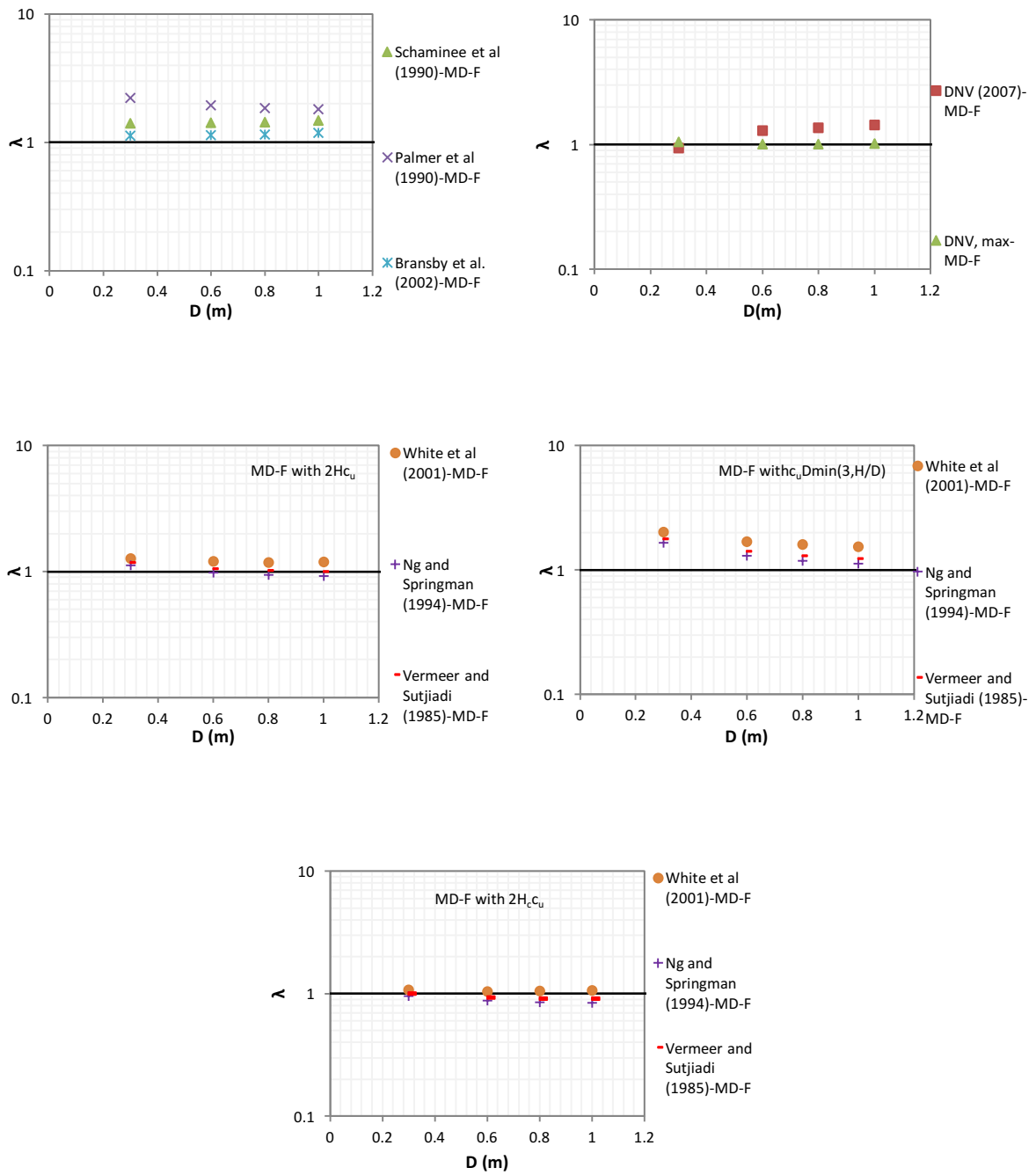


Figure D. 5 Bias Factor versus pipe diameter- Medium Dense Sand with Fines

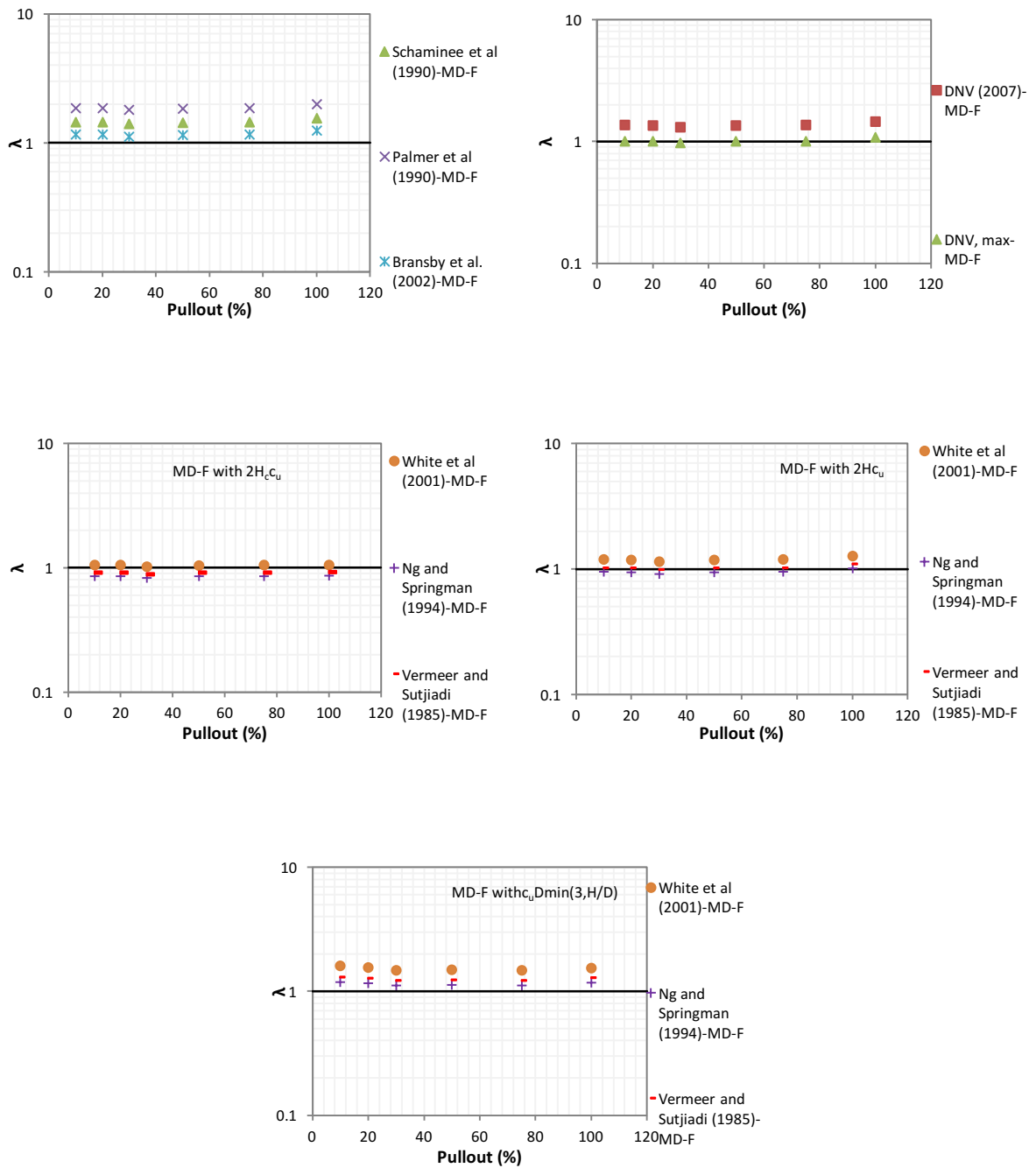


Figure D. 6 Bias Factor versus pullout length- Medium Dense Sand with Fines

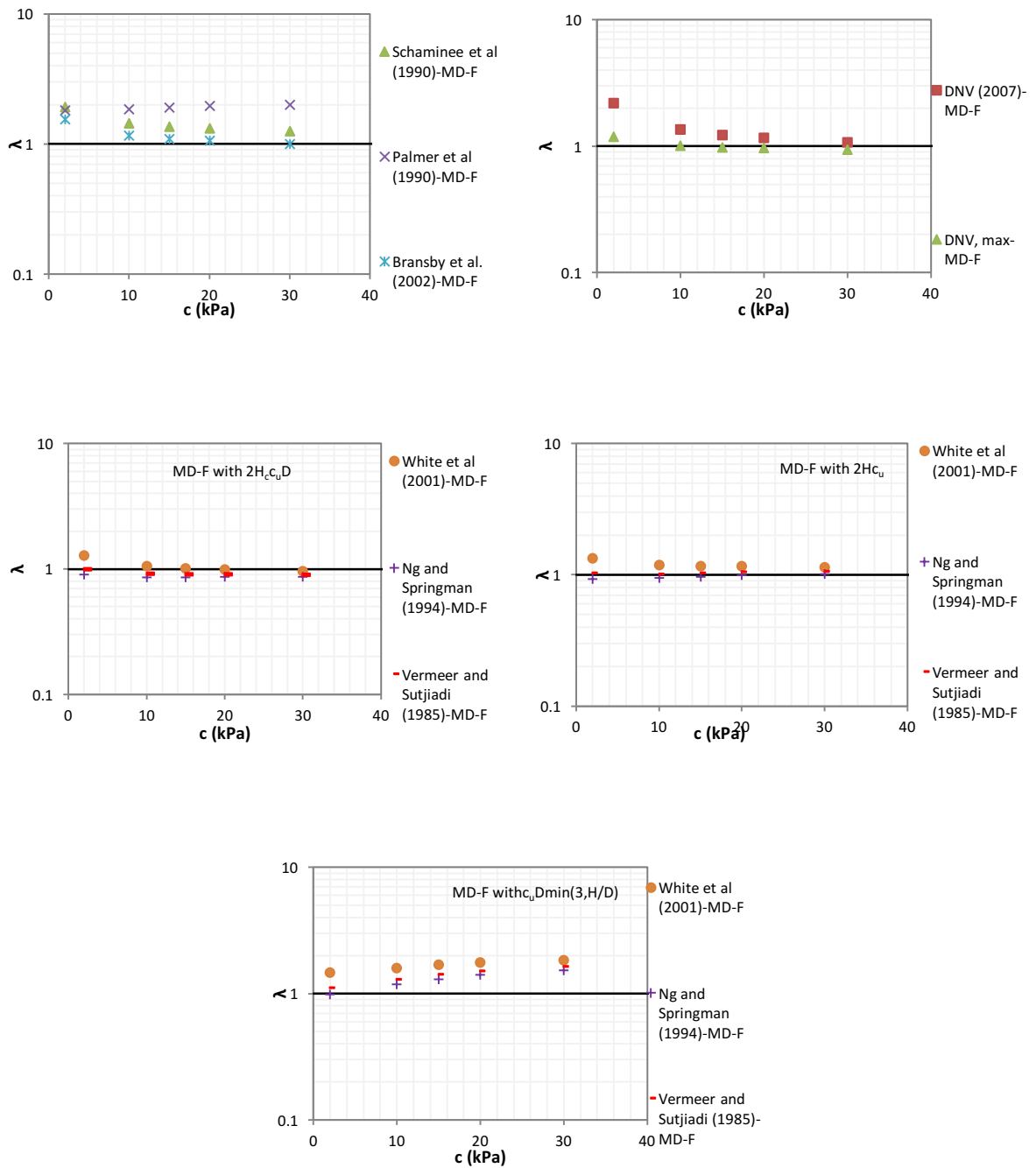


Figure D. 7 Bias Factor versus soil cohesion- Medium Dense Sand with Fines

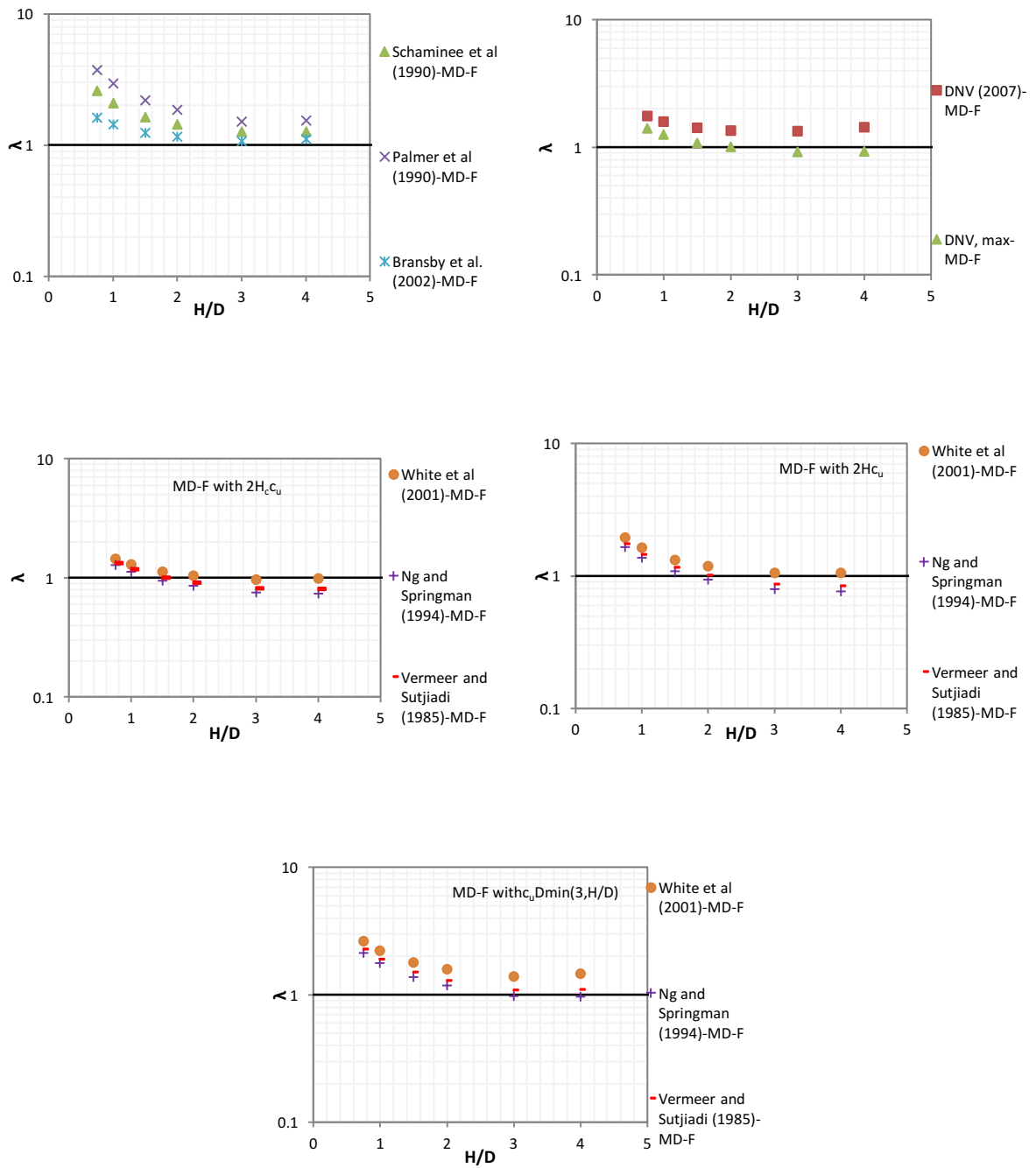


Figure D. 8 Bias Factor versus embedment depth- Medium Dense Sand with Fines

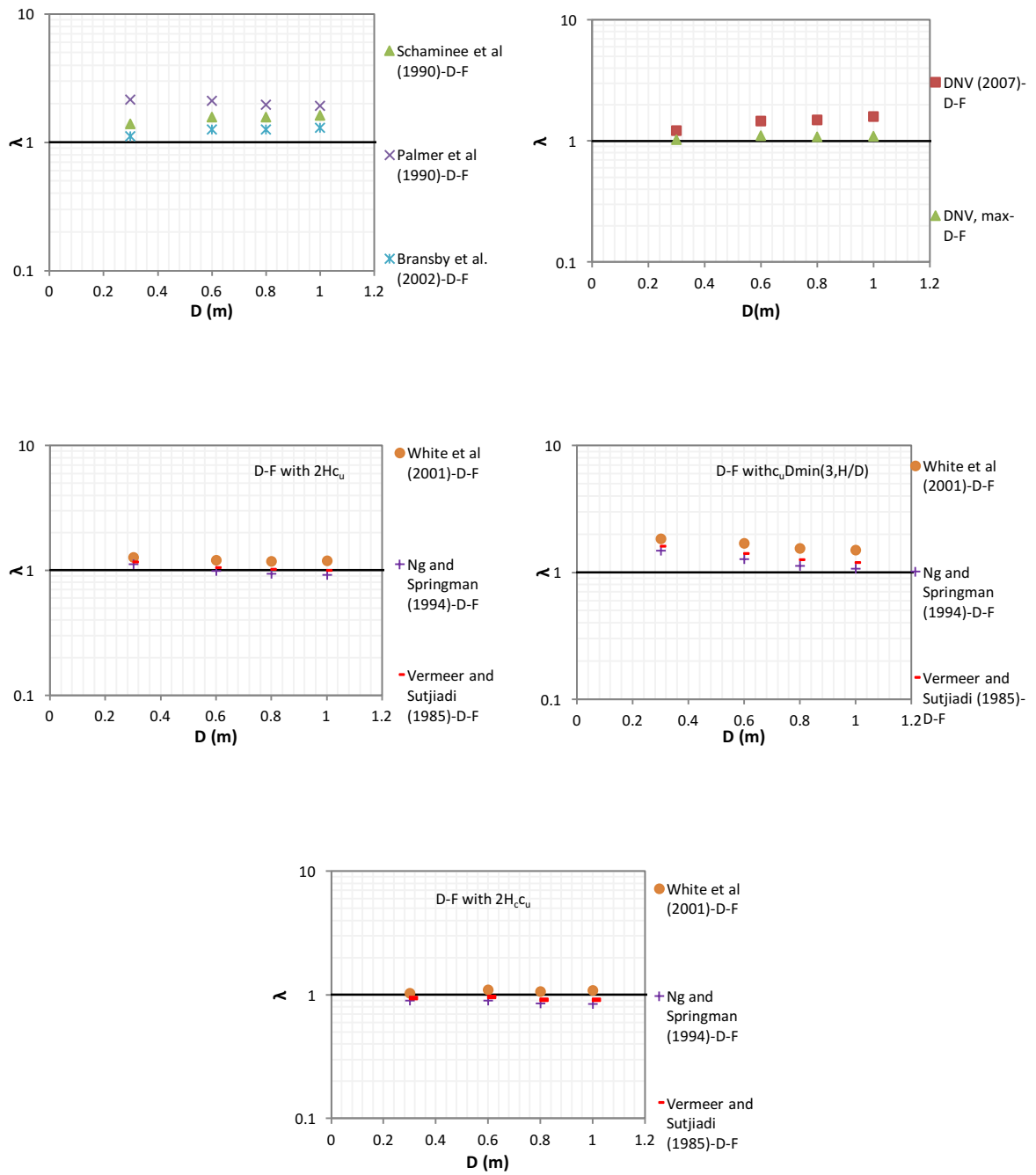


Figure D. 9 Bias Factor versus pipe diameter- Dense Sand with Fines

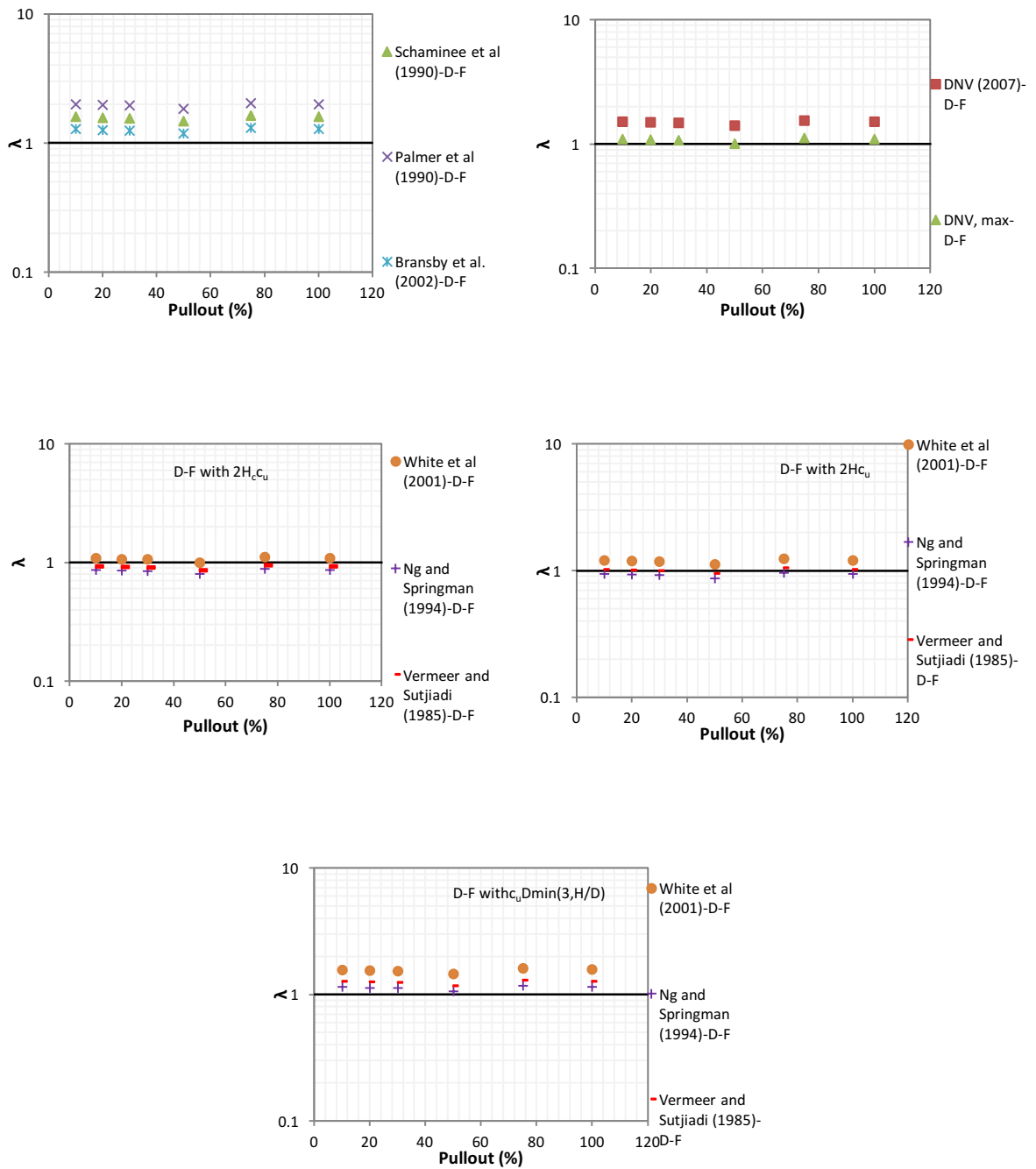


Figure D. 10 Bias Factor versus pullout length- Dense Sand with Fines

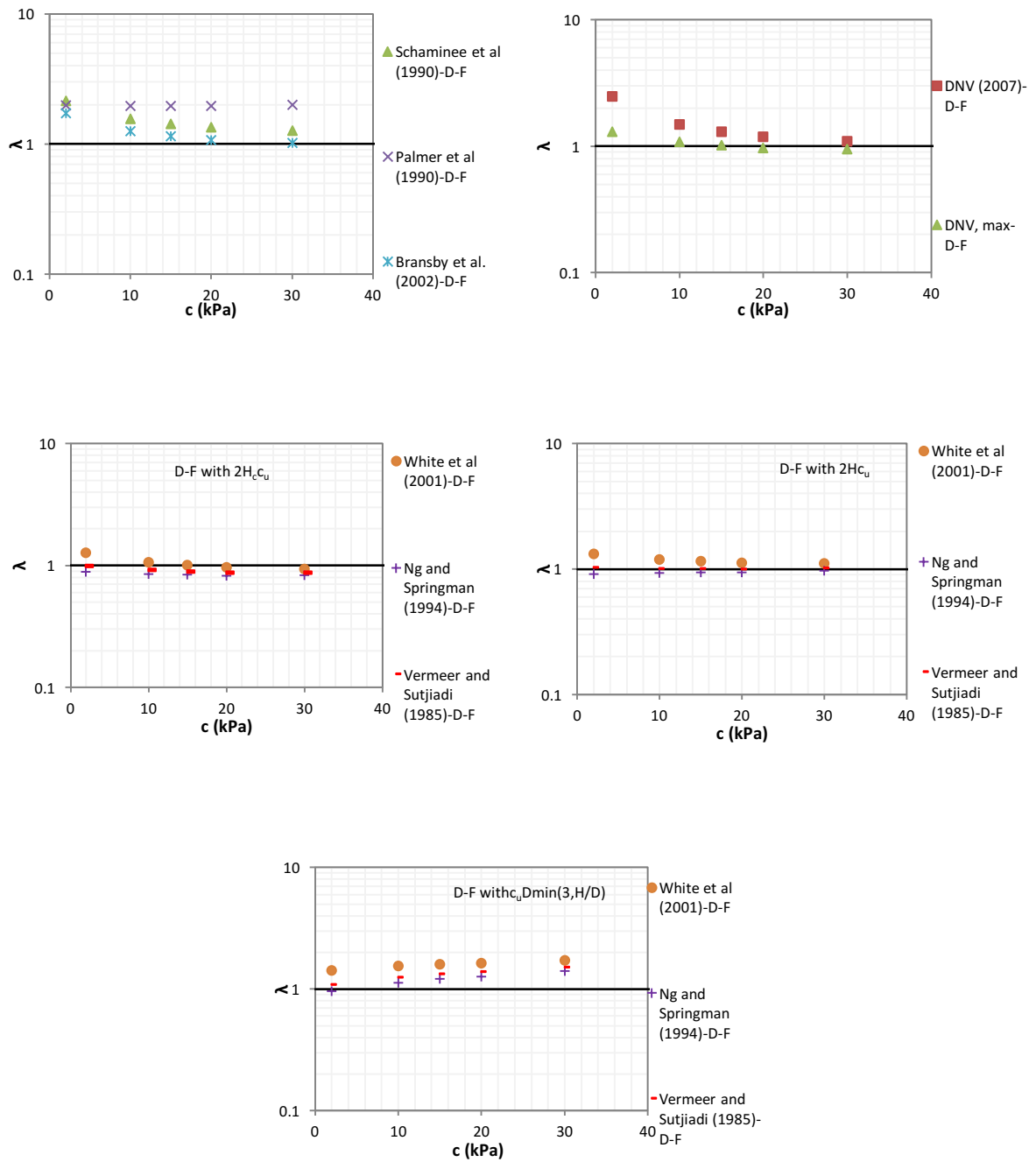


Figure D. 11 Bias Factor versus soil cohesion- Dense Sand with Fines

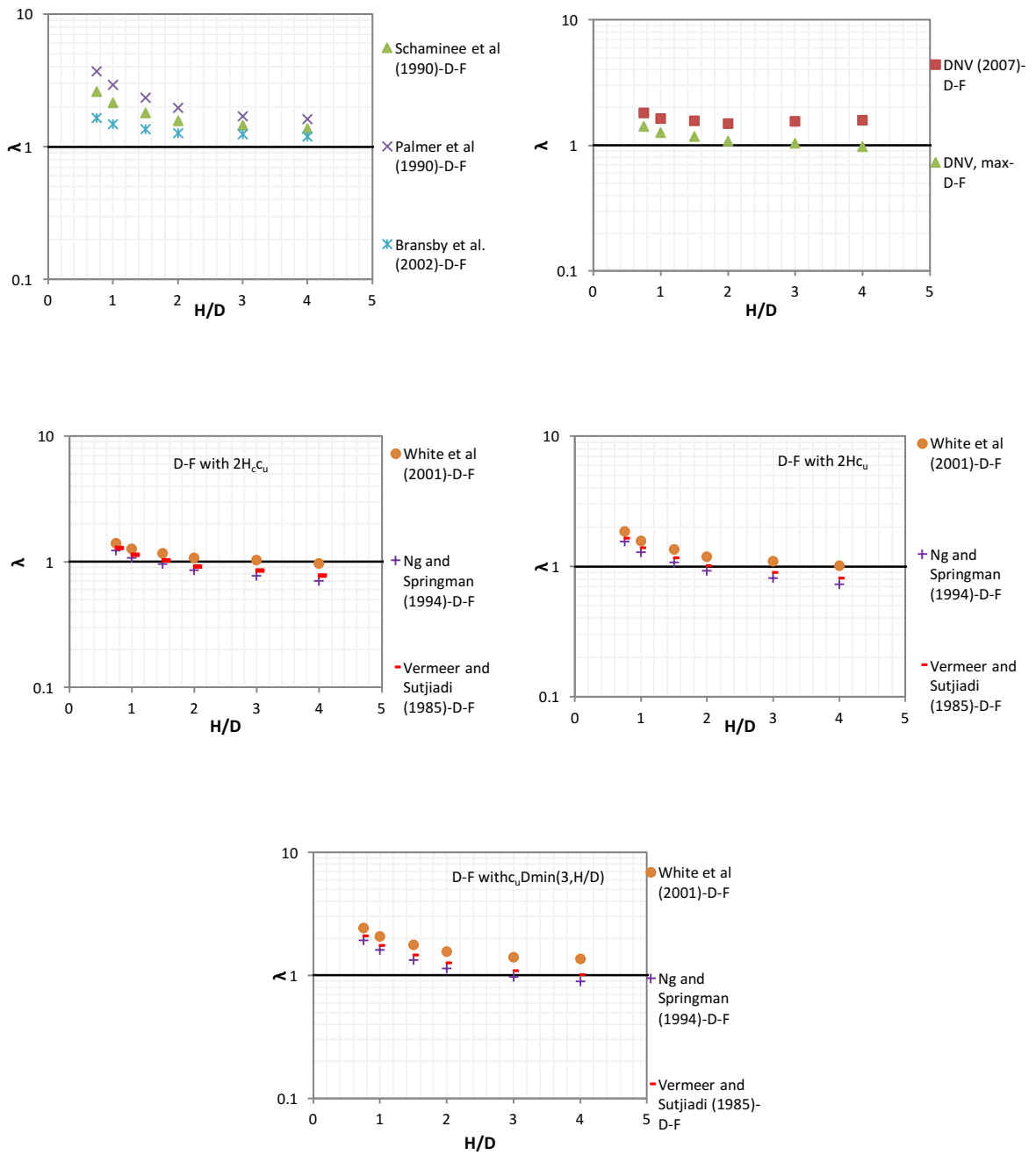


Figure D. 12 Bias Factor versus embedment depth- Dense Sand with Fines

APPENDIX E

SHEAR STRAIN PLOTS

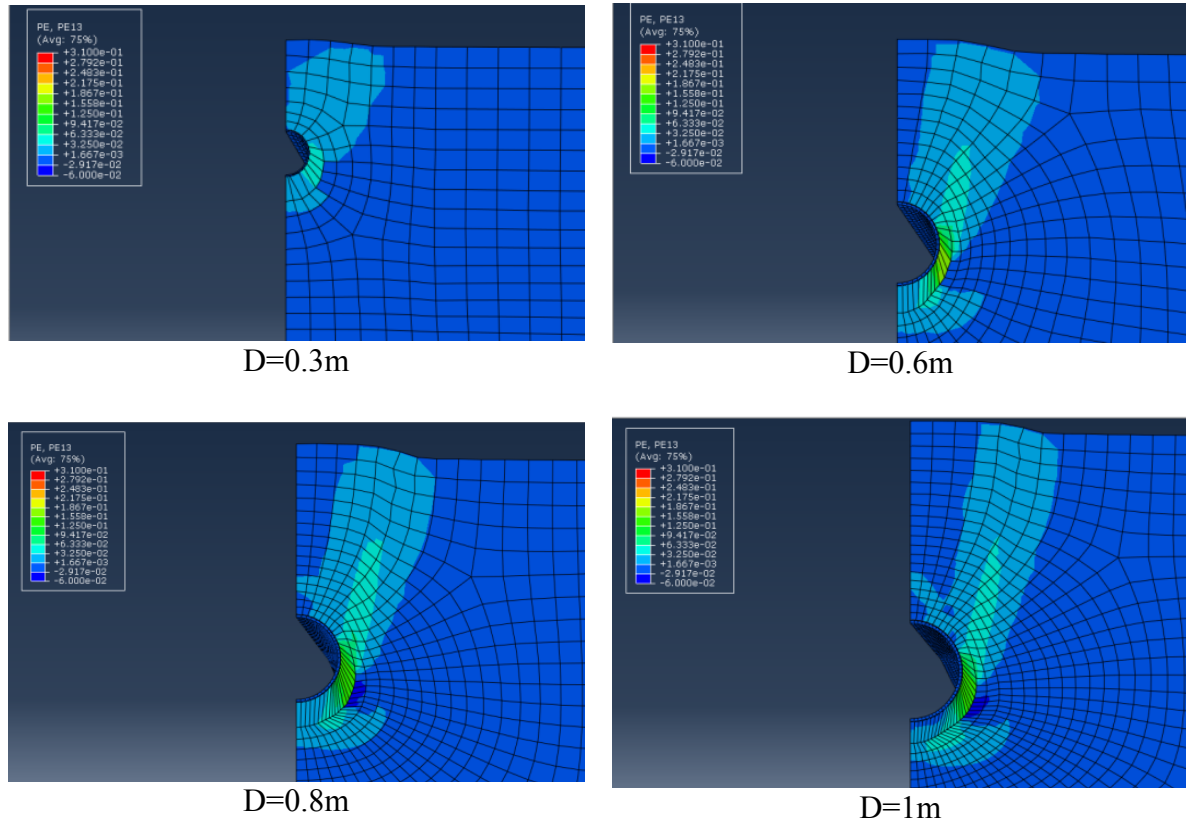


Figure E. 1 Shear strain plots: effect of pipe diameter- medium dense sand with fines

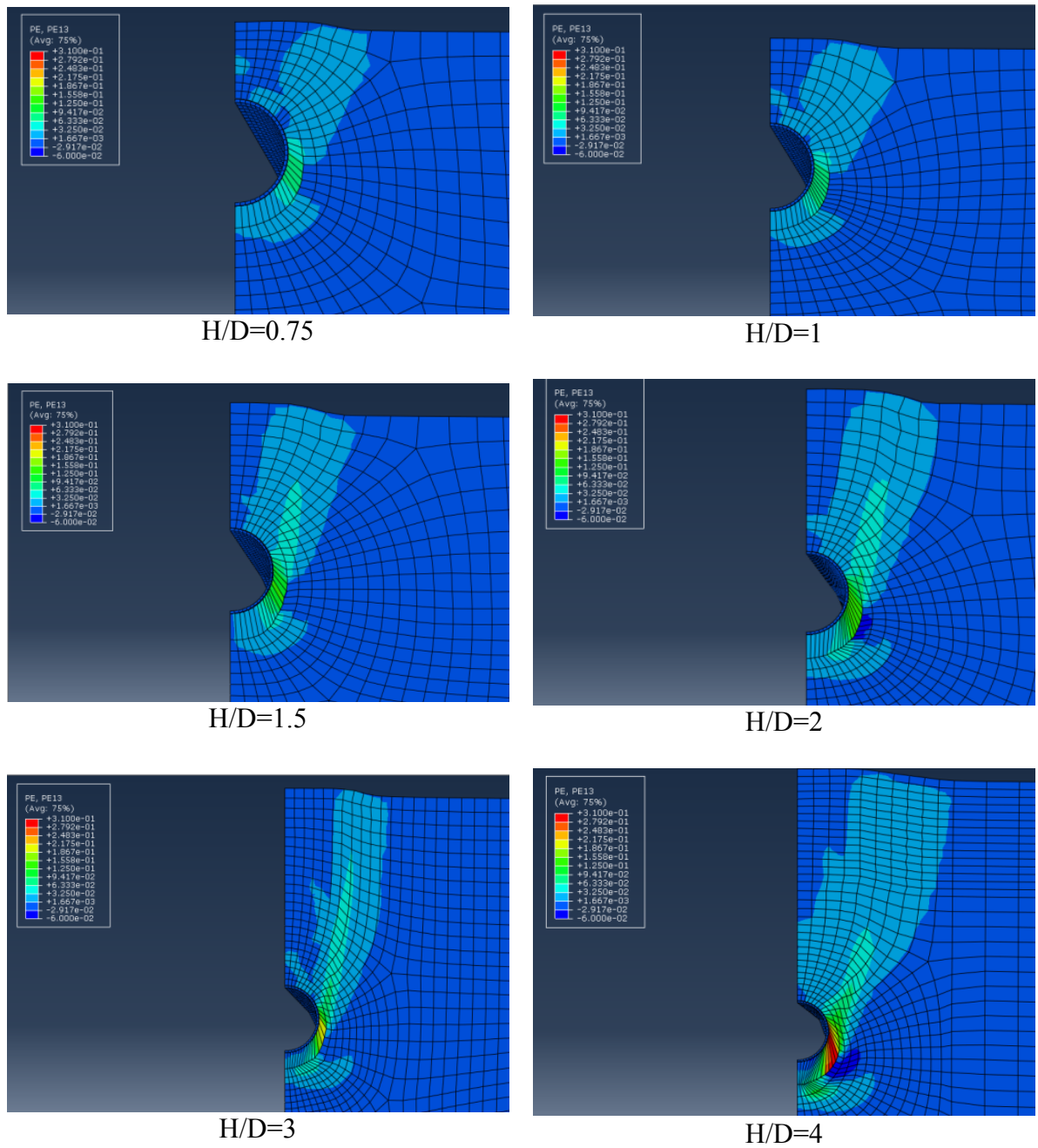
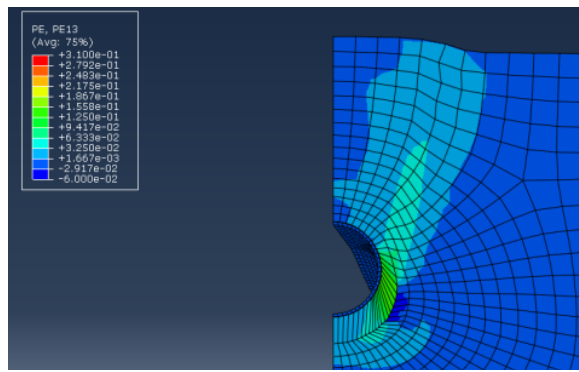
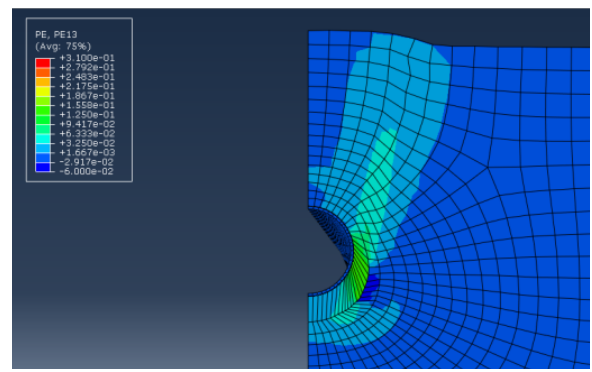


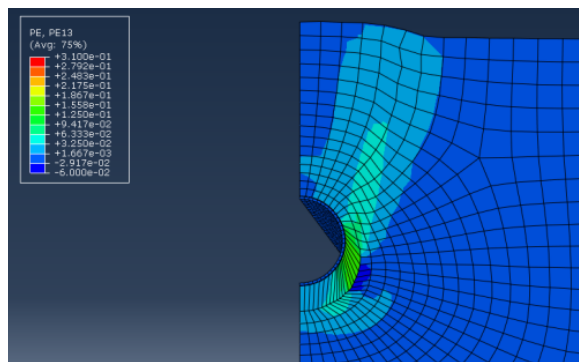
Figure E. 2 Shear strain plots: effect of embedment depth- medium dense sand with fines



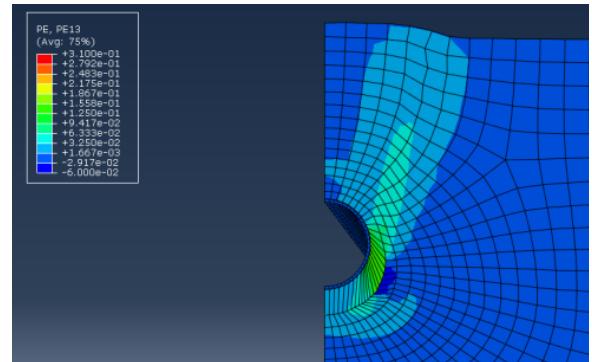
Pullout=10%



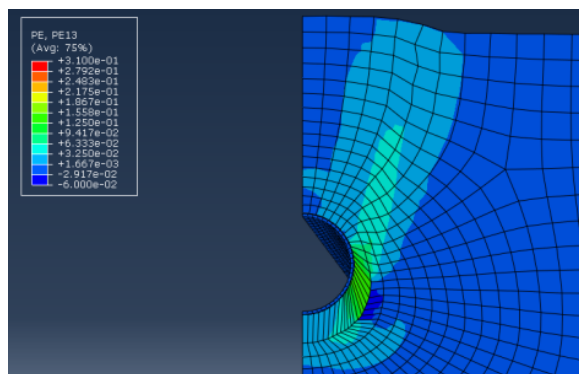
Pullout=20%



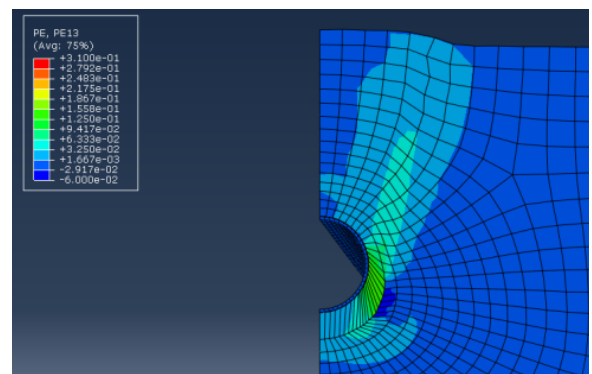
Pullout=30%



Pullout=50%

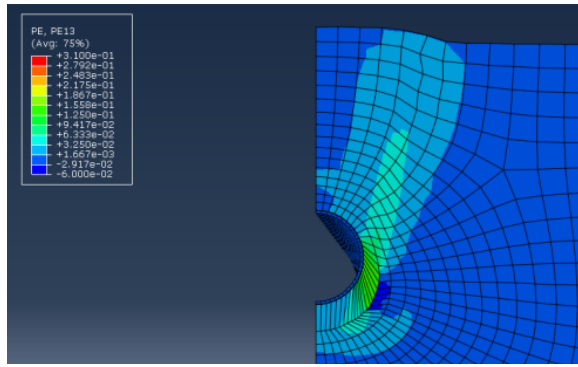


Pullout=75%

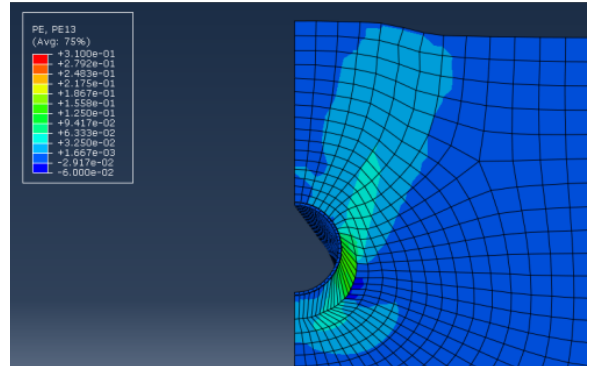


Pullout=100%

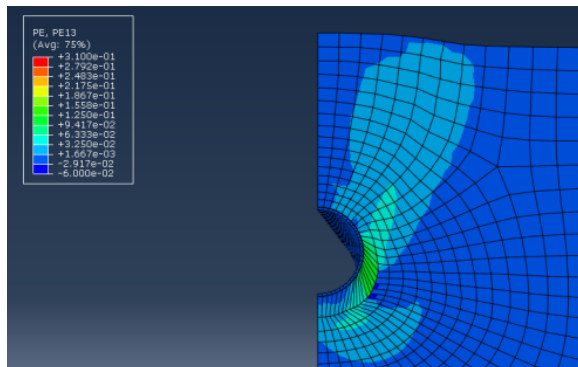
Figure E. 3 Shear strain plots: effect of pullout length- medium dense sand with fines



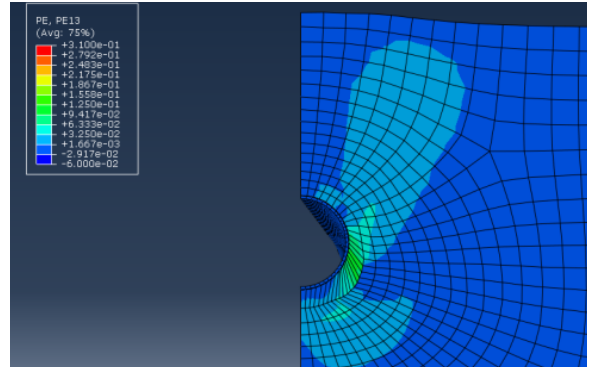
20%-c=10 kPa



20%-c=15 kPa



20%-c=20 kPa



20%-c=30 kPa

Figure E. 4 Shear strain plots: effect of soil cohesion 20% pullout length- medium dense sand with fines

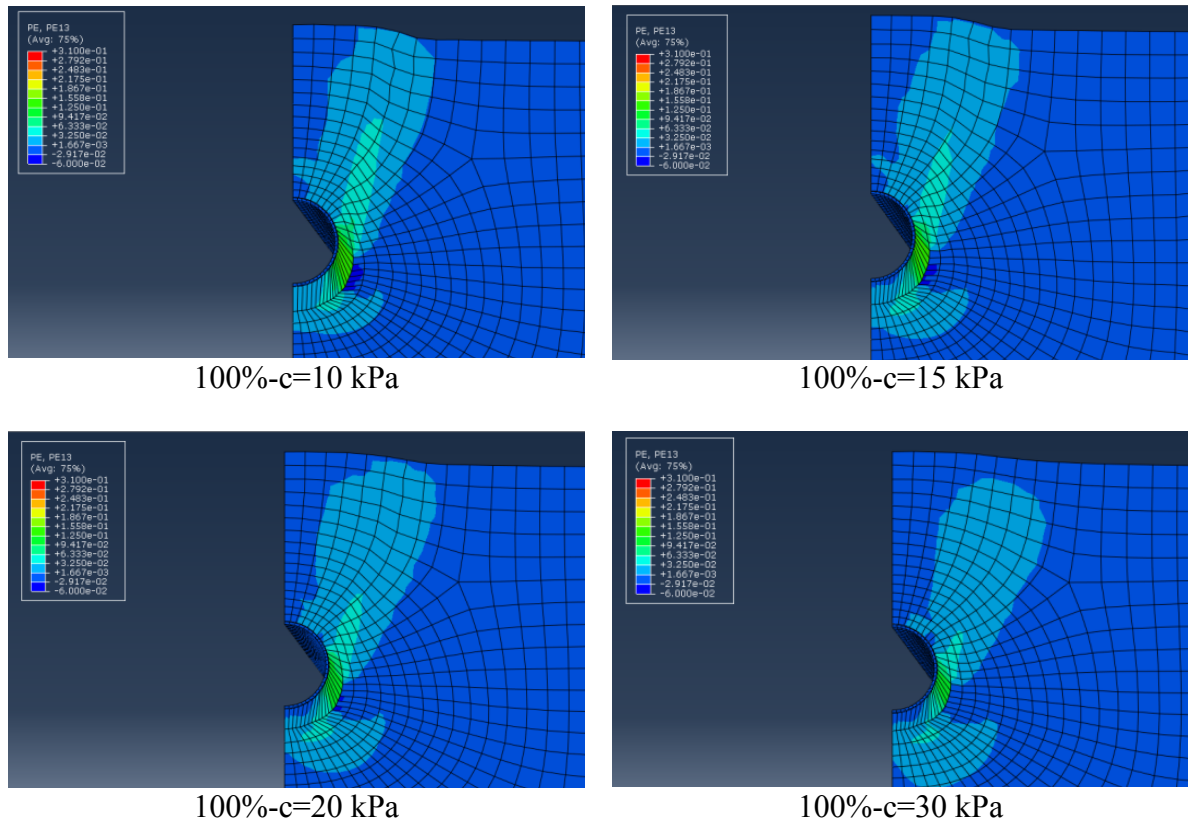


Figure E. 5 Shear strain plots: effect of soil cohesion 100% pullout length- medium dense sand with fines